Stochastic Stability of Flow-Induced Vibration

by

Jinyu Zhu

A thesis
presented to the University of Waterloo
in fulfilment of the
thesis requirement for the degree of
Doctor of Philosophy
in
Civil Engineering

Waterloo, Ontario, Canada, 2008

Author's Declaration

I hereby declare that I am the sole author of this thesis. This is a true copy of the thesis, including any required final revisions, as accepted by my examiners.

I understand that my thesis may be made electronically available to the public.

Abstract

Flow-induced structural vibration is experienced in many engineering applications, such as aerospace industry and civil engineering infrastructures. One of the main mechanisms of flow-induced vibration is instability which can be triggered by parametric excitations or fluid-elastic forces. Experiments show that turbulence has a significant impact on the stability of structures. The objective of this research is to bridge the gap between flow-induced vibration and stochastic stability of structures.

The flow-induced vibration of a spring-supported circular cylinder is studied in this research. The equations of motion for the cylinder placed in a cross-flow are set up, in which the vortex force is modeled by a bounded noise because of its narrow-band characteristics. Since the vibration in the lift direction is more prominent in the lock-in region, the system is reduced to one degree-of-freedom, i.e., only the vibration of the cylinder in the lift direction is considered. The equation of motion for the cylinder can be generalized as a two-dimensional system excited by a bounded noise. Stochastic analysis is used to determine the moment Lyapunov exponents and Lyapunov exponents for the generalized system. The results are then applied to study the parametric instability of a cylinder in the lock-in region.

Fluidelastic instability can occur when the cylinder is placed in a shear flow. The equations of motion are established by using the quasi-steady theory to model the fluid-elastic forces. To study the turbulence effect on the stability of the cylinder, a real noise or an Ornstein-Uhlenbeck process is used to model the grid-generated turbulence. The equations of motion are randomized resulting in a four-dimensional system excited by a real noise. The stability of the stochastic system is studied by determining the moment Lyapunov exponents and Lyapunov exponents. Parameters of the system and the noise are varied to investigate their effects on the stability. It is found that the grid-generated turbulence can stabilize the system when the parameters take certain values, which agrees with the experimental observations.

Many flow-induced vibration problems can be modeled by a two degrees-of-freedom system parametrically excited by a narrow-band process modeled by a bounded noise. The system can be in subharmonic resonance, combination (additive or differential) resonance, or both if the central frequency of the bounded noise takes an appropriate value. The

method for a single degree-of-freedom system is extended to study the stochastic stability of the two degrees-of-freedom system. The moment Lyapunov exponents and Lyapunov exponents for the three cases are obtained using a perturbation method. The effect of noise on various types of parametric resonance, such as subharmonic resonance, combination additive resonance, and combined subharmonic and combination additive resonance, is investigated.

The main contributions of this thesis are stochastic stability analysis of one-degree-of-freedom systems and two-degree-of-freedom systems. Stability analysis for systems under the excitation of real noise and bounded noise is carried out by determining the moment Lyapunov exponents and Lyapunov exponents. Good agreement is obtained between analytical results and those obtained from Monte Carlo simulations. In the two degrees-of-freedom case, the effect of free stream turbulence on cylinder vibration and its stability is examined.

Acknowledgments

I like to take this opportunity to give my sincere appreciation to the people who have helped and supported me for my PhD research. First and foremost, I like to thank my supervisors Dr. Wei-Chau Xie and Dr. Ronald M.C. So for their unending encouragement, advice, and support. I also want to thank Dr. Stanislav Potapenko for his suggestions and cares for my research. I like to thank Dr. X.Q. Wang for his helpful comments and fruitful co-operation. I wish to express my thanks for the valuable discussions with Mr. Qinghua Huang.

In addition, I like to thank the Examinating Committee: Professor Isaac Ellishakoff, Professor Andrew Heunis, Professor Stanislav Potapenko, and Professor Mahesh Pandey.

Many thanks to my friends with whom I have shared the wonderful life in Waterloo for the past four years.

TO

My Family

Contents

List of Figures

CHAPTER 1

Introduction

Flow-induced structural vibration is experienced in numerous fields, including the aerospace industry, power generation or transmission (turbine blades, heat exchanger tubes, nuclear reactor components), civil engineering infrastructures (bridges, tall buildings, smoke stacks), and undersea technology (marine cables). Thus, flow-induced vibration problems are commonplace and their study has become an important area of research.

1.1 Flow-Induced Vibration of Circular Cylinders

Flow-induced vibration of cylinder arrays is an important issue to be considered in the design of heat exchangers since it may cause the failure of heat exchanger tube bundles. Several mechanisms may result in the failure, including vortex shedding resonance, fluidelastic instability and turbulence buffeting. Because of the resulting large vibration amplitudes of the structures, fluidelastic instability is an extremely destructive excitation mechanism. It is of great practical importance to avoid or to alleviate in any case. It has been demonstrated experimentally that the large galloping motions of an elastic cylinder in a cross-flow resulting from fluidelastic instability can be stabilized by additional grid-generated turbulence. Hence, stochastic stabilization of structural vibration has attracted the interest of many researchers.

1.1.1 Introduction of Excitation Mechanisms

For arrays of circular cylinders subject to cross-flow, which can be seen in Figure 1.1, possibilities exist for structural vibrations induced by the flowing fluid via one or more of the following mechanisms:

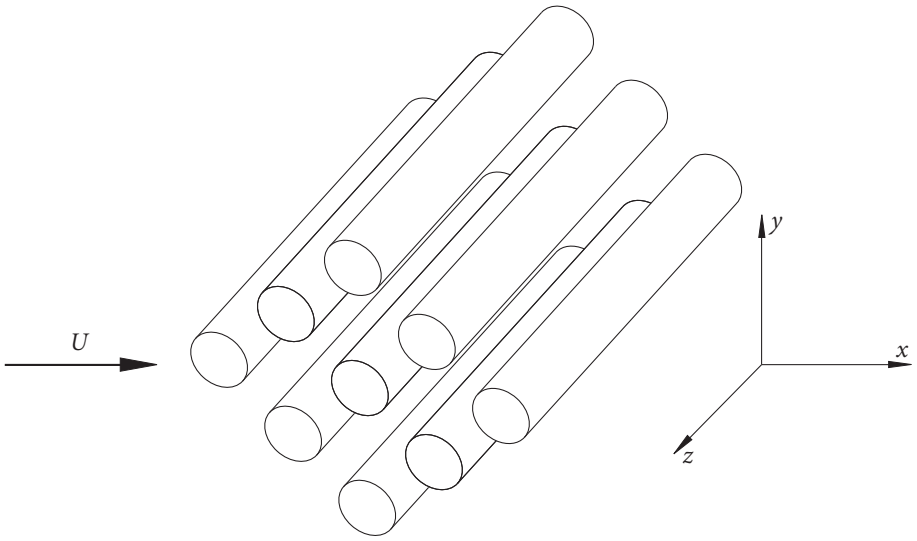

Figure 1.1 A group of cylinders in cross-flow

- **Turbulent Excitation**. In a cylinder array, there exist random noises, including turbulent pressure fluctuations and far-field flow noises. These randomly varying pressures on the surfaces of the cylinders generally produce relatively low-amplitude vibrations. Unlike vortex-induced vibration or fluidelastic instability, which can be eliminated or whose effects minimized by design, turbulence-induced vibration cannot be avoided in virtually all industrial applications. In industrial applications, flow channels are often designed to generate turbulence in order to improve the heat or mass transfer efficiencies or to suppress the vortex shedding or other instability phenomena. A very good review for turbulence-induced vibration can be found in Blevins [16].

- **Vortex-Induced Vibration**. These vibrations are induced by periodic vortex shedding from cylinders. The vortices exert a fluctuating excitation force on the cylinder. For one cylinder in cross-flow, the component of this force in the lift direction (perpendicular to the flow direction) has a frequency equal to vortex-shedding frequency f_s,

while that in the drag direction (direction of flow) has a frequency equal to $2f_s$. The vortex shedding frequency can be written as

$$f_s = \frac{SU}{D}, \tag{1.1.1}$$

where S is the Strouhal number, U is the free stream velocity, and D is the diameter of the cylinder.

In general, the force component in the drag direction is much smaller than the force component in the lift direction. When the cylinder is flexible with characteristic natural frequencies which are close to those of vortex shedding, a phenomenon called lock-in resonance may happen. When one of the structural modal frequencies is close to f_s or $2f_s$, the vortex-shedding frequency f_s (or $2f_s$) may actually shift from its value for a stationary cylinder to the nearest natural frequency of the cylinder, resulting in large amplitude, resonant vibration. Lock-in resonance can occur in either the lift or the drag direction. The resulting structural response will then change its form from forced vibration to resonant vibration, with larger vibration amplitudes. While vortex shedding initiates cylinder vibration, the vortex shedding process can be modified by cylinder motions and synchronized with cylinder vibrations. More details can be found in [15], [89], [93] and [74].

- **Fluidelastic Instability**. When a bundle of cylinders is subjected to cross-flow with increasing velocity, it will come to a point at which the responses of the cylinders suddenly and rapidly increase without bound, until cylinder-to-cylinder impacting or other non-linear effects limit the cylinder vibrations. This phenomena is known as fluidelastic instability. The velocity at which the vibration amplitudes of the cylinders suddenly increase is called the critical velocity. Unlike vortex shedding, the amplitudes of a fluidelastic unstable cylinder bundle will continue to increase even when the critical velocity is exceeded. The motions of the cylinders in the bundle become correlated and have definite phase relationship to one another. The dominant fluid forces are the motion-dependent fluid forces. Fluidelastic instability appears in two different mechanisms, i.e. *damping-controlled* (galloping), in which a negative non-conservative fluid damping force is generated when the fluid force has a component in-phase with the cylinder vibration velocity, and *stiffness-controlled*, which results

from the coupling effects of several cylinders in an array by the fluid. The subject of fluidelastic instability in an array of cylinders has been reviewed in detail by, for example, Price [66] and Weaver and Fitzpatrick [87].

These mechanisms, which are generally investigated separately, influence each other. Particularly the intensity of the turbulence can have a significant influence on the onset of instability. Figure 1.2 illustrates the experimental determination of the stability threshold for a cylinder within a bundle. Here, the amplitude $\hat{a}$ related to the cylinder diameter d is plotted as a function of the reduced gap velocity V_r (Figure 1.2a). To represent the stability behavior, the Connors diagram (Figure 1.2b) shows the stability boundaries as a function of mass-damping parameter $\delta_r = \mu\delta/(\rho d^2)$ and the reduced gap velocity $V_r = u/(f_1 d)$, where μ is the mass per unit length, δ is the logarithmic decrement of damping, ρ is the fluid density, u is the velocity in the gap between the cylinders, and f_1 is the fundamental natural frequency of the cylinder.

Mathematically, the equations of motion for cylinders in a cross-flow can be described by a general equation

$$(\mathbf{M}_s + \mathbf{M}_f)\ddot{\mathbf{q}} + (\mathbf{C}_s + \mathbf{C}_f)\dot{\mathbf{q}} + (\mathbf{K}_s + \mathbf{K}_f)\mathbf{q} = \mathbf{F}, \tag{1.1.2}$$

where $\mathbf{q}$, $\dot{\mathbf{q}}$, and $\ddot{\mathbf{q}}$ are the generalized structure displacement, velocity, and acceleration, respectively, and $\mathbf{F}$ represents excitation forces, such as vortex shedding and turbulence. Mass matrices include structural mass $\mathbf{M}_s$ and added mass $\mathbf{M}_f$, damping matrices include structural damping $\mathbf{C}_s$ and fluid damping $\mathbf{C}_f$, and stiffness matrices include structural stiffness $\mathbf{K}_s$ and fluid stiffness $\mathbf{K}_f$. Fluidelastic instability can be one of the fluid-damping-controlled instability (galloping), fluid-stiffness-controlled instability, and parametric resonances depending on the dominant terms in equation (1.1.2). Moreover, it is possible that a combination of three effects occurs. The coefficients in equation (1.1.2), such as $\mathbf{C}_f$ and $\mathbf{K}_f$, can be random due to the influence of turbulence. For more details, see Weaver *et al.* [88].

1.1.2 Mathematical Models for Vortex Shedding

Much effort has been made to investigate the underlying mechanism of the fluid-structure interaction resulting from vortex-induced cylinder vibration. The investigations include experimental, numerical, empirical and theoretical studies. In the latest review by Gabbai and Benaroya [30], the mathematical models for vortex shedding are classified into four groups:

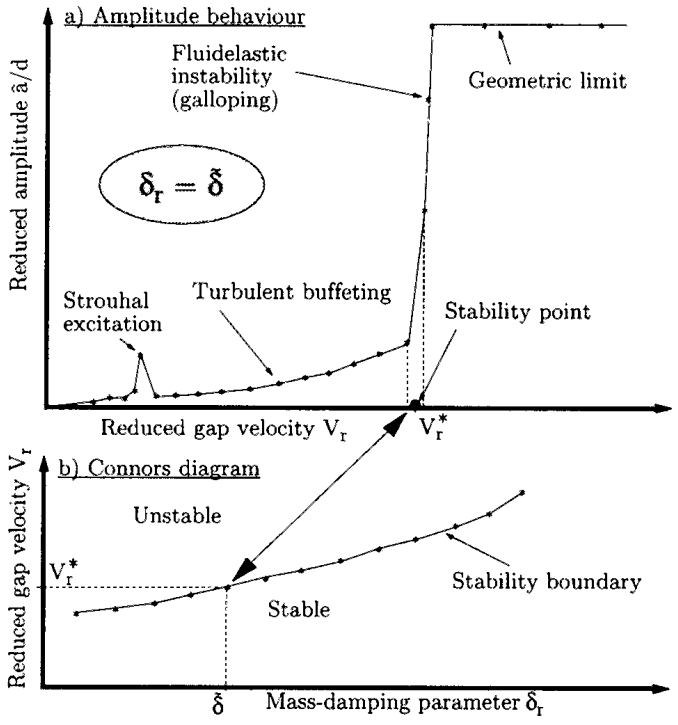

Figure 1.2 Experimental determination of the stability boundary of a flexible tube in a bundle subjected to cross-flow, a) amplitude behaviour, b) Connors diagram (Popp and Romberg [64])

wake oscillator model, single degree-of-freedom model, force decomposition model, and other approaches. A similar classification can be found in Wang *et al.* [85]. For the present study, a force decomposition model [85] is used for modeling the vortex-induced vibration.

Sarpkaya [72] introduced the concept of force decomposition and used it to analyze vortex-induced vibration of an elastically supported rigid cylinder. The fluid force was decomposed into two components, a fluid inertia force and a fluid damping force related to the cylinder displacement and velocity, respectively. Griffin and Koopmann [33] and Griffin [34] divided the fluid force into an excitation part and a reaction part, the latter included all motion-dependent fluid forces. Chen *et al.* [23] presented an unsteady flow theory to model vortex-induced vibration of a cylinder in cross-flow. The fluid force was assumed to be dependent on the displacement, velocity, and acceleration of the cylinder. The force was expressed as a linear combination of the motion-dependent components. In all these models, data measured from experiments was used to determine the fluid force

coefficients and they were shown to be dependent on the reduced velocity $U_r = UD/f$ and Y (dimensionless displacement in the lift direction). When the model was used to predict X and Y, Sarpkaya [72] suggested an iteration technique, thus allowing the fluid-structure interaction effects to be accounted for, at least partially. In Wang *et al.* [85], the models were classified into two groups under (1) wake oscillator models, and (2) force decomposition models. The single degree-of-freedom models reviewed in Gabbai and Benaroya [30] were considered as simplified wake oscillator models. The nonlinear fluid force model proposed by Wang *et al.* [85] can also be regarded as a simplified wake oscillator model rather than a force decomposition model, where a novel model of fluid-structure interaction was proposed. Interestingly, the analytical expression of this model, which can be obtained only when a linear approximation of the fluid-structure interaction is invoked, appears similar to the force decomposition model proposed by Sarpkaya [72]. This suggests that wake oscillator models and force decomposition models are essentially equivalent.

For a stationary cylinder in cross-flow, vortex-induced forces are assumed to be sinusoidal at the vortex shedding frequency f_s and at $2f_s$ in the drag and lift directions, respectively. Hence, they can be expressed as

$$\begin{aligned} c_D(t) &= \frac{1}{2}\rho U^2 D C_D + \frac{1}{2}\rho U^2 D C'_D \sin(\Omega_D t + \phi_D), \\ c_L(t) &= \frac{1}{2}\rho U^2 D C_L + \frac{1}{2}\rho U^2 D C'_L \sin(\Omega_L t + \phi_L), \end{aligned} \tag{1.1.3}$$

where C_D (C_L) is the steady drag (lift) coefficient, C'_D (C'_L) is the fluctuating flow excitation in the drag (lift) direction, ϕ_D (ϕ_L) is the corresponding phase angle with respect to a particular fluid-force component.

When the cylinder is vibrating, the fluid-structure interaction is taken into account by following the approach proposed by Wang *et al.* [85]. The basic idea is that the velocity of cylinder vibration changes the angle at which the incoming flow attacks the cylinder, as seen in Figure 1.3, thus the fluid forces applied to the cylinder are expressed as

$$\begin{aligned} c^X(t) &= c_D(t) \cdot \cos\theta + c_L(t) \cdot \sin\theta, \\ c^Y(t) &= c_L(t) \cdot \cos\theta - c_D(t) \cdot \sin\theta, \end{aligned} \tag{1.1.4}$$

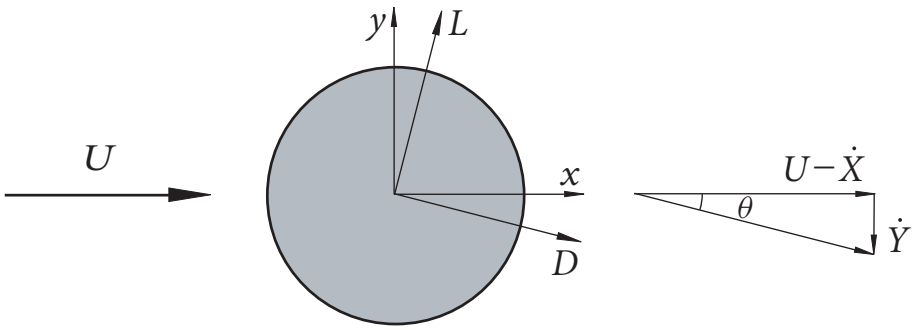

Figure 1.3 Drag and lift force components acting on a cylinder

where θ is the angle between the x-axis and the instantaneous velocity vector of the cylinder motion and is given by

$$\theta = \tan^{-1}\left\{\frac{\dot{Y}(t)}{U - \dot{X}(t)}\right\}.$$

Since the cylinder vibrations will change the flow field and the fluid forces applied on the cylinder, an iteration process can be used to determine the vortex-induced forces applied on the cylinder. More details can be found in Reference [85].

1.1.3 Theoretical Models for Fluidelastic Instability

Several theoretical models for fluidelastic instability are briefly introduced here [88].

Quasi-Static Flow Theory

Only fluid-stiffness forces are considered. At any instant in time, the flow-induced forces of vibrating cylinders in a cross-flow are considered to be the same as those of the corresponding stationary cylinders with the same configuration. The fluid forces depend on the change from a reference of steady state, i.e., the fluid forces on a cylinder depend only on its displacements relative to other displacements of other cylinders, but not the velocities and accelerations of other cylinders. In this case, the fluid forces are determined uniquely by the cylinder array configuration only. However, these models are not applicable for fluid-damping-controlled instability. This is the approach used by Connors [25] and Blevins [15].

The change in steady fluid force per unit length on the jth cylinder in the x- and y-directions (F_x^j, F_y^j) can be written as a function of the jth cylinder displacements (x_j, y_j)

relative to the displacements of the neighboring $(j+1)$th and $(j-1)$th cylinders:

$$\begin{aligned} F_x^j &= \rho U^2 g_x(x_{j+1}-x_j, x_j-x_{j-1}, y_{j+1}-y_j, y_j-y_{j-1})/4, \\ F_y^j &= \rho U^2 g_y(x_{j+1}-x_j, x_j-x_{j-1}, y_{j+1}-y_j, y_j-y_{j-1})/4, \end{aligned} \tag{1.1.5}$$

where ρ is fluid density and U is the flow velocity. The functions g_x and g_y have units of 1/length and express the change of fluid forces on a cylinder due to its relative motion to adjacent cylinders. The analytical expressions for g_x and g_y can be determined based on potential flow theory (see, e.g., Païdoussis *et al.* [58]) or measured experimentally (see, e.g., Connors [25]).

Quasi-Steady Flow Theory

In the quasi-steady theory, both fluid-damping and fluid-stiffness forces are included. At any instant in time, the flow-induced forces of vibrating cylinders in a cross-flow are considered to be the same as those cylinders moving with constant velocities equal to the actual instantaneous values. The fluid forces depend on the configuration of cylinders and are proportional to the motion. This is reflected by the changes of amplitude and phase of the fluid force with respect to cylinder motion. The fluid-stiffness force coefficients are constant and the fluid-damping force coefficients are a function of the reduced flow velocity. This approach has been used by Price and Païdoussis [65] and Granger and Païdoussis [32]. The fluid forces can be written as

$$\begin{aligned} F_j^X &= \frac{1}{2}\rho U^2 LD\Big[C_D\Big(1-\frac{2D}{Ua}\dot{X}_j\Big)+C_L\frac{D}{Ua}\dot{Y}_j\Big], \\ F_j^Y &= \frac{1}{2}\rho U^2 LD\Big[C_L\Big(1-\frac{2D}{Ua}\dot{X}_j\Big)+C_D\frac{D}{Ua}\dot{Y}_j\Big], \end{aligned} \tag{1.1.6}$$

where C_L and C_D are the lift and drag coefficients, respectively, X_j and Y_j are the non-dimensional form of the cylinder motions, i.e.,

$$X_j=\frac{x_j}{D}, \qquad Y_j=\frac{y_j}{D}, \qquad a=\frac{T}{T-\frac{1}{2}D}.$$

Unsteady Flow Theory

The unsteady fluid forces acting on a cylinder are considered to be the same as those acting on a cylinder which is undergoing periodic movements. The flow-induced forces are a linear combination of the displacements, velocities, and accelerations of cylinders. This approach

was used by Tanaka and Takahara [83], Lever and Weaver [43], and Chen [24]. The fluid forces applied on the jth cylinder can be written as

$$\begin{aligned} f_j^X &= -\sum_{k=1}^{n}\left\{\left[\bar{\alpha}_{jk}\frac{\partial^2 X_k}{\partial t^2}+\bar{\alpha}'_{jk}\frac{\partial X_k}{\partial t}+\bar{\alpha}''_{jk}X_k\right]+\left[\bar{\sigma}_{jk}\frac{\partial^2 Y_k}{\partial t^2}+\bar{\sigma}'_{jk}\frac{\partial Y_k}{\partial t}+\bar{\sigma}''_{jk}Y_k\right]\right\}, \\ f_j^Y &= -\sum_{k=1}^{n}\left\{\left[\bar{\tau}_{jk}\frac{\partial^2 X_k}{\partial t^2}+\bar{\tau}'_{jk}\frac{\partial X_k}{\partial t}+\bar{\tau}''_{jk}X_k\right]+\left[\bar{\beta}_{jk}\frac{\partial^2 Y_k}{\partial t^2}+\bar{\beta}'_{jk}\frac{\partial Y_k}{\partial t}+\bar{\beta}''_{jk}Y_k\right]\right\}. \end{aligned} \tag{1.1.7}$$

Experimental results have shown that the fluid-damping and fluid-stiffness coefficients are functions of the reduced flow velocity [82]. Using the following dimensionless force coefficients

$$\begin{aligned} &\bar{\alpha}_{jk}=\tfrac{1}{4}\rho\pi D^2\alpha_{jk}, && \bar{\alpha}'_{jk}=-\frac{\rho U^2}{\omega}\alpha'_{jk}, && \bar{\alpha}''_{jk}=-\rho U^2\alpha''_{jk}, \\ &\bar{\sigma}_{jk}=\tfrac{1}{4}\rho\pi D^2\sigma_{jk}, && \bar{\sigma}'_{jk}=-\frac{\rho U^2}{\omega}\sigma'_{jk}, && \bar{\sigma}''_{jk}=-\rho U^2\sigma''_{jk}, \\ &\bar{\tau}_{jk}=\rho\pi R^2\tau_{jk}, && \bar{\tau}'_{jk}=-\frac{\rho U^2}{\omega}\tau'_{jk}, && \bar{\tau}''_{jk}=-\rho U^2\tau''_{jk}, \\ &\bar{\beta}_{jk}=\rho\pi R^2\beta_{jk}, && \bar{\beta}'_{jk}=-\frac{\rho U^2}{\omega}\beta'_{jk}, && \bar{\beta}''_{jk}=-\rho U^2\beta''_{jk}, \end{aligned}$$

equations (1.1.7) can be written as

$$\begin{aligned} f_j^X =& -\tfrac{1}{4}\rho\pi D^2\sum_{k=1}^{n}\left(\alpha_{jk}\frac{\partial^2 X_k}{\partial t^2}+\sigma_{jk}\frac{\partial^2 Y_k}{\partial t^2}\right)+\frac{\rho U^2}{\omega}\sum_{k=1}^{n}\left(\alpha'_{jk}\frac{\partial X_k}{\partial t}+\sigma'_{jk}\frac{\partial Y_k}{\partial t}\right) \\ &+\rho U^2\sum_{k=1}^{n}\left(\alpha''_{jk}X_k+\sigma''_{jk}Y_k\right), \\ f_j^Y =& -\tfrac{1}{4}\rho\pi D^2\sum_{k=1}^{n}\left(\tau_{jk}\frac{\partial^2 X_k}{\partial t^2}+\beta_{jk}\frac{\partial^2 Y_k}{\partial t^2}\right)+\frac{\rho U^2}{\omega}\sum_{k=1}^{n}\left(\tau'_{jk}\frac{\partial X_k}{\partial t}+\beta'_{jk}\frac{\partial Y_k}{\partial t}\right) \\ &+\rho U^2\sum_{k=1}^{n}\left(\tau''_{jk}X_k+\beta''_{jk}Y_k\right), \end{aligned} \tag{1.1.8}$$

where ρ is fluid density, D is the cylinder diameter, t is time, ω is the circular frequency of cylinder vibrations, α_{jk}, σ_{jk}, τ_{jk}, and β_{jk} are added mass coefficients, α'_{jk}, σ'_{jk}, τ'_{jk}, and β'_{jk} are fluid damping coefficients, and α''_{jk}, σ''_{jk}, τ''_{jk}, β''_{jk} are fluid stiffness coefficients.

The various coefficients in equation (1.1.8) generally depend on structural displacement, velocity, acceleration, and flow velocity. Fluid force coefficients can be determined by

measuring the fluid forces acting on the cylinders due to vibrations of a particular cylinder ([23] and [22]).

The added-mass coefficients α_{jk} and τ_{jk} can be calculated from the potential flow theory [24]; they can also be measured from the excitation of the cylinder in stationary fluid. The added damping and stiffness coefficients can be obtained experimentally or numerically.

Motion-dependent fluid force coefficients are traditionally obtained analytically or experimentally. However, they can also be calculated using a computational fluid dynamics (CFD) method, based on the unsteady flow theory [90]. The CFD calculation procedure follows the steps in the experimental method [105]. The CFD results agree qualitatively with experimental data. This method is cost-effective and has more flexibility.

From the measured data, some general characteristics of motion-dependent force coefficients are observed as follows.

- **High Reduced Flow Velocity**. When the reduced flow velocity U_r is high, e.g., $U_r > 20$ and sometimes even $U_r > 10$, all motion-dependent force coefficients are approximately independent of reduced flow velocity. This shows that when the flow velocity is high relative to cylinder velocity, the fluid forces resulting from the cylinder motion can be measured at a specific velocity and the measured data can be applied to other flow velocities.

- **Reynolds Number**. At low reduced flow velocities, motion-dependent force coefficients depend on the reduced flow velocity, Reynolds number, and excitation amplitude. The peak values decrease with the flow velocity and are shifted toward larger U_r. Similar characteristics have been observed for a single cylinder in a cross-flow [23]. At lower reduced flow velocities, motion-dependent force coefficients are much more complicated. In general, motion-dependent force coefficients are highly nonlinear and extensive experiments have to be done to measure them.

More details about the theoretical models for fluidelastic instability can be found in the comprehensive review paper by Price [66]. Despite significant differences among the theoretical models, the general conclusions obtained from the various models agree to some extent. Price showed that the most important factor for predicting fluidelastic instability

in cylinder arrays was the unsteady nature of the flow, specifically the phase lag between cylinder motion and the flow-induced forces.

1.1.4 Turbulence Buffeting Force

To take the turbulence buffeting force into account, the model of Pettigrew and Gorman [9] is used. Based on experimental measurements, the power spectral density of the random, homogeneous field of turbulence per unit cylinder length, G_F, is assumed to be proportional to the square of the flow dynamic head expressed in terms of the pitch velocity, $U_P = UT/(T-D)$, i.e.

$$G_F = \left[\tfrac{1}{2} C_r(f) \rho D U_P^2\right]^2, \tag{1.1.9}$$

where ρ is the fluid density, D is the cylinder diameter, and T is the cylinder pitch. The random lift coefficient, $C_r(f)$, defines the shape of the turbulence spectrum. The random lift coefficient is a function of the frequency, and also depends on the position of the cylinder. An approximation to the random lift coefficient is given by

$$\begin{cases} C_r = 0.025, & 0 < f < 40\,\text{Hz}, \\ C_r = 0.108 \times 10^{-0.0159 f}, & f \geqslant 40\,\text{Hz}. \end{cases}$$

The general shapes of the power spectral density curves for drag and lift forces are qualitatively the same [24]. Equation (1.1.9) may be used, via inverse Fourier transformation, to generate the turbulence excitation force on the jth cylinder

$$\begin{aligned} f_{Tj}^X(t) &= \Big(\int_0^{+\infty} G_F \cdot \mathrm{e}^{2\pi f t}\mathrm{d}f\Big)^{\frac{1}{2}} = \tfrac{1}{2}\rho D U_P^2 \Big(\int_0^{+\infty} C_r^2 \cdot \mathrm{e}^{2\pi f t}\mathrm{d}f\Big)^{\frac{1}{2}} = \tfrac{1}{2}\rho D U_P^2 C_{Tj}, \\ f_{Tj}^Y(t) &= \Big(\int_0^{+\infty} G_F \cdot \mathrm{e}^{2\pi f t}\mathrm{d}f\Big)^{\frac{1}{2}} = \tfrac{1}{2}\rho D U_P^2 \Big(\int_0^{+\infty} C_r^2 \cdot \mathrm{e}^{2\pi f t}\mathrm{d}f\Big)^{\frac{1}{2}} = \tfrac{1}{2}\rho D U_P^2 C_{Tj}, \end{aligned} \tag{1.1.10}$$

where

$$C_{Tj} = \Big(\int_0^{+\infty} C_r^2 \cdot \mathrm{e}^{2\pi f t}\mathrm{d}f\Big)^{\frac{1}{2}}.$$

Otherwise, the turbulence buffeting force can also be modeled as a Gaussian colored noise [67].

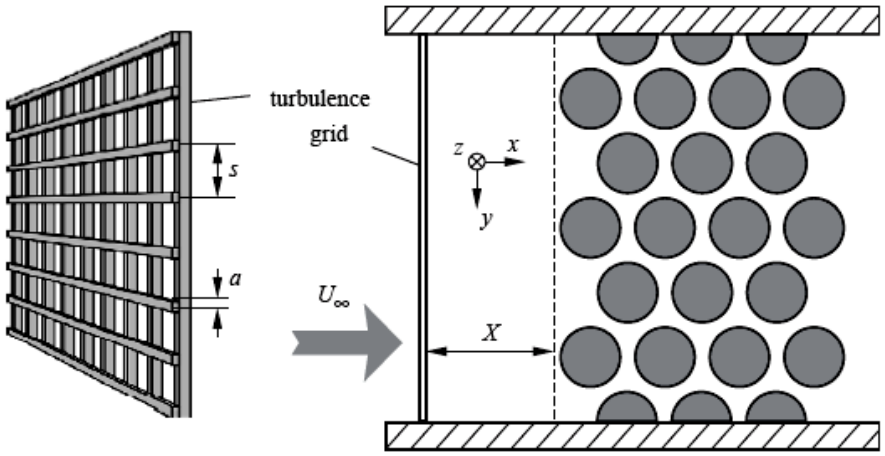

Figure 1.4 Experimental set-up for increasing the turbulence at the inlet of the tube bundle (Rottmann and Popp [69])

1.1.5 Stochastic Influences on Flow-Induced Vibration

Popp and Romberg [64] presented some interesting stability results from carefully carried out experiments on flow-induced vibrations of a flexibly mounted cylinder in an otherwise fixed cylinder array. The experiment set-up is shown in Figure 1.4. They considered both fluidelastic instability and turbulent buffeting, and showed that large galloping motion can be stabilized by grid-generated turbulence, as seen in Figures 1.5 and 1.6. In one of their experiments, Popp and Romberg [64] considered a cylinder with a very small structural damping. The damping measured in the flow direction is high, and the cylinder undergoes a galloping motion in the cross-flow (lift) direction at certain reduced velocity $V_{r,\mathrm{cr}}$. Naturally, turbulence occurs in cylinder bundles during cross-flow due to upstream cylinder bundles acting as turbulence generators. Additional turbulence was generated in this experiment by placing a turbulence grid in front of the cylinder at a distinct distance. It was observed that as the turbulence was increased in the flow, a significant stabilization took place and the galloping instability did not occur for reduced velocity values substantially higher than $V_{r,\mathrm{cr}}$.

The stabilizing effect of turbulence has also been reported in the literature for bridge structures under turbulent winds (e.g., Bucher and Lin [19]). An intuitive explanation has been given which says that turbulence may help to feed energy from the least stable mode

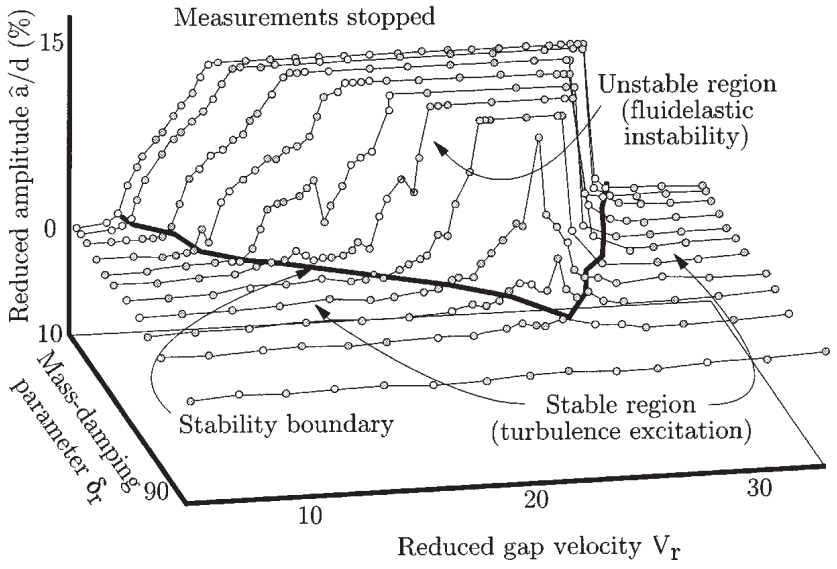

Figure 1.5 Measured reduced amplitudes as a function of V_r and δ_r for one single flexibly mounted tube in the third row of an otherwise fixed array with ideal geometry (Popp and Romberg [64])

to the more stable modes. Therefore, coupled modes have to be considered in the stability analysis. In the study of stochastic dynamical systems, stabilizing a system by noise is an important topic (e.g., Arnold *et al.* [3] and Arnold [8]). For linear systems it is found that stabilization by white noise is possible if and only if the trace of the system matrix, i.e. the sum of the eigenvalues, is negative. Pandey and Ariaratnam [59] analyzed the stability of wind-induced torsional motion of slender bridges under stochastic wind turbulence. They used a periodic excitation with random phase modulation to model the turbulence in wind velocity. They found that the turbulence had small stabilizing effect on the bridge stability, although an increase in the bandwidth of the excitation process tends to stabilize the bridge motion.

Rzentkowski and Lever [71] used a nonlinear model to study the turbulence effect on fluidelastic instability in tube arrays and found that turbulence either reduced or had negligible effect on the stability boundary depending on the vibration pattern. Poirel and Price [62] also found that turbulence could lower the speed of flutter speed of a two-dimensional airfoil. They used the Dryden model to represent the longitudinal turbulence. The stability boundary is determined by obtaining the largest Lyapunov exponent via

Monte Carlo simulation. Namachchivaya and Vedula [55] theoretically proved that a four-dimensional system could be stabilized by a real noise. They used a second order filter to model the noise and examined the moment stability and sample stability of the system by obtaining the moment Lyapunov exponent and Lyapunov exponent. However, they did not validate the analytical results by comparing with numerical results obtained by Monte Carlo simulation. The noise is very narrow-banded, which seems to be unrealistic for practical turbulence. For more information, Ibrahim [36] gave a detailed review about the noise effects, such as stabilization by multiplicative noise and noise-enhanced stability (NES), noise-induced transition, and stochastic resonance, on the stability of dynamical systems.

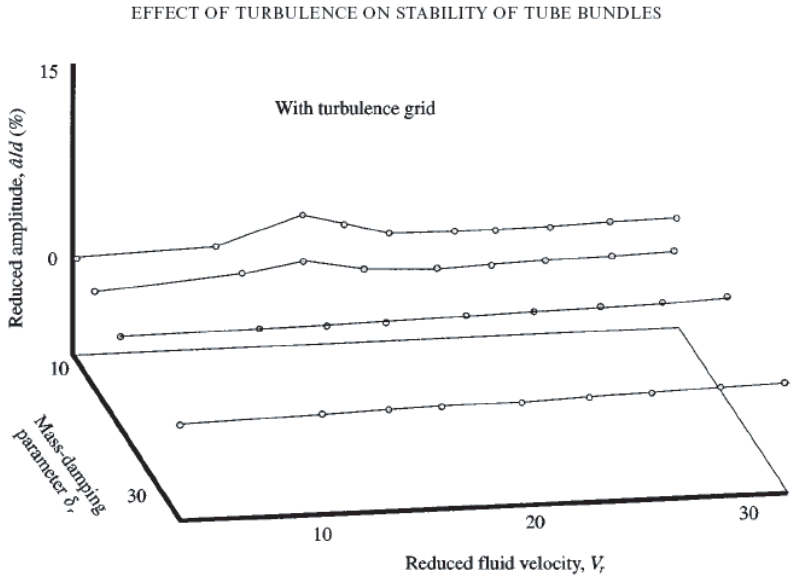

Figure 1.6 Measured reduced amplitudes as a function of V_r and δ_r for one single flexibly mounted tube in the third row of an otherwise fixed array with increased turbulence (Popp and Romberg [64])

Corless and Parkinson ([26] and [27]) used a combined mathematical model to study the interactions of vortex-induced vibration and galloping of a cylinder of square cross-section in cross-flow. The Hartlen-Currie model and the quasi-steady model of Parkinson and Smith were used for vortex-induced vibration and galloping, respectively. The resulting nonlinear equations were solved by the method of multiple scales. Rzentkowski and Lever [71] studied the effect of turbulence on fluidelastic instability in tube bundles. A

simplified, nonlinear model was applied to model the fluidelastic forces for a single flexible tube surrounded by rigid neighbors and constrained to move transverse to the mean flow. The turbulence excitation was expressed as a flat power spectral density function. Rüdinger and Krenk [70] used a nonlinear stochastic single degree-of-freedom system to model the vortex-induced vibration of a structural element. Across-wind turbulence and along-wind turbulence are assumed to be white noise processes and incorporated into the equation of motion as an additive excitation and a parametric excitation term, respectively.

1.2 General Introduction of Stochastic Stability

1.2.1 Stochastic Differential Equations

Many physical processes can be approximated as a Markov process. The simplest example for a Markov process is perhaps the Wiener process or Brownian motion process. The Wiener process can be used as a building block in the stochastic modeling of physical phenomena in science and engineering.

Wiener Process

A Wiener process, denoted as $W(t)$, is defined by

1. $W(t)$ is a Gaussian process;

2. $W(t)$ has mean zero, i.e. $\mathrm{E}\big[W(t)\big]=0$;

3. $\mathrm{E}\big[W(t)W(s)\big]=R(t,s)=\sigma^2\min(t,s)=\begin{cases}\sigma^2 t, & \text{if } t<s,\\ \sigma^2 s, & \text{if } t>s.\end{cases}$

If $\sigma=1$, $W(t)=\sigma\tilde{W}(t)$ and $\mathrm{E}\big[\big|\mathrm{d}\tilde{W}(t)\big|^2\big]=\mathrm{d}t$. $\tilde{W}(t)$ is called the *unit* or *standard* Wiener process.

Itô's Stochastic Differential Equations

An arbitrary scalar Markov diffusion process can be generated from the stochastic differential equation

$$\mathrm{d}X(t)=m(X,t)\,\mathrm{d}t+\sigma(X,t)\,\mathrm{d}W(t),\quad 0\leqslant t\leqslant T, \tag{1.2.1a}$$

or the equivalent integral equation

$$X(t) = x_0 + \int_0^t m(X,t)\,\mathrm{d}t + \int_0^t \sigma(X,t)\,\mathrm{d}W(t), \tag{1.2.1b}$$

if $m(X,t)$ and $\sigma(X,t)$ satisfy the Lipschitz and linear growth conditions in X, i.e., there exists a constant $C>0$ such that the following inequalities hold for all $0 \leqslant t \leqslant T$ and $X, Y \in \mathcal{R}$:

$$\begin{aligned} &\big|m(X,t) - m(Y,t)\big| \leqslant C\big|X - Y\big|, \quad \big|\sigma(X,t) - \sigma(Y,t)\big| \leqslant C\big|X - Y\big|, \\ &\big|m(X,t)\big|^2 \leqslant C\big(1 + |X|^2\big), \qquad \big|\sigma(X,t)\big|^2 \leqslant C\big(1 + |X|^2\big), \end{aligned}$$

and $m(X,t)$ and $\sigma(X,t)$ are continuous functions. $a = m(X,t)$ and $b = \sigma^2(X,t)$ are called the drift and diffusion coefficients, respectively.

The transition probability density $q\big(\xi, t \,\big|\, \xi_0, t_0\big)$ of $X(t)$ satisfies the equations:

$$\begin{aligned} &\Big(\frac{\partial}{\partial t_0} + \mathscr{L}_{\xi_0}\Big) q(\xi, t \,|\, \xi_0, t_0) = 0, \quad \text{Backward Kolmogorov equation,} \\ &\Big(-\frac{\partial}{\partial t} + \mathscr{L}_{\xi}^{*}\Big) q(\xi, t \,|\, \xi_0, t_0) = 0, \quad \begin{array}{l}\text{Forward Kolmogorov equation} \\ \text{or Fokker-Planck equation,}\end{array} \end{aligned} \tag{1.2.2}$$

where

$$\begin{aligned} \mathscr{L}_{\xi_0}(\cdot) &= m(\xi_0, t_0)\frac{\partial(\cdot)}{\partial \xi_0} + \frac{1}{2}\sigma^2(\xi_0, t_0)\frac{\partial^2(\cdot)}{\partial \xi_0^2}, \\ \mathscr{L}_{\xi}^{*}(\cdot) &= -\frac{\partial}{\partial \xi}\big[m(\xi,t)(\cdot)\big] + \frac{1}{2}\frac{\partial^2}{\partial \xi^2}\big[\sigma^2(\xi,t)(\cdot)\big]. \end{aligned}$$

Equation (1.2.1) can be extended to the vector case. More details about the stochastic differential equations can be found in [76] and [39].

Ornstein-Uhlenbeck Process

An Ornstein-Uhlenbeck process $X(t)$ is defined by the one-dimensional Itô stochastic differential equation

$$\mathrm{d}X(t) = -\alpha\, X(t)\,\mathrm{d}t + \sigma\,\mathrm{d}W(t), \quad X(t_0) = X_0. \tag{1.2.3}$$

For the given initial condition $X(t_0) = X_0$ at time t_0, the transition probability denoted as $q(X, t \,|\, X_0, t_0)$ is the solution of the forward Kolmogorov equation or the Fokker-Planck

equation (1.2.2), i.e. for the initial condition t_0 and X_0 fixed,

$$\begin{aligned} &\left[\frac{\partial}{\partial t} - \frac{\sigma^2}{2}\frac{\partial^2}{\partial X^2} + \frac{\partial}{\partial X}(-\alpha X)\right] q(X,t \mid X_0,t_0) = 0, \qquad t > t_0, \\ &q(X,t_0 \mid X_0,t_0) = \lim_{t\downarrow t_0} q(X,t \mid X_0,t_0) = \delta(X - X_0). \end{aligned} \tag{1.2.4}$$

Applying the Fourier transformation

$$\varphi(k,t \mid X_0,t_0) = \int_{-\infty}^{\infty} \mathrm{e}^{-\mathrm{i}kX} q(X,t \mid X_0,t_0)\,\mathrm{d}X.$$

to equation (1.2.4) leads to

$$\frac{\partial \varphi}{\partial t} + \alpha k \frac{\partial \varphi}{\partial k} = -\frac{\sigma^2 k^2}{2}\varphi, \qquad \varphi(k,t_0 \mid X_0,t_0) = \mathrm{e}^{-\mathrm{i}kX_0}. \tag{1.2.5}$$

Equation (1.2.5) can be solved using the method of characteristics to give

$$\varphi(k,t \mid X_0,t_0) = \exp\left\{-\mathrm{i}kX_0\mathrm{e}^{-\alpha(t-t_0)} + \frac{\sigma^2}{4\alpha}k^2\left[\mathrm{e}^{-2\alpha(t-t_0)} - 1\right]\right\}. \tag{1.2.6}$$

Applying the inverse Fourier transformation

$$q(X,t \mid X_0,t_0) = \frac{1}{2\pi}\int_{-\infty}^{\infty} \mathrm{e}^{\mathrm{i}kX}\varphi(k,t \mid X_0,t_0)\,\mathrm{d}k,$$

to equation (1.2.6) leads to

$$q(X,t \mid X_0,t_0) = \frac{1}{\sqrt{2\pi}\,\sigma_{X(t)}}\exp\left\{-\frac{\left[X - \mu_{X(t)}\right]^2}{2\,\sigma_{X(t)}^2}\right\}, \tag{1.2.7}$$

with $\mu_{X(t)}$ and $\sigma_{X(t)}$ given by

$$\mu_{X(t)} = X_0\,\mathrm{e}^{-\alpha(t-t_0)}, \qquad \sigma_{X(t)}^2 = \frac{\sigma^2\left[1 - \mathrm{e}^{-2\alpha(t-t_0)}\right]}{2\alpha}. \tag{1.2.8}$$

Equation (1.2.7) implies that $X(t)$, for given $X_0 = X(t_0)$, is normally distributed with mean $\mu_{X(t)}$ and standard deviation $\sigma_{X(t)}$.

For arbitrary initial condition X_0,

$$\mathrm{E}\left[X(t)\right] \to 0, \quad \mathrm{Var}\left[X(t)\right] \to \frac{\sigma^2}{2\alpha}, \quad \text{as } t \to \infty,$$

i.e. the distribution of $X(t)$ approaches $N\left(0, \sigma^2/(2\alpha)\right)$ as $t \to \infty$.

If the initial condition X_0 is normal with mean 0 and variance $\sigma^2/(2\alpha)$, i.e. $X_0 \sim N\big(0, \sigma^2/(2\alpha)\big)$, then $X(t)$ is a stationary Gaussian process with mean zero, $\mathrm{E}\big[X(t)\big]=0$, and the correlation function is

$$R(\tau) = \mathrm{E}\big[X(t)\,X(t+\tau)\big] = \frac{\sigma^2}{2\alpha}\,\mathrm{e}^{-\alpha|\tau|}. \tag{1.2.9}$$

The power spectral density function is given by

$$\begin{aligned} S(\omega) &= \int_{-\infty}^{+\infty} R(\tau)\,\mathrm{e}^{-\mathrm{i}\omega\tau}\mathrm{d}\tau = \frac{\sigma^2}{2\alpha}\int_{-\infty}^{+\infty} \mathrm{e}^{-\alpha|\tau|}\,\mathrm{e}^{-\mathrm{i}\omega\tau}\mathrm{d}\tau \\ &= \frac{\sigma^2}{\alpha^2+\omega^2} = \frac{\sigma^2}{\alpha^2}\frac{1}{1+\left(\dfrac{\omega}{\alpha}\right)^2}. \end{aligned} \tag{1.2.10}$$

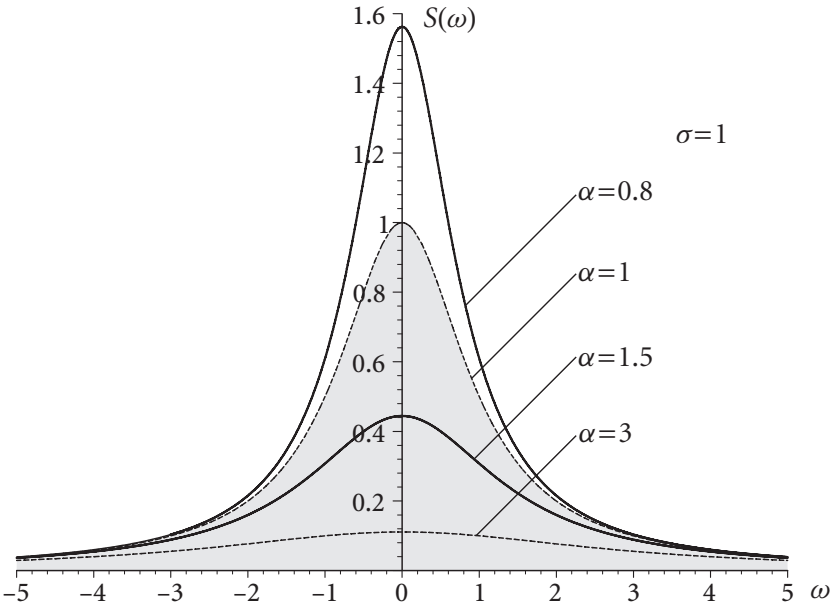

Figure 1.7 Power spectral density function of an Ornstein-Uhlenbeck process.

From equation (1.2.10), it is seen that the parameter α characterizes the bandwidth of the process and $(\sigma/\alpha)^2$ is proportional to the spectral density of the process. Typical plots of the power spectral density $S(\omega)$ are shown in Figure 1.7 for $\sigma=1$ and various values of α. When α is increased, $S(\omega)$ becomes flat in a wide frequency range. For the special case when $\sigma=\alpha\sqrt{S_0}\to\infty$, the Ornstein-Uhlenbeck process $X(t)$ approaches Gaussian white noise process with constant spectral density $S(\omega)=S_0$, i.e. the Ornstein-Uhlenbeck process

$X(t)=\sqrt{S_0}\,\xi(t)$, where $\xi(t)$ is a unit Gaussian white noise process. In summary, Ornstein-Uhlenbeck process is a simple, Gaussian, explicitly representable stationary process that is often used to model a realizable noise process. As a result, it is also called a real noise process. Ornstein-Uhlenbeck process is widely used in the engineering applications (see, e.g., Moshchuk *et al.* [50]).

Bounded Noise Process

Since an Ornstein-Uhlenbeck process defined by equation (1.2.3) is a normally distributed random variable, it is not bounded and may take arbitrarily large values with small probabilities. As a result, it may not be a realistic model of noise in many engineering applications. To overcome this problem, a bounded noise process defined as follows is often used to model noise

$$\zeta(t) = \cos\big[\nu t + \sigma W(t) + \theta\big], \tag{1.2.11}$$

in which θ is a uniformly distributed random number in $(0,\ 2\pi)$ and is independent of $W(t)$. The inclusion of the phase angle θ in equation (1.2.11) makes $\zeta(t)$ a stationary process. Equation (1.2.11) can be written as

$$\begin{cases} \zeta(t) = \cos\eta(t), \\ \mathrm{d}\eta(t) = \nu\,\mathrm{d}t + \sigma\,\mathrm{d}W(t), \end{cases} \tag{1.2.12}$$

where the initial condition of $\eta(t)$ is $\eta(0)=\theta$. The correlation function of $\zeta(t)$ is given by

$$R(\tau) = \mathrm{E}\big[\zeta(t)\zeta(t+\tau)\big] = \frac{1}{2}\cos\nu\tau\ \exp\left(-\frac{\sigma^2}{2}\,|\tau|\right). \tag{1.2.13}$$

The spectral density function of $\zeta(t)$ is

$$S(\omega) = \frac{\sigma^2\left(\omega^2+\nu^2+\frac{1}{4}\sigma^4\right)}{2\left[(\omega-\nu)^2+\frac{1}{4}\sigma^4\right]\left[(\omega+\nu)^2+\frac{1}{4}\sigma^4\right]}. \tag{1.2.14}$$

It may be noted that the mean-square value of the bounded noise process $\zeta(t)$ is fixed at

$$\mathrm{E}\big[\zeta^2(t)\big] = R(0) = \frac{1}{2}.$$

Typical plots of the power spectral density function $S(\omega)$ are shown in Figure 1.8 for various values of the parameters σ and ν. The spectral density function can be used to approximate the well-known Dryden and von Karman spectra of wind turbulence by adjusting the values of the parameters ν and σ. In a recent paper, Wang *et al.* [86] applied

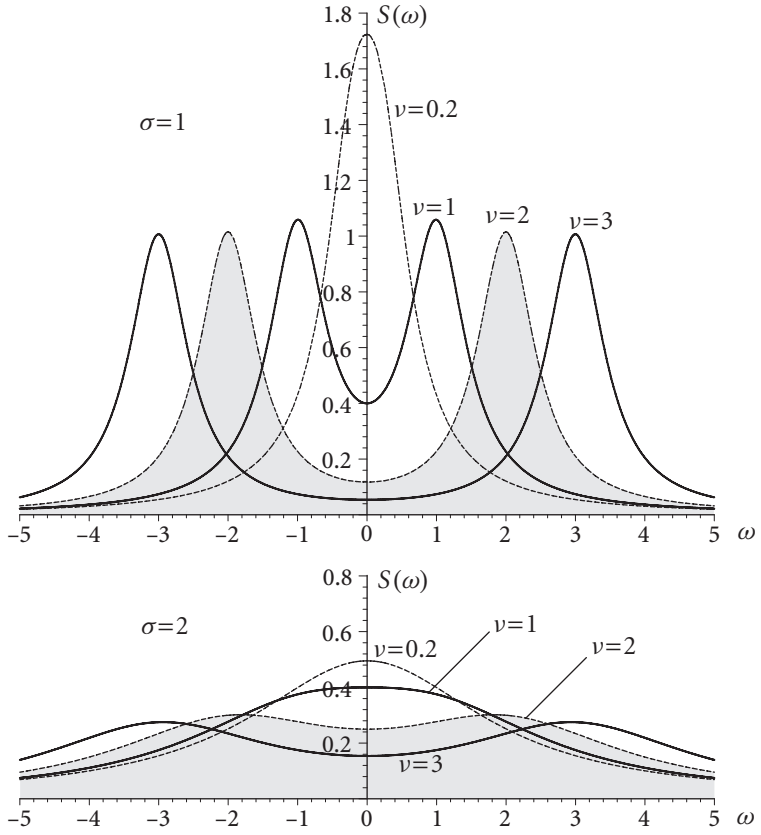

Figure 1.8 Power spectral density function of a bounded noise process.

the bounded noise to model the vortex-induce force of a spring-mounted cylinder in a cross-flow.

When σ is small, from Figure 1.8, it can be seen that the bounded noise can be used to model a narrow band process with the central frequency ν. If σ approaches zero, the bounded noise becomes a deterministic sinusoidal function. When σ is increased, the power spectral density curve becomes flat. For large values of σ, the bounded noise approximates a white noise process. However, since the mean-square value is fixed at $\frac{1}{2}$, the spectral density level of the white noise goes to zero when $\sigma \to \infty$.

The bounded noise process (1.2.11) was first employed by Stratonovich [81] and has since been used to model many engineering problems ([2], [29], [44], and [92]). For more information about modeling of bounded stochastic processes, refer to Cai and Wu [20].

1.2.2 Definitions of Stochastic Stability

In this section, the almost-sure stability (or stability with probability 1) and the moment stability of a stochastic dynamical system are defined [99].

Consider the n-dimensional stochastic system of the form

$$\dot{\mathbf{x}} = \mathbf{f}\big(\mathbf{x}, t, \boldsymbol{\xi}(t)\big), \tag{1.2.15}$$

where the initial condition is $\mathbf{x}(0) = \mathbf{x}_0$, with probability 1 (w.p.1), and $\boldsymbol{\xi}(t)$ is an m-dimensional vector of stochastic processes.

Without the loss of generality, one may take $\mathbf{x}(0) = \mathbf{0}$ and $\mathbf{f}\big(\mathbf{0}, t, \boldsymbol{\xi}(t)\big) = \mathbf{0}$ so that, w.p.1, $\mathbf{x}(t) \equiv \mathbf{0}$ is a solution.

Almost-Sure (a.s.) Stability or Stability with Probability 1 (w.p.1)

The solution $\mathbf{x}(t) = \mathbf{0}$ is stable almost-surely if, for any $\varepsilon > 0$ and $\rho > 0$, one can find $\delta(\varepsilon, \rho) > 0$ such that

$$P\Big\{ \sup_{t>0} \big\|\mathbf{x}(t)\big\| > \varepsilon \Big\} < \rho, \tag{1.2.16}$$

whenever $\big\|\mathbf{x}(0)\big\| < \delta$.

Almost-Sure Asymptotic Stability

If condition for almost-sure stability is satisfied and if

$$P\Big\{ \lim_{t\to\infty} \big\|\mathbf{x}(t)\big\| = 0 \Big\} = 1, \tag{1.2.17}$$

then the trivial solution $\mathbf{x}(t) = \mathbf{0}$ is asymptotically stable almost-surely.

Moment Stability

The trivial solution is stable in the pth moment if, given $\varepsilon > 0$, there exists $\delta > 0$ such that

$$\mathrm{E}\big[\big\|\mathbf{x}(t)\big\|^p\big] < \varepsilon, \qquad \text{for all } t \geqslant 0 \text{ and } \big\|\mathbf{x}(0)\big\| < \delta. \tag{1.2.18}$$

From Jensen's inequality, it can be concluded that higher moment stability implies lower moment stability. Furthermore, mean square stability ($p = 2$) implies almost-sure stability, which can be concluded from Chebyshev's inequality (see, e.g., Xie [99]).

1.3 Lyapunov Exponent and Moment Lyapunov Exponent

Lyapunov Exponent

Lyapunov exponents were first introduced by Lyapunov [47] for investigating the stability of dynamical systems described by nonlinear ordinary differential equations. The theory of Lyapunov exponents was further advanced by Oseledec [57] in the well-known *Multiplicative Ergodic Theorem*. Oseledec showed that for continuous dynamical systems, both deterministic and stochastic, there exist *deterministic, real* numbers characterizing the average exponential rates of growth or decay of the solution for large time and called them *Lyapunov exponents*. Since then, Lyapunov exponents have been applied in a variety of branches of science and engineering.

Consider the following stochastic system

$$\dot{\mathbf{x}}(t) = \mathbf{A}\big(\boldsymbol{\xi}(t)\big)\,\mathbf{x}(t), \quad \mathbf{x}(0) = \mathbf{x}_0 \in \mathcal{R}^n \backslash \{\mathbf{0}\}, \tag{1.3.1}$$

where $\mathbf{A} : \mathcal{M} \to \mathcal{R}^{(n,n)}$ is an analytic function from a compact connected smooth manifold $\mathcal{M}$ into the space $\mathcal{R}^{(n,n)}$, and $\boldsymbol{\xi}(t)$ is a stationary ergodic diffusion process on $\mathcal{M}$ described by the stochastic differential equation

$$\mathrm{d}\boldsymbol{\xi}(t) = \mathbf{X}_0(\boldsymbol{\xi})\mathrm{d}t + \sum_{l=1}^{d} \mathbf{X}_l(\boldsymbol{\xi})\mathrm{d}W_l(t).$$

By assuming that $\boldsymbol{\xi}(t)$ is strongly elliptic and satisfies other non-degenerate conditions, one has, for any $\mathbf{x}_0 \neq \mathbf{0}$,

$$\lambda = \lim_{t\to\infty} \frac{1}{t} \log\big\|\mathbf{x}(t;\mathbf{x}_0)\big\|, \quad \text{almost surely,} \tag{1.3.2}$$

where λ is deterministic and equal to the largest Lyapunov exponent from the *Multiplicative Ergodic Theorem*. The Lyapunov exponent λ characterizes the exponential rate of growth or decay of the solutions of system (1.3.1). If the Lyapunov exponent λ is negative, the solutions of system (1.3.1) decay exponentially as $t \to \infty$ and the system is stable almost-surely or with probability 1; otherwise, the system is unstable w.p.1.

Moment Lyapunov Exponent

For certain values of system parameters, the solution of a stochastic system may be stable with probability 1, but its second moment may grow exponentially. The connection between

moment stability and almost-sure stability for an undamped linear two-dimensional system under real noise excitation was established by Molchanov [49]. These results were extended for an arbitrary n-dimensional linear stochastic system by Arnold [7], in which a formula connecting moment and sample stability was established. A systematic study of moment Lyapunov exponents is presented in [6] for linear Itô systems and in [5] for linear stochastic systems under real noise excitations.

Analogous to the Lyapunov exponents, define the pth moment Lyapunov exponent of solutions of the system (1.3.1) as

$$\Lambda(p) = \lim_{t\to\infty} \frac{1}{t} \log \mathrm{E}\big[\|\mathbf{x}(t)\|^p\big]. \tag{1.3.3}$$

The pth moment Lyapunov exponent $\Lambda(p)$ characterizes the exponential rate of growth or decay of the pth moment $\mathrm{E}\big[\|\mathbf{x}(t)\|^p\big]$. If $\Lambda(p)<0$, then the pth moment is asymptotically stable, i.e. $\mathrm{E}\big[\|\mathbf{x}(t)\|^p\big]\to 0$ as $t\to\infty$.

The moment Lyapunov exponent $\Lambda(p)$ possesses the following properties:

1. $\Lambda\big(p,\mathbf{x}(0)\big)=\Lambda(p)$, for all initial conditions $\mathbf{x}(0)$ in the n-dimensional vector space excluding the origin.
2. For all real values of p, $\Lambda(p)$ is real, analytic, and convex.
3. $\Lambda(p)/p$ is increasing and $\Lambda(p)$ passes the origin, $\Lambda(0)=0$, and
$$\lambda = \Lambda'(0) = \lim_{p\to 0} \frac{\Lambda(p)}{p}, \tag{1.3.4}$$
i.e. the slope of $\Lambda(p)$ at the origin is equal to the Lyapunov exponent given by equation (1.3.2).
4. The pth moment Lyapunov exponent $\Lambda(p)$ is the principal eigenvalue of the differential eigenvalue problem
$$\mathscr{L}(p)T(p) = \Lambda(p)T(p), \tag{1.3.5}$$
with non-negative eigenfunction $T(p)$.

Equation (1.3.4) is the most concise relationship between the almost-sure stability and the moment stability of linear system (1.3.1). $\mathscr{L}(p)$ in equation (1.3.5) can be derived from equation (1.3.1) by making use of the Khasminskii's transformation (see, e.g., Arnold *et al.* [5] and [6]). The operator $\mathscr{L}$ can also be obtained in a more straight-forward way which was first used by Wedig [91].

In general, the eigenvalue problem (1.3.5) is very complicated and therefore it is difficult to find the explicit solution to (1.3.5). Alternatively, there are two approximate methods which can yield satisfactory results. One method is Monte Carlo simulation which is briefly introduced in next subsection. The other is the perturbation method which has been used successfully by many researchers (see, e.g., Xie [99]). The two methods are usually used together to validate each other.

For a small noise excitation, Arnold, Doyle, and Namachchivaya [4] obtained an expansion of moment Lyapunov exponent for two dimensional systems with p near zero. Khasminskii and Moshchuk [38] considered the two dimensional linear stochastic system and obtained the asymptotic expansions for the moment Lyapunov exponent and stability index for the oscillator. Namachchivaya *et al.* [52] used a similar perturbation approach to obtain the small-noise expansions of moment Lyapunov exponent for two coupled oscillators with noncommensurable natural frequencies driven by real noise. However, the limitation of small p restricts the utility of the results. Namachchivaya and Roessel [53] improved the method to obtain an asymptotic expansion of moment Lyapunov exponent for finite p. They also used the stochastic averaging method to derive the $\mathscr{L}$ operator and found that it was identical to the one obtained by the perturbation method. In a recent paper, Nachchivaya and Roessel [54] applied both the perturbation method and stochastic averaging method to two coupled oscillators in resonance, i.e., with commensurable natural frequencies.

1.4 Monte Carlo Simulation

For problems involving random variables and random processes with known probability distributions, Monte Carlo simulation can be used. In each simulation, a particular set of values of the random variables and realizations of the random processes generated in accordance with the corresponding probabilistic properties are used. By repeating the process, samples of solutions, each corresponding to a different set of values of the random variables and realizations of random processes, are obtained.

A sample from a Monte Carlo simulation is similar to a sample of experimental observations. Therefore, the results of Monte Carlo simulations may be treated statistically. Monte Carlo simulation is a sampling technique, and the results are subject to sampling

errors. Generally, Monte Carlo simulation requires a sufficiently large sample size to yield satisfactory results.

1.4.1 Simulation of the Standard Wiener Process $W(t)$

In order to simulate $W(t)$ for $0 \leqslant t \leqslant T$, discretize the time interval into K segments: $t_0 = 0,\ t_1,\ t_2,\ \ldots,\ t_K = T$, where $\Delta t_k = t_k - t_{k-1},\ k = 1, 2, \ldots, K$. From the definition of Wiener process, it is well known that $\mathrm{d}W$ is Gaussian with $\mathrm{E}\big[\mathrm{d}W\big] = 0$ and $\mathrm{E}\big[(\mathrm{d}W)^2\big] = \mathrm{d}t$. The random variable $\Delta W^k = W(t_k) - W(t_{k-1})$ is then normally distributed with mean zero and variance Δt_k, i.e. $\Delta W^k = N(0, \Delta t_k)$. Then ΔW^k can be generated as

$$\Delta W^k = n^k \sqrt{\Delta t_k}, \tag{1.4.1}$$

where n^k is a standard normally distributed random number. Hence, for a given initial condition $W^0 = W(0)$, a realization of the standard Wiener process $W(t)$ at time t_k is given by

$$W^k = W^{k-1} + \Delta W^k, \quad k = 1, 2, \ldots, K. \tag{1.4.2}$$

1.4.2 Simulation of the Stochastic Differential Equations

Consider the dynamic responses of a stochastic system governed by an N-dimensional system of autonomous Itô stochastic differential equations of the form

$$\mathrm{d}Y_j = m_j(\mathbf{Y})\,\mathrm{d}t + \sum_{l=1}^{d} \sigma_{jl}(\mathbf{Y})\,\mathrm{d}W_l, \quad j = 1, 2, \ldots, N, \tag{1.4.3}$$

where $\mathbf{Y} = \big\{Y_1, Y_2, \ldots, Y_N\big\}^T$.

The time parameter t is discretized as $t_0 = 0,\ t_1,\ t_2,\ \ldots,$ of equal time step Δ, i.e. $t_k - t_{k-1} = \Delta$.

1.4.2.1 Strong Approximation Schemes

A time discrete approximation $\mathbf{Y}^\Delta$ is said to converge strongly with order $\gamma > 0$ to $\mathbf{Y}$ at time T if there exists a constant $C > 0$, which is independent of Δ, and $\Delta_0 > 0$ such that the error of approximation

$$\epsilon(\Delta) = \mathrm{E}\big[\big\|\mathbf{Y}(T) - \mathbf{Y}^\Delta(T)\big\|\big] \leqslant C\,\Delta^\gamma,$$

for each $0 < \Delta < \Delta_0$.

The Euler Scheme

The Euler scheme is strongly convergent with $\gamma = 0.5$. Equations (1.4.3) yield

$$Y_j^k = Y_j^{k-1} + m_j^{k-1} \cdot \Delta + \sum_{l=1}^{d} \sigma_{jl}^{k-1} \cdot \Delta W_l^{k-1}, \quad j = 1, 2, \ldots, N, \tag{1.4.4}$$

where the superscript k denotes that the quantity is evaluated at time t_k.

1.4.2.2 Weak Approximation Schemes

In certain applications, it is not necessary to obtain path-wise approximation of the solution of the stochastic differential equations (1.4.3). For example, one may be interested in the pth moment of the solution at time T, i.e. $\mathrm{E}\big[\|\mathbf{Y}(T)\|^p\big]$. In these cases, only a much weaker form of convergence in probability distribution is required.

A time discrete approximation $\mathbf{Y}^\Delta$ is said to converge weakly with order $\gamma > 0$ to $\mathbf{Y}$ at time T if there exists a constant $C > 0$, which is independent of Δ, and $\Delta_0 > 0$ such that the error of approximation, for each $0 < \Delta < \Delta_0$,

$$\epsilon(\Delta) = \Big|\mathrm{E}\big[g\{\mathbf{Y}(T)\}\big] - \mathrm{E}\big[g\{\mathbf{Y}^\Delta(T)\}\big]\Big| \leqslant C\,\Delta^\gamma,$$

where g is any function that is at least $2(\gamma+1)$ times continuously differentiable.

The Euler Scheme

The Euler scheme given by equations (1.4.4) has the order of weak convergence $\gamma = 1.0$ if the drift and diffusion coefficients are four times continuously differentiable.

There exist other discretization schemes, such as Milstein scheme and Taylor scheme, which have their own advantages and disadvantages. A detailed source of numerical solutions of stochastic differential equations is given in [39].

1.4.3 Simulation of Moment Lyapunov Exponent

The determination of the pth moment Lyapunov exponent is in general very difficult. For most practical engineering structures, numerical approaches have to be applied. The Monte Carlo simulation method presented in this Section is a condensed version of that in Xie [99].

Consider an N-dimensional system of linear autonomouse Itô stochastic differential equations

$$\mathrm{d}\mathbf{Y} = \mathbf{M}\mathbf{Y}\,\mathrm{d}t + \sum_{l=1}^{d} \boldsymbol{\sigma}_l \mathbf{Y}\,\mathrm{d}W_l, \tag{1.4.5}$$

where $\mathbf{M}$ and $\boldsymbol{\sigma}_l$ $(l=1,2,\ldots,d)$ are $N\times N$ matrixes, $\mathbf{Y}=\{Y_1, Y_2, \ldots, Y_N\}^T$, in which $Y_j = X_j$, for $j=1,2,\ldots,n$. Vector $\mathbf{X}$ and the vector containing the first n elements of vector $\mathbf{Y}$ are interchangeable for the easy of presentation.

Since the moment Lyapunov exponent is related to the exponential rate of growth or decay of the pth moment, only the numerical approximation of the pth moment of the solution of system (1.4.5) is of interest in the Monte Carlo simulation. As a result, pathwise approximations of the solutions of the stochastic differential equations (1.4.5) are not necessary. Only a much weaker form of convergence in probability distribution is required.

For the numerical solutions of the stochastic differential equations (1.4.5), weak Taylor approximations, such as the order 2.0 weak Taylor scheme, may be applied. To evaluate the pth moment $\mathrm{E}[\|\mathbf{X}\|^p]$, S samples of the solutions of equations (1.4.5) are generated. The sample size S must be a large number since the evaluation of expectation depends on it.

Generally, the solution of equations (1.4.5) grows or decays exponentially in time, periodic normalization of the solution must be applied in order to avoid numerical overflow or underflow and to correctly determine the moment Lyapunov exponent.

Take the initial condition of $\mathbf{X}(0)$ such that $\|\mathbf{X}(0)\|=1$. Note that $Y_j=X_j$, for $j=1, 2, \ldots, n$. Normalization of the first n elements of the state vector $\mathbf{Y}$ is applied after every time period $(K\Delta)$. Note that the value of K should be chosen judiciously. A small value of K is not necessary and numerically inefficient, since in a small period of time $(K\Delta)$, the system does not show appreciable growth or decay.

At the time instance t in the mth period, $m=1,2,\ldots,M$, the solution can be normalized as

$$\mathbf{X}_m(t) = \frac{\mathbf{X}\big((m-1)(K\Delta)+t, \mathbf{X}_0\big)}{\|\mathbf{X}\big((m-1)(K\Delta), \mathbf{X}_0\big)\|}, \quad \text{for } m=1,\ 2,\ \ldots,\ M, \tag{1.4.6}$$

with the initial value given by

$$\mathbf{X}_m(0) = \frac{\mathbf{X}\big((m-1)(K\Delta), \mathbf{X}_0\big)}{\|\mathbf{X}\big((m-1)(K\Delta), \mathbf{X}_0\big)\|}.$$

After the normalization, numerical solution of the stochastic differential equations is continued.

From equation (1.4.6), it can be easily shown that

$$\begin{aligned}\left\|\mathbf{X}\big(M(K\Delta)\big)\right\| &= \left\|\mathbf{X}\big(M(K\Delta),\mathbf{X}_0\big)\right\| \\ &= \prod_{m=1}^{M}\frac{\left\|\mathbf{X}\big(m(K\Delta)\big)\right\|}{\left\|\mathbf{X}\big((m-1)(K\Delta)\big)\right\|} = \prod_{m=1}^{M}\left\|\mathbf{X}_m(K\Delta)\right\|. \end{aligned} \tag{1.4.7}$$

Using equations (1.3.3) and (1.4.7), the pth moment Lyapunov exponent is given by, for all values of p of interest,

$$\Lambda_{\mathbf{X}}(p) = \frac{1}{M(K\Delta)}\log \mathsf{E}\Big[\prod_{m=1}^{M}\left\|\mathbf{X}_m(K\Delta)\right\|^{p}\Big]. \tag{1.4.8}$$

More details about the approximation of expectation can be found in Xie and Huang [95].

The Monte Carlo simulation presented in this Section can be easily applied to higher dimensional systems and any noise excitations, even for those with only time series available.

1.5 Organization of the Thesis

It is quite obvious, from the review above, that there has been a large amount of research done in both flow-induced vibration of cylinders in cross-flow and dynamic stability of stochastic systems. However, it seems that the research in these two areas has been conducted separately. Flow-induced vibration has been studied mainly using deterministic tools. On the other hand, the investigations of dynamic stability of stochastic systems are mainly for structures under externally applied loads. For a limited number of publications on stability of structures under fluid-dynamic loads, only considerably simplified structure models and fluid dynamic force models, such as white noise process, have been used.

The present research bridges the gaps between these two important engineering disciplines. The spring-supported cylinder in a cross-flow or a shear flow is considered, which vibrates in both the drag and lift directions. In the lock-in region, the flow-induced vibration of a cylinder is a combination of forced vibration and instability. The vortex-induced force is modeled by a bounded noise due to its narrow-band characteristics. Thus, the equations of motion are established and the stability of the cylinder is investigated by determining the moment Lyapunov exponent and Lyapunov exponent. For a cylinder in a shear flow,

the large-amplitude vibration in the region of high reduced velocity mainly results from the fluidelastic instability especially when the cylinder is placed in a light fluid such as air. A quasi-steady model is used to model the flow-induced force in this case. Since turbulent flow occurs in cylinder arrays in a cross-flow with the upstream cylinders acting as turbulence generators and additional turbulence is generated to stabilize the flow-induced vibration, the flow field can be described satisfactorily only in probabilistic terms. Thus an appropriate stochastic model for turbulence has to be applied to account for the influence of turbulence on the stability of the system. The equations of motion of the cylinder is established with both the flow and cylinder modeled as close to reality as possible. The resulting equations of motion are of the form of parametrically excited stochastic differential equations. The Lyapunov exponents and pth moment Lyapunov exponents of the system are evaluated to determine the dynamic stability of the cylinder.

In Chapter 1, the three main mechanisms of fluid-induced vibration of circular cylinders in a cross-flow are introduced. The experimental observations of stabilizing effect of turbulence are reviewed. On the other hand, a brief introduction of stochastic stability is presented. Since Lyapunov exponent and moment Lyapunov exponent are extremely important in stochastic stability, the concepts and their simulation methods are briefed. Real noise and bounded noise are two common types of stochastic processes, which have wide applications in engineering practices. Hence, they are also briefly introduced here.

Chapter 2 introduces a force decomposition model, in which the motion-dependent forces are included, for the flow-induced vibration of a cylinder in a cross-flow. The model for a spring-mounted cylinder placed in a cross-flow is established and the vortex-induced force is modeled by a bounded noise due to its narrow-band characteristics. In the lock-in region, the vibration of the cylinder in the drag direction is relatively small and can be neglected. Thus, the model is reduced to a single degree-of-freedom system under bounded noise excitation. Then, the model is extended to be applicable to a cylinder placed in a shear flow. In the region of high reduced velocity, the cylinder in a shear flow can be subjected to fluidelastic instability. To capture the instability, a quasi steady model is used to model the flow-induced forces. For the grid-generated turbulence, the flow velocity can be decomposed into a mean component and a fluctuating component. The latter can be modeled as a real noise since the grid-generated turbulence is nearly Gaussian and has

zero mean. After considering the influence of turbulence, the vortex-induced forces and motion-dependent forces include stochastic terms. Hence, the equations of motion become a four dimensional stochastic differential equations.

Parametric instability of a single cylinder in the lock-in range is introduced in Chapter 3. The model developed in Chapter 2 for a cylinder in a cross-flow can be generalized to represent a class of two-dimensional dynamic systems subjected to parametric excitations in the damping term, which is described by a narrow-band bounded noise process. The dynamic stability of the system is studied by determining the moment Lyapunov exponents and the Lyapunov exponents. Based on the stability analysis results of a two-dimensional general dynamic system, an example is given to demonstrate the role of parametric instability in vortex-induced vibration of a single cylinder in a cross-flow. The effects on the stability of some crucial parameters, such as the mass ratio and fluid damping coefficient, are studied.

In Chapter 4, the fluidelastic instability of a single cylinder in shear flow is considered. The grid-generated turbulence is modeled as an Ornstein-Uhlenbeck process, which is included in the equations of motion as a perturbation when the turbulence intensity is small. The stability of the deterministic system is studied by varying the critical parameter (frequency ratio k). It is shown that fluidelastic instability can be stabilized by the turbulence under certain conditions. Parametric studies are performed to demonstrate the significant effects of noise parameters α and σ, on the stability of the cylinder. Analytical results and those obtained from numerical simulations are compared to validate the approach.

The method presented in Chapter 3 is extended and applied to the case for a two degrees-of-freedom system in Chapter 5. For a two degrees-of-freedom system excited by a bounded noise process, the system can be in subharmonic resonance, combination (additive or differential) resonance, or in both, depending on the excitation frequency. The effect of noise on various parametric resonances is investigated. The effects of parameters on the stability are studied. Similarly, analytical results agree well with the numerical results.

Chapter 6 discusses some of the open questions in the current research and makes some suggestions for future research.

CHAPTER 2

Modeling of Flow-Induced Vibration of a Cylinder

Three mechanisms are usually considered to be responsible for flow-induced vibration and/or instability of a cylinder in a cross-flow; they are vortex-induced lock-in resonance, fluidelastic instability, and turbulence-induced buffeting. According to Naudascher and Rockwell [56], these three mechanisms represent three general sources of excitation: the (flow) instability-induced excitation (IIE), the movement-induced excitation (MIE), and the extraneously-excited excitation (EIE), respectively. The total flow-induced force can then be expressed as

$$F = F_V + F_M + F_T, \tag{2.0.1}$$

where the subscripts V, M, and T represent vortex-induced, motion-dependent, and turbulence-induced buffeting forces, respectively. When the cylinder is rigid and fixed, it becomes stationary even though there is a cross-flow. In this case, the total flow-induced force becomes

$$F_0 = F_{V0} + F_{T0}. \tag{2.0.2}$$

The three mechanisms may coexist in any flow-induced vibration problem. When that happens, the dynamic behavior of the fluid-structure system becomes very complex. The task of a theoretical modeling study is thus to formulate the problem in a general way, to simplify the formulation by identifying key mechanism(s), and to demonstrate the main features for specific cases through dynamic analyzes.

For a single circular cylinder in a uniform flow, the main mechanism of unstable motion is considered to be vortex-induced lock-in resonance (Sarpkaya [72] and [74]). In a recent theoretical modeling study, Zhu *et al.* [104] modeled the vortex-induced force as a bounded noise and showed that this lock-in resonance is accompanied by a parametric instability due to the bounded noise excitation. On the other hand, Yu *et al.* [100] showed that a single cylinder could undergo fluidelastic instability if the approach flow is not uniform, e.g., a shear flow. Such instability occurs at very large values of reduced velocity ($U_r > 100$), where the vortex-induced force has no appreciable influence on cylinder vibration. The main mechanism responsible for this type of instability could be attributed to changes of the mean lift and mean drag forces relevant to cylinder motion. Fluidelastic instability may also occur when the single cylinder is in the wake of another cylinder (Bokaian and Geoola [18]), or in cylinder arrays (Price and Paidoussis [65], Chen [24]). It is considered that the motion-dependent fluid force, in the form of fluid-damping force and/or fluid-stiffness force, is responsible for fluidelastic instability in these cases.

Since fluidelastic instability could occur under many different circumstances, its suppression is thus of importance to a variety of engineering applications. In most practical engineering problems, the flow is quite often turbulent. According to So and Savkar [79], under certain flow conditions, free stream turbulence could act to substantially increase the fluctuating vortex-induced forces. Their measurements were carried out on a rigid cylinder. The increased fluctuating forces could, in turn, influence fluidelastic instability of the fluid-structure system. Romberg and Popp [68] presented some interesting stability results from carefully carried out experiments on flow-induced vibrations of a flexibly-mounted cylinder in an otherwise fixed cylinder array. They considered both fluidelastic instability and turbulent buffeting, and showed that large galloping motion can be stabilized by grid-generated turbulence. In one of their experiments, Romberg and Popp [68] considered a cylinder with a very small structural damping. The damping measured in the flow direction is high, and the cylinder undergoes a galloping motion in the cross-flow (lift) direction at certain reduced velocity $U_{r,\mathrm{cr}}$. Naturally, turbulence occurs in cylinder bundles in cross-flow due to upstream cylinder bundles acting as turbulence generators. Additional turbulence was generated in this experiment by placing a turbulence grid in front of the cylinder at a distinct distance. It was observed that as the turbulence was increased in the

flow, a significant stabilization took place and the galloping instability did not occur for reduced velocity values substantially higher than $U_{r,\mathrm{cr}}$. The experiment also showed that the turbulence intensity is a significant factor influencing the stability. Similar effects are observed in the experiments of a parallel triangular tube bundle performed by Rottmann and Popp [69].

In this chapter, a spring-supported cylinder in a cross-flow and a shear flow is considered, respectively. The equations of motion for the two cases are set up and simplified for further analytical analysis.

2.1 A Single Cylinder in Cross-Flow

In view of its fundamental importance, vortex-induced vibrations have been studied extensively, using experimental, numerical, and theoretical modeling methods. A number of review articles are available on this subject, e.g., Anagnostopoulos [1], Gabbai and Benaroya [30], and Sarpkaya [73], [74]. Since the present study is concerned with the theoretical modeling of vortex-induced vibrations, only relevant work is reviewed and discussed.

Due to the complex nature of fluid-structure interaction in vortex-induced vibration, theoretical modeling is usually carried out in a semi-analytical and semi-empirical way. The developed models can be classified into two groups; one is the force decomposition model, and the other is the wake oscillator model.

In the force decomposition model, the force acting on the cylinder is decomposed into several components representing the forces due to vortex shedding and arising from fluid-structure interaction. This type of model was first proposed by Sarpkaya [72], who divided the total force into a fluid inertia and a fluid damping component. Griffin and Koopmann [33] and Griffin [34] decomposed the total force into a fluid excitation component and a fluid reaction component, the latter representing the force arising from fluid-structure interaction. It was found that fluid damping decreased dramatically in the lock-in range. This implies that fluid damping plays a crucial role in vortex-induced vibration. Based on unsteady flow theory, Chen *et al.* [23] represented the force arising from the fluid-structure interaction by three linear motion-dependent components, i.e., a fluid inertia, a fluid damping, and a fluid stiffness component. They were combined with a vortex-induced excitation force to give the total force, and Chen *et al.* [23] concluded that vortex-induced

vibration is made up of instability and forced vibration. However, they did not point out explicitly which component is the source that leads to instability.

In the wake oscillator model, a van der Pol oscillator was invoked to represent the dynamics of the lift force due to vortex shedding. It was combined with the equation of motion of the cylinder to form the governing equations for the fluid-structure system. Certain terms related to cylinder motion were assumed in the wake oscillator to represent the effect of structural motion on the lift force, thereby taking the fluid-structure interaction into account. Hartlen and Currie [35] were the first to propose the wake-oscillator model. The model was later modified by a number of researchers, e.g., Skop and Griffin [75], Landl [41], Berger [12], and Balasubramanian and Skop [10], in order to obtain a better agreement with experimental measurements and to replicate experimental observations.

Wang *et al.* [85] proposed a model for vortex-induced vibration in both cross-flow and stream-wise directions. In the model, the quasi-steady flow theory was invoked to account for fluid-structure interactions. This model avoids using the assumed fluid-structure interaction terms as in the wake-oscillator model, but is limited to weak fluid-structure interaction cases only. This is because the condition for the quasi-steady flow theory to hold is that the velocity of structural vibration is small compared to the free-stream velocity of the approach flow. If the fluid-structure interaction is strong, the induced structural vibration becomes significant, and the velocity of structural vibration is large, thus the quasi-steady flow theory might not be applicable. An analytical expression of vortex-induced force could be obtained when a linear approximation of fluid-structure interaction was made. This model requires only the parameters for a stationary cylinder compared with the wake-oscillator model, thus avoiding the use of the assumed fluid-structure interaction terms whose coefficients are to be determined from free or forced vibration tests. Using this model, an analytical expression of vortex-induced force could be deduced using a linear approximation of fluid-structure interaction. The expression is similar to that proposed by Sarpkaya [72], but additional nonlinear terms arising from fluid-structure interaction were present. In the Wang *et al.* [85] model, vortex-induced lift and drag forces acting on the stationary cylinder were represented by sinusoidal functions. The model was modified using the bounded noise process to represent vortex-induced lift and drag forces acting on the stationary cylinder (Wang *et al.* [86]) and based on the narrow-band characteristic of the

vortex-induced force shown by Vickery and Basu [84]. The modified model was validated against experimental measurements in the literature. The predicted power spectra of the flow-induced force and the cylinder vibration are very similar to experimental results.

In the present study, the model developed by Wang *et al.* [86] is further extended to include the motion-dependent fluid forces, in an attempt to investigate whether they could induce instability which coexists with vortex-induced vibration and to identify the source of instability. The motion-dependent forces are taken into account using a linear model proposed by Chen *et al.* [23], and the vortex shedding forces are modeled by a bounded noise. The stability of the resultant model will be studied by the determination of Lyapunov exponents and moment Lyapunov exponents which are presented in Chapter 3 for stochastically excited systems.

In previous models of vortex-induced vibration, vortex-induced forces are usually represented by sinusoidal functions. However, the shape of the narrow-banded spectrum is very similar to that of a bounded noise (see, e.g., Vickery and Basu [84]). Therefore, a bounded noise would be a more appropriate model. In this model, vortex-induced lift and drag forces are modeled by bounded noise processes, while the fluid-structure interaction is accounted for using a quasi-steady flow theory. As a result, the interaction between the drag and lift directions is taken into account.

2.1.1 Equations of Motion for a Cylinder in Cross-Flow

Consider an elastically supported rigid cylinder in a cross-flow. The approaching flow is assumed to be uniform and two-dimensional. The equations of motion of the cylinder are

$$\begin{aligned} \ddot{X}(t) + 2\zeta_s\omega_0\dot{X}(t) + \omega_0^2 X(t) &= \frac{F^X(t)}{M}, \\ \ddot{Y}(t) + 2\zeta_s\omega_0\dot{Y}(t) + \omega_0^2 Y(t) &= \frac{F^Y(t)}{M}, \end{aligned} \tag{2.1.1}$$

where $X(t)$ and $Y(t)$ are cylinder displacements in the stream-wise and the cross-flow directions, respectively, ω_0 is the natural frequency, ζ_s is the structural damping coefficient, and M is the mass per unit length of the cylinder.

In equations (2.1.1), $F^X(t)$ and $F^Y(t)$ are flow-induced forces per unit length acting on the cylinder in the stream-wise and the cross-flow directions, respectively. For the present case, flow-induced forces may be divided into two components: one arising from vortex

shedding, and the other due to the feedback effect of cylinder motion. Hence, they can be written as

$$\begin{aligned} F^X(t) &= F_V^X(t) + F_M^X(t), \\ F^Y(t) &= F_V^Y(t) + F_M^Y(t), \end{aligned} \tag{2.1.2}$$

where the subscripts "V" and "M" represent "vortex-induced" and "motion-dependent", respectively.

When the cylinder is stationary, the motion-dependent fluid forces, $F_M^X(t)$ and $F_M^Y(t)$, are absent, and only vortex-induced forces are applied to the cylinder. These are denoted as $F_{V_0}^X(t)$ and $F_{V_0}^Y(t)$ in order to differentiate them from their counterparts when the cylinder is in motion. Once the cylinder is vibrating under the action of vortex-induced forces, its motion can alter vortex shedding, thus changing vortex-induced forces not only in their magnitudes but also in their dominant frequencies.

In addition to vortex-induced excitation, fluid flow will also affect the dynamics of the cylinder in the form of added mass, fluid damping, etc. They are all included into the motion-dependent forces, $F_M^X(t)$ and $F_M^Y(t)$, in the present formulation.

In general, both vortex-induced and motion-dependent forces are nonlinear and dependent on a number of parameters, such as the Reynolds number, the reduced velocity, structural damping, and their expressions are complex. In order to carry out a theoretical analysis, approximate modeling is necessary.

2.1.1.1 Modeling of Vortex-Induced Forces

In the present study, a model proposed by Wang *et al.* [86] is invoked for vortex-induced forces. In the model, vortex-induced forces acting on a vibrating cylinder are modeled based on the quasi-steady flow theory, and the basic idea is illustrated in Figure 2.1. When the velocity of cylinder vibration is small compared with the flow velocity, the quasi-steady theory is valid. Vortex-induced forces acting on a vibrating cylinder are equal to those acting on the same but stationary cylinder at the instantaneous position, with the direction of the approach flow changed by the velocity of cylinder vibration. Vortex-induced forces are thus expressed as

$$\begin{aligned} F_V^X(t) &= F_{V_0}^X(t) \cdot \cos\theta(t) + F_{V_0}^Y(t) \cdot \sin\theta(t), \\ F_V^Y(t) &= F_{V_0}^Y(t) \cdot \cos\theta(t) - F_{V_0}^X(t) \cdot \sin\theta(t), \end{aligned} \tag{2.1.3}$$

where θ is the angle between the x-axis and the instantaneous velocity vector of cylinder vibration given by

$$\theta(t) = \tan^{-1} \frac{\dot{Y}}{U - \dot{X}}. \tag{2.1.4}$$

In equations (2.1.3), $F^X_{V_0}(t)$ and $F^Y_{V_0}(t)$ are the drag and lift forces acting on the stationary cylinder subjected to a cross-flow of free-stream velocity $V(t) = \sqrt{(U-\dot{X})^2 + \dot{Y}^2}$ at the angle θ. When the cylinder velocity is much smaller than the flow velocity, i.e., $\dot{X}(t) \ll U$ and $\dot{Y}(t) \ll U$,

$$V(t) = \sqrt{\left(U - \dot{X}\right)^2 + \dot{Y}^2} \approx U. \tag{2.1.5}$$

Therefore, the lift and drag forces acting on the stationary cylinder can be used to deduce vortex-induced forces applied to the vibrating cylinder. In the literature, the lift and drag forces are usually represented by sinusoidal functions at the Strouhal and the double Strouhal frequencies, respectively. However, Vickery and Basu [84] have shown that the spectrum of vortex-induced force is of narrow-band, even though the approaching flow is uniform. Wang *et al.* [86] showed that the bounded noise process has similar spectral distribution to that of the vortex-induced force, and is thus appropriate for the force modeling. Using the bounded noise process, the drag and lift forces acting on the stationary cylinder can be expressed as

$$\begin{aligned} F^X_{V_0}(t) &= F_D(t) = \tfrac{1}{2}\rho U^2 D \bar{C}_D + \tfrac{1}{2}\rho U^2 D C_D \cos\left[\nu_D t + \sigma_D W(t) + \phi_D\right], \\ F^Y_{V_0}(t) &= F_L(t) = \tfrac{1}{2}\rho U^2 D C_L \cos\left[\nu_L t + \sigma_L W(t) + \phi_L\right], \end{aligned} \tag{2.1.6}$$

where ρ is the density of the fluid, $\bar{C}_D$ is the mean drag coefficient, C_D (C_L) is the amplitude of the fluctuating drag (lift) coefficients, ν_D (ν_L) and σ_D (σ_L) are the frequencies and bandwidths of the vortex-induced force in the drag(lift) direction, respectively, $W(t)$ is the standard Wiener process, and ϕ_D and ϕ_L are uniformly distributed random numbers to make the bounded noise processes stationary.

In general, an iteration process is needed to obtain the expressions of vortex-induced forces using equations (2.1.3) since the flow-induced forces and the cylinder vibrations have an interactive relationship through the angle θ, which is nonlinearly related to cylinder motion. For small amplitude vibration, however, a linear approximation can be invoked in

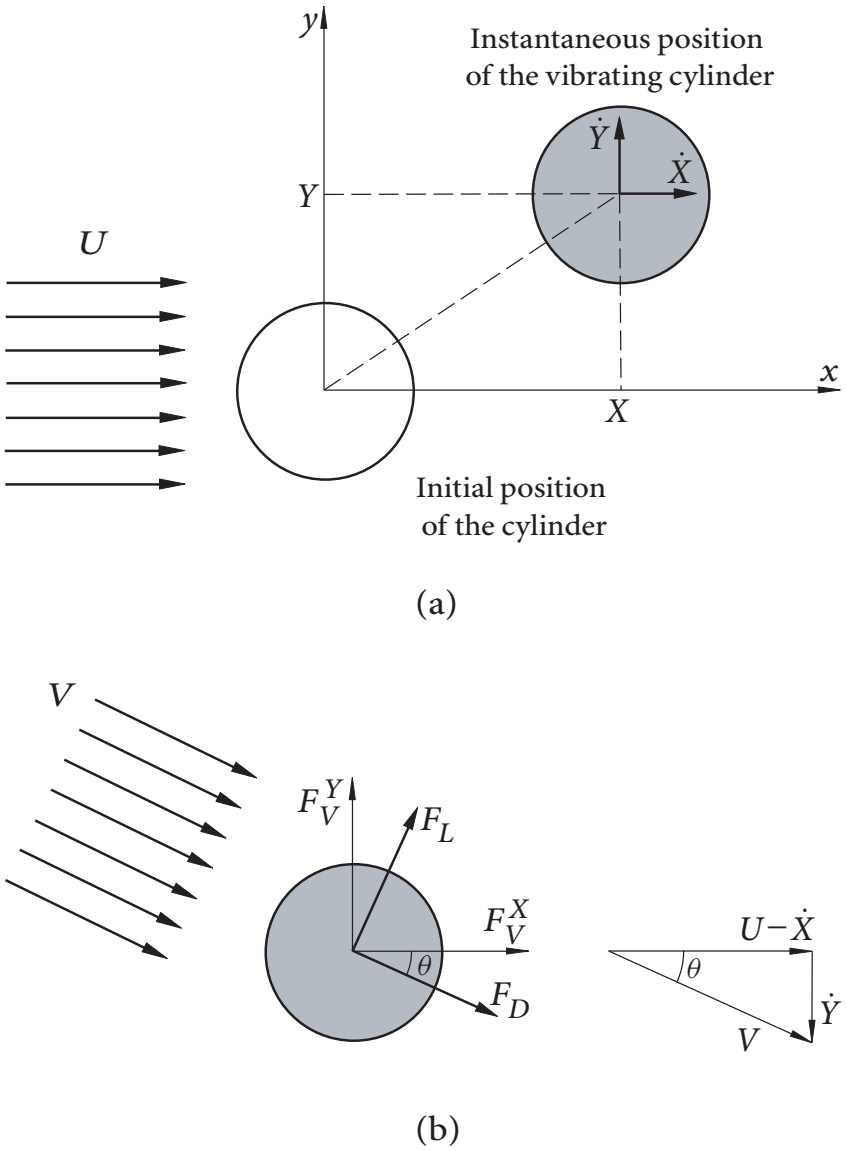

Figure 2.1 Illustration of the quasi-steady flow theory. (a) a cylinder subjected to a cross-flow; (b) vortex-induced forces acting on the vibrating cylinder according to the quasi-steady flow theory.

the present study, i.e.,

$$\begin{aligned} \sin\theta(t) &= \frac{\dot{Y}(t)}{\sqrt{[U-\dot{X}(t)]^2+\dot{Y}^2(t)}} \approx \frac{\dot{Y}(t)}{U}, \\ \cos\theta(t) &= \frac{U-\dot{X}(t)}{\sqrt{[U-\dot{X}(t)]^2+\dot{Y}^2(t)}} \approx 1. \end{aligned} \tag{2.1.7}$$

It follows then that the vortex-induced forces can be expressed as

$$\begin{aligned} F_V^X(t) &= F_D(t) + F_L(t) \cdot \frac{\dot{Y}(t)}{U}, \\ F_V^Y(t) &= F_L(t) - F_D(t) \cdot \frac{\dot{Y}(t)}{U}. \end{aligned} \tag{2.1.8}$$

Substituting equations (2.1.8) into equations (2.1.1), the equations of motion are written as

$$\begin{aligned} \ddot{X}(t) + 2\zeta_s\omega_0\dot{X}(t) + \omega_0^2 X(t) &= \frac{1}{M}\Big[F_D(t) + F_L(t)\frac{\dot{Y}(t)}{U} + F_M^X(t)\Big], \\ \ddot{Y}(t) + 2\zeta_s\omega_0\dot{Y}(t) + \omega_0^2 Y(t) &= \frac{1}{M}\Big[F_L(t) - F_D(t)\frac{\dot{Y}(t)}{U} + F_M^Y(t)\Big]. \end{aligned} \tag{2.1.9}$$

Since the present study is focused on the cylinder vibration in the cross-flow direction, only equation (2.1.9) is retained and rewritten as

$$\ddot{Y}(t) + \Big[2\zeta_s\omega_0 + \frac{1}{M}\frac{F_D(t)}{U}\Big]\dot{Y}(t) + \omega_0^2 Y(t) = \frac{1}{M}\big[F_L(t) + F_M^Y(t)\big]. \tag{2.1.10}$$

2.1.1.2 Modeling of Motion-Dependent Forces

Cylinder vibration also induces other fluid forces, such as the inertia force due to added mass and the fluid damping force, which are not considered in the above model. In the present study, they are included in the motion-dependent fluid force as

$$F_M^Y = -\frac{\rho\pi D^2}{4}c_m\ddot{Y} + \frac{\rho U^2}{\bar{\omega}_0}c_d\dot{Y} + \rho U^2 c_k Y, \tag{2.1.11}$$

where c_m, c_d, and c_k are the added mass, the fluid damping, and the fluid stiffness coefficients, respectively, and $\bar{\omega}_0$ is the natural frequency of the system, whose expression is given in subsection 2.1.1.3. In general, $c_m = 1$ since the added mass is considered to be equal to the mass of fluid displaced by the vibrating cylinder. As a first approximation, the fluid damping force is assumed to be proportional to the velocity of cylinder vibration. The fluid stiffness term affects only the natural frequency of the fluid-structure system.

2.1.1.3 Model for Vortex-Induced Vibration

Substituting equation (2.1.11) into equation (2.1.10) yields

$$\ddot{Y}(t) + \Big[2\zeta_s\omega_0 + \frac{1}{M}\frac{F_D(t)}{U}\Big]\dot{Y}(t) + \omega_0^2 Y(t) = \frac{1}{M}\Big[F_L(t) - \frac{\rho\pi D^2}{4}c_m\ddot{Y} + \frac{\rho U^2}{\bar{\omega}_0}c_d\dot{Y} + \rho U^2 c_k Y\Big]. \tag{2.1.12}$$

After some manipulation, equation (2.1.12) can be written as

$$\left(M+\frac{\rho\pi D^2}{4}\right)\ddot{Y}(t)+\left[2\zeta_s\omega_0 M+\frac{F_D(t)}{U}-\frac{\rho U^2}{\bar{\omega}_0}c_d\right]\dot{Y}(t)+\left(M\omega_0^2-\rho U^2 c_k\right)Y(t)=F_L(t). \tag{2.1.13}$$

Using equations (2.1.6), equation (2.1.13) can be simplified as

$$\ddot{Y}(t)+\left\{2\bar{\zeta}_s\bar{\omega}_0+\frac{U\left[\bar{C}_D+C_D\cos\eta_D(t)\right]}{2DM_r}-\frac{U^2}{\bar{\omega}_0 D^2 M_r}c_d\right\}\dot{Y}(t)+\bar{\omega}_0^2 Y(t)=\frac{U^2}{2DM_r}C_L\cos\eta_L(t), \tag{2.1.14}$$

where

$$\bar{M}=M+\frac{\rho\pi D^2}{4}, \qquad M_r=\frac{\bar{M}}{\rho D^2},$$

$$\bar{\omega}_0=\sqrt{\frac{M\omega_0^2-\rho U^2 c_k}{\bar{M}}}, \qquad \bar{\zeta}_s=\frac{\omega_0 M}{\bar{\omega}_0\bar{M}}\zeta_s,$$

$$\eta_D(t)=\nu_D t+\sigma_D W(t)+\phi_D, \qquad \eta_L(t)=\nu_L t+\sigma_L W(t)+\phi_L.$$

Non-dimensionalizing equation (2.1.14) with respect to U and D, and applying the time scaling $\tau=\bar{\omega}_0 t$, the equation becomes

$$Y''(\tau)+\left[2\bar{\zeta}_s+\frac{\bar{U}_{r0}}{2\pi}\frac{\bar{C}_D+C_D\cos\tilde{\eta}_D(\tau)}{2M_r}-\frac{\bar{U}_{r0}^2}{4\pi^2}\frac{c_d}{M_r}\right]Y'(\tau)+Y(\tau)=\frac{\bar{U}_{r0}^2}{4\pi^2}\frac{C_L}{M_r}\cos\tilde{\eta}_L(\tau), \tag{2.1.15}$$

where

$$\bar{U}_{r0}=\frac{2\pi U}{\bar{\omega}_0 D}=\text{the reduced velocity},$$

$$\tilde{\eta}_D(t)=\tilde{\nu}_D t+\tilde{\sigma}_D W(t)+\phi_D, \qquad \tilde{\nu}_D=\frac{\nu_D}{\bar{\omega}_0}, \qquad \tilde{\sigma}_D=\frac{\sigma_D}{\sqrt{\bar{\omega}_0}},$$

$$\tilde{\eta}_L(t)=\tilde{\nu}_L t+\tilde{\sigma}_L W(t)+\phi_L, \qquad \tilde{\nu}_L=\frac{\nu_L}{\bar{\omega}_0}, \qquad \tilde{\sigma}_L=\frac{\sigma_L}{\sqrt{\bar{\omega}_0}}.$$

Letting

$$\beta=2\bar{\zeta}_s+\frac{\bar{U}_{r0}}{2\pi}\frac{\bar{C}_D}{2M_r}-\frac{\bar{U}_{r0}^2}{4\pi^2}\frac{c_d}{M_r}, \qquad \mu_D=\frac{\bar{U}_{r0}}{2\pi}\frac{C_D}{M_r}, \qquad \mu_L=\frac{\bar{U}_{r0}^2}{4\pi^2}\frac{C_L}{M_r}, \tag{2.1.16}$$

equation (2.1.15) can be written as

$$Y''(\tau)+\left[\beta+\mu_D\cos\tilde{\eta}_D(\tau)\right]Y'(\tau)+Y(\tau)=\mu_L\cos\tilde{\eta}_L(\tau). \tag{2.1.17}$$

From equation (2.1.17), one can see that two sources are responsible for cylinder vibration: $\mu_L \cos\tilde{\eta}_L(\tau)$, which may lead to the main resonance if $\tilde{\nu}_L = \nu_L/\bar{\omega}_0 = 1$, and $\beta + \mu_D \cos\tilde{\eta}_D(\tau)$, which may give rise to a negative-damping-induced instability or a parametric instability depending on the relationship between β, μ_D, and $\tilde{\eta}_D(\tau)$. This is studied in detail in the following chapter.

2.2 A Spring-Supported Cylinder in Shear Flow

In the present study, a single circular cylinder in a shear flow with free stream turbulence is considered and it is hoped that through the investigation the mechanisms that contribute to fluid-structure instability could be identified and the stabilizing effect of free stream turbulence could be analyzed in detail.

In the present study, the model developed in Zhu *et al.* [104] is extended to take the effects of shear flow and free stream turbulence into account. A general model is first proposed. It is then reduced to a simplified one for dynamic analysis of a single cylinder in a turbulent shear flow at large U_r values.

2.2.1 Deterministic Modeling

Consider an elastically supported rigid cylinder in a cross-flow. The approaching flow is assumed to be a linear shear flow and two-dimensional. The equations of motion of the cylinder can be written as

$$\begin{aligned} \ddot{x}(t) + 2\zeta_s\omega_x\dot{x}(t) + \omega_x^2 x(t) &= \frac{F^X(t)}{M}, \\ \ddot{y}(t) + 2\zeta_s\omega_y\dot{y}(t) + \omega_y^2 y(t) &= \frac{F^Y(t)}{M}, \end{aligned} \tag{2.2.1}$$

where $x(t)$ and $y(t)$ are cylinder displacements in the stream-wise and the cross-flow directions, respectively, ω_x and ω_y are the natural frequencies, ζ_s is the nondimensional structural damping coefficient, and M is the mass per unit length of the cylinder. $F^X(t)$ and $F^Y(t)$ are flow-induced forces per unit length acting on the cylinder in the stream-wise and the cross-flow directions, respectively, and they are defined in equations (2.1.2)

2.2.1.1 Modeling of Motion-Dependent Forces

Cylinder vibration induces fluid forces, such as the added mass and the fluid damping force. In the present study, they are approximated in a linear combination as

$$\left\{ \begin{array}{c} F_M^X \\ F_M^Y \end{array} \right\} = -\frac{\rho\pi D^2}{4} \left[\begin{array}{cc} c_m^x & c_m^{xy} \\ c_m^{yx} & c_m^y \end{array} \right] \left\{ \begin{array}{c} \ddot{x} \\ \ddot{y} \end{array} \right\} + \frac{\rho U^2}{\omega_0} \left[\begin{array}{cc} c_d^x & c_d^{xy} \\ c_d^{yx} & c_d^y \end{array} \right] \left\{ \begin{array}{c} \dot{x} \\ \dot{y} \end{array} \right\} + \rho U^2 \left[\begin{array}{cc} c_k^x & c_k^{xy} \\ c_k^{yx} & c_k^y \end{array} \right] \left\{ \begin{array}{c} x \\ y \end{array} \right\}, \tag{2.2.2}$$

where c_m, c_d, and c_k are the added mass, the fluid damping, and the fluid stiffness coefficients, respectively. In general, the added mass is considered to be equal to the mass of fluid pushed by the vibrating cylinder. In light fluids such as air, the added mass is usually negligible. As a first approximation, the fluid damping force is assumed to be proportional to the velocity of cylinder vibration. The fluid stiffness term affects only the natural frequency of the fluid-structure system.

2.2.1.2 Modeling of Vortex-Induced Forces

The model developed by Zhu *et al.* [104] is extended to represent vortex-induced forces acting on a vibrating cylinder in shear flow. The basic idea of this model is illustrated in Figure 2.2. According to the model, when the velocity of cylinder vibration is small compared with the flow velocity, it is considered that the unsteady vortex-induced forces acting on a vibrating cylinder are equal to the vortex-induced forces acting on the same but stationary cylinder at the instantaneous position, but with the direction of the approach flow changed by the velocity of cylinder vibration. For the stationary cylinder as at its initial position, vortex-induced forces are steady-state and can be represented by the bounded noise processes. Vortex-induced forces are thus expressed as

$$\begin{aligned} F^X(t) &= F_{V_0}^X(t) \cdot \cos\theta(t) + F_{V_0}^Y(t) \cdot \sin\theta(t), \\ F^Y(t) &= F_{V_0}^Y(t) \cdot \cos\theta(t) - F_{V_0}^X(t) \cdot \sin\theta(t), \end{aligned} \tag{2.2.3}$$

where $F_{V_0}^X(t)$ and $F_{V_0}^Y(t)$ are the drag and lift forces acting on the stationary cylinder, θ is the angle between the x-axis and the instantaneous velocity vector of cylinder vibration given by

$$\theta(t) = \tan^{-1} \frac{\dot{Y}}{U - \dot{x}}.$$

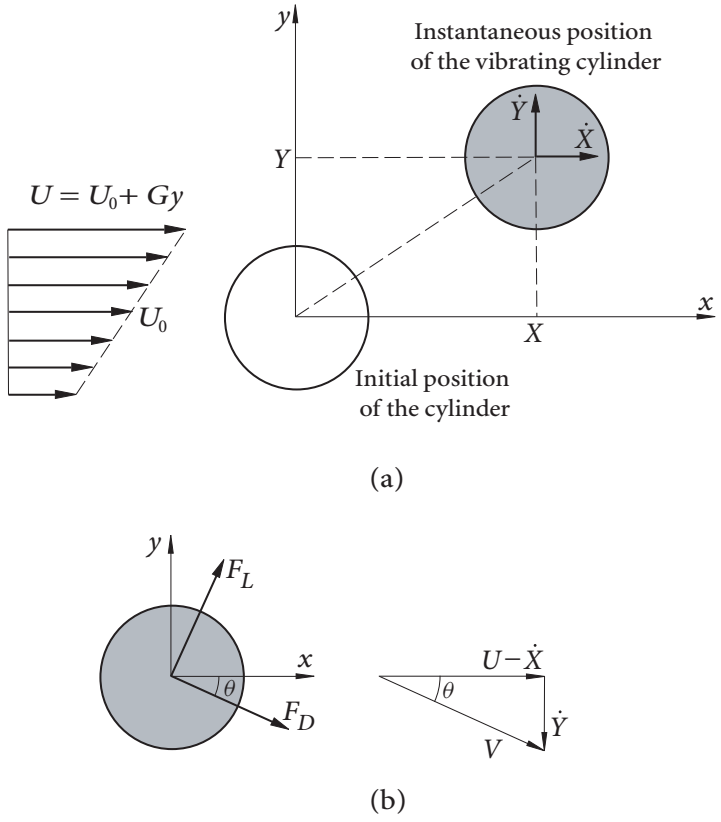

Figure 2.2 Illustration of the flow-induced forces. (a) a cylinder subjected to a shear flow; (b) drag and lift forcesacting on the vibrating cylinder.

In a shear flow, the force coefficients can be expanded in terms of small displacements of the cylinder, x and y, from its original position $(0,0)$, i.e.,

$$F^X_{V_0}(t) = \tfrac{1}{2}\rho V^2 D\Big[C_D(0,0,t) + \frac{\partial C_D(0,0,t)}{\partial x}x + \frac{\partial C_D(0,0,t)}{\partial y}y\Big],$$

$$F^Y_{V_0}(t) = \tfrac{1}{2}\rho V^2 D\Big[C_L(0,0,t) + \frac{\partial C_L(0,0,t)}{\partial x}x + \frac{\partial C_L(0,0,t)}{\partial y}y\Big],$$

where V is the relative velocity.

Since the local velocity is also a function of the coordinate y, i.e., $U = U_0 + Gy$, where G is the flow velocity gradient, the derivatives with respect to x are zero, i.e., $\partial C_D/\partial x = \partial C_L/\partial x = 0$, in the expressions above. When the cylinder velocity is much smaller than the flow velocity, i.e., $\dot{x}(t) \ll U$ and $\dot{y}(t) \ll U$, the relative velocity can be approximated as

$$V^2(t) = \big(U_0 + Gy - \dot{x}\big)^2 + \dot{y}^2 \approx U_0^2\Big(1 + 2\frac{Gy - \dot{x}}{U_0}\Big).$$

For small amplitude vibration, however, a linear approximation can be invoked in the present study, i.e.,

$$\sin\theta(t) = \frac{\dot{y}(t)}{\sqrt{\left[U_0 + Gy - \dot{x}(t)\right]^2 + \dot{y}^2(t)}} \approx \frac{\dot{y}(t)}{U_0},$$
$$\cos\theta(t) = \frac{U_0 + Gy - \dot{x}(t)}{\sqrt{\left[U_0 + Gy - \dot{x}(t)\right]^2 + \dot{y}^2(t)}} \approx 1.$$

Hence, the vortex forces can be approximated as

$$\begin{aligned} F_V^X &= \tfrac{1}{2}\rho U_0^2 D\Big(C_D + \frac{\partial C_D}{\partial y}y + 2\frac{Gy - \dot{x}}{U_0}C_D + \frac{\dot{y}}{U_0}C_L\Big), \\ F_V^Y &= \tfrac{1}{2}\rho U_0^2 D\Big(C_L + \frac{\partial C_L}{\partial y}y + 2\frac{Gy - \dot{x}}{U_0}C_L - \frac{\dot{y}}{U_0}C_D\Big). \end{aligned} \tag{2.2.4}$$

2.2.2 Description and Effect of Turbulence

The effects of turbulence are considered in two aspects: one is the effect on the free-stream velocity of the incoming flow, and the other is the effect on the flow-induced forces applied to the cylinder. The latter effect exists even though the incoming flow is smooth in cylinder arrays, because the upstream cylinders act as the turbulence generators. For the description of a turbulent flow field statistical methods are commonly used.

2.2.2.1 Statistical Description of Turbulence

For the case of one dimensional flow, the flow velocity can be written as the sum of the mean value $\bar{U}(x)$ and the fluctuating part $\tilde{U}(t)$.

$$U(x,t) = \bar{U}(x) + \tilde{U}(x,t) = \bar{U}(x)\big[1 + \xi(t)\big], \tag{2.2.5}$$

where $\xi(t)$ is a random process of mean zero.

A common assumption for the flow field is that the velocity is a normally distributed stationary random process. Then the velocity distribution is well-defined by the mean value $\bar{U}$ and the standard deviation σ. If the velocity is further assumed as an ergodic process, the ensemble mean value and the standard deviation can be obtained from a sufficiently long averaging in time,

$$\bar{U}(x) = \lim_{T\to\infty}\frac{1}{T}\int_0^T U(x,t)\mathrm{d}t,$$

$$\sigma^2(x) = \lim_{T\to\infty} \frac{1}{T} \int_0^T \left[U(x,t) - \bar{U}(x)\right]^2 \mathrm{d}t.$$

Combining these two values for a flow with the main flow direction x, the turbulence intensity T_u can be defined

$$T_u = \frac{\sigma}{\bar{U}}. \tag{2.2.6}$$

Furthermore, the flow states are correlated in space and time, which can be described by the space-time covariance function

$$R(x,t,\Delta x,\tau) = \lim_{T\to\infty} \frac{1}{T} \int_0^T \tilde{U}(x,t)\tilde{U}(x+\Delta x, t+\tau)\mathrm{d}t, \tag{2.2.7}$$

where Δx is the offset distance and τ is the offset time. From the space-time covariance function the length scale of turbulence, which describes the average length of a turbulence eddy,

$$L_x = \frac{1}{R(x,t,0,0)} \int_0^{+\infty} R(x,t,y,0)\mathrm{d}y \tag{2.2.8}$$

can be calculated as the spatial character of the flow field. If the flow field is homogeneous, the covariance function is even and the length scale is independent of the position x. Then L_x can be determined at any position x_0 by

$$L_x = \frac{1}{\sigma^2(x_0)} \int_0^{+\infty} R(x_0,t,y,0)\mathrm{d}y. \tag{2.2.9}$$

More details on the statistical description of turbulence can be found in [40] and [69].

2.2.2.2 Stochastic Model of Turbulence

Turbulence can be modeled as a stochastic process. Depending on the characteristics of the power spectral density functions of the turbulent flow, various random processes may be used to model the turbulence. A wind turbulence model was presented by Lin and Li [45] to account for the fluctuating stream-wise velocity of the incoming turbulent flow. The model is essentially a bounded noise process whose spectrum fits experimental measurement of wind velocity spectrum well. The model was used for stability analysis of bridge deck in turbulent flow. The same idea was employed by Namachchivaya and Vedula [55] to explain the stabilizing effect of turbulence on two cylinders. In Namachchivaya and Vedula [55], the quasi-steady flow theory was used to derive the fluid forces, and a real noise process was applied to model the turbulent flow. Moshchuk *et al.* [50] modeled the Gaussian random

sea waves as the output of a shaping filter. They used different shaping filters and compared the results. Solari and Piccardo [77] reviewed the turbulence modeling and proposed a three dimensional turbulence model tailored to determine the gust buffeting response of structures. The parameters in their turbulence model were derived from the experimental measurements.

2.2.2.3 Modeling of Grid-Generated Turbulence

One of the objectives in this study is to develop the proper models of grid-generated turbulence in cross-flow to account for the effects of turbulence on the fluid forces, which is discussed as follows.

The effect of free stream turbulence is considered as the disturbance to the main flow velocity of the incoming flow, which furthermore affects the fluid forces applied to the cylinder. Due to the random behavior of turbulence, statistical methods are commonly used to describe the turbulence. Grid-generated turbulence is approximately stationary, homogeneous, and isotropic (see, e.g., Batchelor [11]), which can be modeled by a stochastic process. To simplify the problem, only the turbulence in the main flow direction is considered.

For the case of one dimensional flow, the flow velocity can be written as the sum of the mean value $\bar{U}$ and the fluctuating part $\tilde{U}$

$$U(t) = \bar{U} + \tilde{U} = \bar{U} + \eta(t),$$

where $\eta(t)$ is a random process of mean zero.

Experiments have shown that the space correlation function $f(r)$ has the form

$$f(r) = f(0)\exp(-r/L_x),$$

where r is the distance between two correlated points in the x direction, and L_x is the length scale of turbulence defined by equation (2.2.9).

If the field of fluctuating velocity is superimposed upon a mean flow of velocity $\bar{U}$ in the x-direction, and if the turbulence is small compared with the mean flow, the turbulence can be thought of being convected by the mean velocity $\bar{U}$ without evolution, which is known as Taylor's hypothesis. Thus, it is possible to interchange time and space variables. The correlation function in time is related to the correlation function in space by replacing the time τ by $r/\bar{U}$, i.e.

$$\mathrm{E}\big[\tilde{U}(t)\tilde{U}(t+\tau)\big] = R(\tau) = f(\tau U), \tag{2.2.10}$$

where $R(\tau)$ is the correlation function in time.

Hence, the corresponding time correlation function is given by

$$R(\tau) = f(\tau U) = R(0)\exp\left(-|\tau|\bar{U}/L_x\right). \tag{2.2.11}$$

Since $R(0) = f(0) = \sigma_x^2$, the time correlation function (2.2.11) at some fixed point in the flow field can be described by

$$R(\tau) = \sigma_x^2 \exp\left(-|\tau|\bar{U}/L_x\right). \tag{2.2.12}$$

Based on the experimental observations of grid-generated turbulence, the fluctuating velocity $\tilde{U}$ can be modeled by an Ornstein-Uhlenbeck process (see, e.g., Pope [63]). An Ornstein-Uhlenbeck process $\eta(t)$ is defined by the one-dimensional Itô stochastic differential equation

$$\mathrm{d}\eta(t) = -\alpha\,\eta(t)\,\mathrm{d}t + \sigma\,\mathrm{d}W(t), \quad \eta(t_0) = \eta_0.$$

The probability density function $f(\eta, t)$ evolves by the Fokker-Planck equation

$$\frac{\partial f}{\partial t} = \frac{\sigma^2}{2}\frac{\partial^2 f}{\partial \eta^2} + \alpha\frac{\partial (f\eta)}{\partial \eta}. \tag{2.2.13}$$

If the initial condition η_0 is normal with mean 0 and variance $\sigma^2/(2\alpha)$, i.e., $\eta_0 \sim N\left(0, \sigma^2/(2\alpha)\right)$, then $\eta(t)$ is a stationary Gaussian process with mean zero, $\mathrm{E}\left[\eta(t)\right] = 0$, and the correlation function is given by

$$R(\tau) = \mathrm{E}\left[\eta(t)\,\eta(t+\tau)\right] = \frac{\sigma^2}{2\alpha}\,\mathrm{e}^{-\alpha|\tau|}. \tag{2.2.14}$$

A limitation of an Ornstein-Uhlenbeck process is that $\eta(t)$ is nowhere differentiable, which is incorrect in reality. For further details, refer to the book by Pope [63].

Comparing the correlation function of the grid-generated turbulence with that of the Ornstein-Uhlenbeck process, from equations (2.2.12) and (2.2.14), one obtains

$$\sigma_x^2 = \frac{\sigma^2}{2\alpha}, \qquad \frac{\bar{U}}{L_x} = \alpha. \tag{2.2.15}$$

Simplifying equations (2.2.15) yields

$$\sigma = \sqrt{\frac{2\bar{U}}{L_x}}\sigma_x, \qquad \alpha = \frac{\bar{U}}{L_x}.$$

For the following analysis of perturbation, let

$$\eta(t) = \sigma_0\,\xi(t),$$

where σ_0 is a small parameter.

By following Itô's formula, one can obtain the governing stochastic differential equation for $\xi(t)$

$$\mathrm{d}\xi(t) = -\alpha\,\xi(t)\,\mathrm{d}t + \sigma_\xi\,\mathrm{d}W(t), \quad \xi(t_0) = \xi_0,$$

where $\sigma_\xi = \sigma/\sigma_0$.

2.2.3 Randomizing Equations of Motion for a Cylinder in Shear Flow

Since the fluctuating velocity is small compared to the mean velocity $\bar{U} = U_0$, one has the following approximation:

$$U^2 = U_0^2\Big[1 + \frac{\sigma_0}{U_0}\xi(t)\Big]^2 \approx U_0^2\big[1 + 2\mu\xi(t)\big].$$

where $\mu = \sigma_0/U_0$ is the noise intensity.

Substituting the above approximate expression into equations (2.2.4), one obtains

$$\begin{aligned} F_{VT}^X &= \tfrac{1}{2}\rho U_0^2 D\big[1 + 2\mu\xi(t)\big]\Big(C_D + \frac{\partial C_D}{\partial y}y\Big) + \tfrac{1}{2}\rho U_0 D\big[1 + \mu\xi(t)\big]\big[2(Gy - \dot{x})C_D + \dot{y}C_L\big], \\ F_{VT}^Y &= \tfrac{1}{2}\rho U_0^2 D\big[1 + 2\mu\xi(t)\big]\Big(C_L + \frac{\partial C_L}{\partial y}y\Big) + \tfrac{1}{2}\rho U_0 D\big[1 + \mu\xi(t)\big]\big[2(Gy - \dot{x})C_L - \dot{y}C_D\big]. \end{aligned} \tag{2.2.16}$$

Similarly, the randomized motion-dependent force is given by

$$\begin{aligned} \begin{Bmatrix} F_M^X \\ F_M^Y \end{Bmatrix} = &-\frac{\rho\pi D^2}{4}\begin{bmatrix} c_m^x & c_m^{xy} \\ c_m^{yx} & c_m^y \end{bmatrix}\begin{Bmatrix} \ddot{x} \\ \ddot{y} \end{Bmatrix} + \frac{\rho U_0^2\big[1 + 2\mu\xi(t)\big]}{\omega_0}\begin{bmatrix} c_d^x & c_d^{xy} \\ c_d^{yx} & c_d^y \end{bmatrix}\begin{Bmatrix} \dot{x} \\ \dot{y} \end{Bmatrix} \\ &+ \rho U_0^2\big[1 + 2\mu\xi(t)\big]\begin{bmatrix} c_k^x & c_k^{xy} \\ c_k^{yx} & c_k^y \end{bmatrix}\begin{Bmatrix} x \\ y \end{Bmatrix}. \end{aligned} \tag{2.2.17}$$

Substituting equations (2.2.16) and (2.2.17) into equation (2.2.1), one can obtain the equations of motion for a cylinder in turbulent shear flow, which includes vortex-induced force, motion-dependent force, and turbulence. When the effects of free-stream turbulence and shear flow are removed, this general model is reduced to the model of Zhu *et al.* [104] for a cylinder in uniform cross-flow. Zhu *et al.* [104] showed that parametric resonance could occur due to the interaction between x- and y-directions at lock-in range. Both motion-dependent force and vortex shedding play a significant role in the vibration.

Yu *et al.* [100] found experimentally that the fluidelastic instability would occur at high reduced velocity ($U_r > 100$) from Re = 8 to 120. At this range of high U_r, the experimental results of Chen *et al.* [21] showed that the motion-dependent damping and stiffness forces approached zero for a single cylinder in the cross-flow, which can be neglected. Thus, the model is reduced to that of Yu *et al.* [100]. Non-dimensionalizing the equations of motion with respect to U_0 and D, and applying the time scaling $\tau = \omega_x t$, the equations of motion become

$$X'' + \left\{2\zeta + \frac{U_r\left[1+\mu\xi(\tau)\right]C_D}{M_r}\right\}X' + X - \left\{\frac{U_r^2\left[1+2\mu\xi(\tau)\right]}{2M_r}\frac{\partial C_D}{\partial Y} + \frac{U_r^2\left[1+2\mu\xi(\tau)\right]KC_D}{M_r}\right\}Y - \frac{U_r\left[1+\mu\xi(\tau)\right]C_L}{2M_r}Y' = \frac{U_r^2\left[1+2\mu\xi(\tau)\right]C_D}{2M_r}, \quad (2.2.18a)$$

$$Y'' + k\left\{2\zeta + \frac{U_r\left[1+\mu\xi(\tau)\right]C_D}{2M_r}\right\}Y' + k^2\left\{1 - \frac{U_r^2\left[1+2\mu\xi(\tau)\right]}{2M_r}\frac{\partial C_L}{\partial Y} - \frac{U_r^2\left[1+2\mu\xi(\tau)\right]KC_L}{M_r}\right\}Y + \frac{kU_r\left[1+2\mu\xi(\tau)\right]C_L}{M_r}X' = \frac{k^2U_r^2\left[1+2\mu\xi(\tau)\right]C_L}{2M_r}, \quad (2.2.18b)$$

where

$$M_r = \frac{M}{\rho D^2}, \quad K = \frac{GD}{U_0}, \quad U_r = \frac{U_0}{\omega_x D}, \quad k = \frac{\omega_y}{\omega_x}, \quad X = \frac{x}{D}, \quad Y = \frac{y}{D}.$$

At this range of Reynolds number, the vortex shedding frequency varies slightly between 0.13 and 0.2 (Kang, [37]), which is far away from the natural frequency of the cylinder. Besides, the mass ratio in this study is chosen to be quite high ($M_r = 5112$). Hence, the forced vibration due to vortex shedding is negligible. Furthermore, additive noise does not affect the stability of the system although additive noise could increase the random vibration and delay the exit time of system response to an unstable region (Ibrahim, [36]). For the analysis of fluidelastic instability, one can neglect the right-hand-side forces in equation (2.2.18) yielding, in the "state-space" form,

$$\mathbf{Z}' = \tilde{\mathbf{A}}\mathbf{Z} + \mu\xi(\tau)\tilde{\mathbf{B}}\mathbf{Z}, \quad (2.2.19)$$

where $\mathbf{Z}=[X, Y, X', Y']$,

$$\tilde{\mathbf{A}} = \begin{bmatrix} 0 & 0 & 1 & 0 \\ 0 & 0 & 0 & 1 \\ -1 & \dfrac{U_r^2}{2M_r}\dfrac{\partial C_D}{\partial Y} + \dfrac{U_r^2 K C_D}{M_r} & -\left(2\zeta + \dfrac{U_r C_D}{M_r}\right) & \dfrac{U_r C_L}{2M_r} \\ 0 & k^2\left(-1 + \dfrac{U_r^2}{2M}\dfrac{\partial C_L}{\partial Y} + \dfrac{U_r^2 K C_L}{M_r}\right) & -\dfrac{k U_r C_L}{M_r} & -k\left(2\zeta + \dfrac{U_r C_D}{2M_r}\right) \end{bmatrix},$$

$$\tilde{\mathbf{B}} = \begin{bmatrix} 0 & 0 & 0 & 0 \\ 0 & 0 & 0 & 0 \\ 0 & 2\left(\dfrac{U_r^2}{2M_r}\dfrac{\partial C_D}{\partial Y} + \dfrac{U_r^2 K C_D}{M_r}\right) & -\dfrac{U_r C_D}{M_r} & \dfrac{U_r C_L}{2M_r} \\ 0 & 2k^2\left(\dfrac{U_r^2}{2M_r}\dfrac{\partial C_L}{\partial Y} + \dfrac{U_r^2 K C_L}{M_r}\right) & -\dfrac{k U_r C_L}{M_r} & -\dfrac{k U_r C_D}{2M_r} \end{bmatrix}.$$

If there is no turbulence in the approach flow, the stability of (2.2.19) is determined by the eigenvalues of system matrix $\tilde{\mathbf{A}}$. If the real part of an eigenvalue is positive, the system is unstable. When upstream turbulence is significant, the stability of (2.2.19) depends on $\tilde{\mathbf{A}}$, $\tilde{\mathbf{B}}$, and the characteristics of noise term $\xi(t)$. Thus, a stochastic method has to be applied to explore the stability of the system, which is introduced in Chapter 4.

2.3 Conclusion

In this Chapter, a model previously proposed to study vortex-induced vibration of a single cylinder in a cross-flow is extended to include motion-dependent fluid forces, in an attempt to understand its dynamic behavior, especially in the lock-in region. The equations of motion for the cylinder placed in a uniform cross-flow are set up, in which the vortex force is modeled by a bounded noise because of its narrow-band characteristics. Since the vibration in the lift direction is more prominent in the lock-in region, the system is reduced to one degree-of-freedom, i.e., only the vibration of the cylinder in the lift direction is considered. The resulting equation of motion indicates that the system can be in main resonance or undergo parametric instability due to the bounded noise; the latter case is studied in Chapter 3 using the theory of stochastic dynamic stability.

For a cylinder in a shear flow, the shear effect has to be taken into account to explain the fluidelastic instability of the cylinder when the reduced velocity is high. A quasi-steady

model is used to model the vortex-induced forces, while the motion- dependent forces are neglected since they are quite small for high reduced velocity. To investigate the effects of turbulence on the stability, the grid-generated turbulence is modeled by an Ornstein-Uhlenbeck process with Gaussian distribution and zero mean. Thus, the equations of motion are randomized, resulting in a four-dimensional system excited by a real noise. The stability of the four-dimensional stochastic system is studied in Chapter 4.

CHAPTER 3

Flow-Induced Instability under Bounded Noise Excitation in Cross-Flow

The equation of motion for many problems of flow-induced vibration is of the general form (see, e.g., equation (2.1.17) in Chapter 2)

$$q''(\tau) + \left[2\varepsilon_0\beta + \varepsilon_0\mu\zeta(\tau)\right]q'(\tau) + \omega_0^2 q(\tau) + f\left(q, q', \varepsilon_0\zeta(\tau)\right) = 0, \tag{3.0.1}$$

where the prime denotes differentiation with respect to the time variable τ, q is the generalized coordinate, β the damping constant, ω_0 the circular natural frequency, ε_0 a small fluctuation parameter, $f\left(q, q', \varepsilon_0\zeta(\tau)\right)$ a nonlinear function, and $\zeta(\tau)$ a stochastic process describing the random property of the flow.

It is natural to ask how the parametric random fluctuation $\zeta(\tau)$ can influence the dynamic stability of system (3.0.1). The dynamical stability of the trivial solution of system (3.0.1) is governed by the stability of the trivial solution of the linearized equation

$$q''(\tau) + \left[2\varepsilon_0\beta + \varepsilon_0\mu\zeta(\tau)\right]q'(\tau) + \omega_0^2 q(\tau) = 0. \tag{3.0.2}$$

Systems excited by stochastic processes in the damping term or stiffness term could become unstable through parametric resonance. Bobryk and Chrzeszczyk [17] determined the mean square stability of a harmonic oscillator which is under parametric resonance induced by a colored Gaussian noise. Xie [97] studied the parametric stability of a two-dimensional system under real noise excitation. In this chapter, the Lyapunov exponent and

moment Lyapunov exponent of the system under bounded noise excitation in the damping term are determined. Analytical results and numerical results are compared to validate the approach.

In Section 3.2, the results obtained in Section 3.1 are used to explore the stability of a cylinder in a cross-flow. It is shown that parametric instability could occur, other than the large-amplitude forced vibration, in the lock-in range, which gives more insight into the mechanism of the lock-in phenomenon.

3.1 Stability of a Two-Dimensional System under Stochastic Parametric Excitation

For a single degree-of-freedom system described by (2.1.17)

$$Y''(\tau) + \left[\beta + \mu_D \cos\tilde{\eta}_D(\tau)\right] Y'(\tau) + Y(\tau) = \mu_L \cos\tilde{\eta}_L(\tau),$$

there exist two types of excitations: the forcing excitation $\mu_L \cos\tilde{\eta}_L(\tau)$ on the right-hand-sid of the equation and the parametric excitation $\beta+\mu_D \cos\tilde{\eta}_D(\tau)$ on the left-hand-side of the equation. The forcing excitation induces main resonance when its frequency is close to the natural frequency of the system, at which point large amplitude vibration occurs when the system damping is small. In particular, if the system is undamped, the amplitude of response grows linearly with time.

The parametric excitation occurs in the damping of the system, $\beta+\mu_D \cos\tilde{\eta}_D(\tau)$; the system damping consists of a constant component and a time-dependent component expressed in the form of a bounded noise. When the constant system damping β is negative, the system becomes unstable regardless of the value of $\mu_D \cos\tilde{\eta}(\tau)$. It can be seen that β is related to three quantities: the structural damping ζ_s, the mean drag coefficient $\bar{C}_D$, and the motion-dependent fluid damping c_d. Both ζ_s and $\bar{C}_D$ are positive and their effect is to increase the system damping, thus would not induce unstable motion of the system. The one which may induce negative system damping is the fluid damping coefficient c_d. The condition for $\beta < 0$ is given by

$$c_d > \frac{4\pi^2 M_r}{U_r^2}\left(2\bar{\zeta}_s + \frac{\bar{U}_{r0}}{2\pi}\frac{\bar{C}_D}{2M_r}\right). \tag{3.1.1}$$

Equation (3.1.1) shows that once c_d is large enough, the system becomes unstable. Such instability can be termed as a constant-fluid-damping-induced instability.

When β is positive and its value is larger than μ_D ($\beta > \mu_D$), the system is stable. In this case, the main resonance due to the forcing excitation plays a dominant role in the response. When β is positive and its value is smaller than μ_D ($\beta < \mu_D$), the stability of the system depends on the time-dependent fluid-damping component $\mu_D \cos\tilde{\eta}(\tau)$. Whatever value β might have, the time-dependent fluid-damping component $\mu_D \cos\tilde{\eta}(\tau)$ always tends to destabilize the system provided that its dominant frequency is in the vicinity of twice of the natural frequency of the system. When parametric instability is induced, the amplitude of cylinder vibration grows exponentially even when $\beta \neq 0$. In this case, parametric resonance becomes much more pronounced than the main resonance. The theory of stochastic instability has to be applied to investigate the parametric stability of the system, as presented in the following. Since the forcing term does not affect the parametric instability, it is dropped in the following stability analysis.

3.1.1 Formulation

Consider the dynamic behaviour of the following parametrically excited, two-dimensional system

$$\begin{aligned} &\frac{\mathrm{d}^2 q(\tau)}{\mathrm{d}\tau^2} + \left[2\varepsilon_0\beta + \varepsilon_0\mu\cos\eta(\tau)\right]\frac{\mathrm{d}q(\tau)}{\mathrm{d}\tau} + \omega_0^2 q(\tau) = 0, \\ &\eta(\tau) = \nu_0\tau + \sigma_0 W(\tau) + \theta, \end{aligned} \tag{3.1.2}$$

in which $\cos\eta(\tau)$ is a bounded noise, and θ is a uniformly distributed random number in $(0, 2\pi)$ that makes $\cos\eta(\tau)$ a stationary process.

For the two-dimensional system (3.1.2), the damping term can be removed by the transformation $q(\tau) = x(\tau)\mathrm{e}^{-\varepsilon_0\beta\tau}$ and further simplified using the time scaling $t = \omega\tau$, where $\omega^2 = \omega_0^2 - \varepsilon_0^2\beta^2$, to yield

$$\begin{aligned} &\frac{\mathrm{d}^2 x(t)}{\mathrm{d}t^2} + \varepsilon\mu\cos\tilde{\eta}(t)\frac{\mathrm{d}x(t)}{\mathrm{d}t} + \left[1 - \varepsilon^2\mu\beta\cos\tilde{\eta}(t)\right]x(t) = 0, \\ &\mathrm{d}\tilde{\eta}(t) = \nu\,\mathrm{d}t + \sigma\,\mathrm{d}W(t), \end{aligned} \tag{3.1.3}$$

where $\varepsilon = \varepsilon_0/\omega$, $\nu = \nu_0/\omega$, and $\sigma = \sigma_0/\sqrt{\omega}$. The Lyapunov exponents and the moment Lyapunov exponents of systems (3.1.2) and (3.1.3) are related by

$$\lambda_{q(\tau)} = -\varepsilon_0\beta + \omega\lambda_{x(t)}, \qquad \Lambda_{q(\tau)}(p) = -p\cdot\varepsilon_0\beta + \omega\Lambda_{x(t)}(p).$$

In the absence of noise, i.e. when $\sigma=0$, the bounded noise reduces to a sinusoidal function and system (3.1.3) is in primary parametric resonance when ν is in the vicinity of 2 (see, e.g., Xie [99]). In order to have an understanding of the effect of noise on the parametric resonance, it is important and interesting to study the dynamic stability of system (3.1.3) under the excitation of a narrow-band process about $\nu=2$, which can be achieved with the bounded noise for small values of σ.

Hence, the following two-dimensional system under bounded noise excitation is considered

$$\begin{aligned} &\frac{\mathrm{d}^2y(t)}{\mathrm{d}t^2}+\varepsilon\mu\cos\eta(t)\frac{\mathrm{d}y(t)}{\mathrm{d}t}+\left[1-\varepsilon^2\mu\beta\cos\eta(t)\right]y(t)=0,\\ &\mathrm{d}\eta(t)=\nu\,\mathrm{d}t+\varepsilon^{1/2}\sigma\,\mathrm{d}W(t). \end{aligned} \tag{3.1.4}$$

The introduction of the scaling parameter $\varepsilon^{1/2}$ in the noise fluctuation term $\sigma\,\mathrm{d}W(t)$ renders the bounded noise a narrow-band process for $\varepsilon=o(1)$ and $\sigma=\mathcal{O}(1)$.

The eigenvalue problem governing the moment Lyapunov exponent of system (3.1.4) can be set up using Wedig's approach [91]. System (3.1.4) can be rewritten as a three-dimensional system

$$\mathrm{d}\begin{Bmatrix} y_1\\ y_2\\ \eta\end{Bmatrix}=\begin{Bmatrix} y_2\\ -\left(1-\varepsilon^2\mu\beta\cos\eta\right)y_1-\varepsilon\mu\cos\eta\, y_2\\ \nu\end{Bmatrix}\mathrm{d}t+\begin{Bmatrix} 0\\ 0\\ \varepsilon^{1/2}\sigma\end{Bmatrix}\mathrm{d}W.$$

Khasminskii's transformation

$$\cos\varphi=\frac{y_1}{a},\qquad \sin\varphi=\frac{y_2}{a},\qquad a=\|\mathbf{y}\|=\left(y_1^2+y_2^2\right)^{1/2},$$

can be applied to transform the Cartesian coordinates (y_1,y_2) to the polar coordinates (a,φ), and the pth norm of $\mathbf{y}=\{y_1,y_2\}^T$ is defined as $P=a^p$. The Itô equations for P and φ can be derived using Itô's Lemma

$$\mathrm{d}P=pP\sin\varphi\cos\eta\,(-\varepsilon\mu\sin\varphi+\varepsilon^2\beta\mu\cos\varphi)\mathrm{d}t,$$

$$\mathrm{d}\varphi=(-1-\varepsilon\mu\sin\varphi\cos\varphi\cos\eta+\varepsilon^2\mu\beta\cos^2\varphi\cos\eta)\,\mathrm{d}t.$$

Applying a linear stochastic transformation

$$S=T(\eta,\varphi)P,\quad P=T^{-1}(\eta,\varphi)S,\quad -\infty<\eta<+\infty,\quad 0\leqslant\varphi<\pi,$$

the Itô equation for the transformed pth norm process S can also be derived using Itô's Lemma

$$\begin{aligned} \mathrm{d}S = \Big[\tfrac{1}{2}\varepsilon\sigma^2 T_{\eta\eta} + \nu T_\eta - \big(1 + \varepsilon\mu\sin\varphi\cos\varphi\cos\eta - \varepsilon^2\mu\beta\cos^2\varphi\cos\eta\big) T_\varphi \\ + pP\sin\varphi\cos\eta\big(-\varepsilon\mu\sin\varphi + \varepsilon^2\beta\mu\cos\varphi\big) T \Big] P\,\mathrm{d}t + \varepsilon^{1/2}\sigma T_\eta P\,\mathrm{d}W. \end{aligned} \tag{3.1.5}$$

For bounded and non-singular transformation $T(\eta,\varphi)$, both processes P and S are expected to have the same stability behaviour. Therefore, $T(\eta,\varphi)$ is chosen so that the drift term of the Itô differential equation (3.1.5) is independent of the noise process $\eta(t)$ and the phase process φ so that

$$\mathrm{d}S = \Lambda S\,\mathrm{d}t + \varepsilon^{1/2}\sigma T_\eta T^{-1} S\,\mathrm{d}W. \tag{3.1.6}$$

Comparing equations (3.1.6) and (3.1.5), it is seen that such a transformation $T(\eta,\varphi)$ is given by the following equation

$$\begin{aligned} &\tfrac{1}{2}\varepsilon\sigma^2 T_{\eta\eta} + \nu T_\eta - \big(1 + \varepsilon\mu\sin\varphi\cos\varphi\cos\eta - \varepsilon^2\mu\beta\cos^2\varphi\cos\eta\big) T_\varphi \\ &+ pP\sin\varphi\cos\eta\big(-\varepsilon\mu\sin\varphi + \varepsilon^2\beta\mu\cos\varphi\big) T = \Lambda T, \quad -\infty < \eta < +\infty, \quad 0 \leqslant \varphi < \pi, \end{aligned} \tag{3.1.7}$$

in which $T(\eta,\varphi)$ is a periodic function in φ of period π and is bounded when $\eta \to \pm\infty$. Equation (3.1.7) defines an eigenvalue problem of a second-order differential operator with Λ being the eigenvalue and $T(\eta,\varphi)$ the associated eigenfunction. From equation (3.1.6), the eigenvalue Λ is seen to be the Lyapunov exponent of the pth moment of system (3.1.4), i.e. $\Lambda = \Lambda_{y(t)}(p)$.

3.1.2 Weak Noise Expansions of the Moment Lyapunov Exponent

3.1.2.1 Perturbation Expansion

For weak noise excitation, i.e. for $0 < \varepsilon \ll 1$, perturbation methods can be applied to solve the partial differential eigenvalue problem (3.1.7) for the perturbative expansions of the moment Lyapunov exponent $\Lambda_{y(t)}(p)$. Since the small parameter ε appears as a coefficient of the term $T_{\eta\eta}$, a method of singular perturbation (see, e.g., Zauderer [101]) must be applied.

Define $\nu = \nu_0 + \varepsilon\Delta$, where $\nu_0 = 2$ corresponds to the primary parametric resonance in the absence of noise and Δ is the detuning parameter. Applying the transformation

$$\eta = \varepsilon^{1/2}\xi - \nu_0\varphi, \qquad \xi = \varepsilon^{-1/2}(\eta + \nu_0\varphi),$$

equation (3.1.7) becomes

$$\frac{\sigma^2}{2}T_{\xi\xi} - T_\varphi + \varepsilon^{1/2}\Delta T_\xi + \mu\cos\varphi\cos(\varepsilon^{1/2}\xi - 2\varphi)\big(-\varepsilon\sin\varphi + \varepsilon^2\beta\cos\varphi\big)\big(T_\varphi + 2\varepsilon^{-1/2}T_\xi\big) + \mu p\sin\varphi\cos(\varepsilon^{1/2}\xi - 2\varphi)\big(-\varepsilon\sin\varphi + \varepsilon^2\beta\cos\varphi\big)T = \Lambda T, \quad (3.1.8)$$

in which the eigenfunction T is treated as a function of ξ, φ, and ε. Denoting $z = \varepsilon^{1/2}\xi$, the eigenfunction $T(\xi,\varphi,\varepsilon)$ becomes $Y(\xi,z,\varphi,\varepsilon)$. It can be shown that

$$T_\xi = Y_\xi + \varepsilon^{1/2}Y_z, \qquad T_{\xi\xi} = Y_{\xi\xi} + 2\varepsilon^{1/2}Y_{\xi z} + \varepsilon Y_{zz}. \quad (3.1.9)$$

Substituting equation (3.1.9) into equation (3.1.8) leads to

$$\mathscr{L}(p)Y = \Lambda_{y(t)}(p)\,Y, \quad \mathscr{L}(p)Y = \mathscr{L}_0 Y + \varepsilon^{1/2}\mathscr{L}_1 Y + \varepsilon\mathscr{L}_2 Y + \varepsilon^{3/2}\mathscr{L}_3 Y + \varepsilon^2\mathscr{L}_4 Y, \quad (3.1.10)$$

where

$$\mathscr{L}_0 Y = \tfrac{1}{2}\sigma^2 Y_{\xi\xi} - Y_\varphi,$$
$$\mathscr{L}_1 Y = \sigma^2 Y_{\xi z} + \big[\Delta - 2\mu\cos(z-2\varphi)\sin\varphi\cos\varphi\big]Y_\xi,$$
$$\mathscr{L}_2 Y = \tfrac{1}{2}\sigma^2 Y_{zz} + \Delta Y_z - \mu\cos(z-2\varphi)\sin\varphi\cos\varphi(2Y_z + Y_\varphi) - \mu p\cos(z-2\varphi)\sin^2\varphi\, Y\big],$$
$$\mathscr{L}_3 Y = 2\mu\beta\cos(z-2\varphi)\cos^2\varphi Y_\xi,$$
$$\mathscr{L}_4 Y = \mu\cos\varphi\cos(z-2\varphi)\big[\beta\cos\varphi(2Y_z + Y_\varphi) + p\sin\varphi\, Y\big].$$

The eigenvalue $\Lambda_{y(t)}(p)$ and the eigenfunction $Y(\xi,z,\varphi)$ can be expanded in powers series of $\varepsilon^{1/2}$ as

$$\Lambda_{y(t)}(p) = \sum_{n=0}^{\infty}\varepsilon^{n/2}\Lambda_n, \qquad Y(\xi,z,\varphi) = \sum_{n=0}^{\infty}\varepsilon^{n/2}Y_n(\xi,z,\varphi), \quad (3.1.11)$$

where $Y_n(\xi, z, \varphi)$ are periodic functions in φ of period π. Substituting equations (3.1.11) into (3.1.10) yields the following sequence of equations

$$\begin{aligned}
&\mathcal{O}(1): \quad \mathscr{L}_0 Y_0 = \Lambda_0 Y_0,\\
&\mathcal{O}\left(\varepsilon^{1/2}\right): \quad \mathscr{L}_0 Y_1 + \mathscr{L}_1 Y_0 = \Lambda_0 Y_1 + \Lambda_1 Y_0,\\
&\mathcal{O}\left(\varepsilon^{1}\right): \quad \mathscr{L}_0 Y_2 + \mathscr{L}_1 Y_1 + \mathscr{L}_2 Y_0 = \sum_{i=0}^{2} \Lambda_i Y_{n-i},\\
&\mathcal{O}\left(\varepsilon^{3/2}\right): \quad \mathscr{L}_0 Y_3 + \mathscr{L}_1 Y_2 + \mathscr{L}_2 Y_1 + \mathscr{L}_3 Y_0 = \sum_{i=0}^{3} \Lambda_i Y_{n-i},\\
&\mathcal{O}\left(\varepsilon^{n/2}\right): \quad \mathscr{L}_0 Y_n + \mathscr{L}_1 Y_{n-1} + \mathscr{L}_2 Y_{n-2} + \mathscr{L}_3 Y_{n-3} + \mathscr{L}_4 Y_{n-4} = \sum_{i=0}^{n} \Lambda_i Y_{n-i},\\
&\qquad\qquad n = 4, 5, \ldots.
\end{aligned} \tag{3.1.12}$$

3.1.2.2 Zeroth-order perturbation

The zeroth-order perturbation equation is $\mathscr{L}_0 Y_0 = \Lambda_0 Y_0$, or

$$\frac{\sigma^2}{2}\frac{\partial^2 Y_0}{\partial \xi^2} - \frac{\partial Y_0}{\partial \varphi} = \Lambda_0 Y_0. \tag{3.1.13}$$

Since the moment Lyapunov exponent $\Lambda_{y(t)}(p)$ passes through the origin, i.e.

$$\Lambda_{y(t)}(0) = \Lambda_0(0) + \varepsilon^{1/2}\Lambda_1(0) + \varepsilon\Lambda_2(0) + \cdots = 0,$$

one obtains $\Lambda_0(0) = \Lambda_1(0) = \Lambda_2(0) = \cdots = 0$. Because equation (3.1.13) does not contain p explicitly, $\Lambda_0(0) = 0$ implies $\Lambda_0(p) = 0$. Applying the method of separation of variables and letting $Y_0(\xi, z, \varphi) = X_0(\xi) Z_0(z) \Phi_0(\varphi)$, equation (3.1.13) becomes

$$\frac{\sigma^2}{2}\frac{\ddot{X}_0}{X_0} = \frac{\Phi_0'}{\Phi_0} = \kappa.$$

Solving the $\Phi_0(\varphi)$ equation yields $\Phi_0(\varphi) = Ce^{\kappa\varphi}$. For $\Phi_0(\varphi)$ to be a periodic function of period π, the constant $\kappa = 0$ and hence $\Phi_0(\varphi) = C$. The $X_0(\xi)$ equation results in $X_0(\xi) = D_0 + D_1\xi$. For $X_0(\xi)$ to be a bounded function as $\xi \to \pm\infty$, it is required that $D_1 = 0$ and hence $X_0(\xi) = D_0$. The zeroth-order perturbation of the eigenfunction is therefore $Y_0(\xi, z, \varphi) = Z_0(z)$, where $Z_0(z)$ is an arbitrary function of z.

The adjoint equation of (3.1.13) is

$$\frac{\sigma^2}{2}\frac{\partial^2 Y_0^*}{\partial \xi^2} + \frac{\partial Y_0^*}{\partial \varphi} = \Lambda_0 Y_0^*. \tag{5.2.7′}$$

Employing the method of separation of variables with $Y_0^*(\xi,z,\varphi)=X_0^*(\xi)Z_0^*(z)\Phi_0^*(\varphi)$, it is easy to show that

$$\begin{aligned}&\Phi_0^*(\varphi)=\frac{1}{\pi}, && 0\leqslant\varphi<\pi,\\ &X_0^*(\xi)=\text{constant}, && -\infty<\xi<+\infty,\\ &Y_0^*(\xi,z,\varphi)=Z_0^*(z),\end{aligned} \tag{3.1.14}$$

where $Z_0^*(z)$ is an arbitrary function of z.

3.1.2.3 First-order perturbation

Since $\Lambda_0=0$, the first-order perturbation equation becomes

$$\mathscr{L}_0 Y_1=\Lambda_1 Y_0-\mathscr{L}_1 Y_0. \tag{3.1.15}$$

From the Fredholm Alternative (see Appendix A.1), for equation (3.1.15) to have a non-zero solution, it is required that

$$\left(\Lambda_1 Y_0-\mathscr{L}_1 Y_0,\, Y_0^*\right)=0, \tag{3.1.16}$$

where (f,g) denotes the inner product of functions $f(\xi,z,\varphi)$ and $g(\xi,z,\varphi)$ defined as

$$(f,g)=\int_{z=-\infty}^{+\infty}\int_{\xi=-\infty}^{+\infty}\int_{\varphi=0}^{\pi} f(\xi,z,\varphi)\,g(\xi,z,\varphi)\,\mathrm{d}\varphi\,\mathrm{d}\xi\,\mathrm{d}z.$$

Since $Y_0(\xi,z,\varphi)=Z_0(z)$, which leads to $\mathscr{L}_1 Y_0=0$, equation (3.1.16) results in $\Lambda_1(p)=0$. Equation (3.1.15) then becomes $\mathscr{L}_0 Y_1=0$. Following the same procedure as in Section 3.1.2.2, it is easy to show that $Y_1(\xi,z,\varphi)=Z_1(z)$.

3.1.2.4 Second-order perturbation

Since $\Lambda_0=\Lambda_1=0$, $\mathscr{L}_1 Y_1=0$, the second-order perturbation equation becomes

$$\mathscr{L}_0 Y_2=\Lambda_2 Y_0-\mathscr{L}_2 Y_0. \tag{3.1.17}$$

From the Fredholm Alternative, for equation (3.1.17) to have non-trivial solutions, it is required that

$$\left(\Lambda_2 Y_0-\mathscr{L}_2 Y_0,\, Y_0^*\right)=0,$$

which can be reduced to

$$\int_{z=-\infty}^{+\infty} Z_0^*(z)\left\{\int_{\varphi=0}^{\pi}\left\{\frac{\sigma^2}{2}\ddot{Z}_0(z)+\left[\Delta-2\mu\sin\varphi\cos\varphi\cos(z-2\varphi)\right]\dot{Z}_0(z)\right.\right.$$

$$+\left[-\mu p\sin^2\varphi\cos(z-2\varphi)-\Lambda_2\right]Z_0(z)\Big\}\,\mathrm{d}\varphi\Big\}\,\mathrm{d}z=0. \quad (3.1.18)$$

Since equation (3.1.18) holds for arbitrary $Z_0^*(z)$, it results in

$$\int_{\varphi=0}^{\pi}\left\{\frac{\sigma^2}{2}\ddot{Z}_0(z)+\left[\Delta-2\mu\sin\varphi\cos\varphi\cos(z-2\varphi)\right]\dot{Z}_0(z)\right.$$
$$\left.+\left[-\mu p\sin^2\varphi\cos(z-2\varphi)-\Lambda_2\right]Z_0(z)\right\}\mathrm{d}\varphi=0,$$

which, after performing the integration, leads to

$$\tfrac{1}{2}\sigma^2\ddot{Z}_0(z)+\left(\Delta-\tfrac{1}{2}\mu\sin z\right)\dot{Z}_0(z)+\left(\tfrac{1}{4}\mu p\cos z-\Lambda_2\right)Z_0(z)=0. \quad (3.1.19)$$

This is a second-order ordinary differential eigenvalue problem; Λ_2 is the eigenvalue and $Z_0(z)$ is the corresponding eigenfunction. Equation (3.1.19) can be solved using the Fourier series

$$Z_0(z)=C_0+\sum_{n=1}^{N}\left(C_n\cos nz+S_n\sin nz\right), \quad (3.1.20)$$

where C_0, C_n, S_n, $n=1, 2, \ldots, N$, are constant coefficients to be determined. For the calculation efficiency, the Fourier series is truncated to include N sine and cosine terms.

Substituting equation (3.1.20) into (3.1.19), multiplying the resulting equation by $\cos nz$ and $\sin nz$, for $n=0, 1, \ldots, N$, respectively, lead to a set of $2N+1$ homogeneous linear algebraic equations for C_0, C_n, S_n, $n=1, 2, \ldots, N$. These equations can be written in the matrix form

$$\left[\mathbf{A}-\Lambda_2^{(N)}\mathbf{B}\right]\mathbf{X}=\mathbf{0}, \quad (3.1.21)$$

where the superscript "(N)" signifies that the Fourier series is truncated to include N harmonic terms, $\mathbf{X}=\left\{C_0; C_1, S_1; C_2, S_2; \ldots; C_N, S_N\right\}^T$, and $\mathbf{A}$, $\mathbf{B}$ are matrices of dimension $(2N+1)\times(2N+1)$.

For system (3.1.21) to have non-trivial solutions, the determinant of the coefficient matrix must be zero, i.e.

$$\left|\mathbf{A}-\Lambda_2^{(N)}\mathbf{B}\right|=0,$$

which leads to a polynomial equation for Λ_2 of degree $2N+1$

$$\left[\Lambda_2^{(N)}\right]^{2N+1}+d_{2N}^{(N)}\left[\Lambda_2^{(N)}\right]^{2N}+d_{2N-1}^{(N)}\left[\Lambda_2^{(N)}\right]^{2N-1}+\cdots+d_1^{(N)}\Lambda_2^{(N)}+d_0^{(N)}=0. \quad (3.1.22)$$

Solving equation (3.1.22), one can obtain an approximation of $\Lambda_2^{(N)}$. As a result, the moment Lyapunov exponent can be approximated by

$$\Lambda_{y(t)}(p) \approx \varepsilon \Lambda_2^{(N)}. \tag{3.1.23}$$

Using equation (1.3.4), an approximation of the Lyapunov exponent can be easily obtained

$$\lambda_{y(t)} \approx \varepsilon \lambda_2^{(N)}, \qquad \lambda_2^{(N)} = \lim_{p\to 0} \frac{\Lambda_2^{(N)}}{p}. \tag{3.1.24}$$

equation (3.1.24) implies that $\Lambda_2^{(N)} = \mathcal{O}(p)$ as $p \to 0$, and hence $\left[\Lambda_2^{(N)}\right]^n = o(p)$, for $n \geqslant 2$. From equation (3.1.22), one obtains

$$\lambda_2^{(N)} = -\lim_{p\to 0} \frac{d_0^{(N)}}{d_1^{(N)} p}. \tag{3.1.25}$$

Three dimensional plots of $\Lambda_2^{(12)}$ are shown in Figure 3.1 for $\sigma = 1.0$. It is clearly seen that, for small noise fluctuation parameter σ, i.e. when the bounded noise is a narrow-band process, the effect of parametric resonance is very significant. When the value of σ is increased, the bandwidth of the bounded noise process $\eta(t)$ increases, resulting in a less prominent effect of the parametric resonance.

3.1.2.5 Monte Carlo Simulation

Equation (3.1.4) can be discretized using the Euler scheme, for iterations $k = 0, 1, 2, \ldots$,

$$\begin{aligned}
y_1^k &= y_1^{k-1} + y_2^{k-1} \cdot \Delta t, \\
y_2^k &= y_2^{k-1} - \left[\left(1 - \varepsilon^2 \mu\beta \cos\eta^{k-1}\right) y_1^{k-1} + \varepsilon\mu \cos\eta^{k-1} y_2^{k-1}\right] \cdot \Delta t, \\
\eta^k &= \eta^{k-1} + \nu \cdot \Delta t + \varepsilon^{1/2}\sigma \cdot \Delta W^{k-1}.
\end{aligned}$$

These equations can be simulated iteratively and the numerical algorithm for determining the Lyapunov exponents (Wolf *et al.* [94]) can be applied to evaluate $\lambda_{y(t)}$. In the Monte Carlo simulation, the time step is chosen as $\Delta t = 0.0005$, and the number of iterations is 10^9. A comparison of the Lyapunov exponents $\lambda_{y(t)}$ obtained using equations (3.1.24)–(3.1.25) and Monte Carlo simulation as shown in Figure 3.2 reveals that there is an excellent agreement between the two results.

A three-dimensional plot of the second-order perturbation of the Lyapunov exponent $\lambda_2^{(16)}$ as obtained using equation (3.1.25) is shown in Figure 3.3. The significant effect of the parametric resonance can be clearly seen for small values of σ.

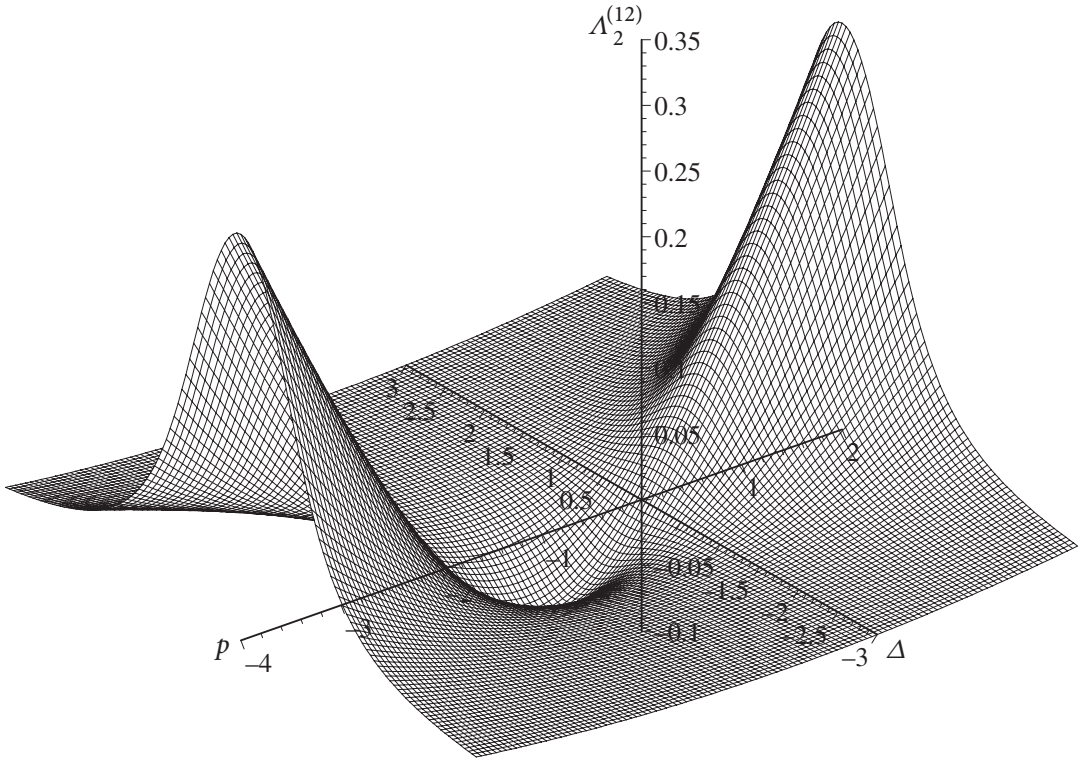

Figure 3.1 Second-order perturbation of the moment Lyapunov exponent $\Lambda_2^{(12)}$ ($\sigma = 1.0$).

According to the presented results, the stability of system (3.1.2) depends on the values of the damping β and parameters of bounded noise—the amplitude μ, the central frequency ν_0, the detuning parameter Δ, and the parameter σ that determines the bandwidth of the bounded noise. The system is unstable if the damping β is negative, which means that energy is fed into the system. The inclusion of the bounded noise makes the system more unstable. If the damping β is positive, the stability of the system depends on the characteristics of bounded noise. The main concern here is the primary parametric instability, namely when ν is in the vicinity of 2. According to the stability analysis, the primary parametric instability may occur when μ and σ take certain values. The parametric instability becomes more significant for larger μ or smaller σ. The Lyapunov exponents can be used to determine the range of the primary parametric instability.

In the following, the results of this section is applied to a single cylinder in cross-flow to study its stability in the lock-in region.

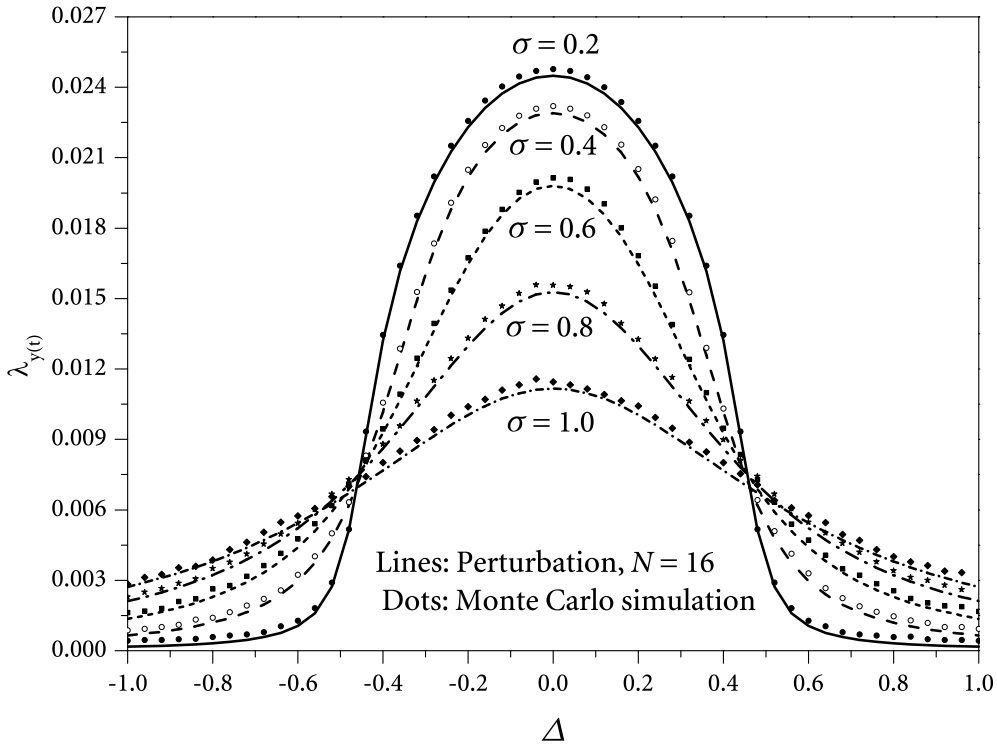

Figure 3.2 Comparison of the Lyapunov exponent $\lambda_{y(t)}$ for $\varepsilon = 0.1$, $\beta = 0.5$, and $\mu = 1.0$.

3.2 Flow-induced instability of a single cylinder in a cross-flow

Stability analysis of the system (2.1.17) shows that vortex-induced vibration of a cylinder is a combination of main resonance and parametric instability in the lock-in region. While the lock-in is associated with main resonance, the parametric instability may occur when the parameters of the time-dependent damping component take certain values and become more significant.

In this section, an example is presented to demonstrate the behavior of parametric instability. In the example, a rigid cylinder supported by elastic springs and viscous dampers in cross-flow is considered. Reynolds number is set at $\mathrm{Re} = 2760$, where data for motion-dependent force coefficients are available in the literature (Chen *et al.* [21]). Fluid inertia coefficients are calculated based on potential flow theory and are approximately unity for

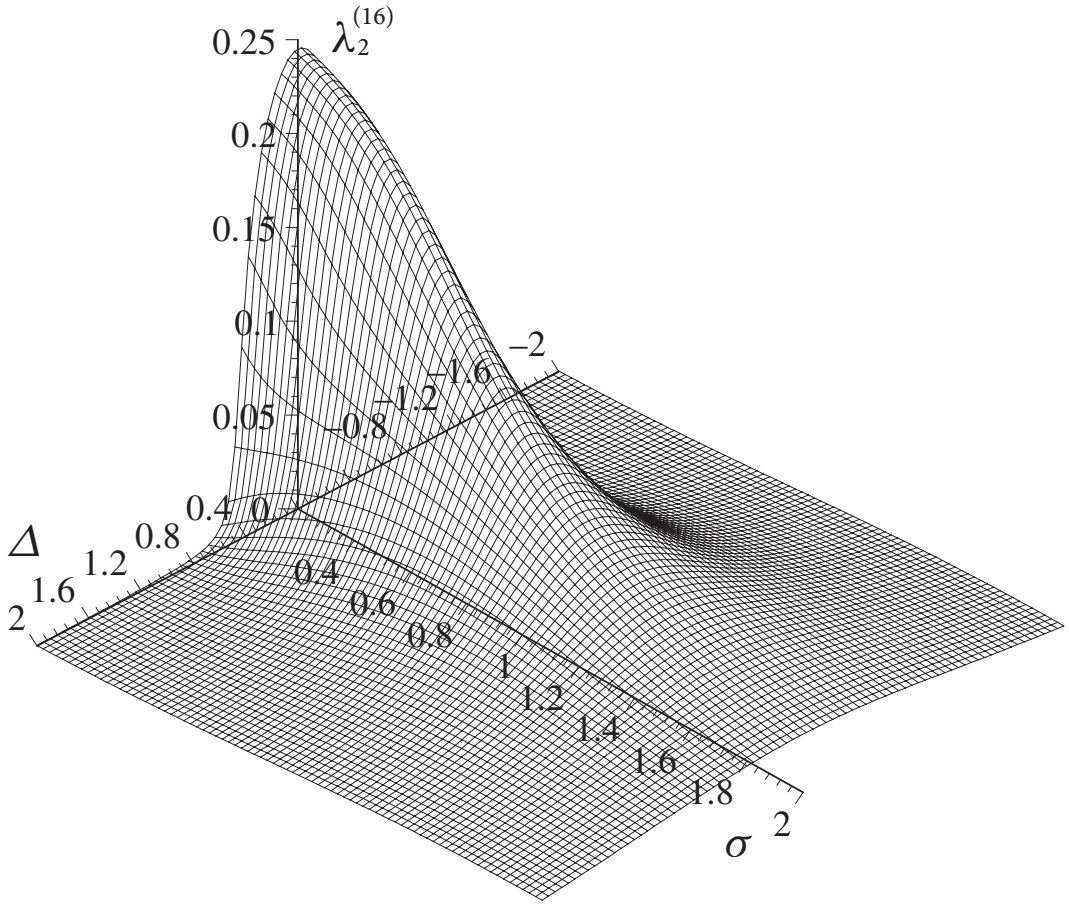

Figure 3.3 Second-order perturbation of the Lyapunov exponent $\lambda_2^{(16)}$.

all $\bar{U}_{r0}$ values investigated. Motion-dependent fluid damping and stiffness coefficients are plotted in Figures 3.4 and 3.5, respectively.

According to So *et al.* [78], the Strouhal number for a stationary cylinder at Re = 2500 is St = 0.2052, and the r.m.s. lift coefficient is $C_L' = 0.68$. These values are assumed for the present case. The mean and r.m.s. drag coefficients can be found in Zdravkovich [102], being $\bar{C}_D = 1.0$ and $C_D' = 0.07$, respectively. It is assumed that the bandwidths of both the lift and drag coefficients are equal, being $\tilde{\sigma}_L = \tilde{\sigma}_D = 0.01$. The reduced velocity is varied in the usual lock-in range of $\bar{U}_{r0} = 5.0$ to 6.6, where it is assumed that $\tilde{\nu}_L \approx 1$ and $\tilde{\nu}_D = 2\tilde{\nu}_L \approx 2$. The parameters are chosen so that the vibration level is similar to that reported by Chen *et al.* [21]. In the present case, the structural damping factor is $\zeta_s = 0.02$, and the mass ratio is varied from $M_r = 15$ to 18 in order to study its effect on the stability.

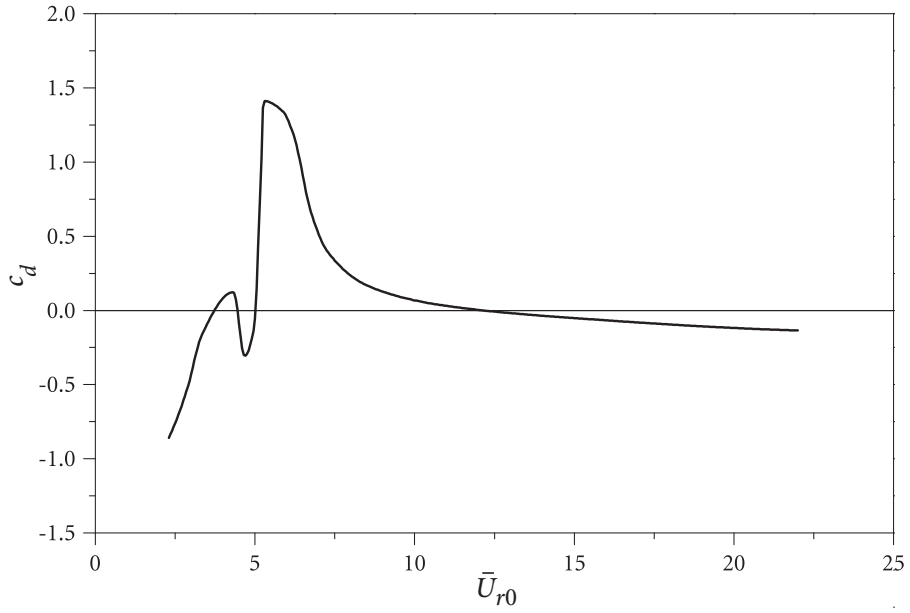

Figure 3.4 Fluid damping coefficient c_d for Re = 2760 and $d = 1.2$ mm (Chen *et al.* [21]).

For $M_r = 18$, the values of β and μ_D as a function of $\bar{U}_{r0}$ are calculated and plotted in Figure 3.6. It can be seen that β is positive in the range of $\bar{U}_{r0}$ concerned, hence constant-fluid-damping-induced instability is not present. However, $\mu_D > \beta$ in the range of $\bar{U}_{r0} = 5.6$ to 6.2, so it is possible for parametric instability to occur. In order to study this possibility, the Lyapunov exponents are obtained following the procedure in Section 3.1, and the results are shown in Figure 3.7.

The Lyapunov exponents for system (2.1.17) can also be obtained by Monte Carlo simulation. In the simulation, the number of iterations is 2×10^9 and the time step is $\Delta t = 10^{-6}$. The two results shown in Figure 3.7 agree with each other quite well.

It can be seen that parametric instability occurs in the range of $\bar{U}_{r0} = 5.85$ to 6.05. Noting that the usual lock-in range is $\bar{U}_{r0} = 4.0$ to 6.0, it can be seen that parametric instability may co-exist with the main resonance due to lock-in.

When the mass ratio is decreased to $M_r = 17$, the values of β and μ_D as a function of $\bar{U}_{r0}$ are plotted in Figure 3.8. It can be seen that this case covers all three situations discussed in Section 3.1, namely, $\beta < 0$, $0 < \beta < \mu_D$, and $\beta > \mu_D$. It is seen that $\beta < 0$ for $\bar{U}_{r0} = 5.72$ to 6.15, suggesting that constant-fluid-damping-induced instability occurs in this range. The Lyapunov exponents are calculated and plotted in Figure 3.9, from which the

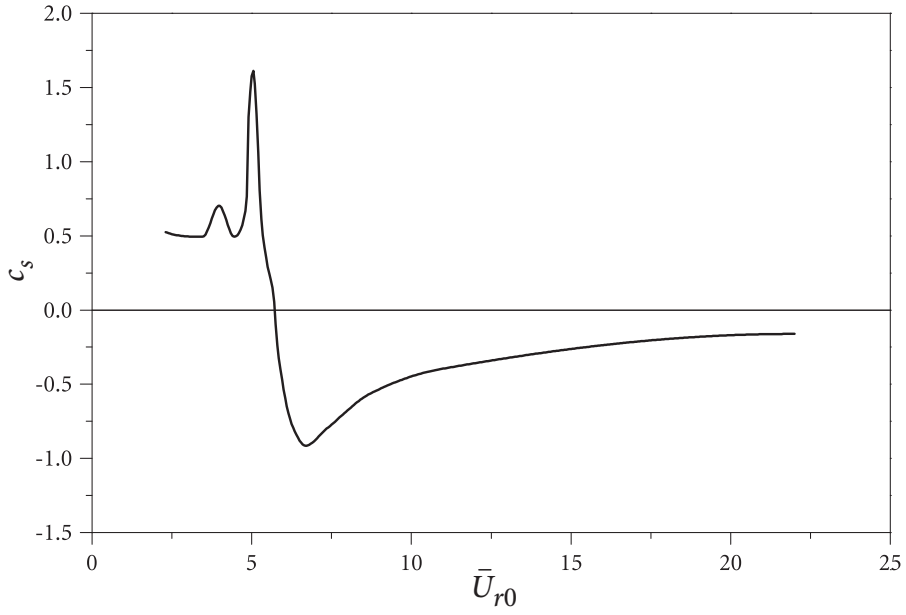

Figure 3.5 Fluid stiffness coefficient c_k for Re = 2760 and $d = 1.2$ mm (Chen *et al.* [21]).

range of instability is determined to be $\bar{U}_{r0} = 5.6$ to 6.22. This means that the parametric resonance enlarges the range of instability. Again, this range overlaps the usual lock-in range. Besides the enlarged instability range, the Lyapunov exponent is larger than that given by only constant-fluid-damping-induced instability alone. It is clearly shown that the time-dependent fluid-damping component $\mu_D \cos\tilde{\eta}(\tau)$ tends to destabilize the system by enlarging the instability range and enabling the response to increase faster (larger Lyapunov exponent).

In Section 3.1, it has been shown that the fluid damping coefficient, c_d, is a crucial parameter. In this example, its effect on parametric instability is studied by varying c_d by $\pm 10\%$ from its original value as reported by Chen *et al.* [21]. The ranges of instability, as determined by the Lyapunov exponents, for the case $M_r = 17$ and a series of c_d values are shown in Figure 3.10. It is seen that the range of instability increases with the increase of c_d, but decreases when c_d is decreased. It even diminishes as c_d is decreased by 5% or more (the system becomes stable in the whole range of $\bar{U}_{r0}$ considered). This is expected since decreasing c_d will increase β, which leads the system towards stable behavior. When the mass ratio is reduced further to $M_r = 15$, however, the system is always unstable in a certain

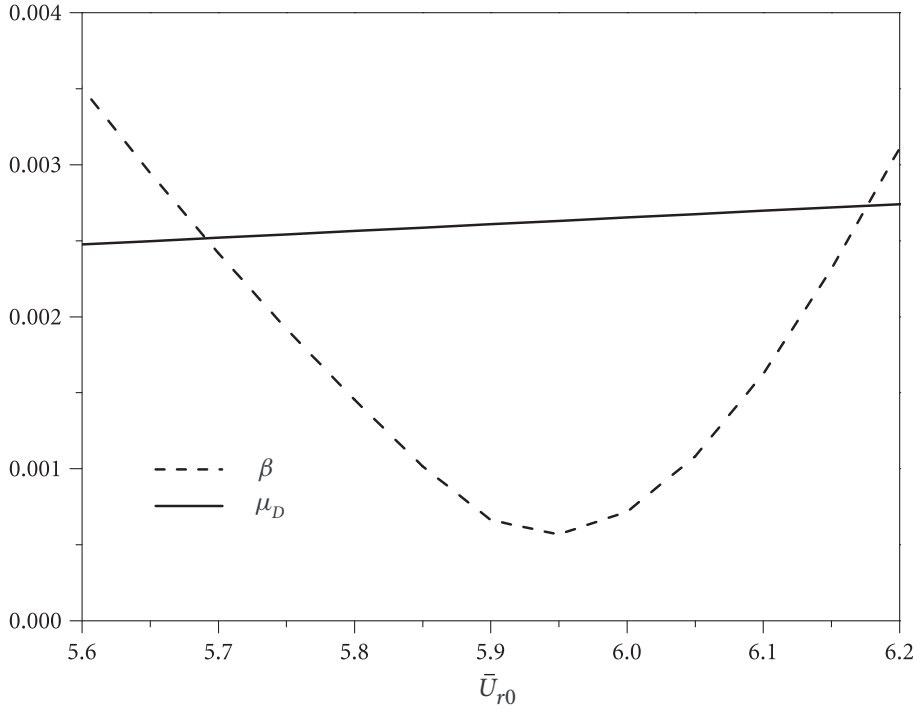

Figure 3.6 Values of β and μ_D in the lock-in range for $M_r = 18$, $\zeta_s = 0.02$, $\bar{C}_D = 1.0$, and $C_D = 0.1$.

range of $\bar{U}_{r0}$ regardless of the variation of c_d as shown in Figure 3.11. In fact, the effect of decreasing M_r is to destabilize the system, which is clearly shown in Figure 3.12.

This range overlaps partially with the usual lock-in range of U_r from 4.0 to 6.0, suggesting that the large-amplitude vibration of the cylinder observed in the lock-in region could include the contribution of parametric instability. It should be noted that the one-cylinder case is a limiting case of multiple cylinders when the distance between adjacent cylinders is large enough. Hence, it is expected that parametric instability might also play a significant role in flow-induced vibration of multiple cylinders. Therefore, a study of instability of multiple cylinders in a cross-flow is in order.

3.3 Conclusion

In this Chapter, possible instability of a cylinder in a cross-flow is discussed based on the extended model developed in Chapter 2. It is found that, apart from the usual vortex-induced large-amplitude vibration in the lock-in region and the instability induced by

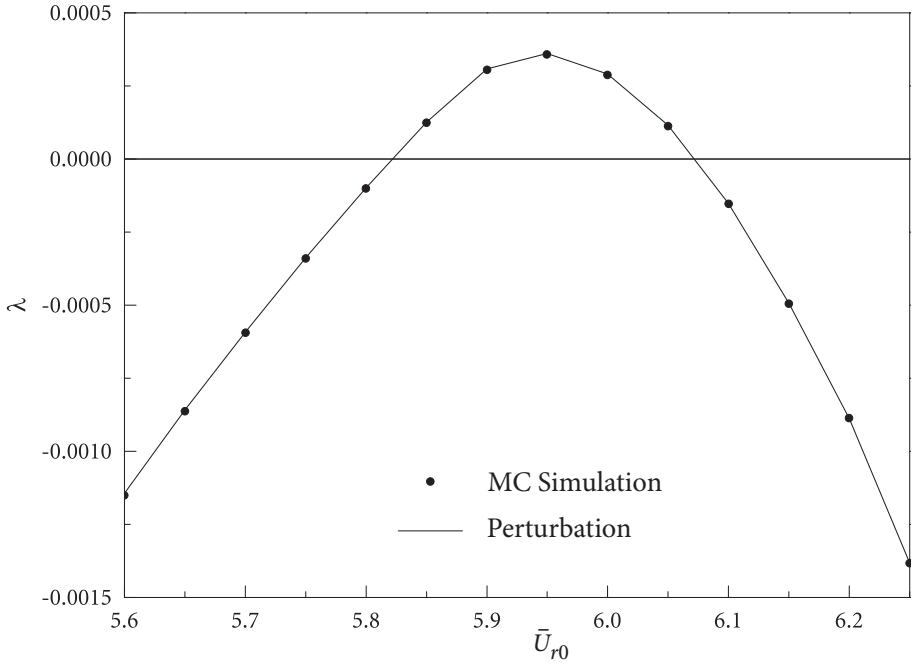

Figure 3.7 Lyapunov exponents for Re = 2760, $\sigma = 0.01$, $\nu = 2$, and $M_r = 18$.

constant fluid-damping force, for which a condition for its occurrence is given, a parametric instability is also possible if the parameters of the system are appropriately selected.

The developed model in Chapter 2 can be generalized to represent a class of two-dimensional dynamic systems subjected to parametric excitations in the damping term, which is described by a narrow-band bounded noise process. The dynamic stability of the system is studied by determining the moment Lyapunov exponents and the Lyapunov exponents. The partial differential eigenvalue problem governing the moment Lyapunov exponent is established using the theory of stochastic dynamical system. For weak noise excitations, a singular perturbation method is employed to obtain second-order expansions of the moment Lyapunov exponents. Lyapunov exponents are then obtained using the relationship between the moment Lyapunov exponent and the Lyapunov exponent. The accuracy of the approximate analytical results are validated and assessed by comparing with numerical results. It is observed that there is an excellent agreement between the analytical results and the numerical results.

Based on the stability analysis results of a two-dimensional general dynamic system, an example is given to demonstrate the role of parametric instability in vortex-induced vibra-

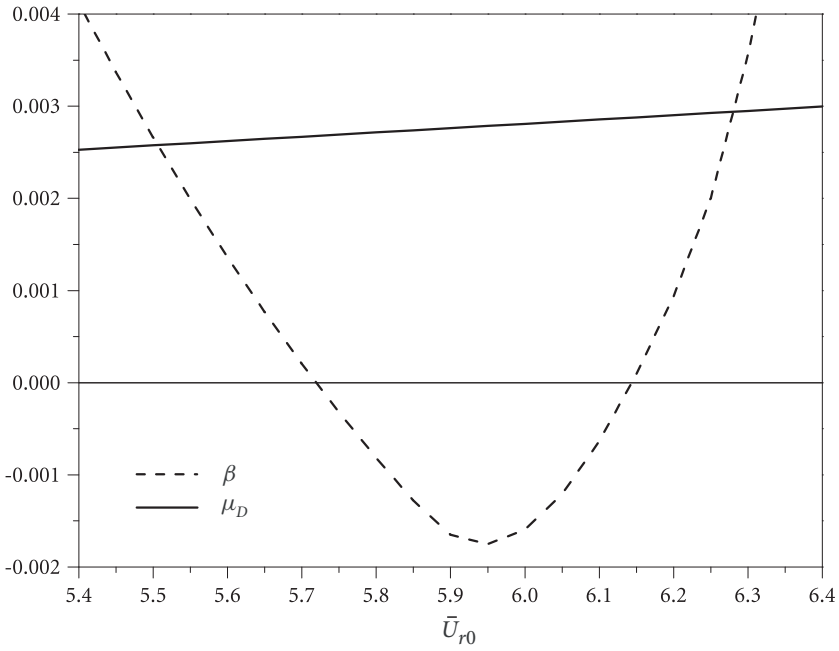

Figure 3.8 Values of β and μ_D in the lock-in range for $M_r = 17$, $\zeta_s = 0.02$, $\bar{C}_D = 1.0$, and $C_D = 0.1$.

tion of a single cylinder in a cross-flow. When appropriate values of the system parameters are taken, it is shown that the vibration of the cylinder is made up of main resonance due to the lock-in forcing, parametric instability due to time-variant fluid damping, and constant-fluid-damping-induced instability in the usual lock-in range. In particular, the primary parametric resonance enlarges the range of instability. The effects of some crucial parameters, such as the mass ratio and the fluid damping coefficient, are studied. It is shown that decreasing the mass ratio or increasing the constant fluid damping has a positive influence on the instability of the system.

As indicated in Chapter 2, fluidelastic instability can occur due to the interaction between the motions in the drag and lift directions at the high reduced velocity region if the cylinder is placed in a shear flow. To study the effect of turbulence on the stability of the cylinder, the grid-generated turbulence is modeled as a real noise and incorporated into the equations of motion. The stability of the resulting random system is studied in Chapter 4.

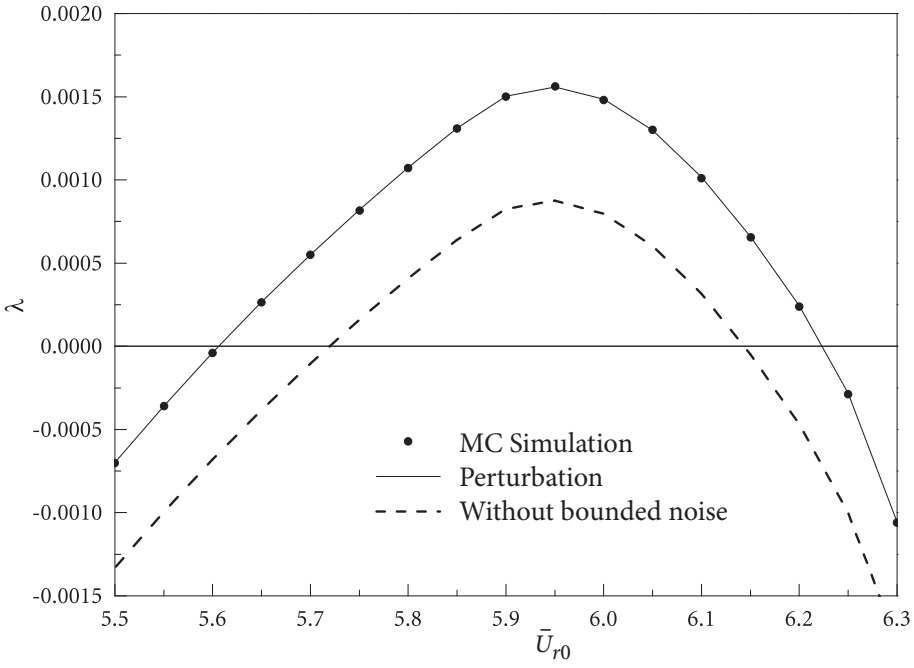

Figure 3.9 Lyapunov exponents for Re = 2760, $\sigma = 0.01$, $\nu = 2$, and $M_r = 17$.

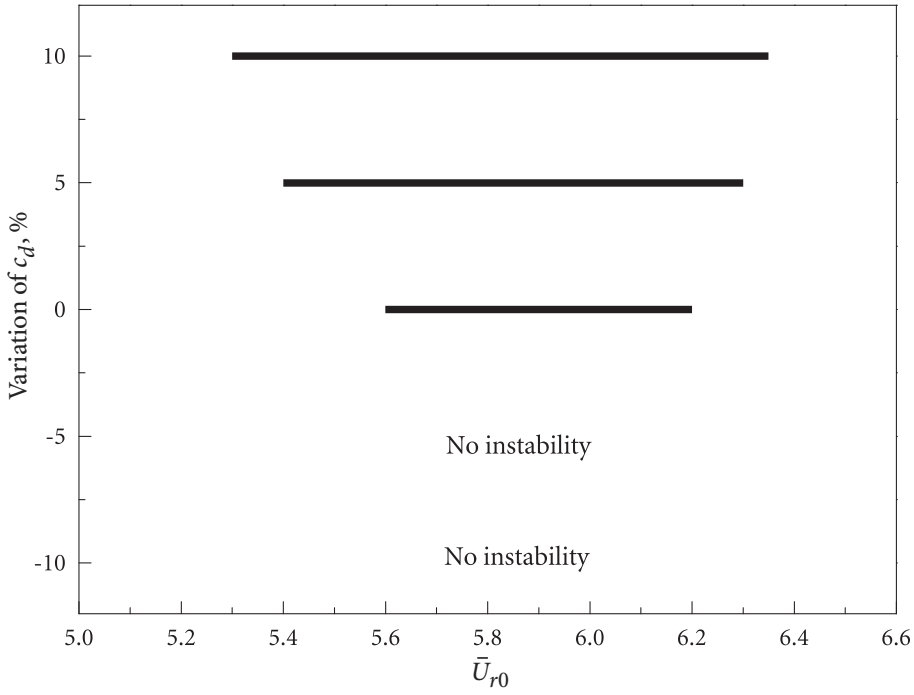

Figure 3.10 Stability range with variation of c_d and $M_r = 17$.

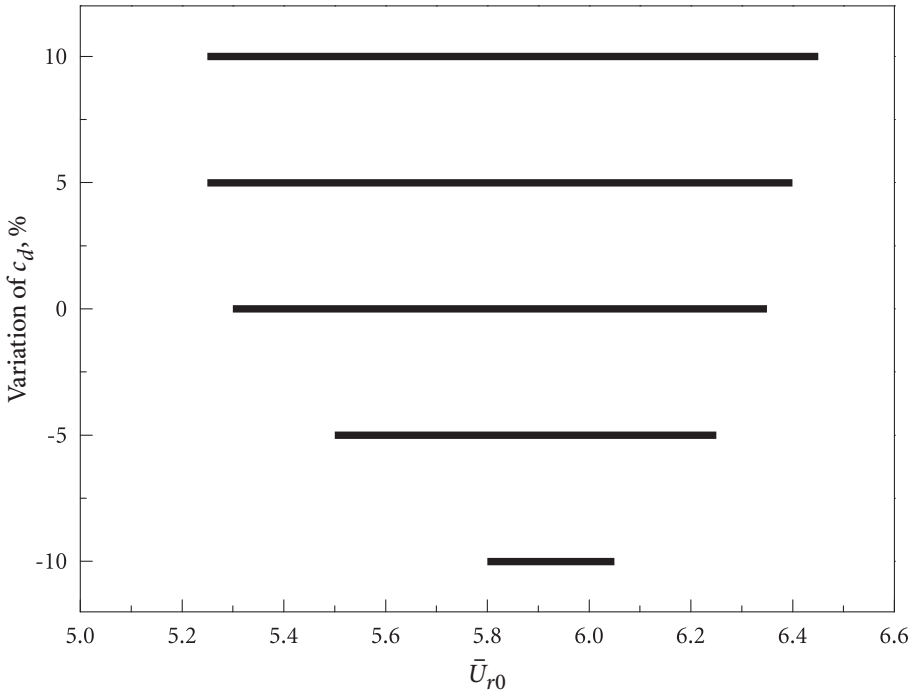

Figure 3.11 Stability range with variation of c_d and $M_r = 15$.

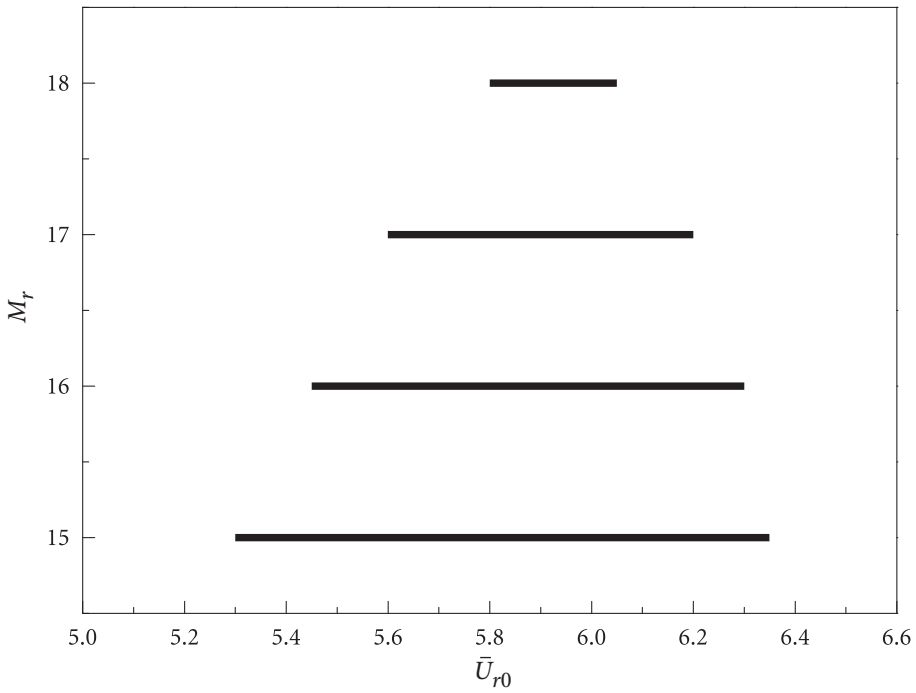

Figure 3.12 Stability range with variation of M_r.

CHAPTER 4

Turbulence Effects on Fluidelastic Instability of a Cylinder in Shear Flow

In this chapter, fluidelastic instability of a single circular cylinder in a shear flow is considered, and the suppression of such instability by free stream turbulence in the approach flow is demonstrated through a stability analysis.

In Section 4.1, the dynamic stability of a four-dimensional system under real noise excitation is studied through the determination of the pth moment Lyapunov exponent and the Lyapunov exponent. The partial differential eigenvalue problem governing the moment Lyapunov exponent is established. For small amplitudes of noise, a method of regular perturbation is applied to determine analytical expansions of the moment Lyapunov exponents and Lyapunov exponents. Thus, both the sample stability and moment stability are studied.

In Section 4.2, the stability of the deterministic system is studied by varying the critical parameter (natural frequency ratio k). The analytical results obtained in Section 4.1 are used to explore the stochastic stability of a cylinder in a shear flow. It is shown that fluidelastic instability can be stabilized by the turbulence under certain conditions. Parametric studies are performed to demonstrate the significant effects of noise parameters α and σ, on the stability of the cylinder. Analytical results and numerical simulations are compared to validate the approach.

4.1 Stability of a Four Dimensional System Excited by a Real Noise

4.1.1 Formulation

Consider a linear stochastic system governed by the following equations of motion

$$\dot{\tilde{\mathbf{x}}} = \tilde{\mathbf{A}}\tilde{\mathbf{x}} + \varepsilon\xi(t)\tilde{\mathbf{B}}\tilde{\mathbf{x}}, \qquad \tilde{x} \in \mathcal{R}^4, \tag{4.1.1}$$

where $\xi(t)$ is an an Ornstein-Uhlenbeck process defined by equation (1.2.3), and ε is a small number.

Assume that system (4.1.1) has one critical mode and one stable mode. Let $\mathbf{x} = \mathbf{T}\tilde{\mathbf{x}}$, where the matrix of transformation $\mathbf{T}$ is constructed from the eigenvectors of $\tilde{\mathbf{A}}$. Specifically, if the eigenvalues consist of two complex-conjugate pairs $\lambda_{1,2} = -\varepsilon^2\delta_1 \pm \mathrm{i}\omega_1$ and $\lambda_{3,4} = -\delta_2 \pm \mathrm{i}\omega_2$, and if the eigenvectors associated with the eigenvalues are $\mathbf{V}_{1R} + \mathrm{i}\mathbf{V}_{1I}$ and $\mathbf{V}_{2R} + \mathrm{i}\mathbf{V}_{2I}$, respectively, $\mathbf{T}$ can be chosen as $\mathbf{T} = [\mathbf{V}_{1R}\ \mathbf{V}_{1I}\ \mathbf{V}_{2R}\ \mathbf{V}_{2I}]$. The transformation yields

$$\dot{\mathbf{x}} = \mathbf{A}\mathbf{x} + \varepsilon\xi(t)\mathbf{B}\mathbf{x}, \quad \mathbf{x} \in \mathcal{R}^4,$$

where

$$\mathbf{A} = \begin{bmatrix} -\varepsilon^2\delta_1 & \omega_1 & 0 & 0 \\ -\omega_1 & -\varepsilon^2\delta_1 & 0 & 0 \\ 0 & 0 & -\delta_2 & \omega_2 \\ 0 & 0 & -\omega_2 & -\delta_2 \end{bmatrix}, \qquad \mathbf{B} = \begin{bmatrix} K_{11} & K_{12} & M_{11} & M_{12} \\ K_{21} & K_{22} & M_{21} & M_{22} \\ N_{11} & N_{12} & L_{11} & L_{12} \\ N_{21} & N_{22} & L_{21} & L_{22} \end{bmatrix}.$$

The quantities $\varepsilon^2\delta_1$ and δ_2 represent the real parts of the eigenvalues of the critical mode and stable mode, respectively.

Applying the transformation

$$x_1 = \mathrm{e}^{\rho}\cos\phi_1\cos\theta, \qquad x_3 = \mathrm{e}^{\rho}\cos\phi_2\sin\theta,$$

$$x_2 = -\mathrm{e}^{\rho}\sin\phi_1\cos\theta, \qquad x_4 = -\mathrm{e}^{\rho}\sin\phi_2\sin\theta,$$

one can obtain the following set of equations for the amplitude ρ, phase variables (ϕ_1, ϕ_2, θ), and noise process ξ:

$$\dot{\rho} = \sum_{j=0}^{2} \varepsilon^j q_j(\xi, \phi_1, \phi_2, \theta), \qquad \dot{\theta} = \sum_{j=0}^{2} \varepsilon^j s_j(\xi, \phi_1, \phi_2, \theta),$$

$$\dot{\phi}_i = \sum_{j=0}^{2} \varepsilon^j h_{ij}(\xi, \phi_1, \phi_2, \theta), \qquad d\xi = -\alpha\xi\, dt + \sigma\, dW(t). \tag{4.1.2}$$

In above expressions, the phase angles ϕ_1 and ϕ_2 are in $(0, 2\pi)$, θ is in $(0, \pi/2)$, and the coefficients q_j, s_j, and h_{ij} are given by

$$\begin{aligned}
q_0(\xi,\phi_1,\phi_2,\theta) &= -\delta_2 \sin^2\theta, \qquad q_2(\xi,\phi_1,\phi_2,\theta) = -\delta_1 \cos^2\theta,\\
q_1(\xi,\phi_1,\phi_2,\theta) &= \Big\{ \tfrac{1}{4}\sin 2\theta\big[(M_{11}+N_{11})(\cos\phi^+ + \cos\phi^-) - (M_{22}+N_{22})(\cos\phi^+ - \cos\phi^-)\\
&\quad - (M_{21}+N_{12})(\sin\phi^+ + \sin\phi^-) - (M_{12}+N_{21})(\sin\phi^+ - \sin\phi^-)\big]\\
&\quad + \sin^2\theta\big[L_{11}\cos^2\phi_2 + L_{22}\sin^2\phi_2 - \tfrac{1}{2}(L_{12}+L_{21})\sin 2\phi_2\big]\\
&\quad + \cos^2\theta\big[K_{11}\cos^2\phi_1 + K_{22}\sin^2\phi_1 - \tfrac{1}{2}(K_{12}+K_{21})\sin 2\phi_1\big]\Big\}\xi(t),\\
h_{10}(\xi,\phi_1,\phi_2,\theta) &= \omega_1, \qquad h_{12}(\xi,\phi_1,\phi_2,\theta) = 0,\\
h_{11}(\xi,\phi_1,\phi_2,\theta) &= \Big\{ K_{12}\sin^2\phi_1 - K_{21}\cos^2\phi_1 - \tfrac{1}{2}(K_{11}-K_{22})\sin 2\phi_1\\
&\quad - \tfrac{1}{2}\tan\theta\big[M_{21}(\cos\phi^+ + \cos\phi^-) + M_{12}(\cos\phi^+ - \cos\phi^-)\\
&\quad + M_{11}(\sin\phi^+ + \sin\phi^-) - M_{22}(\sin\phi^+ - \sin\phi^-)\big]\Big\}\xi(t),\\
h_{20}(\xi,\phi_1,\phi_2,\theta) &= \omega_2, \qquad h_{22}(\xi,\phi_1,\phi_2,\theta) = 0,\\
h_{21}(\xi,\phi_1,\phi_2,\theta) &= \Big\{ L_{12}\sin^2\phi_2 - L_{21}\cos^2\phi_2 - \tfrac{1}{2}(L_{11}-L_{22})\sin 2\phi_2\\
&\quad - \tfrac{1}{2}\cot\theta\big[N_{21}(\cos\phi^+ + \cos\phi^-) + N_{12}(\cos\phi^+ - \cos\phi^-)\\
&\quad - N_{22}(\sin\phi^+ + \sin\phi^-) + N_{11}(\sin\phi^+ - \sin\phi^-)\big]\Big\}\xi(t),\\
s_0(\xi,\phi_1,\phi_2,\theta) &= -\tfrac{1}{2}\delta_2 \sin 2\theta, \qquad s_2(\xi,\phi_1,\phi_2,\theta) = \tfrac{1}{2}\delta_1 \sin 2\theta,\\
s_1(\xi,\phi_1,\phi_2,\theta) &= \Big\{ \tfrac{1}{4}\sin 2\theta\big[2L_{11}\cos^2\phi_2 + 2L_{22}\sin^2\phi_2 - (L_{12}+L_{21})\sin 2\phi_2\\
&\quad - 2K_{11}\cos^2\phi_1 - 2K_{22}\sin^2\phi_1 + (K_{12}+K_{21})\sin 2\phi_1\big]\\
&\quad - \tfrac{1}{2}\sin^2\theta\big[M_{11}(\cos\phi^+ + \cos\phi^-) - M_{22}(\cos\phi^+ - \cos\phi^-)\\
&\quad - M_{12}(\sin\phi^+ - \sin\phi^-) - M_{21}(\sin\phi^+ + \sin\phi^-)\big]\\
&\quad + \tfrac{1}{2}\cos^2\theta\big[N_{11}(\cos\phi^+ + \cos\phi^-) - N_{22}(\cos\phi^+ - \cos\phi^-)
\end{aligned}$$

$$- N_{12}(\sin\phi^+ + \sin\phi^-) - N_{21}(\sin\phi^+ - \sin\phi^-)\Big]\Big\}\xi(t),$$

where $\phi^{\pm} = \phi_1 \pm \phi_2$.

Since the processes $(\xi, \phi_1, \phi_2, \theta)$ do not depend on ρ, the processes alone $(\xi, \phi_1, \phi_2, \theta)$ form a Markov diffusion process and the associated generator is given by

$$L = L_0 + \varepsilon L_1 + \varepsilon^2 L_2,$$

where

$$L_0 = \frac{\sigma^2}{2}\frac{\partial^2}{\partial\xi^2} - \alpha\xi\frac{\partial}{\partial\xi} + \sum_{i=1}^{2}\omega_i\frac{\partial}{\partial\phi_i} + s_0(\phi_1, \phi_2, \theta, \xi)\frac{\partial}{\partial\theta},$$

$$L_1 = s_1(\phi_1, \phi_2, \theta, \xi)\frac{\partial}{\partial\theta} + \sum_{i=1}^{2} h_{i1}(\phi_1, \phi_2, \theta, \xi)\frac{\partial}{\partial\phi_i},$$

$$L_2 = s_2(\phi_1, \phi_2, \theta, \xi)\frac{\partial}{\partial\theta} + \sum_{i=1}^{2} h_{i2}(\phi_1, \phi_2, \theta, \xi)\frac{\partial}{\partial\phi_i}.$$

Arnold *et al.* [5] and [6] proved that $\Lambda(p)$ is an isolated simple eigenvalue of $\mathscr{L}(p)$ with non-negative eigenfunction $T(\xi, \phi_1, \phi_2, \theta)$, i.e.

$$\mathscr{L}(p)T = \Lambda(p)T, \qquad \text{for all real } p, \tag{4.1.4}$$

where

$$\mathscr{L}(p) = \mathscr{L}_0(p) + \varepsilon\mathscr{L}_1(p) + \varepsilon^2\mathscr{L}_2(p),$$

and

$$\mathscr{L}_0(p) = L_0 + pq_0, \quad \mathscr{L}_1(p) = L_1 + pq_1, \quad \mathscr{L}_2(p) = L_2 + pq_2.$$

4.1.2 Weak Noise Expansions of the Moment Lyapunov Exponent

A method of regular perturbation is applied to obtain a weak noise expansion of the moment Lyapunov exponent. Both the eigenvalue $\Lambda(p)$ and the eigenfunction $T(\xi, \phi_1, \phi_2, \theta)$ are expanded in powers of ε:

$$\Lambda(p) = \sum_{n=0}^{\infty}\varepsilon^n\Lambda_n(p), \qquad T(\xi, \phi_1, \phi_2, \theta) = \sum_{n=0}^{\infty}\varepsilon^n T_n(\xi, \phi_1, \phi_2, \theta).$$

Substituting the above expansions into equation (4.1.4), one obtains the following equations:

$$\big[\mathscr{L}_0(p) - \Lambda_0(p)\big]T_0 = 0, \tag{4.1.5}$$

$$\big[\mathscr{L}_0(p) - \Lambda_0(p)\big]T_1 = \Lambda_1(p)T_0 - \mathscr{L}_1(p)T_0, \tag{4.1.6}$$

$$\big[\mathscr{L}_0(p) - \Lambda_0(p)\big]T_2 = \Lambda_2(p)T_0 + \Lambda_1(p)T_1 - \mathscr{L}_2(p)T_0 - \mathscr{L}_1(p)T_1, \tag{4.1.7}$$

$$\cdots \quad \cdots$$

4.1.2.1 Zeroth-Order Perturbation

For zeroth-order perturbation, one has a deterministic system from equation (4.1.2)

$$\dot{\rho} = -\delta_2 \sin^2\theta, \quad \dot{\theta} = -\tfrac{1}{2}\delta_2 \sin 2\theta, \quad \dot{\phi}_i = \omega_i. \tag{4.1.8}$$

Solving equation (4.1.8), one obtains

$$\rho = -\delta_2 \int_0^t \sin^2\theta(s)\mathrm{d}s + \rho_0, \quad \theta = \tan^{-1}\left(\theta_0 \mathrm{e}^{-\delta_2 t}\right), \tag{4.1.9}$$

where ρ_0 and θ_0 are two constants which can be determined by the initial conditions.

It follows from the definition of $\Lambda(p)$

$$\begin{aligned}\Lambda_0(p) &= \lim_{t\to\infty} \frac{1}{t} \log \mathrm{E}\big\|x(t;x_0)\big\|^p, \qquad \text{since the zero-order system is deterministic} \\ &= \lim_{t\to\infty} \frac{1}{t} p \log \|x(t;x_0)\| = p\lambda_0,\end{aligned} \tag{4.1.10}$$

where $\|x\| = \mathrm{e}^{\rho}$ and

$$\begin{aligned}\lambda_0 = \lim_{t\to\infty} \frac{\rho(t)}{t} &= -\delta_2 \lim_{t\to\infty} \frac{1}{t} \int_0^t \sin^2\theta(s)\mathrm{d}s \\ &= -\delta_2 \lim_{t\to\infty} \frac{1}{t} \int_0^t \frac{\tan^2\theta(s)}{1+\tan^2\theta(s)}\mathrm{d}s \\ &= -\delta_2 \lim_{t\to\infty} \frac{1}{t} \int_0^t \frac{\theta_0^2 \mathrm{e}^{-2\delta_2 s}}{1+\theta_0^2 \mathrm{e}^{-2\delta_2 s}}\mathrm{d}s = 0.\end{aligned}$$

Thus, $\Lambda_0(p) \equiv 0$ for all possible p. Equation (4.1.5) reduces to

$$\big(L_0 + pq_0\big)T_0 = 0,$$

where

$$L_0 = \frac{\sigma^2}{2}\frac{\partial^2}{\partial\xi^2} - \alpha\xi\frac{\partial}{\partial\xi} + \omega_1\frac{\partial}{\partial\phi_1} + \omega_2\frac{\partial}{\partial\phi_2} - \tfrac{1}{2}\delta_2 \sin 2\theta \frac{\partial}{\partial\theta}.$$

Applying the method of separation of variables and letting

$$T_0(\xi,\phi_1,\phi_2,\theta) = Z_0(\xi)H_1(\phi_1)H_2(\phi_2)F(\theta)$$

result in

$$\frac{H_1'}{H_1} = a_1, \tag{4.1.11a}$$

$$\frac{H_2'}{H_2} = a_2, \tag{4.1.11b}$$

$$\frac{\sigma^2}{2}\frac{\ddot{Z}_0}{Z_0} - \alpha\zeta\frac{\dot{Z}_0}{Z_0} - \tfrac{1}{2}\delta_2 \sin 2\theta \frac{F_\theta}{F} - p\delta_2 \sin^2\theta = -(a_1 + a_2). \tag{4.1.11c}$$

Solving equation for $H_1(\phi_1)$ yields $H_1(\phi_1) = Ae^{a_1\phi_1}$. For $H_1(\phi_1)$ to be a period function, it is required that $a_1 = 0$ and hence $H_1(\phi_1)$ can be chosen as 1. Similarly, $a_2 = 0$ and $H_2(\phi_2) = 1$. Hence, equation (4.1.11c) reduces to

$$\frac{\sigma^2}{2}\frac{\ddot{Z}_0}{Z_0} - \alpha\zeta\frac{\dot{Z}_0}{Z_0} = a, \tag{4.1.12a}$$

$$\tfrac{1}{2}\delta_2 \sin 2\theta \frac{F_\theta}{F} + p\delta_2 \sin^2\theta = a. \tag{4.1.12b}$$

Equation (4.1.12a) is an eigenvalue problem with the eigenvalues $a = 0, -\alpha, -2\alpha, \cdots$ (see, e.g., Gardiner [31], page 134). However, the left-hand-side of equation (4.1.12b) goes to 0 since θ approaches 0 when $t \to \infty$. Thus, the constant a in equation (4.1.12) should be be taken as 0. The equation for $Z_0(\xi)$ becomes

$$\tfrac{1}{2}\sigma^2\ddot{Z}_0 - \alpha\xi\dot{Z}_0 = 0. \tag{4.1.13}$$

Equation (4.1.13) can be easily solved to yield

$$Z_0(\xi) = C_1 \int \exp\Big(\frac{\alpha}{\sigma^2}\xi^2\Big)\mathrm{d}\xi + C_2, \qquad -\infty < \xi < \infty.$$

For $Z_0(\xi)$ to be bounded, it is required that $C_1 = 0$ and hence $Z_0(\xi)$ can be taken as 1.

The equation for $F(\theta)$ becomes

$$\frac{\mathrm{d}F}{\mathrm{d}\theta} = (-p\tan\theta)F.$$

The solution to this equation is $F(\theta) = (\cos\theta)^p$. Therefore

$$\Lambda_0(p) = 0, \qquad T_0(\xi, \phi_1, \phi_2, \theta) = T_0(\theta) = (\cos\theta)^p. \tag{4.1.14}$$

Since $\Lambda_0(p) = 0$, the associated adjoint differential equation of (4.1.5) is

$$\mathscr{L}_0^* T_0^* = \frac{\sigma^2}{2}\frac{\partial^2 T_0^*}{\partial\xi^2} + \alpha\xi\frac{\partial T_0^*}{\partial\xi} + \alpha T_0^* - \omega_1\frac{\partial T_0^*}{\partial\phi_1} - \omega_2\frac{\partial T_0^*}{\partial\phi_2}$$

$$+\tfrac{1}{2}\delta_2\sin 2\theta\frac{\partial T_0^*}{\partial\theta}+\left(\delta_2\cos 2\theta-p\delta_2\sin^2\theta\right)T_0^*=0. \tag{4.1.15}$$

Applying the method of separation of variables and letting

$$T_0^*(\phi_1,\phi_2,\theta,\xi)=Z_0^*(\xi)H_1^*(\phi_1)H_2^*(\phi_2)F^*(\theta)$$

lead to

$$\frac{(H_1^*)_{\phi_1}}{H_1^*}=b_1, \tag{4.1.16a}$$

$$\frac{(H_2^*)_{\phi_2}}{H_2^*}=b_2, \tag{4.1.16b}$$

$$\frac{\sigma^2}{2}\frac{\ddot{Z}_0^*}{Z_0^*}+\alpha\zeta\frac{\dot{Z}_0^*}{Z_0^*}+\alpha+\tfrac{1}{2}\delta_2\sin 2\theta\frac{(F^*)_\theta}{F^*}+\left(\delta_2\cos 2\theta-p\delta_2\sin^2\theta\right)=-(b_1+b_2). \tag{4.1.16c}$$

The equation for H_1^* yields $H_1^*(\phi_1)=B\mathrm{e}^{-b_1\phi_1}$. For $H_1^*(\phi_1)$ to be a period function, $b_1=0$ and $H_1^*(\phi_1)$ can be taken as

$$H_1^*(\phi_1)=\frac{1}{2\pi},\qquad 0\leqslant\phi_1<2\pi.$$

Similarly, one has

$$H_2^*(\phi_2)=\frac{1}{2\pi},\qquad 0\leqslant\phi_2<2\pi.$$

The above equations show that ϕ_1 and ϕ_2 are uniformly distributed between 0 and 2π.

Hence, equation (4.1.16c) is reduced to

$$\frac{\sigma^2}{2}\frac{\ddot{Z}_0^*}{Z_0^*}+\alpha\zeta\frac{\dot{Z}_0^*}{Z_0^*}+\alpha=b, \tag{4.1.17a}$$

$$-\tfrac{1}{2}\delta_2\sin 2\theta\frac{(F^*)_\theta}{F^*}-\left(\delta_2\cos 2\theta-p\delta_2\sin^2\theta\right)=b. \tag{4.1.17b}$$

Based on the same reasoning as mentioned above, b should be taken as 0. The equation for Z_0^* becomes

$$\tfrac{1}{2}\sigma^2\ddot{Z}_0^*+\alpha\xi\dot{Z}_0^*+\alpha Z_0^*=0, \tag{4.1.18}$$

which is the Fokker-Planck equation for the stationary transition probability density of the Ornstein-Uhlenbeck process $\xi(t)$ as defined in equation (1.2.3). Equation (4.1.18) may be written as

$$\frac{\mathrm{d}}{\mathrm{d}\xi}\left(\frac{\mathrm{d}Z_0^*}{\mathrm{d}\xi}+\frac{2\alpha}{\sigma^2}\zeta Z_0^*\right)=0,$$

or

$$\frac{\mathrm{d}Z_0^*}{\mathrm{d}\xi} + \frac{2\alpha}{\sigma^2}\xi Z_0^* = C_3 = \text{probability current.} \tag{4.1.18$'$}$$

Since the stationary probability density $Z_0^*(\xi)$ and the probability current vanishes when $\xi \to \pm\infty$, the constant of integration $C_3 = 0$. Equation (4.1.18$'$) can be easily solved to give

$$Z_0^*(\xi) = C_4 \exp\Big(-\frac{\alpha}{\sigma^2}\xi^2\Big).$$

Since $Z_0^*(\xi)$ is the stationary probability density, normalizing it yields

$$Z_0^*(\xi) = \frac{1}{\sqrt{2\pi}\sigma_z}\exp\bigg(-\frac{\xi^2}{2\sigma_z^2}\bigg), \tag{4.1.19}$$

i.e. the Ornstein-Uhlenbeck process $\xi(t)$ is a normally distributed random variable with mean $\mu_\xi = 0$ and standard deviation $\sigma_z = \sigma_\xi/\sqrt{2\alpha}$.

The equation for $F^*(\theta)$ becomes

$$\tfrac{1}{2}\sin 2\theta\frac{\mathrm{d}F^*}{\mathrm{d}\theta} = \big(\cos 2\theta - p\sin^2\theta\big)F^*. \tag{4.1.20}$$

The solution to equation (4.1.20) is not unique due to the singularities at $\theta = 0$ and $\pi/2$. Since $\theta = 0$ is a stable equilibrium point of system (4.1.8), by following Pardoux and Wihstutz [61] the solution can be chosen as

$$F^*(\theta) = \delta(\theta - 0),$$

where $\delta(\theta - 0)$ is the Dirac delta function at 0.

Hence, the solution to equation (4.1.15) is obtained as

$$T_0^*(\xi, \phi_1, \phi_2, \theta) = \frac{Z_0^*(\xi)\delta(\theta - 0)}{4\pi^2}.$$

4.1.2.2 Solution of $\mathscr{L}_0 T = f(\xi)g(\phi_1, \phi_2, \theta)$

Consider the partial differential equation $\mathscr{L}_0 T = f(\xi)g(\phi_1, \phi_2, \theta)$, or

$$\bigg(\frac{\sigma^2}{2}\frac{\partial^2}{\partial\xi^2} - \alpha\xi\frac{\partial}{\partial\xi} + \omega_1\frac{\partial}{\partial\phi_1} + \omega_2\frac{\partial}{\partial\phi_2} - \tfrac{1}{2}\delta_2\sin 2\theta\frac{\partial}{\partial\theta} - p\delta_2\sin^2\theta\bigg)T(\xi, \phi_1, \phi_2, \theta)$$
$$= f(\xi)g(\phi_1, \phi_2, \theta). \tag{4.1.21}$$

Introducing an auxiliary time t to equation (4.1.21) leads to

$$\left(\frac{\partial}{\partial t}+\frac{\sigma^2}{2}\frac{\partial^2}{\partial\xi^2}-\alpha\xi\frac{\partial}{\partial\xi}+\omega_1\frac{\partial}{\partial\phi_1}+\omega_2\frac{\partial}{\partial\phi_2}-\tfrac{1}{2}\delta_2\sin 2\theta\frac{\partial}{\partial\theta}\right.$$
$$\left.-\,p\delta_2\sin^2\theta\right)\Psi(t,\xi,\phi_1,\phi_2,\theta)=f(\xi)g(\phi_1,\phi_2,\theta). \quad (4.1.22)$$

Applying the following transformation

$$\tilde{t}=\frac{t}{4}+\frac{\phi_1}{4\omega_1}+\frac{\phi_2}{4\omega_2}-\frac{\ln(\tan\theta)}{4\delta_2},\qquad \tilde{s}=\frac{t}{4}-\frac{\phi_1}{4\omega_1}-\frac{\phi_2}{4\omega_2}-\frac{\ln(\tan\theta)}{4\delta_2},$$
$$\gamma_1=\omega_2\phi_1-\omega_1\phi_2,\qquad \gamma_2=2\omega_1\omega_2 t-\omega_2\phi_1-\omega_1\phi_2,$$

with the inverse transformation given by

$$t=\tilde{t}-\tilde{s}+\frac{\gamma_2}{2\omega_1\omega_2},\qquad \theta=\tan^{-1}\left\{\exp\left[\delta_2\Big(\frac{\gamma_2}{2\omega_1\omega_2}-\tilde{t}-3\tilde{s}\Big)\right]\right\},$$
$$\phi_1=\omega_1(\tilde{t}-\tilde{s})+\frac{\gamma_1}{2\omega_2},\qquad \phi_2=\omega_2(\tilde{t}-\tilde{s})-\frac{\gamma_1}{2\omega_1},$$

equation (4.1.22) becomes

$$\left(\frac{\partial}{\partial\tilde{t}}+\frac{\sigma^2}{2}\frac{\partial^2}{\partial\xi^2}-\alpha\xi\frac{\partial}{\partial\xi}-p\delta_2\sin^2\theta\right)\tilde{\Psi}(\tilde{t},\tilde{s},\gamma_1,\gamma_2,\xi)=f(\xi)\tilde{g}(\tilde{t},\tilde{s},\gamma_1,\gamma_2), \quad (4.1.23)$$

where

$$\tilde{\Psi}(\tilde{t},\tilde{s},\gamma_1,\gamma_2,\xi)=\Psi(t,\xi,\phi_1,\phi_2,\theta),\quad \tilde{g}(\tilde{t},\tilde{s},\gamma_1,\gamma_2)=g(\phi_1,\phi_2,\theta).$$

In order to remove the $\sin^2\theta$ term, introduce the function W defined by

$$\Upsilon(\tilde{t},\tilde{s},\gamma_1,\gamma_2,\xi)=\tilde{\Psi}\exp\left\{-\int^{\tilde{t}}p\delta_2\sin^2\theta(r)\mathrm{d}r\right\}, \quad (4.1.24)$$

Hence equation (4.1.23) becomes

$$\left(\frac{\partial}{\partial\tilde{t}}+\frac{\sigma^2}{2}\frac{\partial^2}{\partial\xi^2}-\alpha\xi\frac{\partial}{\partial\xi}\right)\Upsilon(\tilde{t},\tilde{s},\gamma_1,\gamma_2,\xi)=f(\xi)\tilde{g}(\tilde{t},\tilde{s},\gamma_1,\gamma_2)R_\Upsilon(\tilde{t},\tilde{s},\gamma_1,\gamma_2), \quad (4.1.25)$$

where

$$R_\Upsilon(\tilde{t},\tilde{s},\gamma_1,\gamma_2)=\exp\left\{-\int^{\tilde{t}}p\delta_2\sin^2\theta(r)\mathrm{d}r\right\}$$
$$=\left\{1+\exp\left[2\delta_2\Big(\frac{\gamma_2}{2\omega_1\omega_2}-\tilde{t}-3\tilde{s}\Big)\right]\right\}^{\frac{p}{2}}.$$

Applying Duhamel's Principle (see, e.g., Zauderer [101]), the solution $\Upsilon(\tilde{t},\tilde{s},\gamma_1,\gamma_2,\xi)$ to equation (4.1.25) is given by

$$\Upsilon(\tilde{t},\tilde{s},\gamma_1,\gamma_2,\xi)=\int_0^{\tilde{t}}V(\tilde{t},\tilde{s},\gamma_1,\gamma_2,\xi;r)\,\mathrm{d}r, \quad (4.1.26)$$

where $V(\tilde{t},\tilde{s},\gamma_1,\gamma_2,\xi;r)$ is the solution of the homogeneous equation

$$\begin{aligned}&\left(\frac{\partial}{\partial\tilde{t}}+\frac{\sigma^2}{2}\frac{\partial^2}{\partial\xi^2}-\alpha\xi\frac{\partial}{\partial\xi}\right)V(\tilde{t},\tilde{s},\gamma_1,\gamma_2,\xi;r)=0,\qquad \text{for } \tilde{t}>r,\\ &V(r,\tilde{s},\gamma_1,\gamma_2,\xi;r)=f(\xi)\tilde{g}(r,\tilde{s},\gamma_1,\gamma_2)R_\Upsilon(r,\tilde{s},\gamma_1,\gamma_2),\qquad \text{for } \tilde{t}=r.\end{aligned}\tag{4.1.27}$$

To solve equation (4.1.27), consider the equation

$$\begin{aligned}&\left(\frac{\partial}{\partial\tilde{t}}+\frac{\sigma^2}{2}\frac{\partial^2}{\partial\xi^2}-\alpha\xi\frac{\partial}{\partial\xi}\right)P(\tilde{t},\xi;\tau,z)=0,\qquad \tilde{t}<\tau,\\ &P(\tau,\xi;\tau,z)=\lim_{\tilde{t}\uparrow\tau}P(\tilde{t},\xi;\tau,z)=\delta(z-\xi).\end{aligned}\tag{4.1.28}$$

Equation (4.1.28) is the backward Kolmogorov equation for the transition probability function $P(\tilde{t},\xi;\tau,z)$. It is known that the transition probability $P(\tilde{t},\xi;\tau,z)$ is also the solution of the forward Kolmogorov or Fokker-Planck equation, i.e. for the initial condition $\tilde{t}$ and ξ fixed,

$$\begin{aligned}&\left[\frac{\partial}{\partial\tau}-\frac{\sigma^2}{2}\frac{\partial^2}{\partial z^2}+\frac{\partial}{\partial z}(-\alpha z)\right]P(\tilde{t},\xi;\tau,z)=0,\qquad \tau>\tilde{t},\\ &P(\tilde{t},\xi;\tilde{t},z)=\lim_{\tau\downarrow\tilde{t}}P(\tilde{t},\xi;\tau,z)=\delta(z-\xi).\end{aligned}\tag{4.1.29}$$

The solution of equation (4.1.29) is given by,

$$P(\tilde{t},\xi;\tau,z)=\frac{1}{\sqrt{2\pi}\sigma_{z(\tau)}}\exp\left\{-\frac{\left[z-\mu_{z(\tau)}\right]^2}{2\sigma^2_{z(\tau)}}\right\},\tag{4.1.30}$$

where

$$\mu_{z(\tau)}=\xi\,\mathrm{e}^{-\alpha(\tau-\tilde{t})},\qquad \sigma^2_{z(\tau)}=\frac{\sigma^2\left[1-\mathrm{e}^{-2\alpha(\tau-\tilde{t})}\right]}{2\alpha}.$$

For the initial condition $\xi(\tilde{t})$ fixed, $z(\tau)$ is a normally distributed random variable with mean $\mu_{z(\tau)}$ and standard deviation $\sigma_{z(\tau)}$.

From equations (4.1.27) and (4.1.28), the solution $V(\tilde{t},\tilde{s},\gamma_1,\gamma_2,\xi;r)$ to (4.1.27) is given by

$$V(\tilde{t},\tilde{s},\gamma_1,\gamma_2,\xi;r)=\tilde{g}(r,\tilde{s},\gamma_1,\gamma_2)R_\Upsilon(r,\tilde{s},\gamma_1,\gamma_2)\int_{-\infty}^{\infty}f(z)\,P(\tilde{t},\xi;r,z)\,\mathrm{d}r,\tag{4.1.31}$$

where

$$\mathrm{E}\left[f\left(z(r)\right)\right]=\int_{-\infty}^{\infty}f(z)\,P(\tilde{t},\xi;r,z)\,\mathrm{d}z$$

is the expected value of the random variable $f\big(z(r)\big)$ with $z(r)$ being the normally distributed random variable as defined in (4.1.30).

Combining equations (4.1.26) and (4.1.31), the solution to equation (4.1.23) is given by

$$\Upsilon(\tilde{t},\tilde{s},\gamma_1,\gamma_2,\xi)=\int_0^{\tilde{t}}\tilde{g}(r,\tilde{s},\gamma_1,\gamma_2)R_\Upsilon(r,\tilde{s},\gamma_1,\gamma_2)\,\mathrm{E}\big[f\big(z(r)\big)\big]\,\mathrm{d}r. \tag{4.1.32}$$

Hence, from equation (4.1.24), one has

$$\tilde{\Psi}(\tilde{t},\tilde{s},\gamma_1,\gamma_2,\xi)=\frac{\Upsilon}{R_\Upsilon}. \tag{4.1.33}$$

The solution $T(\xi,\phi_1,\phi_2,\theta)$ to equation (4.1.21) is obtained by using the inverse transformation and passing the limit $\tilde{t}\to-\infty$,

4.1.2.3 First-Order Perturbation

Substituting the above expression for $T_0(\theta)$ into equation (4.1.6) results in

$$\mathscr{L}_0T_1=-s_1(\xi,\phi_1,\phi_2,\theta)\frac{\mathrm{d}T_0}{\mathrm{d}\theta}+\big[\Lambda_1(p)-pq_1(\xi,\phi_1,\phi_2,\theta)\big]T_0. \tag{4.1.34}$$

From the Fredholm Alternative, for equation (4.1.34) to have a nontrivial solution it is required that

$$\big(-s_1T_0'+\big[\Lambda_1(p)-pq_1\big]T_0,T_0^*\big)=0,$$

i.e.

$$\Lambda_1(p)=\big(s_1T_0'+pq_1T_0,T_0^*\big)=\frac{1}{16\pi^2}\big(\xi g(\phi_1,\phi_2,\theta),Z_0^*(\xi)\delta(\theta-0)\big)=0, \tag{4.1.35}$$

where $\big((\cdot),(\cdot\cdot)\big)$ is the inner product defined by

$$(\cdot,\cdot\cdot)=\int_0^{\pi/2}\int_{-\infty}^{+\infty}\int_0^{2\pi}\int_0^{2\pi}(\cdot)(\cdot\cdot)\mathrm{d}\phi_1\mathrm{d}\phi_2\mathrm{d}\xi\,\mathrm{d}\theta,$$

$$\begin{aligned}g(\phi_1,\phi_2,\theta)=&p(\cos\theta)^p\Big\{K_{22}\sin^2\phi_1+K_{11}\cos^2\phi_1-\tfrac{1}{2}(K_{12}+K_{21})\sin2\phi_1\\&+\tfrac{1}{2}\tan\theta\big[M_{11}(\cos\phi^+-\cos\phi^-)-M_{22}(\cos\phi^+-\cos\phi^-)\\&-M_{12}(\sin\phi^+-\sin\phi^-)-M_{21}(\sin\phi^++\sin\phi^-)\big]\Big\}.\end{aligned}$$

The equality in equation (4.1.35) results from the fact that q_1 and s_1 is periodic in ϕ_1 and ϕ_2, and ξ is a zero mean process. Hence, equation (4.1.34) reduces to

$$\mathscr{L}_0T_1=-\xi g(\phi_1,\phi_2,\theta). \tag{4.1.36}$$

Equation (4.1.36) can be solved by applying Duhamel's Principle and making use of the solution of the Fokker-Planck equation (1.2.7).

Since, from Section 4.1.2.2, $\mathrm{E}\big[z(r)\big]=\mu_{z(r)}=\xi\,\mathrm{e}^{-\alpha(r-\tilde{t})}$, the solution of equation (4.1.36) is obtained as

$$\Upsilon(\tilde{t},\tilde{s},\gamma_1,\gamma_2,\xi)=\int_0^{\tilde{t}}\tilde{g}(r,\tilde{s},\gamma_1,\gamma_2)\,R_\Upsilon(r,\tilde{s},\gamma_1,\gamma_2)\mathrm{e}^{-\alpha(r-\tilde{t})}\,\mathrm{d}r\cdot\xi. \tag{4.1.37}$$

and

$$\tilde{\Psi}_1(\tilde{t},\tilde{s},\gamma_1,\gamma_2,\xi)=\frac{\Upsilon}{R_\Upsilon}. \tag{4.1.38}$$

or

$$\begin{aligned}T_1(\xi,\phi_1,\phi_2,\theta)=-\tfrac{1}{2}p(\cos\theta)^p\Big\{&K_{11}\Big[G(2\phi_1)-\frac{1}{\alpha}\Big]-K_{22}\Big[G(2\phi_1)+\frac{1}{\alpha}\Big]\\&-(K_{12}+K_{21})H(2\phi_1)+\tan\theta\Big\{M_{11}\big[G(\phi^+)+G(\phi^-)\big]-M_{22}\big[G(\phi^+)-G(\phi^-)\big]\\&-M_{12}\big[H(\phi^+)-H(\phi^-)\big]-M_{21}\big[H(\phi^+)+H(\phi^-)\big]\Big\}\Big\}\xi(t),\end{aligned}$$

where

$$G(2\phi_1)=\lim_{\tilde{t}\to-\infty}\int_0^{\tilde{t}}\mathrm{e}^{-\alpha(r-\tilde{t})}\cos2\phi_1(r)\,\mathrm{d}r=\frac{2\omega_1\sin2\phi_1-\alpha\cos2\phi_1}{\alpha^2+4\omega_1^2},$$

$$H(2\phi_1)=\lim_{\tilde{t}\to-\infty}\int_0^{\tilde{t}}\mathrm{e}^{-\alpha(r-\tilde{t})}\sin2\phi_1(r)\,\mathrm{d}r=-\frac{2\omega_1\cos2\phi_1+\alpha\sin2\phi_1}{\alpha^2+4\omega_1^2},$$

$$\begin{aligned}G(\phi^-)&=\lim_{\tilde{t}\to-\infty}\int_0^{\tilde{t}}\mathrm{e}^{-\alpha(r-\tilde{t})}\cos\big[\phi_1(r)-\phi_2(r)\big]\tan\theta(r)\,\mathrm{d}r\\&=-\frac{\tan\theta\big[(\omega_2-\omega_1)\sin\phi^-+(\delta_2+\alpha)\cos\phi^-\big]}{\delta_2^2+2\,\delta_2\alpha+\alpha^2+\omega_1^2-2\,\omega_1\omega_2+\omega_2^2},\end{aligned}$$

$$\begin{aligned}G(\phi^+)&=\lim_{\tilde{t}\to-\infty}\int_0^{\tilde{t}}\mathrm{e}^{-\alpha(r-\tilde{t})}\cos\big[\phi_1(r)+\phi_2(r)\big]\tan\theta(r)\,\mathrm{d}r\\&=\frac{\tan\theta\big[(\omega_1+\omega_2)\sin\phi^+-(\delta_2+\alpha)\cos\phi^+\big]}{\delta_2^2+2\,\delta_2\alpha+\alpha^2+\omega_1^2+2\,\omega_1\omega_2+\omega_2^2},\end{aligned}$$

$$\begin{aligned}H(\phi^-)&=\lim_{\tilde{t}\to-\infty}\int_0^{\tilde{t}}\mathrm{e}^{-\alpha(r-\tilde{t})}\sin\big[\phi_1(r)-\phi_2(r)\big]\tan\theta(r)\,\mathrm{d}r\\&=-\frac{\tan\theta\big[(\omega_1-\omega_2)\cos\phi^-+(\delta_2+\alpha)\sin\phi^-\big]}{\delta_2^2+2\,\delta_2\alpha+\alpha^2+\omega_1^2-2\,\omega_1\omega_2+\omega_2^2},\end{aligned}$$

$$H(\phi^+) = \lim_{\tilde{t}\to-\infty} \int_0^{\tilde{t}} \mathrm{e}^{-\alpha(r-\tilde{t})} \sin\big[\phi_1(r)+\phi_2(r)\big] \tan\theta(r)\,\mathrm{d}r$$
$$= -\frac{\tan\theta\big[(\omega_1+\omega_2)\cos\phi^+ + (\delta_2+\alpha)\sin\phi^+\big]}{\delta_2^2 + 2\,\delta_2\alpha + \alpha^2 + \omega_1^2 + 2\,\omega_1\omega_2 + \omega_2^2}.$$

4.1.2.4 Second-order perturbation

The equation for the second-order perturbation is

$$\mathscr{L}_0 T_2 = \big[\Lambda_2(p) - \mathscr{L}_2\big]T_0 - \mathscr{L}_1 T_1. \tag{4.1.39}$$

From the Fredholm Alternative, for equation (4.1.39) to have a nontrivial solution it is required that

$$\big(\big[\Lambda_2(p) - \mathscr{L}_2\big]T_0 - \mathscr{L}_1 T_1, T_0^*\big) = 0,$$

i.e.

$$\Lambda_2(p) = \big(\mathscr{L}_2 T_0 + \mathscr{L}_1 T_1, T_0^*\big)$$
$$= \Big(\big(s_2\frac{\partial}{\partial\theta} + pq_2\big)T_0 + \big(s_1\frac{\partial}{\partial\theta} + h_{11}\frac{\partial}{\partial\phi_1} + h_{21}\frac{\partial}{\partial\phi_2} + pq_1\big)T_1, T_0^*\Big).$$

After performing the integration, one obtains

$$\Lambda_2(p) = \big[-8\delta_1 + \big(\kappa_2 F_0 + \kappa_3 F_1 + \kappa_4 F_2 + \kappa_5 F_3 + \kappa_6 F_4\big)\big]\frac{p}{8} + \big(\kappa_2 F_0 + \frac{2\kappa_1}{\alpha}\big)\frac{p^2}{16}, \tag{4.1.40}$$

where

$$\kappa_1 = (K_{11}+K_{22})^2, \qquad \kappa_2 = (K_{12}+K_{21})^2 + (K_{11}-K_{22})^2,$$
$$\kappa_3 = (N_{12}+N_{21})(M_{11}-M_{22}) - (N_{11}-N_{22})(M_{12}+M_{21}),$$
$$\kappa_4 = (N_{12}+N_{21})(M_{12}+M_{21}) + (N_{11}-N_{22})(M_{11}-M_{22}),$$
$$\kappa_5 = (N_{11}+N_{22})(M_{12}-M_{21}) + (N_{12}-N_{21})(M_{11}+M_{22}),$$
$$\kappa_6 = (N_{11}+N_{22})(M_{11}+M_{22}) - (N_{12}-N_{21})(M_{12}-M_{21}),$$

and

$$F_0 = \frac{\sigma^2}{\alpha^2 + 4\omega_1^2},$$

$$F_1 = \frac{\sigma^2(\omega_1+\omega_2)}{\alpha[(\delta_2+\alpha)^2 + (\omega_1+\omega_2)^2]}, \qquad F_2 = \frac{\sigma^2(\delta_2+\alpha)}{\alpha[(\delta_2+\alpha)^2 + (\omega_1+\omega_2)^2]},$$

$$F_3 = \frac{\sigma^2(\omega_1-\omega_2)}{\alpha[(\delta_2+\alpha)^2+(\omega_1-\omega_2)^2]}, \qquad F_4 = \frac{\sigma^2(\delta_2+\alpha)}{\alpha[(\delta_2+\alpha)^2+(\omega_1-\omega_2)^2]}.$$

The largest Lyapunov exponent can be calculated by equation (1.3.4) as

$$\lambda = \lim_{p\to 0}\frac{\Lambda(p)}{p} = \varepsilon^2\Big[-\delta_1 + \frac{1}{8}\big(\kappa_2 F_0 + \kappa_3 F_1 + \kappa_4 F_2 + \kappa_5 F_3 + \kappa_6 F_4\big)\Big]. \tag{4.1.41}$$

From the above expressions, κ_1 and κ_2 are always positive. κ_3, κ_4, κ_5, and κ_6 could take positive and negative values depending on the values of the elements of matrix **B**. Similarly, the parameters F_0, F_1, F_2, and F_4 are always positive. However, the parameter F_3 could take positive and negative values depending on the difference between two modal frequencies. From equation (4.1.41), one can see that the stabilization is possible if the total contribution of the turbulence is negative.

If only the motion in the x-direction is considered, the previous equations are reduced to include only $\kappa_2 = 1$ and F_0, i.e.,

$$\Lambda(p) = \varepsilon^2\Big[-\delta_1 p + \frac{p(p+2)\sigma^2}{16(\alpha^2+4\omega_1^2)}\Big] + o(\varepsilon^2), \tag{4.1.42}$$

$$\lambda = \varepsilon^2\Big[-\delta_1 + \frac{\sigma^2}{8(\alpha^2+4\omega_1^2)}\Big] + o(\varepsilon^2). \tag{4.1.43}$$

Equations (4.1.42) and (4.1.43) agree with the results of Xie [97]. Equations (4.1.42) and (4.1.43) also show that the real noise destabilizes the one degree-of-freedom system.

Note that all F_i $(i=0,1,\cdots,4)$ include the term σ^2/α, which represents the noise intensity. Thus, increasing the noise intensity can assist the stabilizing or destabilizing effect of noise.

4.2 Study of Stabilization

4.2.1 Deterministic System

Uniform Flow

As presented in Chapter 2, the model will be reduced to that of Zhu *et al.* [104] at lock-in range when the flow is uniform and laminar

$$Y''(\tau) + \Big[2\bar{\zeta}_s + \frac{\bar{U}_{r0}}{2\pi}\frac{\bar{C}_D + C_D\cos\tilde{\eta}_D(\tau)}{2M_r} - \frac{\bar{U}_{r0}^2}{4\pi^2}\frac{c_d}{M_r}\Big]Y'(\tau) + Y(\tau) = \frac{\bar{U}_{r0}^2}{4\pi^2}\frac{C_L}{M_r}\cos\tilde{\eta}_L(\tau).$$

At lock-in range, it is shown that the vibration of the cylinder is made up of main resonance due to the lock-in forcing, parametric instability due to time-variant fluid damping, and constant-fluid-damping-induced instability in the usual lock-in range. The critical parameters are the motion-dependent damping coefficient and the bandwidth of vortex shedding. At high reduced velocities ($U_r > 20$), motion-dependent force coefficients approach zero and can be neglected (Chen *et al.* [21]). Furthermore, the vortex shedding frequency is far away from the natural frequency of the cylinder, which eliminates the forced vibration due to vortex shedding. Hence, the system is expected to be stable.

Shear Flow

At high reduced velocity, motion-dependent forces are assumed to be negligible. The equations of motion are thus reduced to those of Yu *et al.* [100]

$$X'' + \Big(2\zeta + \frac{U_r C_D}{M_r}\Big)X' + X - \Big(\frac{U_r^2}{2M_r}\frac{C_D}{\partial Y} + \frac{U_r^2 K C_D}{M_r}\Big)Y - \frac{U_r C_L}{2M_r}Y' = \frac{U_r^2}{2M_r}C_D, \quad (4.2.1a)$$

$$Y'' + k\Big(2\zeta + \frac{U_r C_D}{2M_r}\Big)Y' + k^2\Big(1 - \frac{U_r^2}{2M_r}\frac{C_L}{\partial Y} - \frac{U_r^2 K C_L}{M_r}\Big)Y + \frac{kU_r C_L}{M_r}X' = \frac{k^2 U_r^2}{2M_r}C_L. \quad (4.2.1b)$$

The equations of motion (4.2.1) have similar forms as those for wake galloping in which the derivative $\partial C_L/\partial x$ is a critical parameter that determines the instability (Blevins, [15]). Similarly, the lift coefficient C_L and its derivative $\partial C_L/\partial y$ are expected to play a significant role in the stability of a cylinder in a shear flow.

For a cylinder in a shear flow, the drag and lift force coefficients (C_D and C_L) are functions of Reynolds number ($\mathrm{Re} = UD/\nu$, where ν is the kinematic viscosity of the fluid) and shear parameter ($K = GD/U$). Since $U = U_0 + Gy$ is a function of only y, the derivatives of C_D and C_L with respect to x are zero. The derivatives of C_D and C_L with respect to y can be evaluated as

$$\frac{\partial C_D}{\partial y} = \frac{\partial C_D}{\partial \mathrm{Re}}\frac{\partial \mathrm{Re}}{\partial y} + \frac{\partial C_D}{\partial \mathrm{K}}\frac{\partial K}{\partial y}, \quad (4.2.2a)$$

$$\frac{\partial C_L}{\partial y} = \frac{\partial C_L}{\partial \mathrm{Re}}\frac{\partial \mathrm{Re}}{\partial y} + \frac{\partial C_L}{\partial \mathrm{K}}\frac{\partial K}{\partial y}. \quad (4.2.2b)$$

The derivatives with respect to y in equation (4.2.2) can be evaluated as

$$\frac{\partial \mathrm{Re}}{\partial y} = \frac{\partial U}{\partial y}\cdot\frac{D}{\nu} = \frac{GD}{\nu} = \frac{1}{D}\cdot\frac{UD}{\nu}\cdot\frac{GD}{U} = \frac{\mathrm{Re}K}{D}, \quad (4.2.3a)$$

$$\frac{\partial K}{\partial y} = \frac{\partial}{\partial U}\left(\frac{GD}{U}\right)\cdot\frac{\partial U}{\partial y} = -\frac{GD}{U^2}G = -\frac{1}{D}\frac{G^2D^2}{U^2} = -\frac{K^2}{D}. \tag{4.2.3b}$$

Substituting equations (4.2.3) into equations (4.2.2) and normalizing them with respect to D yield

$$\frac{\partial C_D}{\partial Y} = \frac{\partial C_D}{\partial \mathrm{Re}}\mathrm{Re}\,K - \frac{\partial C_D}{\partial K}K^2, \tag{4.2.4a}$$

$$\frac{\partial C_L}{\partial Y} = \frac{\partial C_L}{\partial \mathrm{Re}}\mathrm{Re}\,K - \frac{\partial C_L}{\partial K}K^2. \tag{4.2.4b}$$

If extensive data of $C_D(\mathrm{Re}, K)$ and $C_L(\mathrm{Re}, K)$ are known, their derivatives with respect to Y can be calculated by equations (4.2.4).

In order to demonstrate the fluidelastic instability of the system described by equations (4.2.1), consider an example with the parameters $\mathrm{Re}=100$, $M_r=5112$, and $\zeta=0.007$. At this Reynolds number, the drag and lift coefficients are available (Lei *et al.* [42]) for calculating their derivatives, which are given by

$$C_D = 1.486, \quad \frac{\partial C_D}{\partial K} = -0.32, \quad \frac{\partial C_D}{\partial \mathrm{Re}} = -0.0016,$$

$$C_L = -0.126, \quad \frac{\partial C_L}{\partial K} = -1.0, \quad \frac{\partial C_L}{\partial \mathrm{Re}} = 0.0005.$$

The stability depends on the eigenvalues of the system matrix **A**. If the real parts of the eigenvalues are negative, the system is stable. When the reduced velocity increases to a critical value, the largest real part of the eigenvalues become positive, i.e., the cylinder becomes unstable. Increasing the shear parameter also tends to destabilize the cylinder. For example, the critical velocity for $k=\omega_y/\omega_x=1.0$ is $U_{r,\mathrm{cr}}=256$ at $K=0.1$ and decreases to about $U_{r,\mathrm{cr}}=112$ at $K=0.2$. The stability boundary for a cylinder with $M_r=5112$ is determined experimentally by Yu *et al.* [100] as $U_rK^{1.44}/2\pi=5$ approximately, which yields $U_{r,\mathrm{cr}}=865$ at $K=0.1$. The present result does not agree quantitatively with the stability boundary obtained by Yu *et al.* [100] since Reynolds number changed from 8 to 120 in the experiment while the present result is obtained at $\mathrm{Re}=100$. The lift and drag force coefficients are dependent on the Reynolds number at this range. However, the effects of U_r and K on the stability are qualitatively the same as the experimental observations which shows that increasing U_r or K can destabilize the cylinder. On the contrary, increasing M_r, decreasing U_r, or decreasing K would weaken the effect of C_L, which makes the system more stable.

Similarly as wake galloping, the fluidelastic instability for a cylinder in a shear flow turns out to be sensitive to the ratio of natural frequencies in the two coordinate directions. Small changes of frequency can significantly shift the critical velocity, which is shown in Figure 4.1. The minimum critical reduced velocity occurs at about $k=0.95$, and then the critical reduced velocity will increase rapidly with larger detuning in the frequencies. This phenomenon is also observed in the flutter of a two-dimensional linear airfoil by Poirel and Price [62].

4.2.2 Stochastic System

Uniform Flow

Recent experimental results (So *et al.* [80]) showed that the effect of free stream turbulence on a single cylinder in a cross-flow is to increase the amplitude of cylinder vibration in the U_r range of 1.45 – 12.08. This is accomplished by increasing the vortex-induced force in the U_r range of 1.45 – 7.25 while increasing the fluid damping force in the U_r range of 8.21 – 12.08. However, the cylinder is still stable even though the U_r investigated straddles across the lock-in range. When U_r is increased to very large values as considered in the present study, it is expected that the cylinder would still remain stable.

Shear Flow

When grid-generated turbulence is added in front of the cylinder in a shear flow, the governing equations of motion (2.2.18) are random differential equations . The Lyapunov exponent and moment Lyapunov exponent of the system can be determined using the analytical method developed in Section 4.1. The critical reduced velocity for the deterministic and stochastic systems are obtained and shown in Figure 4.1. From Figure 4.1(a), one can see that turbulence can shift the critical reduced velocity to a higher value and hence stabilize the system. Figure 4.1(b) gives the stabilized percentage $r_{U_{r,\mathrm{cr}}}$ of the critical reduced velocity, which is defined as

$$r_{U_{r,\mathrm{cr}}} = \frac{U^T_{r,\mathrm{cr}} - U_{r,\mathrm{cr}}}{U_{r,\mathrm{cr}}},$$

where $U_{r,\mathrm{cr}}$ and $U^T_{r,\mathrm{cr}}$ are the critical velocities in the uniform flow and turbulent flow, respectively. Figure 4.1(b) also shows that the stabilizing effect becomes smaller when α, which characterizes the bandwidth of the real noise, increases from 0.3 to 0.6. In both cases,

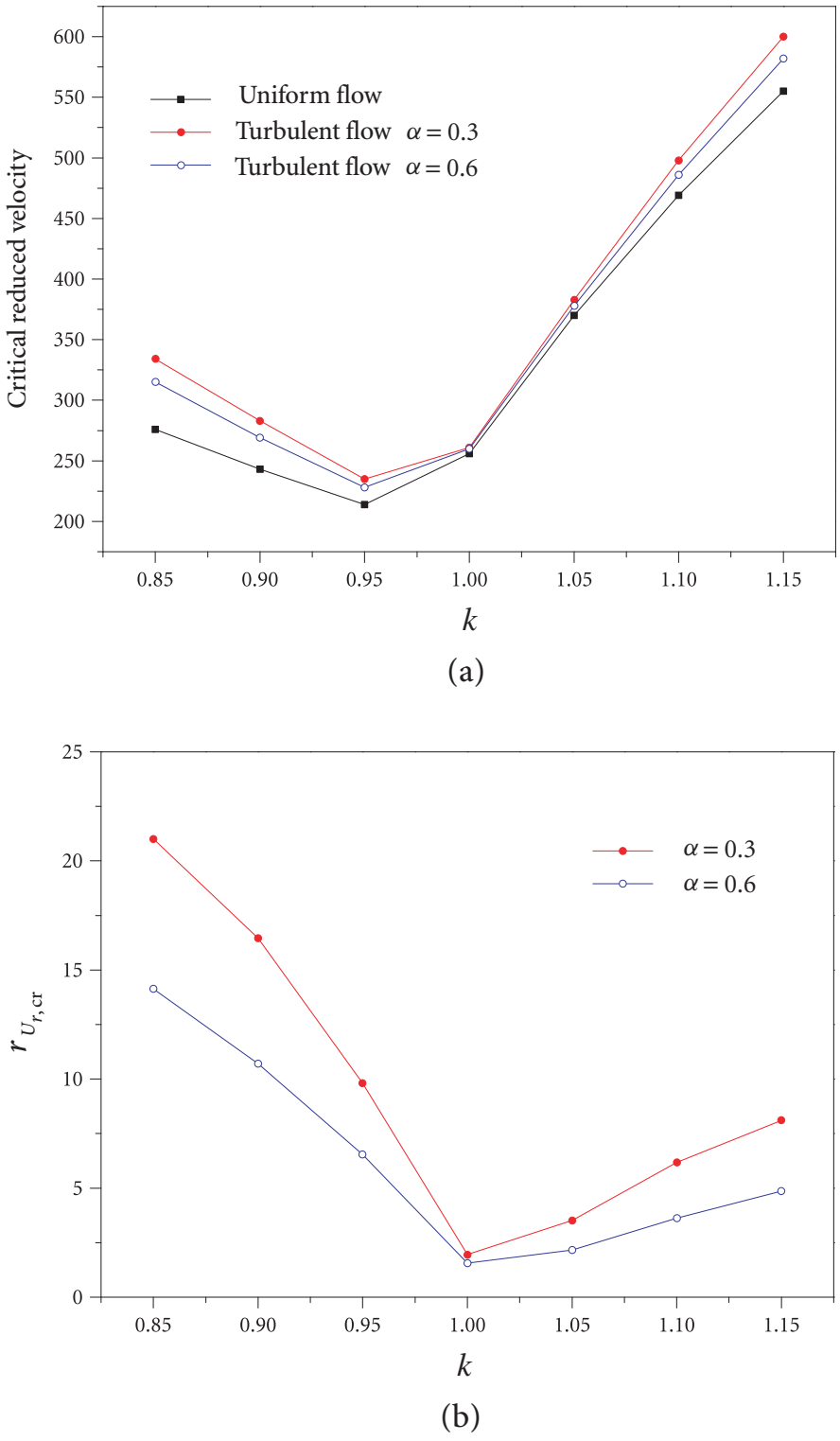

Figure 4.1 The critical reduced velocity for different k.

the amplitude of the noise μ changes with α from 1.0 to $\sqrt{2}$ to make the turbulence intensity fixed. This result indicates that the length scale of turbulence L_x is a key parameter for the stabilization since α is related to L_x. The effect of μ on the stability is shown in Figure 4.2. When μ increases, the critical reduced velocity at which the Lyapunov exponent is zero is shifted to a higher value. Since α is fixed and σ_ξ is chosen to be 0.5 for all cases, this means that higher turbulence intensity can achieve a better stabilizing effect.

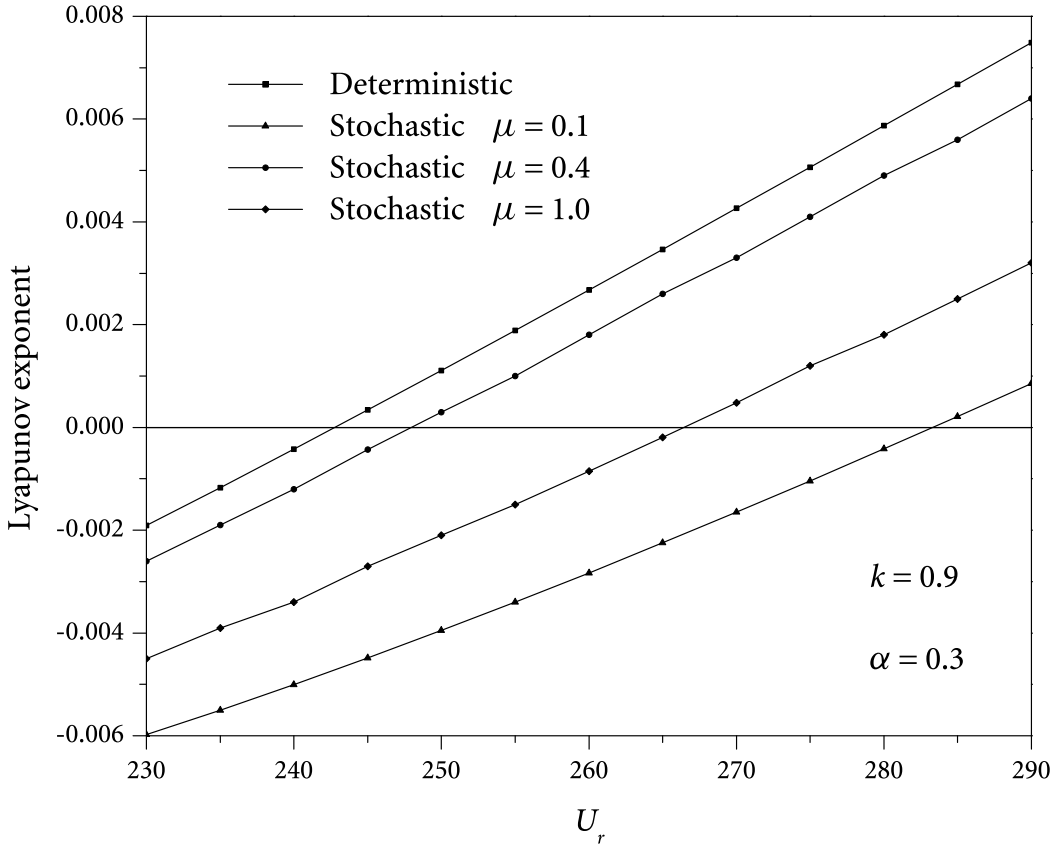

Figure 4.2 Stability boundary for $k=0.9$.

It is also found that the stabilizing effect of turbulence is sensitive to the ratio of frequencies k, as shown in Figure 4.1. Comparison of the critical velocities for different cases ($k=0.85$ to 1.15) in Figure 4.1 shows that the stabilizing effect is more significant with larger detuning in frequencies. When there is no detuning ($k=1$), the turbulence increases the critical reduced velocity slightly from $U_{r,\mathrm{cr}}=256$ to 261. When k decreases or increases from 1, the critical reduced velocity increases significantly. For example, the critical reduced

velocity increases from $U_{r,\mathrm{cr}}=243$ to 283 for $k=0.9$. To illustrate the influence of k, two cases ($k=1$ and $k=0.9$) are considered here. For a cylinder in a shear flow with $k=1.0$ and $U_r=280$, the system matrix $\mathbf{A}$ and $\mathbf{B}$ are given by

$$\mathbf{A}=\begin{bmatrix} 0.00215 & 0.97696 & 0 & 0 \\ -0.97696 & 0.00215 & 0 & 0 \\ 0 & 0 & -0.07719 & 1.06005 \\ 0 & 0 & -1.06005 & -0.07719 \end{bmatrix},$$

$$\mathbf{B}=\begin{bmatrix} -0.00610 & -0.01270 & -0.05120 & 0.00657 \\ 0.04164 & 0.05830 & -0.01271 & 0.08690 \\ 0.04965 & 0.05741 & -0.16954 & 0.15978 \\ -0.01000 & -0.01749 & -0.04129 & -0.00474 \end{bmatrix}.$$

The Lyapunov exponents can be calculated from equation (4.1.41) for different α and μ and are shown in Figure 4.3. It can be seen that Lyapunov exponents are decreased slightly when α is decreased or μ is increased. However, the stabilizing effect is quite small and not enough to stabilize the system. This is due to the weak interaction between the two modes, which can be seen from matrix $\mathbf{B}$. The elements M_{ij} and N_{ij} in the upper right submatrix and lower left submatrix are relatively small. Thus, the sum of the product of κ_{i+2} and F_i ($i=0,1,\cdots,4$) in equation (4.1.41) is small and not enough to make the largest Lyapunov exponent negative.

When $k=0.9$ and $U_r=260$, the system matrix $\mathbf{A}$ and $\mathbf{B}$ are given by

$$\mathbf{A}=\begin{bmatrix} 0.00267 & 0.91588 & 0 & 0 \\ -0.91588 & 0.00267 & 0 & 0 \\ 0 & 0 & -0.07076 & 1.01278 \\ 0 & 0 & -1.01278 & -0.07076 \end{bmatrix},$$

$$\mathbf{B}=\begin{bmatrix} 0.07601 & 0.02414 & 0.06375 & -0.01045 \\ 0.01608 & 0.00607 & -0.02520 & -0.00767 \\ -0.31696 & -0.10233 & -0.19893 & 0.05301 \\ -0.05759 & -0.01817 & -0.05297 & 0.00725 \end{bmatrix}.$$

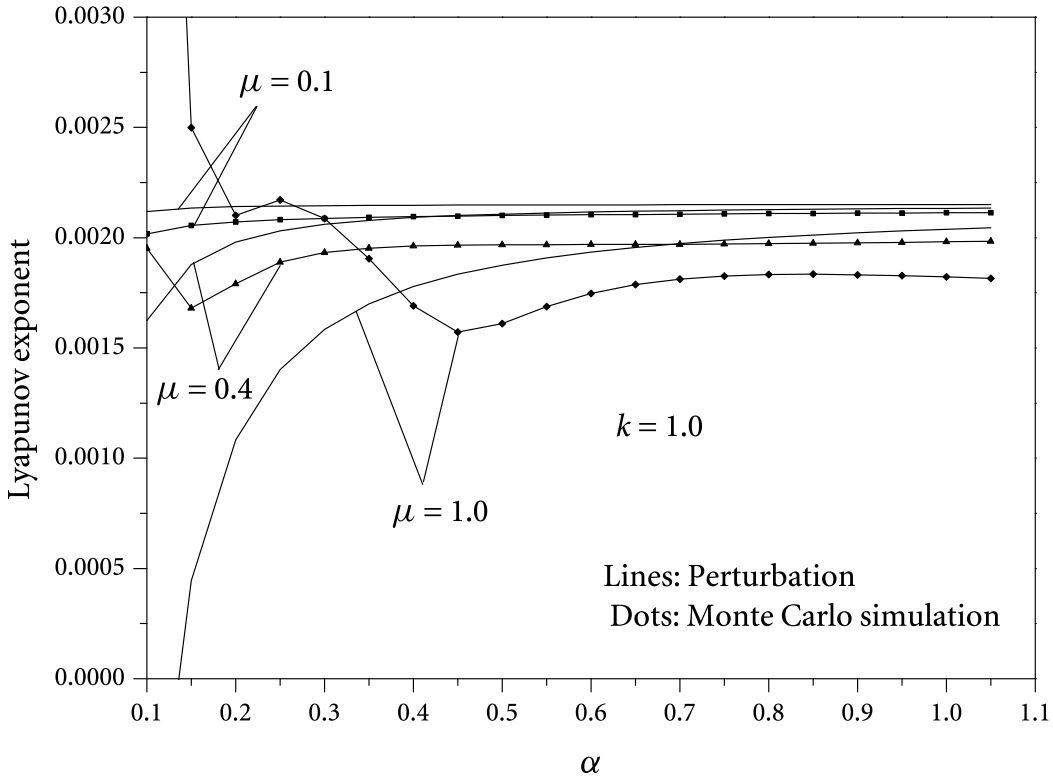

Figure 4.3 Lyapunov exponent for $k=1.0$ and $U_r=280$.

These two cases have similar matrix **A**. However, N_{11} and N_{12} in matrix **B** for $k=0.9$ are relatively large compared to those for $k=1$, which means that stronger interactions between two modes exist when the difference of frequencies increases. Thus, the energy can be transmitted from the critical mode to the stable mode via the turbulence, which results in the stabilization. Rottmann and Popp [69] also reported an experimental observation that the rocking mode of vibration switched from stable to unstable at high turbulence intensities in the fully flexible bundle while the translational mode was stabilized. This partially explained the energy transfer between two coupling modes.

The Lyapunov exponents for $k=0.9$ is shown in Figure 4.4. The stabilizing effect increases with the decrease of α or increase of the amplitude of noise μ. The same conclusion can be drawn from moment Lyapunov exponents shown in Figures 4.5 and 4.6. It can be seen that the slope at $p=0$ for $\mu=0.1$ is positive, which means that the system is unstable. When μ increases, the slope at $p=0$ becomes negative and the system becomes stable. Furthermore,

the moment Lyapunov exponents are negative between $p=0$ and 0.8 for $\mu=1$, which indicates the moment stability of the system. From these figures, it is found that the system is stabilized in the sense of both sample stability and moment stability.

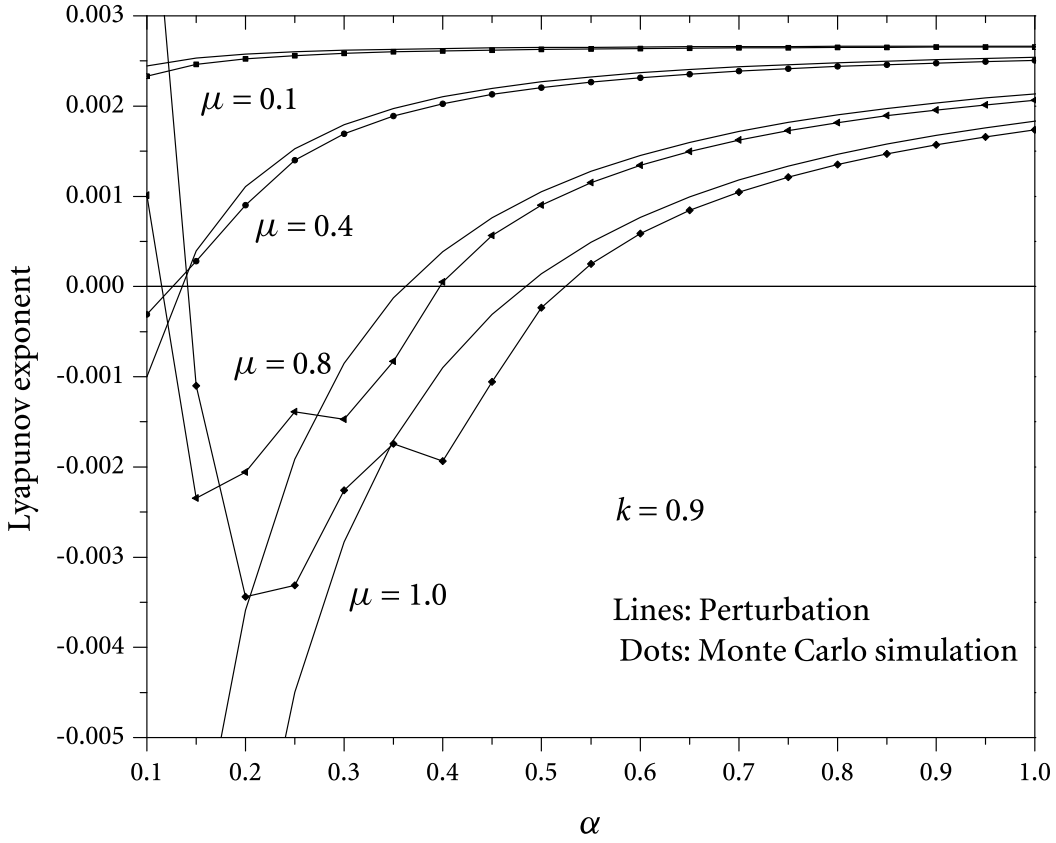

Figure 4.4 Lyapunov exponent for $k=0.9$ and $U_r=260$.

The Lyapunov exponents and moment Lyapunov exponents can also be obtained by Monte Carlo simulation (see, e.g., Xie [99]). In the simulation, the system can be discretized using the Euler scheme and the time step is $\Delta t=10^{-6}$. 5000 sample paths are simulated to calculate the moment Lyapunov exponents. As shown in Figures 4.4–4.8, the numerical results agree well with the analytical results for larger α. One exception is Figure 4.3 which shows significant discrepancies even when α is large. This is because all the elements of matrix **B** are small compared to the value of μ, which impairs the results of perturbation method. For all the cases, the discrepancy grows with the decrease of α. Figures 4.5 and 4.6 for moment Lyapunov exponents also show that the perturbation results are better with

relatively large α. The power spectrum of real noise is more narrow-banded with smaller α. Numerical results show that turbulence can destabilize the system when $\alpha < 0.1$. One possible explanation is that the destabilization is due to the parametric resonance. When α is small, the energy of the real noise is located at lower frequency range. Since the difference between ω_1 and ω_2 is small, the parametric resonance corresponding to a combination difference type could occur (Poirel and Price [62]).

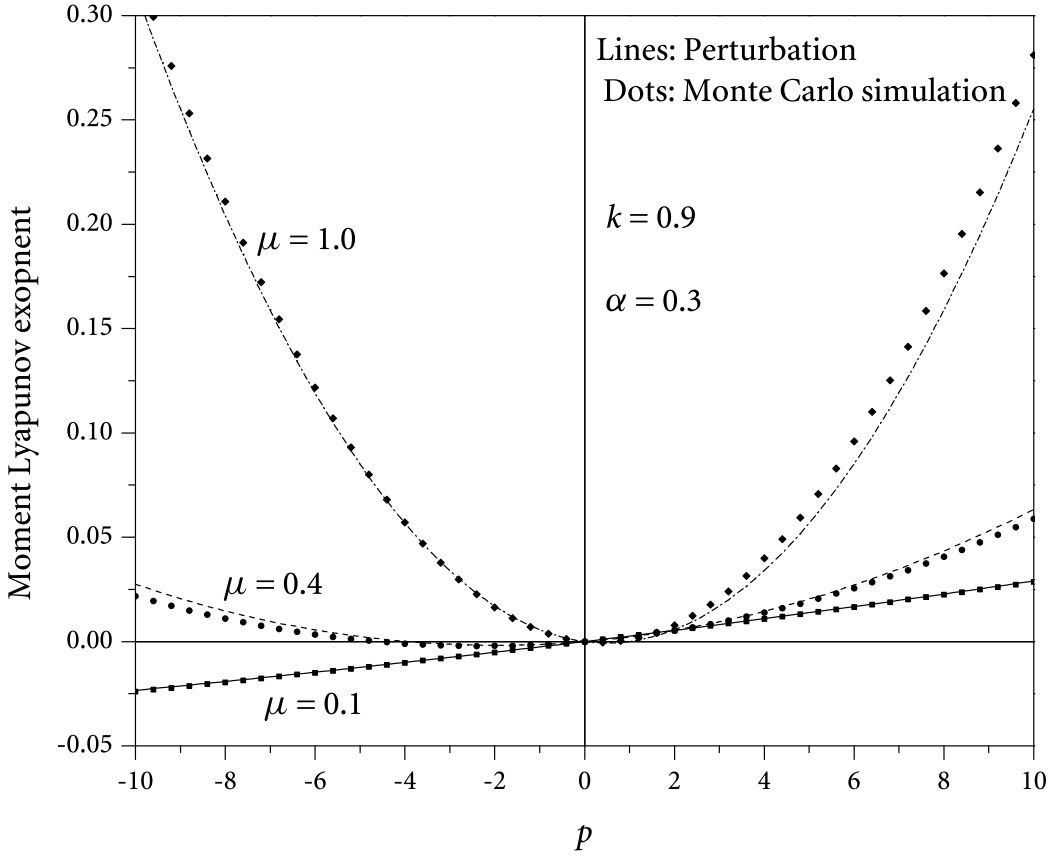

Figure 4.5 Moment Lyapunov exponent for $\alpha = 0.3$, $k = 0.9$, and $U_r = 260$.

As mentioned in Section 4.1, the stabilizing effect is more significant with decreasing α or increasing μ. Noting

$$\sigma = \sigma_0 \sigma_\xi, \qquad \mu = \frac{\sigma_0}{U_0},$$

the turbulence intensity defined by equation (2.2.6) is given by

$$T_u = \frac{\sigma/\sqrt{2\alpha}}{U_0} = \frac{\sigma_0}{U_0} \cdot \frac{\sigma_\xi}{\sqrt{2\alpha}} = \frac{\mu \sigma_\xi}{\sqrt{2\alpha}}. \tag{4.2.5}$$

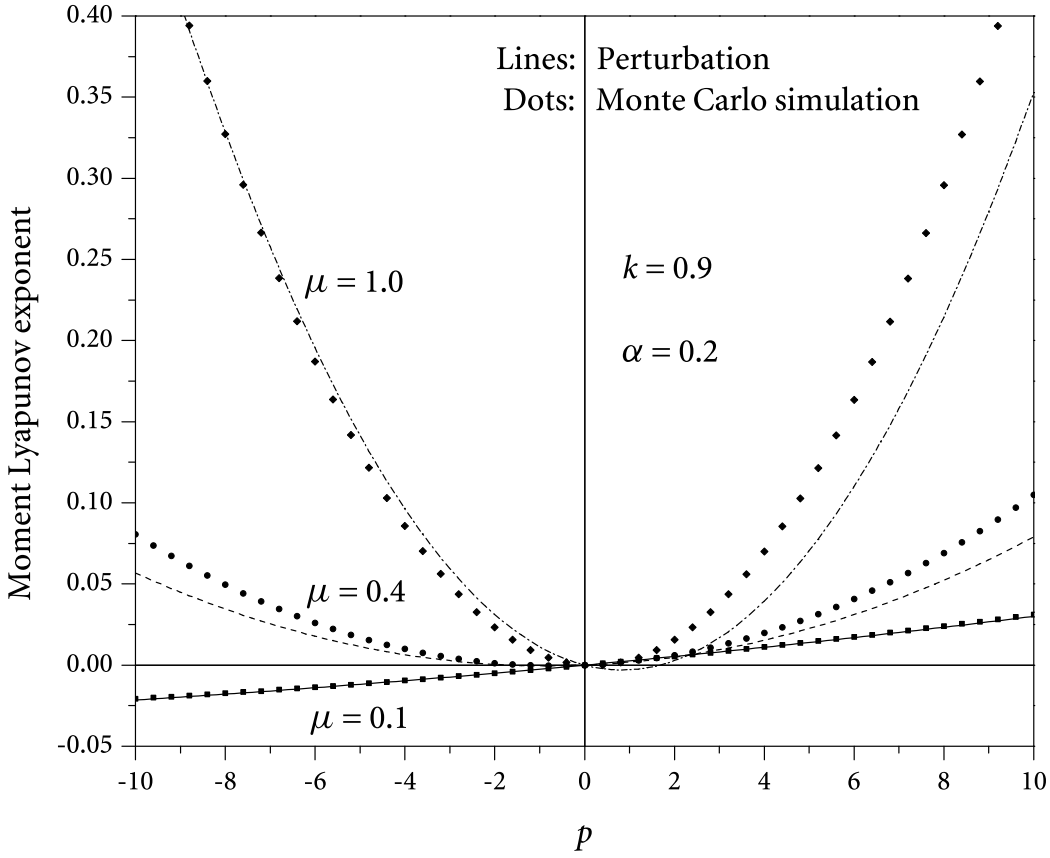

Figure 4.6 Moment Lyapunov exponent for $\alpha = 0.2$, $k = 0.9$, and $U_r = 260$.

Thus, the stabilizing effect is proportional to the turbulence intensity, which agrees with the experimental observations by Rottmann and Popp [69]. Experiments by Romberg and Popp [68] show that stabilization can be observed when the turbulence intensity T_u is larger than 13%. In the present study, stabilization could occur at $T_u = 6.5\%$ ($\mu = 0.1$ and $\alpha = 0.3$) for the cylinder with $k = 0.9$ (see Figure 4.2). However, the effect of turbulence on the fluid force coefficients is not taken into account. In the above study, it is assumed that the drag and lift force coefficients do not change for different cases due to the lack of experimental data for a cylinder in a shear flow. In fact, the coefficients can be influenced by the turbulence intensity and Reynolds number (So and Savkar [79], and Blackburn and Melbourne [13], [14]). Further experimental investigation on the effect of turbulence needs to be conducted in future research.

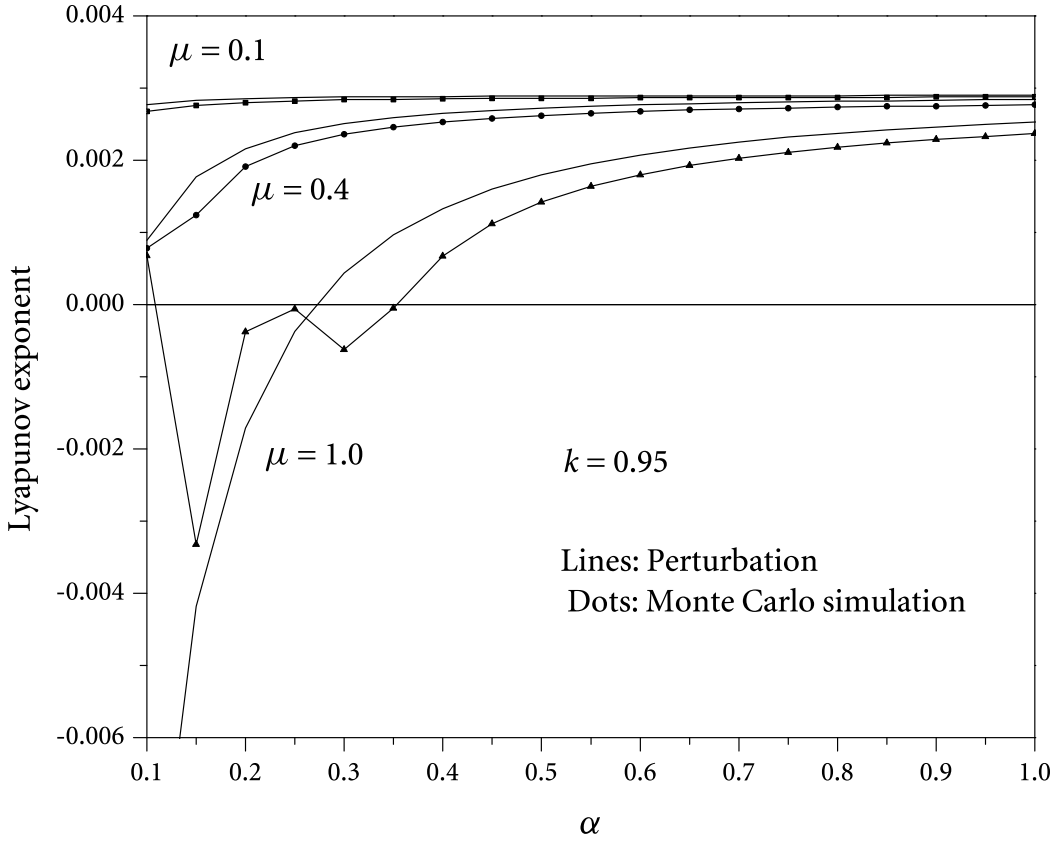

Figure 4.7 Lyapunov exponent for $\alpha = 0.3$, $k = 0.95$, and $U_r = 240$.

4.3 Conclusion

In this chapter, the effect of real noise on the stability of a parametrically excited four-dimensional system is considered. The dynamic stability of the system is studied by determining the moment Lyapunov exponents and the Lyapunov exponents. For weak noise excitations, a regular perturbation method is employed to obtain second-order expansions of the moment Lyapunov exponents. The Lyapunov exponent is then obtained using the relationship between the moment Lyapunov exponent and the Lyapunov exponent. The correctness and the accuracy of the approximate analytical results are validated and assessed by comparing with numerical simulations.

The analytical method is applied to a circular cylinder in a shear flow, which is subjected to fluidelastic instability. The analysis demonstrates that the cylinder can be stabilized by the real noise with proper parameters in the sense of both sample stability and moment

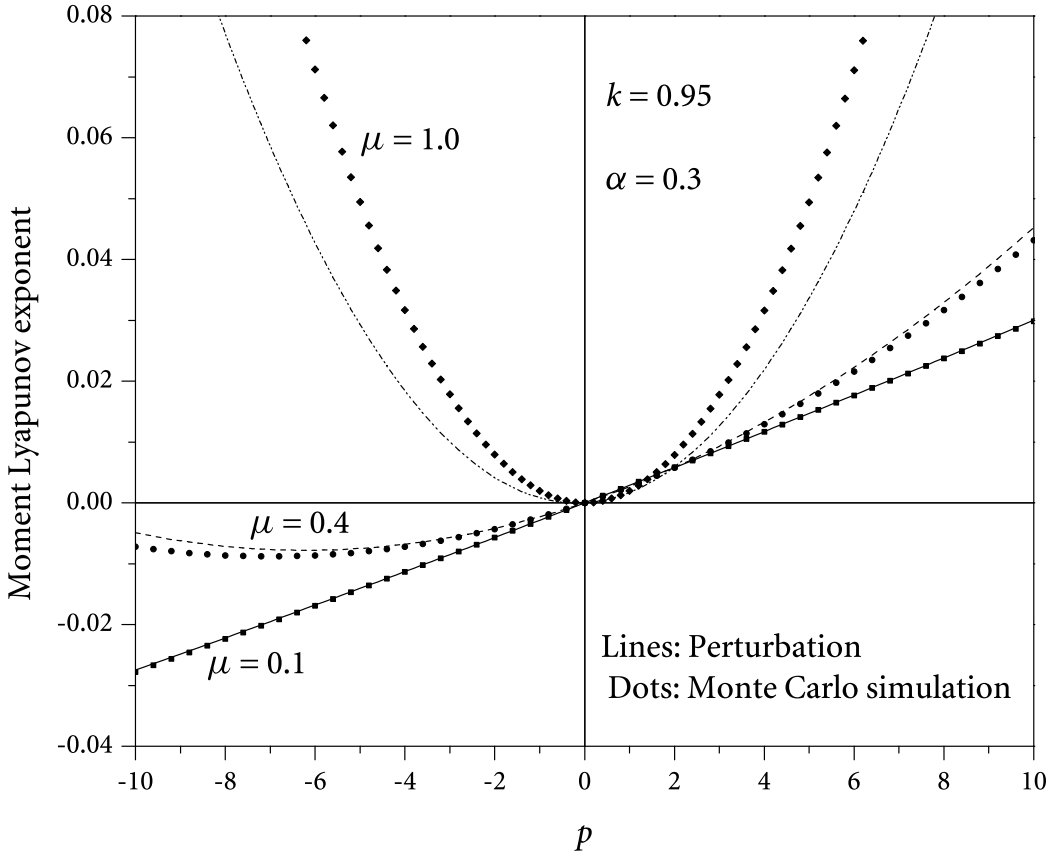

Figure 4.8 Moment Lyapunov exponent for $\alpha = 0.3$, $k = 0.95$, and $U_r = 240$.

stability. It is found that the stabilization is sensitive to the frequency ratio k. Larger detuning can result in a better stabilizing effect due to stronger coupling between the two modes. Furthermore, the stabilizing effect is proportional to the turbulence intensity, which agrees with the experimental observations.

However, noise can also destabilize a system. A two degrees-of-freedom system excited by a bounded noise can undergo parametric instability if the central frequency of the bounded noise is close to one of the natural frequencies of the system or the sum or difference of two natural frequencies. The stochastic stability of such a system is studied in the next chapter.

CHAPTER 5

Parametric Resonance of a Two Degrees-of-Freedom System Induced by Bounded Noise

The equations of motion for many engineering problems are of the general form:

$$\ddot{q}_i(t) + 2\beta_i \dot{q}_i(t) + \omega_i^2 q_i(t) + \zeta(t)\omega_i \sum_{j=1}^{2} k_{ij} q_j(t) = 0, \quad i = 1, 2, \tag{5.0.1}$$

where q_i's are the generalized coordinates, β_i and ω_i are the ith damping constant and circular natural frequency, respectively, and $\zeta(t)$ is a stochastic process describing the excitation.

Equations (5.0.1) represent a number of practical flow-induced vibration problems encountered in aerospace, power, and structural engineering. Namachchivaya and Vedula [55] used a similar set of equations to study the stability of a downstream cylinder in the wake of upstream cylinder arrays. The two degrees-of-freedom represent the cylinder motions in the lift and the drag directions, respectively. Their interaction would induce unstable motions at certain reduced velocities which are related to ω_i and k_{ij}. Moreover, when the approach flow is turbulent, the coefficients of interaction were modeled by real noise processes, and the stabilizing effect observed experimentally was explained. For a civil engineering structure, such as a bridge deck, the two degrees-of-freedom usually represent the bending motion and the torsional motion (Li and Lin, [45] and [46]). Again, the aerodynamic interaction between the two motions gives rise to unstable motion under certain conditions.

The effect of flow turbulence was also addressed, and it was shown that the turbulence has a stabilizing or destabilizing effect, depending on whether it increases or decreases the mean critical wind velocity. Similar aeroelastic coupling between the translational mode and the tortional mode can also be found in the flutter of an airfoil (Poirel and Price [62]). The flutter speed was found to be decreased by flow turbulence, especially its longitudinal component, and this change of flutter point is mainly due to fluid stiffness.

Xie obtained weak noise expansions of the moment Lyapunov exponent, the Lyapunov exponent, and the stability index of a two-dimensional system under real noise excitation [96] and bounded noise excitation [98] in terms of the small fluctuation parameter. In Chapter 3 (see also Zhu *et al.* [104]), the vortex shedding force of a cylinder in a cross-flow is modeled as a bounded noise process and it is found that parametric instability occurred in the lock-in region.

For a two degrees-of-freedom system, Namachchivaya and Vedula [55] obtained an asymptotic approximation of the moment Lyapunov exponent and the Lyapunov exponent with one critical mode and another asymptotically stable mode driven by a real noise of small intensity. They showed that the system can be stabilized by real noise. Namachchivaya and Roessel [53] studied two coupled oscillators driven by real noise. They set up the eigenvalue problem using the perturbation and stochastic averaging method, respectively, and obtained an approximation for the moment Lyapunov exponents of the two degrees-of-freedom system. Furthermore, Namachchivaya and Roessel [54] determined the moment Lyapunov exponent of two coupled oscillators with commensurable frequencies excited by a real noise using a perturbation method. Li and Lin [46] studied a two degrees-of-freedom system excited by the bounded noise process. They used the stochastic averaging method to determine the Lyapunov exponent of the system and thus determined the boundary of stability of the system.

In this chapter, a two degrees-of-freedom system under bounded noise excitation is considered. Depending on the central frequency of the bounded noise, various types of parametric resonance may occur in the system. The partial differential eigenvalue problem governing the moment Lyapunov exponent is established. For weak noise excitations, a singular perturbation method is employed to obtain second-order expansions of the moment Lyapunov exponents. The effects of the bounded noise and the detuning frequency

on the resonance are investigated. This chapter explores the moment stability as well as sample stability of the system and can be considered as an extension of Li and Lin [46], which studied the sample stability of the two degrees-of-freedom system through stochastic averaging method. Stochastic stability of the system, which is in subharmonic resonance, combination additive resonance, and combined resonance, respectively, when the excitation is a harmonic function, is studied. Numerical results for both the Lyapunov exponents and moment Lyapunov exponents are obtained by Monte Carlo simulation and compared with the analytical results to validate the analytical approach.

5.1 Formulation

Consider the following two degrees-of-freedom system

$$\ddot{q}_1 + 2\varepsilon\beta_1\dot{q}_1 + \omega_1^2 q_1 + \varepsilon\omega_1(k_{11}q_1 + k_{12}q_2)\zeta(t) = 0, \tag{5.1.1a}$$

$$\ddot{q}_2 + 2\varepsilon\beta_2\dot{q}_2 + \omega_2^2 q_2 + \varepsilon\omega_2(k_{21}q_1 + k_{22}q_2)\zeta(t) = 0, \tag{5.1.1b}$$

where $\zeta(t)$ is the excitation process, and ε is a small parameter introduced to make the analytical analysis more convenient.

5.1.1 Deterministic Excitation

If the excitation $\zeta(t)$ is deterministic and harmonic, e.g., $\zeta(t) = \cos\nu t$, system (5.1.1) could be in parametric resonance depending on the frequency ν. When the central frequency ν is not in the vicinities of $2\omega_i$ or $\left|\omega_1 \pm \omega_2\right|$, the system is stable and there is no resonance. If $\nu = 2\omega_i$, the system is in subharmonic resonance in the ith mode. The dynamic stability behavior of the system is the same as that of a single degree-of-freedom system in the first-order approximation. If the excitation frequency ν is in the vicinities of the linear combinations of two natural frequencies, i.e., $\nu = \left|\omega_1 \pm \omega_2\right|$, both modes are excited and the system is in combination resonance. See, e.g., Xie [99], for details on parametric resonance in multiple degrees-of-freedom systems.

5.1.2 Stochastic Excitation

In most practical applications, the excitation $\zeta(t)$ has to be described by a random process and in many cases a narrow-band process. To consider the effect of noise on parametric

resonance, consider the excitation $\zeta(t)$ as a narrow-band process, modeled by a bounded noise,

$$\zeta(t) = \cos\eta(t) = \cos\big[\nu t + \varepsilon^{1/2}\sigma W(t) + \psi\big],$$

in which $W(t)$ is the standard Wiener process, and ψ is a uniformly distributed random number in $(0, 2\pi)$ that makes $\zeta(t)$ a stationary process.

Using the transformation $q_1 = x_1$, $\dot{q}_1 = \omega_1 x_2$, $q_2 = x_3$, and $\dot{q}_2 = \omega_2 x_4$, equations (5.1.1) can be written as

$$\dot{\mathbf{x}} = \mathbf{A}\mathbf{x} + \varepsilon\zeta(t)\mathbf{B}\mathbf{x}, \quad \mathbf{x} \in \mathbb{R}^4, \tag{5.1.2}$$

where

$$\mathbf{A} = \begin{bmatrix} 0 & \omega_1 & 0 & 0 \\ -\omega_1 & -2\varepsilon\beta_1 & 0 & 0 \\ 0 & 0 & 0 & \omega_2 \\ 0 & 0 & -\omega_2 & -2\varepsilon\beta_2 \end{bmatrix}, \qquad \mathbf{B} = \begin{bmatrix} 0 & 0 & 0 & 0 \\ -k_{11} & 0 & -k_{12} & 0 \\ 0 & 0 & 0 & 0 \\ -k_{21} & 0 & -k_{22} & 0 \end{bmatrix}.$$

Applying the transformation

$$\begin{aligned} x_1 &= \mathrm{e}^{\rho}\cos\phi_1\cos\theta, \qquad & x_3 &= \mathrm{e}^{\rho}\cos\phi_2\sin\theta, \\ x_2 &= -\mathrm{e}^{\rho}\sin\phi_1\cos\theta, \qquad & x_4 &= -\mathrm{e}^{\rho}\sin\phi_2\sin\theta, \end{aligned} \tag{5.1.3}$$

one can obtain the following set of equations for the logarithm of amplitude $\rho = \log\|\mathbf{x}\|$, phase variables (ϕ_1, ϕ_2, θ), and noise process η:

$$\begin{aligned} \dot{\rho} &= \sum_{j=0}^{1}\varepsilon^j q_j(\phi_1,\phi_2,\theta,\eta) = m_\rho, & \dot{\theta} &= \sum_{j=0}^{1}\varepsilon^j s_j(\phi_1,\phi_2,\theta,\eta) = m_\theta, \\ \dot{\phi}_i &= \sum_{j=0}^{1}\varepsilon^j h_{ij}(\phi_1,\phi_2,\theta,\eta) = m_{\phi_i}, & \mathrm{d}\eta &= \nu\mathrm{d}t + \varepsilon^{1/2}\sigma\mathrm{d}W(t), \end{aligned} \tag{5.1.4}$$

where

$$\begin{aligned} q_0(\eta,\phi_1,\phi_2,\theta) &= 0, \\ q_1(\eta,\phi_1,\phi_2,\theta) &= \tfrac{1}{4}\big\{(k_{11}\sin2\phi_1 + k_{22}\sin2\phi_2) + (k_{11}\sin2\phi_1 - k_{22}\sin2\phi_2)\cos2\theta \\ &\quad + \big[(k_{12}+k_{21})\sin\phi^+ + (k_{12}-k_{21})\sin\phi^-\big]\sin2\theta\big\}\cos\eta(t) \\ &\quad - \tfrac{1}{2}\big[\beta_1(1-\cos2\phi_1) + \beta_2(1-\cos2\phi_2)\big] \end{aligned}$$

$$- \tfrac{1}{2}\big[\beta_1(1-\cos 2\phi_1) - \beta_2(1-\cos 2\phi_2)\big]\cos 2\theta,$$

$$h_{10}(\eta,\phi_1,\phi_2,\theta) = \omega_1,$$

$$h_{11}(\eta,\phi_1,\phi_2,\theta) = \tfrac{1}{2}\big[k_{11}(1+\cos 2\phi_1) + k_{12}(\cos\phi^+ + \cos\phi^-)\tan\theta\big]\cos\eta(t) - \beta_1 \sin 2\phi_1,$$

$$h_{20}(\eta,\phi_1,\phi_2,\theta) = \omega_2,$$

$$h_{21}(\eta,\phi_1,\phi_2,\theta) = \tfrac{1}{2}\big[k_{22}(1+\cos 2\phi_2) + k_{21}(\cos\phi^+ + \cos\phi^-)\cot\theta\big]\cos\eta(t) - \beta_2 \sin 2\phi_2,$$

$$s_0(\eta,\phi_1,\phi_2,\theta) = 0,$$

$$\begin{aligned} s_1(\eta,\phi_1,\phi_2,\theta) = \tfrac{1}{4}\big\{&(k_{21}-k_{12})\sin\phi^+ - (k_{12}+k_{21})\sin\phi^- \\ &+ (k_{22}\sin 2\phi_2 - k_{11}\sin 2\phi_1)\sin 2\theta \\ &+ \big[(k_{12}+k_{21})\sin\phi^+ + (k_{12}-k_{21})\sin\phi^-\big]\cos 2\theta\big\}\cos\eta(t) \\ &+ \tfrac{1}{2}\big[\beta_1(1-\cos 2\phi_1) - \beta_2(1-\cos 2\phi_2)\big]\sin 2\theta. \end{aligned}$$

In the above expressions, $\phi^{\pm} = \phi_1 \pm \phi_2$.

The pth norm of $\mathbf{x}$ can be written as $P = \|\mathbf{x}\|^p = (e^{\rho})^p = e^{p\rho}$. The Itô equation for P can be derived using the Itô's Lemma

$$dP = \Big(m_\rho \frac{\partial}{\partial\rho} + m_{\phi_1}\frac{\partial}{\partial\phi_1} + m_{\phi_2}\frac{\partial}{\partial\phi_2} + m_\theta\frac{\partial}{\partial\theta}\Big)P dt = p m_\rho P dt. \tag{5.1.5}$$

Applying a linear stochastic transformation

$$S = T(\eta,\phi_1,\phi_2,\theta)P, \qquad P = T^{-1}(\eta,\phi_1,\phi_2,\theta)S,$$

$$-\infty < \eta < +\infty, \quad 0 \leqslant \phi_{1,2} < 2\pi, \quad 0 \leqslant \theta < \frac{\pi}{2},$$

the Itô equation for the transformed pth norm process S can also be derived using Itô's Lemma,

$$dS = \big(\tfrac{1}{2}\varepsilon\sigma^2 T_{\eta\eta} + \nu T_\eta + m_{\phi_1} T_{\phi_1} + m_{\phi_2} T_{\phi_2} + m_\theta T_\theta + m_P T\big)P\,dt + \varepsilon^{1/2}\sigma T_\eta P\,dW. \tag{5.1.6}$$

For bounded and non-singular transformation $T(\eta,\phi_1,\phi_2,\theta)$, both processes P and S are expected to have the same stability behavior. Therefore, $T(\eta,\phi_1,\phi_2,\theta)$ is chosen so that the drift term of the Itô differential equation (5.1.6) is independent of the noise process $\eta(t)$,

the phase processes ϕ_1, ϕ_2, and θ so that

$$\mathrm{d}S = \Lambda S\,\mathrm{d}t + \varepsilon^{1/2}\sigma T_\eta T^{-1} S\,\mathrm{d}W. \tag{5.1.7}$$

Comparing equations (5.1.6) and (5.1.7), it is seen that such a transformation $T(\eta, \phi_1, \phi_2, \theta)$ is given by the following equation

$$\begin{aligned}\tfrac{1}{2}\varepsilon\sigma^2 T_{\eta\eta} + \nu T_\eta + m_{\phi_1} T_{\phi_1} + m_{\phi_2} T_{\phi_2} + m_\theta T_\theta + m_P T = \Lambda T,\\ -\infty < \eta < +\infty, \quad 0 \leqslant \phi_{1,2} < 2\pi, \quad 0 \leqslant \theta < \frac{\pi}{2},\end{aligned} \tag{5.1.8}$$

in which $T(\eta, \phi_1, \phi_2, \theta)$ is a periodic function in ϕ_1 and ϕ_2 of period 2π and is bounded when $\eta \to \pm\infty$. Equation (5.1.8) defines an eigenvalue problem of a second-order differential operator with Λ being the eigenvalue and $T(\eta, \phi_1, \phi_2, \theta)$ the associated eigenfunction. From equation (5.1.7), the eigenvalue Λ is seen to be the Lyapunov exponent of the pth moment of system (5.1.2) or system (5.1.1), i.e. $\Lambda = \Lambda_{\mathbf{x}(t)}(p) = \Lambda_{\mathbf{q}(t)}(p)$.

5.2 Weak Noise Expansions of the Moment Lyapunov Exponent

5.2.1 Singular Perturbation Expansion

For weak noise excitation, i.e. $\varepsilon = o(1)$, perturbation methods can be applied to solve the partial differential eigenvalue problem (5.1.8) for the perturbative expansions of the moment Lyapunov exponent $\Lambda_{\mathbf{x}(t)}(p)$. Since the small parameter ε appears as a coefficient of the term $T_{\eta\eta}$, a method of singular perturbation (see, e.g., [101]) must be applied.

Denote the frequency $\nu = \nu_0 + \varepsilon\Delta$, where ν_0 is the central frequency and Δ is the detuning parameter. Applying the stretching transformation

$$\eta = \varepsilon^{1/2}\xi + (\alpha_1\phi_1 + \alpha_2\phi_2), \qquad \xi = \varepsilon^{-1/2}\big[\eta - (\alpha_1\phi_1 + \alpha_2\phi_2)\big],$$

in which α_1 and α_2 are constants, one has

$$\begin{aligned}\frac{\partial T}{\partial \eta} &= \frac{\partial T}{\partial \xi}\frac{\partial \xi}{\partial \eta} = \varepsilon^{-1/2} T_\xi, \qquad \frac{\partial^2 T}{\partial \eta^2} = \varepsilon^{-1} T_{\xi\xi},\\ \frac{\partial T}{\partial \phi_1} &= \frac{\partial T}{\partial \phi_1} + \frac{\partial T}{\partial \xi}\frac{\partial \xi}{\partial \phi_1} = T_{\phi_1} - \varepsilon^{-1/2}\alpha_1 T_\xi,\\ \frac{\partial T}{\partial \phi_2} &= \frac{\partial T}{\partial \phi_2} + \frac{\partial T}{\partial \xi}\frac{\partial \xi}{\partial \phi_2} = T_{\phi_2} - \varepsilon^{-1/2}\alpha_2 T_\xi.\end{aligned}$$

Thus, equation (5.1.8) becomes

$$\tfrac{1}{2}\sigma^2 T_{\xi\xi} + \omega_1 T_{\phi_1} + \omega_2 T_{\phi_2} + \varepsilon^{-1/2}\big[\nu_0 - (\alpha_1\omega_1 + \alpha_2\omega_2)\big]T_\xi + \varepsilon^{1/2}(\Delta - \alpha_1\bar{h}_{11} - \alpha_2\bar{h}_{21})T_\xi$$
$$+ \varepsilon(\bar{h}_{11}T_{\phi_1} + \bar{h}_{21}T_{\phi_2} + \bar{s}_1 T_\theta + p\bar{q}_1 T) = \Lambda T,$$
$$-\infty < \xi < +\infty, \quad 0 \leqslant \phi_{1,2} < 2\pi, \quad 0 \leqslant \theta < \frac{\pi}{2}, \quad (5.2.1)$$

where

$$\begin{aligned}
&\bar{q}_1(\xi, \phi_1, \phi_2, \theta) \\
&\quad = \tfrac{1}{4}\big\{(k_{11}\sin 2\phi_1 + k_{22}\sin 2\phi_2) + (k_{11}\sin 2\phi_1 - k_{22}\sin 2\phi_2)\cos 2\theta \\
&\qquad + \big[(k_{12}+k_{21})\sin\phi^+ + (k_{12}-k_{21})\sin\phi^-\big]\sin 2\theta\big\}\cos(\varepsilon^{1/2}\xi + \alpha_1\phi_1 + \alpha_2\phi_2) \\
&\qquad - \tfrac{1}{2}\big[\beta_1(1-\cos 2\phi_1) + \beta_2(1-\cos 2\phi_2)\big] \\
&\qquad - \tfrac{1}{2}\big[\beta_1(1-\cos 2\phi_1) - \beta_2(1-\cos 2\phi_2)\big]\cos 2\theta, \\
&\bar{h}_{11}(\xi, \phi_1, \phi_2, \theta) \\
&\quad = \tfrac{1}{2}\big[k_{11}(1+\cos 2\phi_1) + k_{12}(\cos\phi^+ + \cos\phi^-)\tan\theta\big] \\
&\qquad \times \cos(\varepsilon^{1/2}\xi + \alpha_1\phi_1 + \alpha_2\phi_2) - \beta_1\sin 2\phi_1, \\
&\bar{h}_{21}(\xi, \phi_1, \phi_2, \theta) \\
&\quad = \tfrac{1}{2}\big[k_{22}(1+\cos 2\phi_2) + k_{21}(\cos\phi^+ + \cos\phi^-)\cot\theta\big] \\
&\qquad \times \cos(\varepsilon^{1/2}\xi + \alpha_1\phi_1 + \alpha_2\phi_2) - \beta_2\sin 2\phi_2, \\
&\bar{s}_1(\xi, \phi_1, \phi_2, \theta) \\
&\quad = \tfrac{1}{4}\big\{(k_{21}-k_{12})\sin\phi^+ - (k_{12}+k_{21})\sin\phi^- + (k_{22}\sin 2\phi_2 - k_{11}\sin 2\phi_1)\sin 2\theta \\
&\qquad + \big[(k_{12}+k_{21})\sin\phi^+ + (k_{12}-k_{21})\sin\phi^-\big]\cos 2\theta\big\}\cos(\varepsilon^{1/2}\xi + \alpha_1\phi_1 + \alpha_2\phi_2) \\
&\qquad + \tfrac{1}{2}\big[\beta_1(1-\cos 2\phi_1) - \beta_2(1-\cos 2\phi_2)\big]\sin 2\theta.
\end{aligned}$$

If $\nu_0 = \alpha_1\omega_1 + \alpha_2\omega_2$, equation (5.2.1) can be reduced to

$$\tfrac{1}{2}\sigma^2 T_{\xi\xi} + \omega_1 T_{\phi_1} + \omega_2 T_{\phi_2} + \varepsilon^{1/2}\big(\Delta - \alpha_1\bar{h}_{11} - \alpha_2\bar{h}_{21}\big)T_\xi$$

$$+\varepsilon\left(\bar{h}_{11}T_{\phi_1}+\bar{h}_{21}T_{\phi_2}+\bar{s}_1T_\theta+p\bar{q}_1T\right)=\Lambda_{\mathbf{x}(t)}T,$$

$$-\infty<\xi<+\infty,\quad 0\leqslant\phi_{1,2}<2\pi,\quad 0\leqslant\theta<\frac{\pi}{2},\quad (5.2.2)$$

in which the eigenfunction T is treated as a function of ξ, ϕ_1, ϕ_2, θ, and ε. Denoting $z=\varepsilon^{1/2}\xi$, the eigenfunction $T(\xi,\phi_1,\phi_2,\theta,\varepsilon)$ becomes $Y(\xi,z,\phi_1,\phi_2,\theta)$. It can be shown that

$$T_\xi=Y_\xi+\varepsilon^{1/2}Y_z,\qquad T_{\xi\xi}=Y_{\xi\xi}+2\varepsilon^{1/2}Y_{\xi z}+\varepsilon Y_{zz}. \quad (5.2.3)$$

Substituting equation (5.2.3) into equation (5.2.2) leads to

$$\mathscr{L}(p)Y=\Lambda_{\mathbf{x}(t)}(p)Y,\qquad \mathscr{L}(p)Y=\mathscr{L}_0Y+\varepsilon^{1/2}\mathscr{L}_1Y+\varepsilon\mathscr{L}_2Y, \quad (5.2.4)$$

where

$$\mathscr{L}_0Y=\tfrac{1}{2}\sigma^2Y_{\xi\xi}+\omega_1Y_{\phi_1}+\omega_2Y_{\phi_2},$$

$$\mathscr{L}_1Y=\sigma^2Y_{\xi z}+\left(\Delta-\alpha_1\bar{h}_{11}-\alpha_2\bar{h}_{21}\right)Y_\xi,$$

$$\mathscr{L}_2Y=\tfrac{1}{2}\sigma^2Y_{zz}+\left(\Delta-\alpha_1\bar{h}_{11}-\alpha_2\bar{h}_{21}\right)Y_z+\left(\bar{h}_{11}Y_{\phi_1}+\bar{h}_{21}Y_{\phi_2}+\bar{s}_1Y_\theta+p\bar{q}_1Y\right).$$

Expand the eigenvalue $\Lambda_{\mathbf{x}(t)}(p)$ and the eigenfunction $Y(\xi,z,\phi_1,\phi_2,\theta)$ as

$$\Lambda_{\mathbf{x}(t)}(p)=\sum_{n=0}^{\infty}\varepsilon^{n/2}\Lambda_n(p),\qquad Y(\xi,z,\phi_1,\phi_2,\theta)=\sum_{n=0}^{\infty}\varepsilon^{n/2}Y_n(\xi,z,\phi_1,\phi_2,\theta), \quad (5.2.5)$$

where $Y_n(\xi,z,\phi_1,\phi_2,\theta)$ are periodic functions in ϕ_1 and ϕ_2 of period 2π. Substituting equations (5.2.5) into (5.2.4), expanding, and equating terms of the same orders of $\varepsilon^{1/2}$ yields

$$\begin{aligned}
&\mathcal{O}(1): && \mathscr{L}_0Y_0=\Lambda_0Y_0,\\
&\mathcal{O}\left(\varepsilon^{1/2}\right): && \mathscr{L}_0Y_1+\mathscr{L}_1Y_0=\Lambda_0Y_1+\Lambda_1Y_0,\\
&\mathcal{O}\left(\varepsilon^{1}\right): && \mathscr{L}_0Y_2+\mathscr{L}_1Y_1+\mathscr{L}_2Y_0=\sum_{i=0}^{2}\Lambda_iY_{n-i},\\
&\mathcal{O}\left(\varepsilon^{n/2}\right): && \mathscr{L}_0Y_n+\mathscr{L}_1Y_{n-1}+\mathscr{L}_2Y_{n-2}=\sum_{i=0}^{n}\Lambda_iY_{n-i},\quad n=3,4,\ldots.
\end{aligned} \quad (5.2.6)$$

5.2.2 Zeroth-Order Perturbation

The zeroth-order perturbation equation is $\mathscr{L}_0Y_0=\Lambda_0Y_0$, or

$$\frac{\sigma^2}{2}\frac{\partial^2Y_0}{\partial\xi^2}+\omega_1\frac{\partial Y_0}{\partial\phi_1}+\omega_2\frac{\partial Y_0}{\partial\phi_2}=\Lambda_0Y_0. \quad (5.2.7)$$

Since the moment Lyapunov exponent $\Lambda_{\mathbf{x}(t)}(p)$ passes through the origin, i.e.

$$\Lambda_{\mathbf{x}(t)}(0) = \Lambda_0(0) + \varepsilon^{1/2}\Lambda_1(0) + \varepsilon\Lambda_2(0) + \cdots = 0,$$

one obtains $\Lambda_0(0)=\Lambda_1(0)=\Lambda_2(0)=\cdots=0$. Because equation (5.2.7) does not contain p explicitly, $\Lambda_0(0)=0$ implies $\Lambda_0(p)=0$. Applying the method of separation of variables and letting

$$Y_0(\xi, z, \phi_1, \phi_2, \theta) = X_0(\xi)Z_0(z,\theta)\Phi_{01}(\phi_1)\Phi_{02}(\phi_2),$$

equation (5.2.7) becomes

$$\begin{aligned}
\frac{\Phi_{01}'}{\Phi_{01}} &= a_1,\\
\frac{\Phi_{02}'}{\Phi_{02}} &= a_2,\\
\frac{\sigma^2}{2}\frac{\ddot{X}_0}{X_0} &= -(a_1+a_2) = \kappa.
\end{aligned}$$

Solving the $\Phi_{01}(\phi_1)$ equation yields $\Phi_{01}(\phi_1)=Ce^{a_1\phi_1}$. For $\Phi_{01}(\phi_1)$ to be a periodic function of period 2π, the constant $a_1=0$ and hence $\Phi_{01}(\phi_1)=C_1$. Similarly, $a_2=0$ and $\Phi_{02}(\phi_2)=C_2$. The $X_0(\xi)$ equation results in $X_0(\xi)=D_0+D_1\xi$. For $X_0(\xi)$ to be a bounded function as $\xi\to\pm\infty$, it is required that $D_1=0$ and hence $X_0(\xi)=D_0$, which can be chosen as 1. The zeroth-order perturbation of the eigenfunction is therefore $Y_0(\xi, z, \phi_1, \phi_2, \theta)=Z_0(z,\theta)$, where $Z_0(z,\theta)$ is a function to be determined.

The adjoint equation of (5.2.7) is

$$\frac{\sigma^2}{2}\frac{\partial^2 Y_0^*}{\partial\xi^2} - \omega_1\frac{\partial Y_0^*}{\partial\phi_1} - \omega_2\frac{\partial Y_0^*}{\partial\phi_2} = 0. \tag{5.2.7′}$$

Employing the method of separation of variables with

$$Y_0^*(\xi, z, \phi_1, \phi_2, \theta) = X_0^*(\xi)Z_0^*(z,\theta)\Phi_{01}^*(\phi_1)\Phi_{02}^*(\phi_2),$$

it is easy to show that

$$\begin{aligned}
\Phi_{01}^*(\phi_1) &= \frac{1}{2\pi}, && 0\leqslant\phi_1<2\pi,\\
\Phi_{02}^*(\phi_2) &= \frac{1}{2\pi}, && 0\leqslant\phi_2<2\pi,\\
X_0^*(\xi) &= 1, && -\infty<\xi<+\infty,\\
Y_0^*(\xi, z, \phi_1, \phi_2, \theta) &= Z_0^*(z,\theta).
\end{aligned} \tag{5.2.8}$$

5.2.3 First-Order Perturbation

Since $\Lambda_0 = 0$, the first-order perturbation equation becomes

$$\mathscr{L}_0 Y_1 = \Lambda_1 Y_0 - \mathscr{L}_1 Y_0. \tag{5.2.9}$$

From the Fredholm Alternative, for equation (5.2.9) to have nontrivial solutions, it is required that

$$\left(\Lambda_1 Y_0 - \mathscr{L}_1 Y_0,\, Y_0^*\right) = 0, \tag{5.2.10}$$

where $Y_0^*(\xi, z, \phi_1, \phi_2, \theta)$ is the solution (5.2.8) of the adjoint equation (5.2.7′) of the first-order perturbation equation, and (f, g) denotes the inner product of functions $f(\cdot)$ and $g(\cdot\cdot)$ defined as

$$(f, g) = \int_{z=-\infty}^{+\infty} \int_{\xi=-\infty}^{+\infty} \int_{\phi_1=0}^{2\pi} \int_{\phi_2=0}^{2\pi} \int_{\theta=0}^{\frac{\pi}{2}} f(\cdot)\, g(\cdot\cdot)\, \mathrm{d}\theta\, \mathrm{d}\phi_2\, \mathrm{d}\phi_1\, \mathrm{d}\xi\, \mathrm{d}z.$$

Since $Y_0(\xi, z, \phi_1, \phi_2, \theta) = Z_0(z, \theta)$, which leads to $\mathscr{L}_1 Y_0 = 0$, equation (5.2.10) results in $\Lambda_1(p) = 0$. Equation (5.2.9) then becomes $\mathscr{L}_0 Y_1 = 0$. Following the same procedure as in Section 5.2.2, it is easy to show that $Y_1(\xi, z, \phi_1, \phi_2, \theta) = Z_1(z, \theta)$.

5.2.4 Second-Order Perturbation

Since $\Lambda_0 = \Lambda_1 = 0$, $\mathscr{L}_1 Y_1 = 0$, the second-order perturbation equation becomes

$$\mathscr{L}_0 Y_2 = \Lambda_2 Y_0 - \mathscr{L}_2 Y_0. \tag{5.2.11}$$

From the Fredholm Alternative, for equation (5.2.11) to have nontrivial solutions, it is required that

$$\left(\Lambda_2 Y_0 - \mathscr{L}_2 Y_0,\, Y_0^*\right) = 0,$$

which can be written as

$$\int_{z=-\infty}^{+\infty} \int_{\theta=0}^{\frac{\pi}{2}} Z_0^*(z, \theta) \Bigg\{ \int_{\phi_1=0}^{2\pi} \int_{\phi_2=0}^{2\pi} \Bigg[\frac{\sigma^2}{2} \frac{\partial^2 Z_0}{\partial z^2} + \left(\Delta - \alpha_1 \hat{h}_{11} - \alpha_2 \hat{h}_{21}\right) \frac{\partial Z_0}{\partial z} + \hat{s}_1 \frac{\partial Z_0}{\partial \theta} + \left(p\hat{q}_1 - \Lambda_2\right) Z_0 \Bigg] \mathrm{d}\phi_2 \mathrm{d}\phi_1 \Bigg\} \mathrm{d}\theta\, \mathrm{d}z = 0. \tag{5.2.12}$$

Because equation (5.2.12) is valid for an arbitrary function $Z_0^*(z, \theta)$, it results in

$$\int_{\phi_1=0}^{2\pi} \int_{\phi_2=0}^{2\pi} \left[\frac{\sigma^2}{2} \frac{\partial^2 Z_0}{\partial z^2} + \left(\Delta - \alpha_1 \hat{h}_{11} - \alpha_2 \hat{h}_{21}\right) \frac{\partial Z_0}{\partial z} + \hat{s}_1 \frac{\partial Z_0}{\partial \theta} + \left(p\hat{q}_1 - \Lambda_2\right) Z_0 \right] \mathrm{d}\phi_2 \mathrm{d}\phi_1 = 0,$$

which, after performing the integration, leads to

$$L(p)Z_0 = \Lambda_2 Z_0, \tag{5.2.13}$$

where

$$L(p)Z_0 = \frac{\sigma^2}{2}\frac{\partial^2 Z_0}{\partial z^2} + \left(\Delta - \alpha_1\hat{h}_{11} - \alpha_2\hat{h}_{21}\right)\frac{\partial Z_0}{\partial z} + \hat{s}_1\frac{\partial Z_0}{\partial \theta} + p\hat{q}_1 Z_0,$$

$$\hat{h}_{11} = \int_{\phi_1=0}^{2\pi}\int_{\phi_2=0}^{2\pi}\bar{h}_{11}\mathrm{d}\phi_2\mathrm{d}\phi_1, \qquad \hat{h}_{21} = \int_{\phi_1=0}^{2\pi}\int_{\phi_2=0}^{2\pi}\bar{h}_{21}\mathrm{d}\phi_2\mathrm{d}\phi_1,$$

$$\hat{s}_1 = \int_{\phi_1=0}^{2\pi}\int_{\phi_2=0}^{2\pi}\bar{s}_1\mathrm{d}\phi_2\mathrm{d}\phi_1, \qquad \hat{p}_1 = \int_{\phi_1=0}^{2\pi}\int_{\phi_2=0}^{2\pi}\bar{p}_1\mathrm{d}\phi_2\mathrm{d}\phi_1.$$

Hence, the second-order perturbation of the moment Lyapunov exponent Λ_2 is the eigenvalue of a second-order partial differential eigenvalue problem (5.2.13) with function $Z_0(z,\theta)$ being the associated eigenfunction.

Equation (5.2.13) can be solved using a double Fourier series. Since θ is defined on the interval $[0,\pi/2)$, the Fourier series for θ should include $\cos 4n\theta$ and $\sin 4n\theta$ which come from the extension of the interval from $[0,\pi/2)$ to $[0,2\pi)$ (see, e.g., Myint-U and Debnath [51]). Hence, the eigenfunction $Z_0(z,\theta)$ can be expressed as

$$\begin{aligned} Z_0(z,\theta) = CC_{00} &+ \sum_{n=1}^{K} CC_{0n}\cos 4n\theta + \sum_{n=0}^{K}\sum_{m=1}^{K}\left(CC_{mn}\cos mz + SC_{mn}\sin mz\right)\cos 4n\theta \\ &+ \sum_{n=1}^{K} CS_{0n}\sin 4n\theta + \sum_{n=1}^{K}\sum_{m=1}^{K}\left(CS_{mn}\cos mz + SS_{mn}\sin mz\right)\sin 4n\theta, \end{aligned} \tag{5.2.14}$$

or, more concisely,

$$\begin{aligned} Z_0(z,\theta) = \sum_{n=0}^{K}\sum_{m=0}^{K}\Big[&\left(CC_{mn}\cos mz + SC_{mn}\sin mz\right)\cos 4n\theta \\ &+ \left(CS_{mn}\cos mz + SS_{mn}\sin mz\right)\sin 4n\theta\Big], \end{aligned} \tag{5.2.14$'$}$$

in which $SC_{0n} = CS_{m0} = SS_{m0} = SS_{0n} = 0$, for all values of m and n, all the other CC_{mn}, SC_{mn}, CS_{mn}, and SS_{mn} are constant coefficients to be determined. The Fourier series is truncated to include K sine and cosine terms for the purpose of numerical analysis; when $K \to \infty$, the exact result is obtained.

Substituting equation (5.2.14′) into (5.2.13), multiplying it by $\cos rz\cos 4s\theta$, $\sin rz\cos 4s\theta$, $\cos rz\sin 4s\theta$, or $\sin rz\sin 4s\theta$, respectively, and integrating with respect to z from 0 to 2π and with respect to θ from 0 to $\pi/2$ yield a set of equations:

$$\sum_{m=0}^{K}\sum_{n=0}^{K}\begin{bmatrix} L_{mnrs}^{CCCC} & L_{mnrs}^{SCCC} & L_{mnrs}^{CSCC} & L_{mnrs}^{SSCC} \\ L_{mnrs}^{CCSC} & L_{mnrs}^{SCSC} & L_{mnrs}^{CSSC} & L_{mnrs}^{SSSC} \\ L_{mnrs}^{CCCS} & L_{mnrs}^{SCCS} & L_{mnrs}^{CSCS} & L_{mnrs}^{SSCS} \\ L_{mnrs}^{CCSS} & L_{mnrs}^{SCSS} & L_{mnrs}^{CSSS} & L_{mnrs}^{SSSS} \end{bmatrix}\begin{Bmatrix} CC_{mn} \\ SC_{mn} \\ CS_{mn} \\ SS_{mn} \end{Bmatrix} = \Lambda_2\begin{Bmatrix} CC_{rs} \\ SC_{rs} \\ CS_{rs} \\ SS_{rs} \end{Bmatrix},$$

$$r,s = 0,1,\cdots,K, \quad (5.2.15)$$

where

$$L_{mnrs}^{CCCC} = \int_{\theta=0}^{\frac{\pi}{2}}\int_{z=0}^{2\pi} L(p)(\cos mz\cos 4n\theta)\times \cos rz\cos 4s\theta\,\mathrm{d}z\mathrm{d}\theta,$$

$$L_{mnrs}^{SCCC} = \int_{\theta=0}^{\frac{\pi}{2}}\int_{z=0}^{2\pi} L(p)(\sin mz\cos 4n\theta)\times \cos rz\cos 4s\theta\,\mathrm{d}z\mathrm{d}\theta,$$

$$L_{mnrs}^{CSCC} = \int_{\theta=0}^{\frac{\pi}{2}}\int_{z=0}^{2\pi} L(p)(\cos mz\sin 4n\theta)\times \cos rz\cos 4s\theta\,\mathrm{d}z\mathrm{d}\theta,$$

$$L_{mnrs}^{SSCC} = \int_{\theta=0}^{\frac{\pi}{2}}\int_{z=0}^{2\pi} L(p)(\sin mz\sin 4n\theta)\times \cos rz\cos 4s\theta\,\mathrm{d}z\mathrm{d}\theta,$$

$$L_{mnrs}^{CCSC} = \int_{\theta=0}^{\frac{\pi}{2}}\int_{z=0}^{2\pi} L(p)(\cos mz\cos 4n\theta)\times \sin rz\cos 4s\theta\,\mathrm{d}z\mathrm{d}\theta,$$

$$L_{mnrs}^{SCSC} = \int_{\theta=0}^{\frac{\pi}{2}}\int_{z=0}^{2\pi} L(p)(\sin mz\cos 4n\theta)\times \sin rz\cos 4s\theta\,\mathrm{d}z\mathrm{d}\theta,$$

$$L_{mnrs}^{CSSC} = \int_{\theta=0}^{\frac{\pi}{2}}\int_{z=0}^{2\pi} L(p)(\cos mz\sin 4n\theta)\times \sin rz\cos 4s\theta\,\mathrm{d}z\mathrm{d}\theta,$$

$$L_{mnrs}^{SSSC} = \int_{\theta=0}^{\frac{\pi}{2}}\int_{z=0}^{2\pi} L(p)(\sin mz\sin 4n\theta)\times \sin rz\cos 4s\theta\,\mathrm{d}z\mathrm{d}\theta,$$

$$L_{mnrs}^{CCCS} = \int_{\theta=0}^{\frac{\pi}{2}}\int_{z=0}^{2\pi} L(p)(\cos mz\cos 4n\theta)\times \cos rz\sin 4s\theta\,\mathrm{d}z\mathrm{d}\theta,$$

$$L_{mnrs}^{SCCS} = \int_{\theta=0}^{\frac{\pi}{2}}\int_{z=0}^{2\pi} L(p)(\sin mz\cos 4n\theta)\times \cos rz\sin 4s\theta\,\mathrm{d}z\mathrm{d}\theta,$$

$$L_{mnrs}^{CSCS} = \int_{\theta=0}^{\frac{\pi}{2}}\int_{z=0}^{2\pi} L(p)(\cos mz\sin 4n\theta)\times \cos rz\sin 4s\theta\,\mathrm{d}z\mathrm{d}\theta,$$

$$L_{mnrs}^{SSCS} = \int_{\theta=0}^{\frac{\pi}{2}} \int_{z=0}^{2\pi} L(p)(\sin mz \sin 4n\theta) \times \cos rz \sin 4s\theta \, \mathrm{d}z\mathrm{d}\theta,$$

$$L_{mnrs}^{CCSS} = \int_{\theta=0}^{\frac{\pi}{2}} \int_{z=0}^{2\pi} L(p)(\cos mz \cos 4n\theta) \times \sin rz \sin 4s\theta \, \mathrm{d}z\mathrm{d}\theta,$$

$$L_{mnrs}^{SCSS} = \int_{\theta=0}^{\frac{\pi}{2}} \int_{z=0}^{2\pi} L(p)(\sin mz \cos 4n\theta) \times \sin rz \sin 4s\theta \, \mathrm{d}z\mathrm{d}\theta,$$

$$L_{mnrs}^{CSSS} = \int_{\theta=0}^{\frac{\pi}{2}} \int_{z=0}^{2\pi} L(p)(\cos mz \sin 4n\theta) \times \sin rz \sin 4s\theta \, \mathrm{d}z\mathrm{d}\theta,$$

$$L_{mnrs}^{SSSS} = \int_{\theta=0}^{\frac{\pi}{2}} \int_{z=0}^{2\pi} L(p)(\sin mz \sin 4n\theta) \times \sin rz \sin 4s\theta \, \mathrm{d}z\mathrm{d}\theta.$$

Equations (5.2.15) can be further cast into a generalized linear algebraic eigenvalue problem of the form

$$\left[\mathbf{A} - \Lambda_2^{(K)}\mathbf{B}\right]\mathbf{X} = \mathbf{0}, \tag{5.2.16}$$

where the superscript "(K)" signifies that the Fourier series is truncated to include K harmonic terms, $\mathbf{A}$, $\mathbf{B}$ are matrices of dimension $(2K+1)^2 \times (2K+1)^2$, and

$$\begin{aligned}\mathbf{X} = \big\{ & CC_{00}, CC_{01}, \cdots, CC_{0K}; CC_{10}, CC_{11}, \cdots, CC_{1K}, \cdots; CC_{K0}, CC_{K1}, \cdots, CC_{KK}; \\ & SC_{10}, SC_{11}, \cdots, SC_{1K}, \cdots; SC_{K0}, SC_{K1}, \cdots, SC_{KK}; \\ & CS_{01}, CS_{02}, \cdots, CS_{0K}; CS_{11}, CS_{12}, \cdots, CS_{1K}; \cdots; CS_{K1}, CS_{K2}, \cdots, CS_{KK}; \\ & SS_{11}, SS_{12}, \cdots, SS_{1K}; \cdots; SS_{K1}, SS_{K2}, \cdots, SS_{KK}\big\}^T.\end{aligned}$$

For system (5.2.16) to have non-trivial solutions, the determinant of the coefficient matrix must be zero, i.e.

$$\left|\mathbf{A} - \Lambda_2^{(K)}\mathbf{B}\right| = 0.$$

By solving this generalized eigenvalue problem, the moment Lyapunov exponent can be determined.

Having obtained an approximate result of the second-order perturbation $\Lambda_2^{(K)}$ of the moment Lyapunov exponent, an approximation of the moment Lyapunov exponent is given by

$$\Lambda_{\mathbf{x}(t)}(p) \approx \varepsilon \, \Lambda_2^{(K)}. \tag{5.2.17}$$

Using equation (1.3.4), an approximation of the Lyapunov exponent can be easily obtained

$$\lambda_{\mathbf{x}(t)} \approx \varepsilon \lambda_2^{(K)}, \qquad \lambda_2^{(K)} = \lim_{p\to 0} \frac{\Lambda_2^{(K)}}{p}. \tag{5.2.18}$$

5.3 Parametric Resonances

5.3.1 Subharmonic Resonance

To study the subharmonic resonance in the first mode, the central frequency of the bounded noise is taken as $\nu_0 = 2\omega_1$. Assuming $\omega_1 \neq \omega_2$ and $2\omega_1 \neq \omega_2$, the coefficients in equation (5.2.13) are given by

$$\hat{h}_{11} = \tfrac{1}{4}k_{11}\cos z, \qquad \hat{h}_{21} = 0,$$

$$\hat{s}_1 = \tfrac{1}{8}k_{11}\sin 2\theta \sin z + \tfrac{1}{2}(\beta_1 - \beta_2)\sin 2\theta,$$

$$\hat{q}_1 = -\tfrac{1}{8}k_{11}(1 + \cos 2\theta)\sin z - \tfrac{1}{2}\big[(\beta_1 + \beta_2) + (\beta_1 - \beta_2)\cos 2\theta\big].$$

In fact, this is the singular case in which θ approaches zero as time goes to infinity since only one mode of the system is excited. Thus, the coefficients are

$$\hat{h}_{11} = \tfrac{1}{4}k_{11}\cos z, \quad \hat{h}_{21} = 0, \quad \hat{q}_1 = -\tfrac{1}{4}k_{11}\sin z - \beta_1, \quad \hat{s}_1 = 0.$$

Hence, the eigenvalue problem is reduced to that of a single degree-of-freedom problem studied by Xie [98]. The eigenvalue problem can be solved using the Fourier series

$$Z_0(z) = C_0 + \sum_{k=1}^{N}(C_k \cos kz + S_k \sin kz), \tag{5.3.1}$$

where $C_0, C_k, S_k, k = 1, 2, \ldots, N$, are constant coefficients to be determined. Following the same procedure shown in the previous section, the moment Lyapunov exponent can be determined. Hence, the Lyapunov exponent can be evaluated from equation (1.3.4), which is shown in Figure 5.1.

For numerical simulation, the original equation can be discretized using the Euler scheme for iterations $n = 0, 1, 2, \ldots,$

$$x_1^{n+1} = x_1^n + \omega_1 x_2^n \cdot \Delta t,$$
$$x_2^{n+1} = x_2^n + \Big[-\omega_1 x_1^n - 2\varepsilon\beta_1 x_2^n - \varepsilon \cos\eta^n \big(k_{11}x_1^n + k_{12}x_3^n\big)\Big] \cdot \Delta t,$$

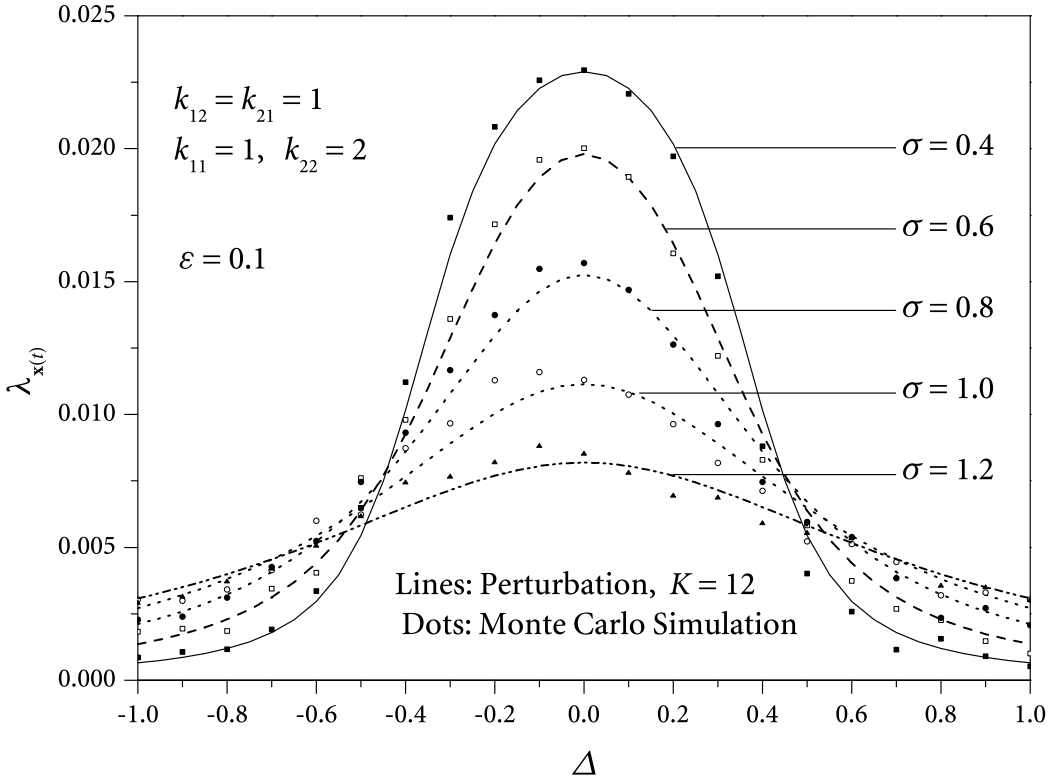

Figure 5.1 Lyapunov exponent for $\beta_1 = \beta_2 = 0$ and $\nu_0 = 2\omega_1$.

$$
\begin{aligned}
x_3^{n+1} &= x_3^n + \omega_2 x_4^n \cdot \Delta t, \\
x_4^{n+1} &= x_4^n + \Big[-\omega_2 x_3^n - 2\varepsilon\beta_2 x_4^n - \varepsilon \cos\eta^n \big(k_{21} x_1^n + k_{22} x_3^n\big) \Big] \cdot \Delta t, \\
\eta^{n+1} &= \eta^n + \nu \cdot \Delta t + \varepsilon^{1/2} \sigma \cdot \Delta W^n.
\end{aligned}
$$

These equations can be simulated iteratively and the numerical algorithm for determining the Lyapunov exponents (Wolf *et al.* [94]) can be applied to evaluate $\lambda_{\mathbf{x}(t)}$. In the Monte Carlo simulation, the time step is chosen as $\Delta t = 10^{-6}$, the frequencies are $\omega_1 = 1$ and $\omega_2 = 4$, and the number of iterations is 2×10^9. A comparison of the Lyapunov exponents $\lambda_{\mathbf{x}(t)}$ obtained by perturbation and Monte Carlo simulation as shown in Figure 5.1 reveals that there is an excellent agreement between the two results. The moment Lyapunov exponents $\Lambda_{\mathbf{x}(t)}$ are shown in Figure 5.2 for $\sigma = 1.0$.

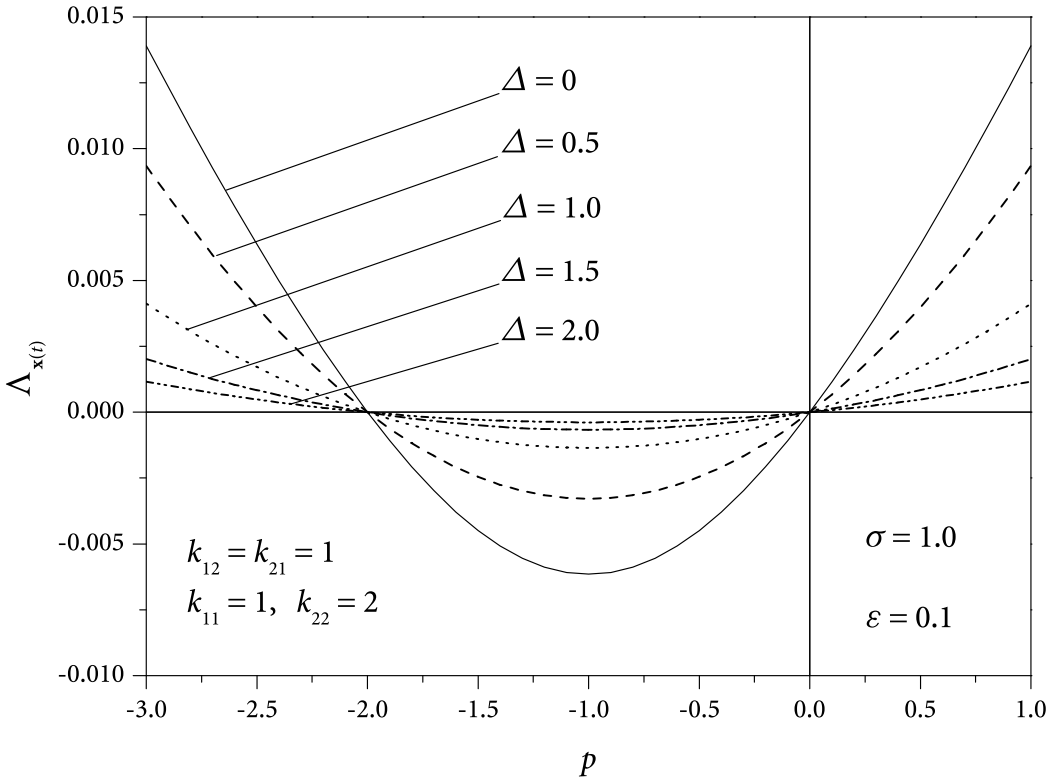

Figure 5.2 Moment Lyapunov exponent for $\beta_1 = \beta_2 = 0$, and $\nu_0 = 2\omega_1$ ($K = 12$).

5.3.2 Combination Additive Resonance

To study the combination additive resonance, the central frequency of the bounded noise is taken as $\nu_0 = \omega_1 + \omega_2$. Assuming $\omega_1 \neq \omega_2$, the coefficients in equation (5.2.13) are given by

$$\begin{aligned}
&\hat{h}_{11} = \tfrac{1}{4} k_{12} \cos z \tan\theta, \qquad \hat{h}_{21} = \tfrac{1}{4} k_{21} \cos z \cot\theta,\\
&\hat{s}_1 = -\tfrac{1}{8}\big[(k_{21} - k_{12}) + (k_{12} + k_{21})\cos 2\theta\big] \sin z + \tfrac{1}{2}(\beta_1 - \beta_2)\sin 2\theta,\\
&\hat{q}_1 = -\tfrac{1}{8}(k_{12} + k_{21})\sin 2\theta \sin z - \tfrac{1}{2}\big[(\beta_1 + \beta_2) + (\beta_1 - \beta_2)\cos 2\theta\big].
\end{aligned} \tag{5.3.2}$$

Note that k_{11} and k_{22} do not appear in the above coefficients, which means that they have no influence on the stability of the system in combination additive resonance. However, their influences have to be taken into account if ω_1 and ω_2 are close, i.e., $\omega_1 + \omega_2 \approx 2\omega_1$. By a suitable scaling of coordinates, it is always possible to take $k_{12} = \pm k_{21} = k > 0$ without loss of generality. Hence, assume $k_{12} = k_{21} = 1$ in the following analysis.

Substituting equation (5.3.2) into equation (5.2.13) and performing some calculations yield

$$\frac{\sigma^2}{2}\frac{\partial^2 Z_0}{\partial z^2}+\left(\Delta-\frac{k_{12}}{2\sin 2\theta}\cos z\right)\frac{\partial Z_0}{\partial z}+\left[-\tfrac{1}{4}k_{12}\cos 2\theta\sin z+\tfrac{1}{2}(\beta_1-\beta_2)\sin 2\theta\right]\frac{\partial Z_0}{\partial \theta}$$
$$+p\left\{-\tfrac{1}{4}k_{12}\sin 2\theta\sin z-\tfrac{1}{2}\left[(\beta_1+\beta_2)+(\beta_1-\beta_2)\cos 2\theta\right]\right\}Z_0=\Lambda_2 Z_0. \quad (5.3.3)$$

To eliminate the singularities at $\theta=0$ or $\pi/2$ in equation (5.3.3), multiplying equation (5.3.3) by $\sin 2\theta$ results in

$$\frac{\sigma^2}{2}\sin 2\theta\frac{\partial^2 Z_0}{\partial z^2}+\left(\Delta\sin 2\theta-\tfrac{1}{2}k_{12}\cos z\right)\frac{\partial Z_0}{\partial z}$$
$$+\left[-\tfrac{1}{4}k_{12}\sin 2\theta\cos 2\theta\sin z+\tfrac{1}{2}(\beta_1-\beta_2)\sin^2 2\theta\right]\frac{\partial Z_0}{\partial \theta}$$
$$+p\left\{-\tfrac{1}{4}k_{12}\sin^2 2\theta\sin z-\tfrac{1}{2}\left[(\beta_1+\beta_2)\sin 2\theta+(\beta_1-\beta_2)\sin 2\theta\cos 2\theta\right]\right\}Z_0=\Lambda_2\sin 2\theta Z_0, \quad (5.3.4)$$

or, after the simplification,

$$\frac{\sigma^2}{2}\sin 2\theta\frac{\partial^2 Z_0}{\partial z^2}+\left(\Delta\sin 2\theta-\tfrac{1}{2}k_{12}\cos z\right)\frac{\partial Z_0}{\partial z}$$
$$+\left[-\tfrac{1}{8}k_{12}\sin 4\theta\sin z+\tfrac{1}{4}(\beta_1-\beta_2)-\tfrac{1}{4}(\beta_1-\beta_2)\cos 4\theta\right]\frac{\partial Z_0}{\partial \theta}$$
$$+p\left[\tfrac{1}{8}k_{12}(1-\cos 4\theta)\sin z-\tfrac{1}{2}(\beta_1+\beta_2)\sin 2\theta-\tfrac{1}{4}(\beta_1-\beta_2)\sin 4\theta\right]Z_0=\Lambda_2\sin 2\theta Z_0, \quad (5.3.5)$$

Following the same procedure as in the previous section, the moment Lyapunov exponents and Lyapunov exponents can be determined and are shown in Figures 5.3–5.9.

The Lyapunov exponents obtained by perturbation and Monte Carlo simulation are shown in Figure 5.3. The frequencies of the system are taken as $\omega_1=1$ and $\omega_2=4$, and the central frequency of the bounded noise is taken as $\nu_0=\omega_1+\omega_2=5$. From Figure 5.3, one can clearly see that the parametric resonance occurs when the frequency detuning Δ is small ($\Delta<0.5$). Figure 5.4 shows the moment Lyapunov exponents for the undamped system. When the system is undamped, the pth moment Lyapunov exponent is positive for all $p>0$. It is seen that when the frequency detuning Δ is increased the effect of combination resonance is reduced, which is similar to the results of one degree-of-freedom system obtained in Xie [98].

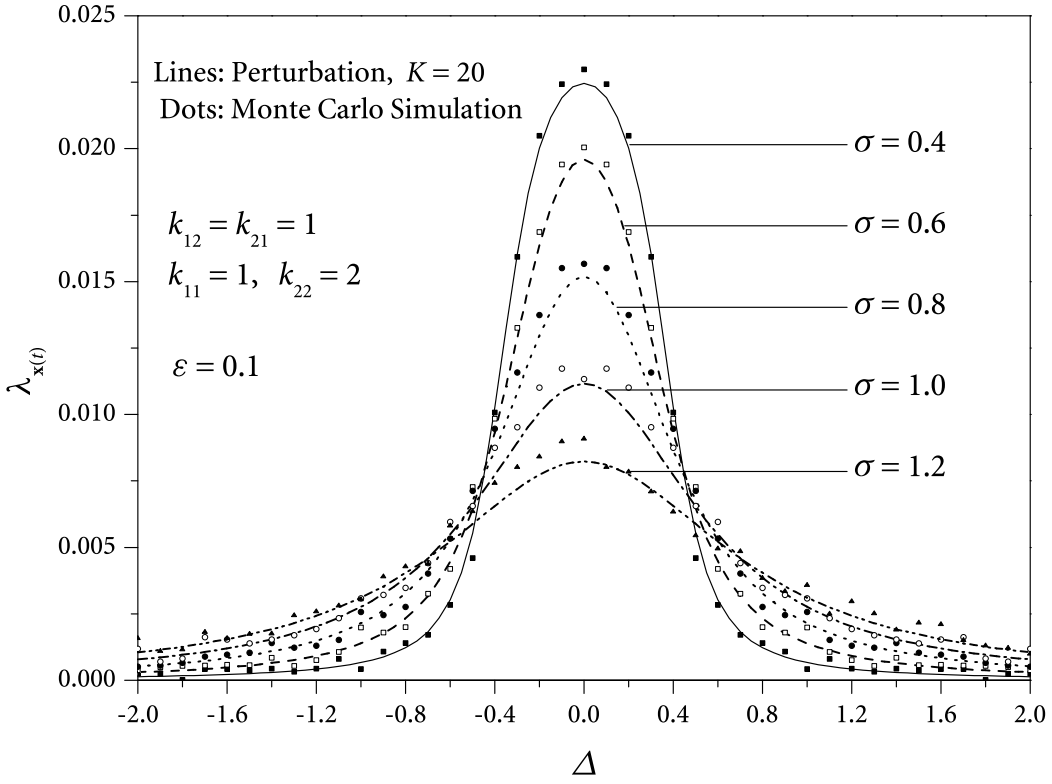

Figure 5.3 Lyapunov exponent for $\beta_1 = \beta_2 = 0$, and $\nu_0 = \omega_1 + \omega_2$.

The numerical results of the moment Lyapunov exponents given by equation (5.2.17) converge when K is sufficiently large. In this study, $K = 20$ yields satisfactory results and is used to calculate the moment Lyapunov exponents for the undamped system. For the damped system, a larger value of K is needed for satisfactory results as shown in Figures 5.5 and 5.6. It is seen that the rate of convergence varies for different system parameters.

The Monte Carlo simulation procedure proposed by Xie and Huang [95] is applied to determine the pth moment Lyapunov exponents of system (5.1.2). Numerical results are presented in Figures 5.8 and 5.9 for $\beta_1 = 0.1$ and 0.2, respectively, with various values of σ. In the simulation, the sample size is chosen as $S = 5000$, time step is $\Delta t = 10^{-5}$, the number of iterations is 2×10^8, the total time of simulation is 2000, and the state vector is normalized after every time period of $t = 20$. Approximate analytical results of $\Lambda(p)$ are also plotted for comparison. The number of harmonic terms in the double Fourier series expansion is

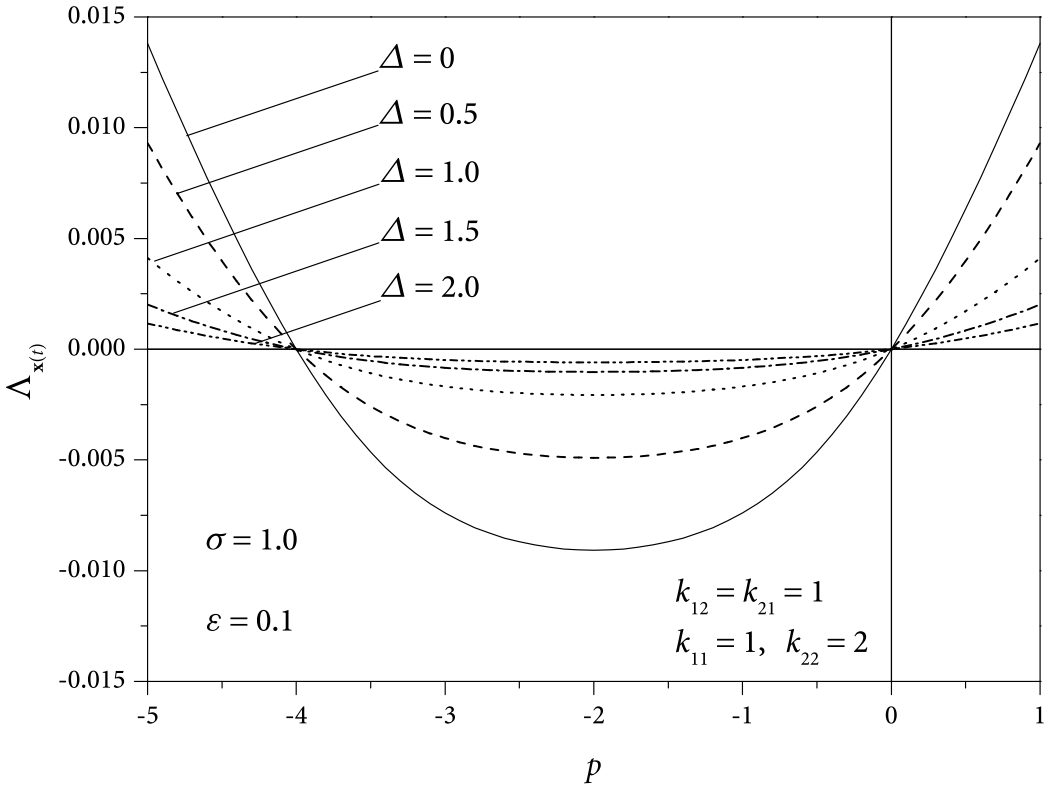

Figure 5.4 Moment Lyapunov exponent for $\beta_1 = \beta_2 = 0$ and $\nu_0 = \omega_1 + \omega_2$ ($K = 20$).

chosen as $K = 40$. It is seen that the approximate analytical results agree quite well with the numerical results.

By increasing the value of σ, the bandwidth of the narrow-band excitation modeled by the bounded noise process increases, and the effect of combination resonance is reduced, as reflected in the decrease of the Lyapunov exponent and the moment Lyapunov exponents, and the increase of the stability index as seen in Figures 5.7–5.9. Figure 5.7 shows that Lyapunov exponent becomes negative for all values of Δ when σ is increased to 0.8, meaning that the system is stable almost surely. Furthermore, the system is unstable in the pth moment, $p > 0$, for small values of σ as shown in Figures 5.8 and 5.9. For instance, Figure 5.9 shows that, when $\sigma = 1.5$, the system is unstable in the pth moment only if $p > 7$. The effect of damping can be seen from the comparison of Figure 5.8 and 5.9. At $\sigma = 1.5$, the stability index is about $p = 2$ for $\beta_1 = \beta_2 = 0.1$ (Figure 5.8). If β_1 is increased to 0.2, the

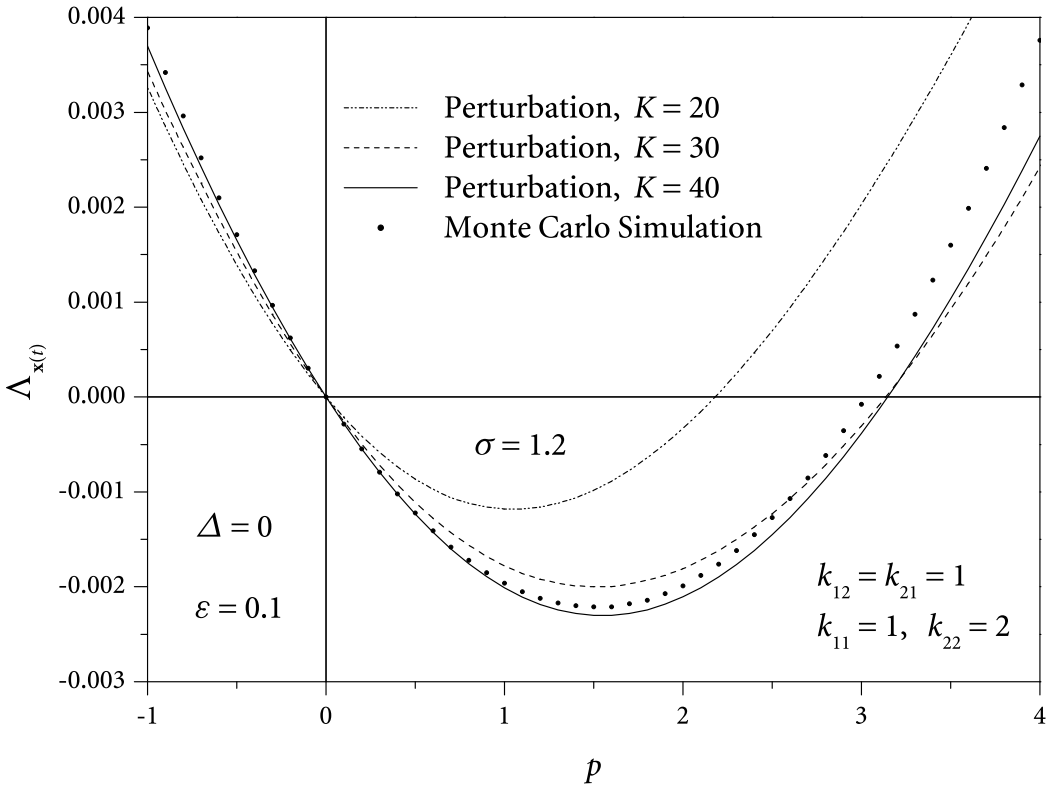

Figure 5.5 Moment Lyapunov exponent for $\beta_1 = 0.2$, $\beta_2 = 0.1$, and $\nu_0 = \omega_1 + \omega_2$.

stability index is about $p = 7$. As expected, increasing the damping always stabilizes the system.

By varying the central frequency ν_0 to $|\omega_1 - \omega_2|$ and following the same procedure, one can easily obtain the moment Lyapunov exponents for combination differential resonance.

5.3.3 Subharmonic and Combination Additive Resonance

Assuming $\omega_1 \approx \omega_2$, one has $2\omega_1 \approx 2\omega_2 \approx \omega_1 + \omega_2$. The central frequency of the bounded noise is taken as $\nu_0 = \omega_1 + \omega_2$. Here, the parameters of the system are $\omega_1 = \omega_2 = 1$ and $\nu_0 = 2$. Thus, the coefficients in equation (5.2.13) are given by

$$\hat{h}_{11} = \tfrac{1}{4}\big(k_{11} + k_{12}\tan\theta\big)\cos z, \qquad \hat{h}_{21} = \tfrac{1}{4}\big(k_{22} + k_{21}\cot\theta\big)\cos z,$$

$$\hat{s}_1 = -\tfrac{1}{8}\big[(k_{21} - k_{12}) + (k_{22} - k_{11})\sin 2\theta + (k_{12} + k_{21})\cos 2\theta\big]\sin z + \tfrac{1}{2}(\beta_1 - \beta_2)\sin 2\theta,$$

$$\hat{q}_1 = -\tfrac{1}{8}\big[(k_{11} + k_{22}) + (k_{11} - k_{22})\cos 2\theta + (k_{12} + k_{21})\sin 2\theta\big]\sin z$$

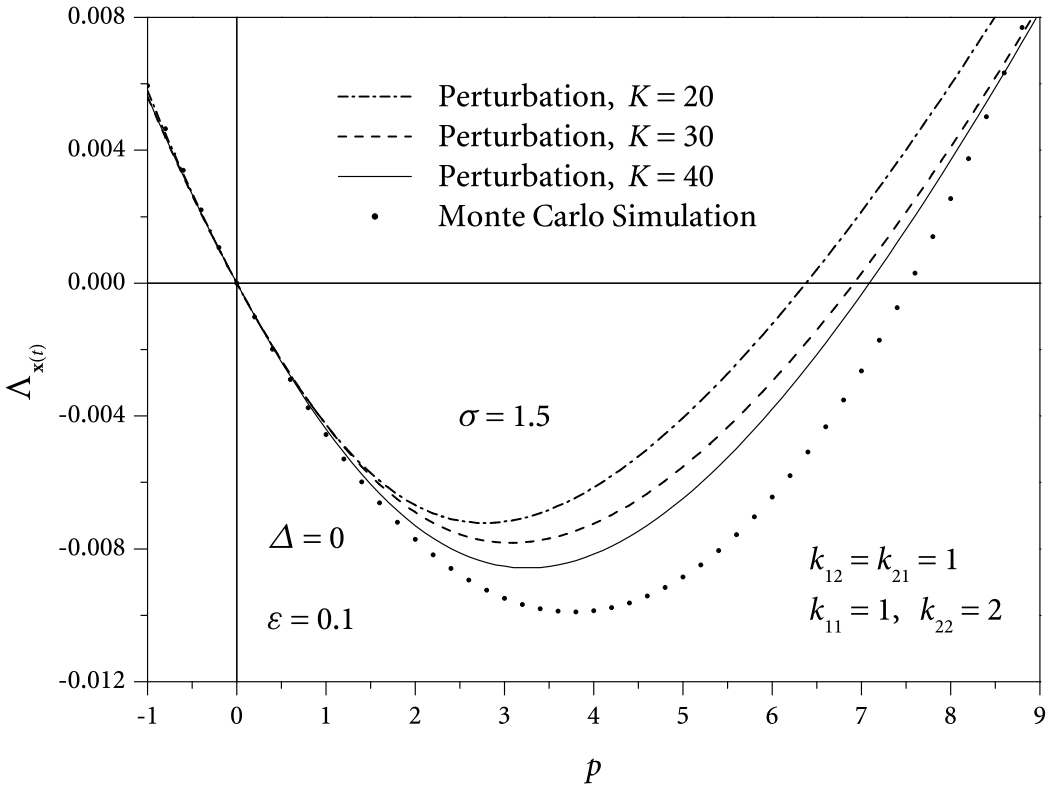

Figure 5.6 Moment Lyapunov exponent for $\beta_1 = 0.2$, $\beta_2 = 0.1$, and $\nu_0 = \omega_1 + \omega_2$.

$$- \tfrac{1}{2}\big[(\beta_1+\beta_2) + (\beta_1-\beta_2)\cos 2\theta\big]. \tag{5.3.6}$$

Substituting equation (5.3.6) into equation (5.2.13) and performing some calculations yield

$$\begin{aligned}
&\frac{\sigma^2}{2}\frac{\partial^2 Z_0}{\partial z^2} + \left[\Delta - \tfrac{1}{4}(k_{11}+k_{22})\cos z - \frac{k_{12}}{2\sin 2\theta}\cos z\right]\frac{\partial Z_0}{\partial z} \\
&\quad + \big[\tfrac{1}{8}(k_{11}-k_{22})\sin 2\theta \sin z - \tfrac{1}{4}k_{12}\cos 2\theta \sin z + \tfrac{1}{2}(\beta_1-\beta_2)\sin 2\theta\big]\frac{\partial Z_0}{\partial \theta} \\
&\quad + p\big\{-\tfrac{1}{8}\big[(k_{11}+k_{22}) + (k_{11}-k_{22})\cos 2\theta + 2k_{12}\sin 2\theta\big]\sin z \\
&\quad - \tfrac{1}{2}\big[(\beta_1+\beta_2) + (\beta_1-\beta_2)\cos 2\theta\big]\big\} Z_0 = \Lambda_2 Z_0.
\end{aligned} \tag{5.3.7}$$

Similarly, multiplying equation (5.3.7) by $\sin 2\theta$ results in

$$\begin{aligned}
&\frac{\sigma^2}{2}\sin 2\theta\frac{\partial^2 Z_0}{\partial z^2} + \big[\Delta \sin 2\theta - \tfrac{1}{4}(k_{11}+k_{22})\sin 2\theta \cos z - \tfrac{1}{2}k_{12}\cos z\big]\frac{\partial Z_0}{\partial z} \\
&\quad + \big[\tfrac{1}{8}(k_{11}-k_{22})\sin^2 2\theta \sin z - \tfrac{1}{4}k_{12}\sin 2\theta \cos 2\theta \sin z + \tfrac{1}{2}(\beta_1-\beta_2)\sin^2 2\theta\big]\frac{\partial Z_0}{\partial \theta}
\end{aligned}$$

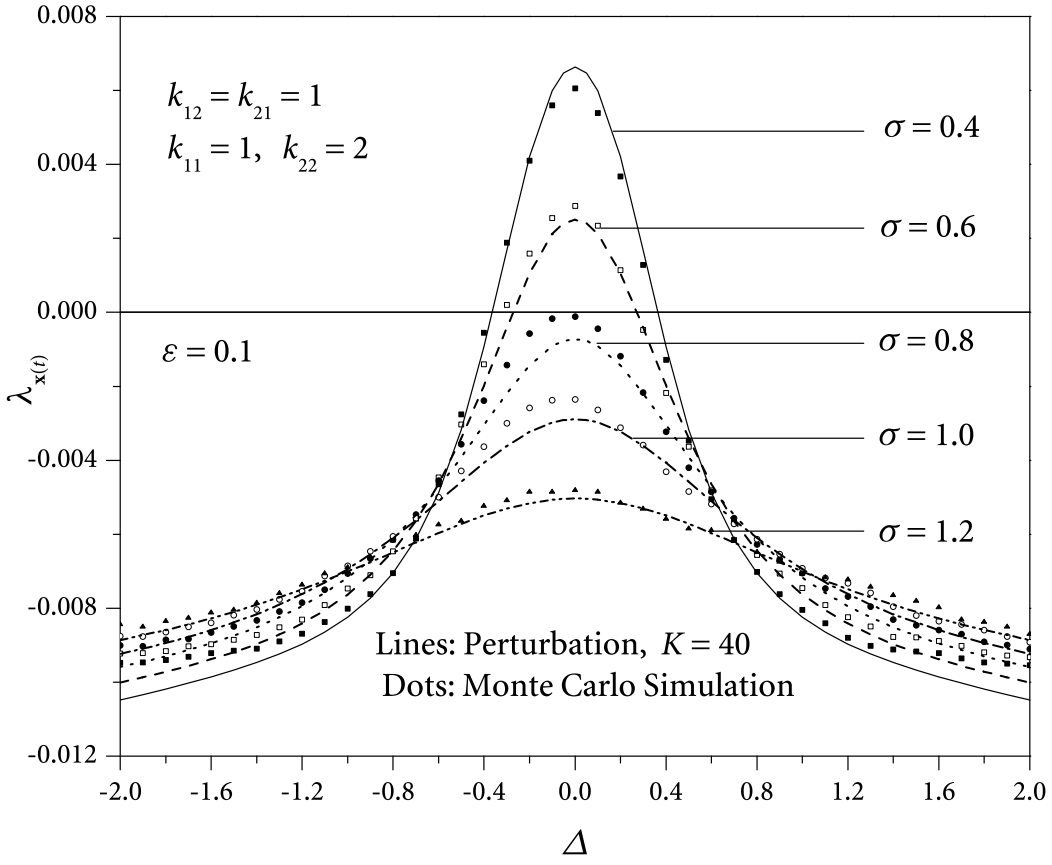

Figure 5.7 Lyapunov exponent for $\beta_1 = 0.2$, $\beta_2 = 0.1$, and $\nu_0 = \omega_1 + \omega_2$.

$$+ p\{-\tfrac{1}{8}[(k_{11}+k_{22})\sin 2\theta + (k_{11}-k_{22})\sin 2\theta\cos 2\theta + 2k_{12}\sin^2 2\theta]\sin z$$
$$- \tfrac{1}{2}[(\beta_1+\beta_2)\sin 2\theta + (\beta_1-\beta_2)\sin 2\theta\cos 2\theta]\}Z_0 = \Lambda_2 \sin 2\theta Z_0, \quad (5.3.8)$$

or, after the simplification,

$$\frac{\sigma^2}{2}\sin 2\theta\frac{\partial^2 Z_0}{\partial z^2} + [\Delta\sin 2\theta - \tfrac{1}{4}(k_{11}+k_{22})\sin 2\theta\cos z - \tfrac{1}{2}k_{12}\cos z]\frac{\partial Z_0}{\partial z}$$
$$+ [\tfrac{1}{16}(k_{11}-k_{22})\sin z - \tfrac{1}{16}(k_{11}-k_{22})\cos 4\theta\sin z - \tfrac{1}{8}k_{12}\sin 4\theta\sin z$$
$$+ \tfrac{1}{4}(\beta_1-\beta_2) - \tfrac{1}{4}(\beta_1-\beta_2)\cos 4\theta]\frac{\partial Z_0}{\partial\theta}$$
$$+ p\{-\tfrac{1}{16}[2(k_{11}+k_{22})\sin 2\theta - (k_{11}-k_{22})\sin 4\theta - 2k_{12}(1-\cos 4\theta)]\sin z$$
$$- \tfrac{1}{4}[2(\beta_1+\beta_2)\sin 2\theta + (\beta_1-\beta_2)\sin 4\theta]\}Z_0 = \Lambda_2\sin 2\theta Z_0, \quad (5.3.9)$$

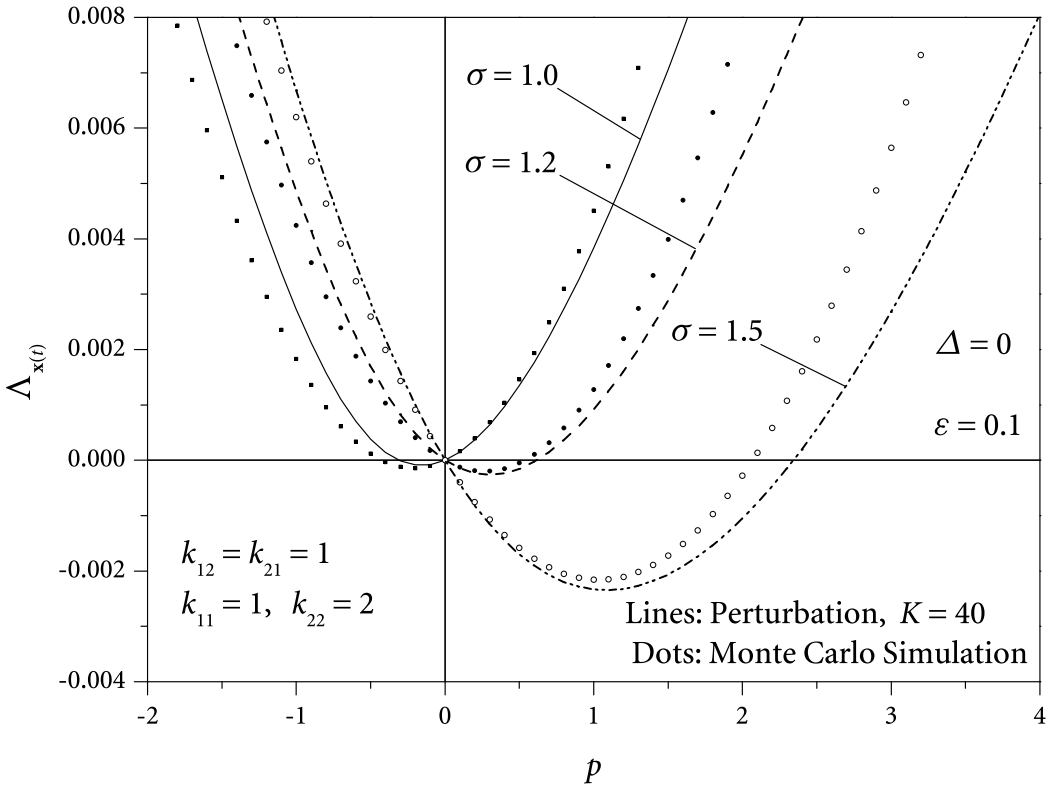

Figure 5.8 Moment Lyapunov exponent for $\beta_1 = \beta_2 = 0.1$, and $\nu_0 = \omega_1 + \omega_2$.

These expressions show that the coefficients are linear combinations of the coefficients for subharmonic and combination additive resonances. Thus, all k_{ij}'s contribute to the resonance of the system. Similarly, increasing the value of σ results in a more stable system, which can be seen from Figures 5.10 and 5.11. One can also draw the conclusion that larger values of k_{22} yields more significant resonances since larger k_{22} means larger amplitude of the bounded noise. Figure 5.12 shows that damping can reduce the resonance significantly, and can even stabilize the system when the value of σ is relatively large. For example, the Lyapunov exponents for $\sigma = 1.5$ are nearly all negative except those close to the central frequency. The moment Lyapunov exponents for the undamped system with $\sigma = 1$ and various detuning parameters Δ are shown in Figure 5.13. The stabilizing effect of damping can also be observed in Figure 5.15 in terms of the moment Lyapunov exponents. Consistently, larger values of σ also make the system more stable in the pth moments for $p > 0$.

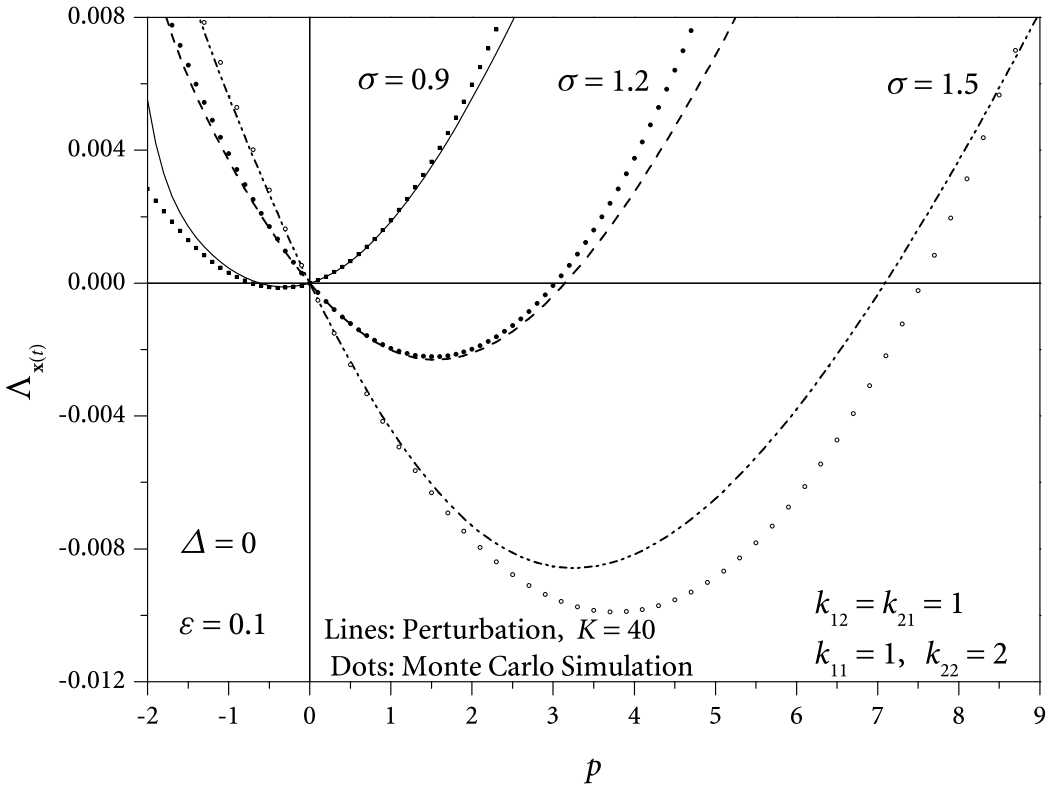

Figure 5.9 Moment Lyapunov exponent for $\beta_1 = 0.2$, $\beta_2 = 0.1$, and $\nu_0 = \omega_1 + \omega_2$.

Comparison of Figures 5.1, 5.3, and 5.11 indicates that the combined effect of subharmonic and combination additive resonances results in not only more significant resonance in terms of larger Lyapunov exponent than either case separately, but also wider resonance region in terms of frequency detuning Δ. This means that parametric resonance can be triggered more easily. For example, the resonance region for subharmonic resonance is around $|\Delta| < 0.5$ from Figure 5.1, while the region is expanded to $|\Delta| < 1.0$ from Figure 5.11 when the effects of subharmonic resonance and combination additive resonance are combined.

As shown above, the coefficients for subharmonic resonance are associated with k_{11} or k_{22} only, while the coefficients for combination additive resonance include only k_{12} and k_{21}, which represents the coupling between the two degrees-of-freedom. When the subharmonic resonance and combination additive resonance occur simultaneously, the resonance results have contributions from all k_{ij}. Depending on the values of the coefficients, the convergent

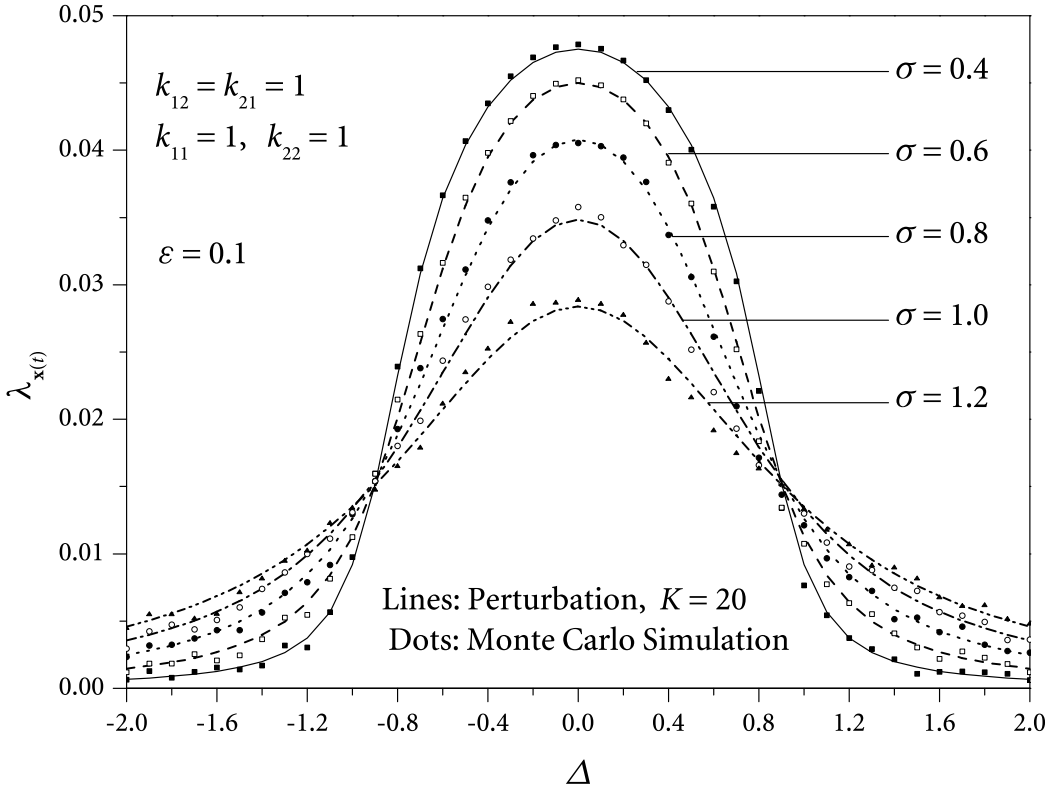

Figure 5.10 Lyapunov exponent for $\beta_1 = \beta_2 = 0$, $\omega_1 = \omega_2$, and $\nu_0 = 2\omega_1$.

rates of the Fourier series are different. For subharmonic resonance, $K = 12$ is sufficient to obtain satisfactory results. However, a relatively large K ($K = 40$) is needed for the combination additive resonance with damping. Meanwhile, other parameters such as the damping coefficients $\beta_{1,2}$, noise intensity σ, and frequency detuning Δ also influence the rates of convergence (see, e.g., Figures 5.5 and 5.6).

Larger values of k_{ij} yield more significant resonance since they are the amplitudes of the bounded noise. Decreasing the value of σ has the same effect on the stability because the power spectrum of the bounded noise is more narrow-banded and the effect of parametric resonance is more prominent. The frequency detuning parameter Δ is also a key parameter to the stability of the system. When the central frequency of the bounded noise is offset from the resonance frequencies, the effect of parametric resonance is significantly reduced. The damping always has a stabilizing effect.

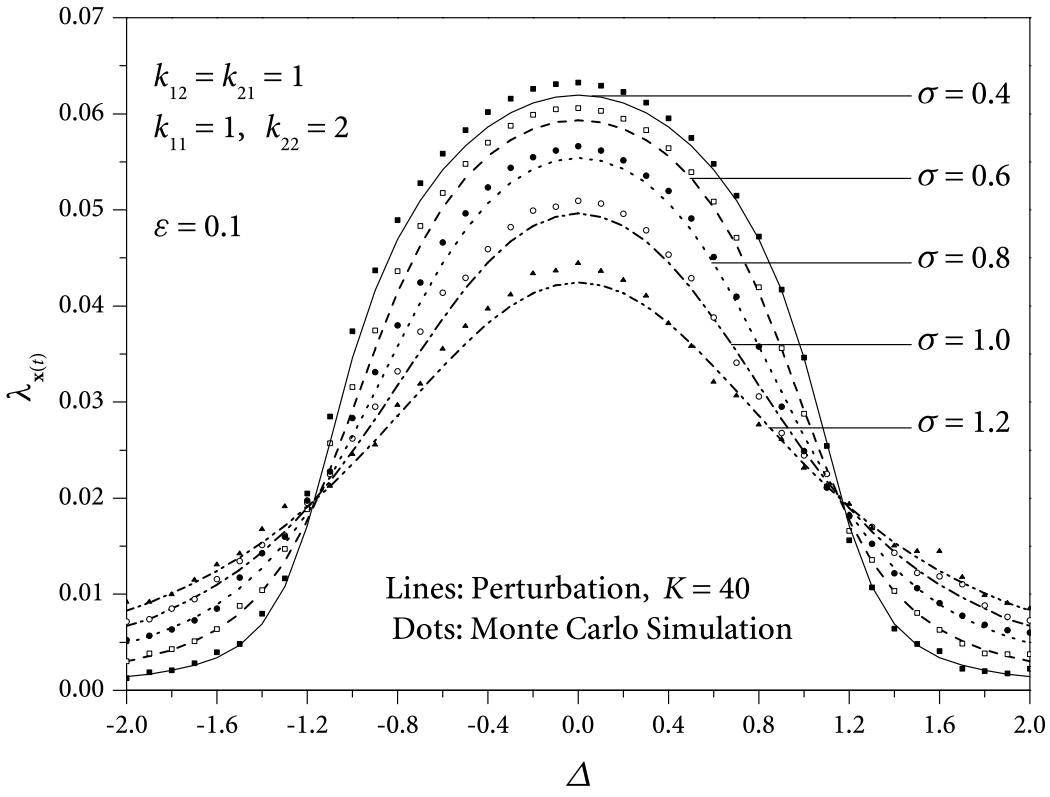

Figure 5.11 Lyapunov exponent for $\beta_1 = \beta_2 = 0$, $\omega_1 = \omega_2$, and $\nu_0 = 2\omega_1$.

5.4 Conclusion

The dynamic stability of a two degrees-of-freedom system subjected to bounded noise excitation is studied by determining the moment Lyapunov exponents. The partial differential eigenvalue problem governing the moment Lyapunov exponent is established using the theory of stochastic dynamical system. For weak noise excitations, a singular perturbation method is employed to obtain second-order expansions of the moment Lyapunov exponents. A double Fourier series is used to solve the eigenvalue problem. The Lyapunov exponent is then obtained using the relationship between the moment Lyapunov exponent and the Lyapunov exponent. The accuracy of the approximate analytical results is validated and assessed by comparing with those obtained using Monte Carlo simulation. It is observed that there is an excellent agreement between the analytical results and the numerical results. The effect of noise on various parametric resonances, such as subharmonic resonance, combination additive resonance, and combined subharmonic and combination

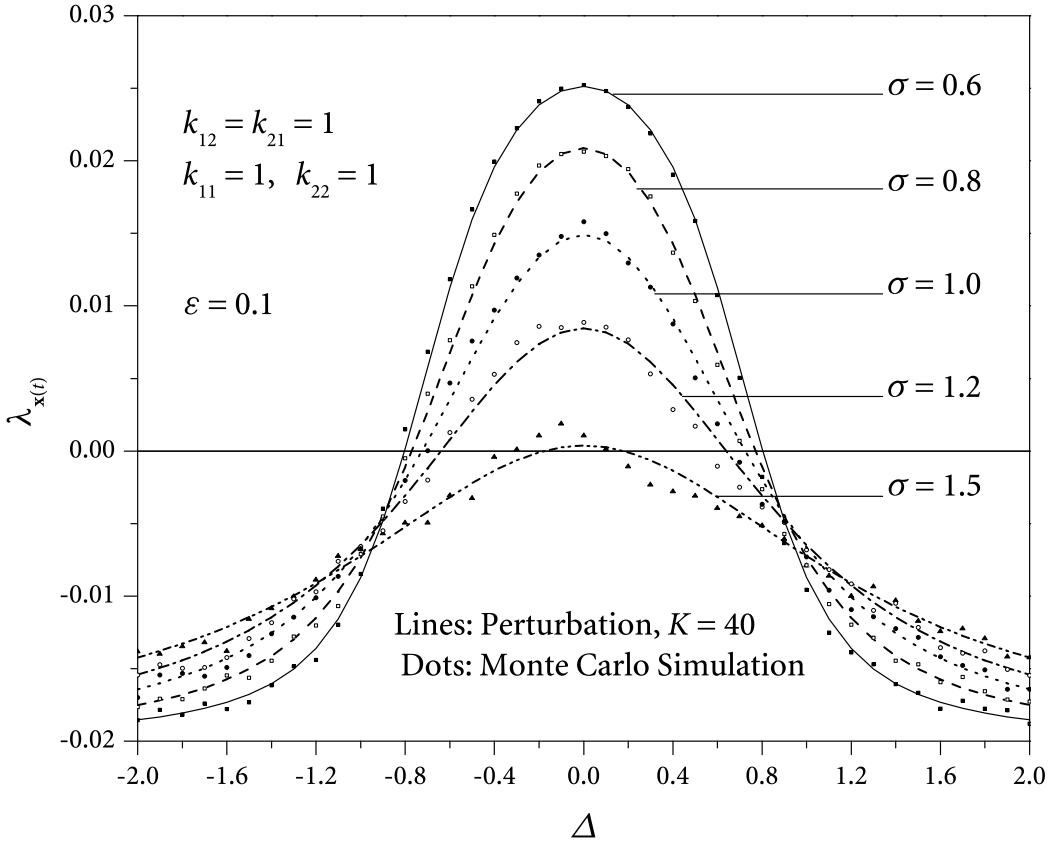

Figure 5.12 Lyapunov exponent for $\beta_1 = \beta_2 = 0.2$, $\omega_1 = \omega_2$, and $\nu_0 = 2\omega_1$.

additive resonance, is investigated. The effects of system parameters on the stability are studied.

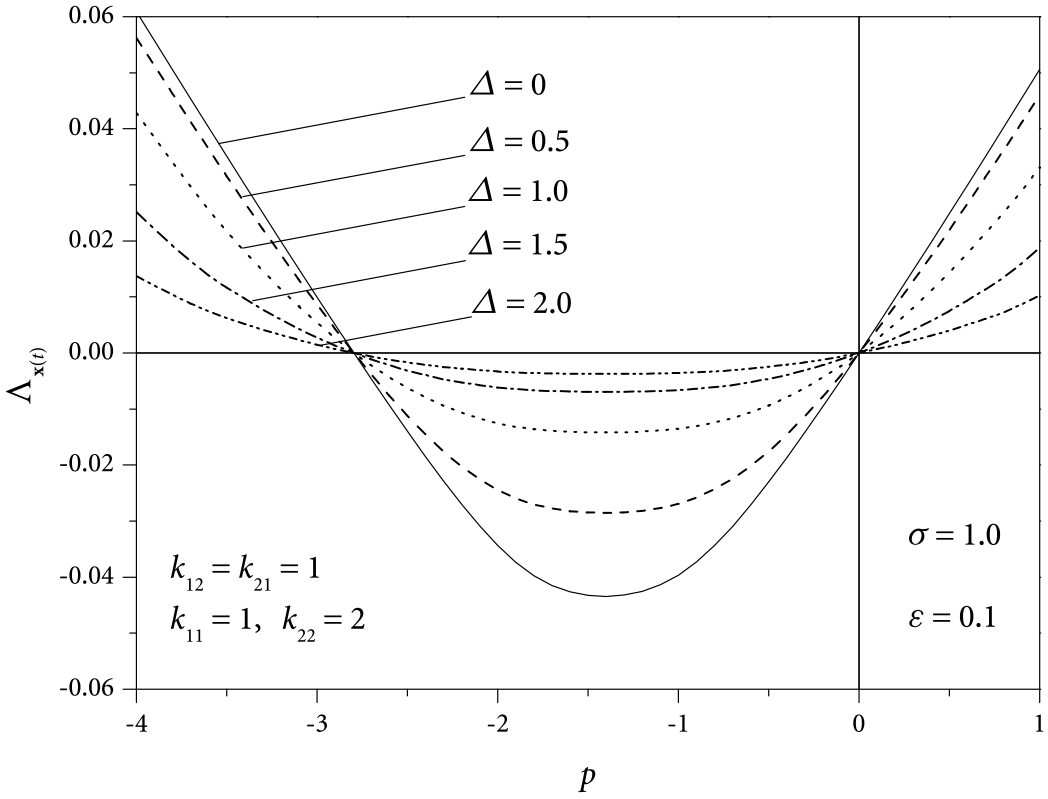

Figure 5.13 Moment Lyapunov exponent for $\beta_1 = \beta_2 = 0$, $\omega_1 = \omega_2$, and $\nu_0 = 2\omega_1$ ($K = 20$).

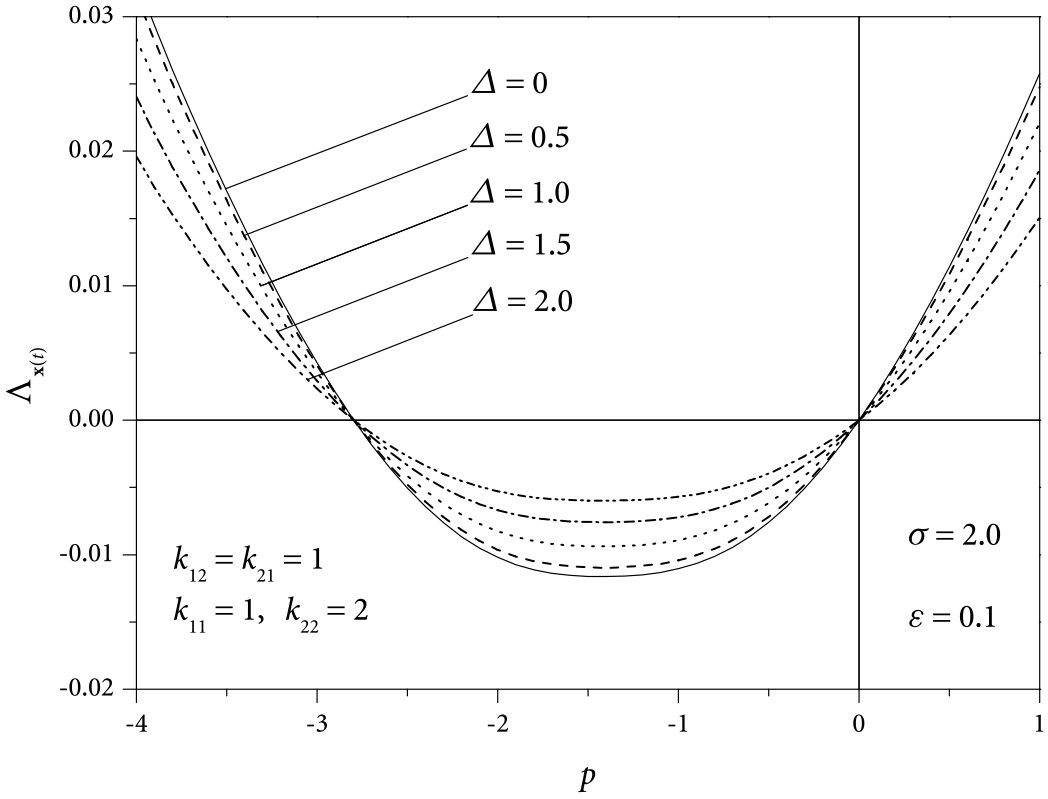

Figure 5.14 Moment Lyapunov exponent for $\beta_1 = \beta_2 = 0$, $\sigma = 2.0$, and $\nu_0 = 2\omega_1$ ($K = 20$).

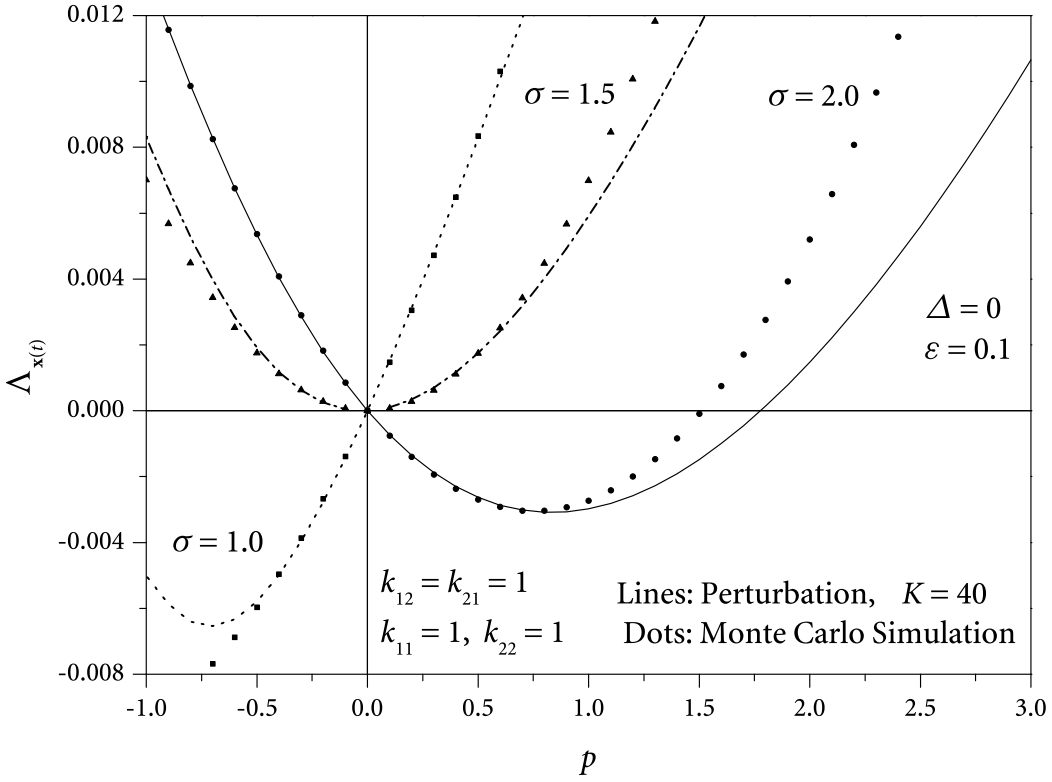

Figure 5.15 Moment Lyapunov exponent for $\beta_1 = \beta_2 = 0.2$, $\omega_1 = \omega_2$, and $\nu_0 = 2\omega_1$.

C H A P T E R 6

Conclusions and Future Work

Flow-induced vibration and dynamic stability of stochastic systems are two important research areas. There is extensive research done in either area. The research in this thesis fills the gap between the two areas and successfully apply the stochastic theory to flow-induced vibration and instability. The effects of noise on flow-induced vibration are investigated.

6.1 Conclusions

Flow-induced vibration of a cylinder in a cross-flow

A spring-supported cylinder is considered in this research. The equations of motion for the cylinder placed in a cross-flow are set up in which the vortex force is modeled by a bounded noise because of its narrow-band characteristics and the motion-dependent forces are also included. Since the vibration of the cylinder in the lift direction is more prominent in the lock-in region, the system is reduced to one degree-of-freedom, i.e., only the vibration of the cylinder in the lift direction is considered. Hence, a general two-dimensional system excited by a bounded noise is considered. The partial differential eigenvalue problem governing the moment Lyapunov exponents is established and a singular perturbation is applied to obtain the second-order expansions of the moment Lyapunov exponents for small noise excitations. The Lyapunov exponents are determined from the relationship between the moment Lyapunov exponents and Lyapunov exponents.

It is found that parametric instability occurs in vortex-induced vibration of a single cylinder in a cross-flow at the lock-in range. When appropriate values of the system

parameters are taken, the vibration of the cylinder is made up of main resonance due to the lock-in forcing, parametric instability due to time-variant fluid damping, and constant-fluid-damping-induced instability in the usual lock-in range. In particular, the primary parametric resonance enlarges the range of instability in terms of the reduced flow velocity. The effects of some crucial parameters, such as the mass ratio and the fluid damping coefficient, are studied. Specifically, decreasing the mass ratio or increasing the constant fluid damping has a positive influence on the instability of the system. The analytical results agree very well with those obtained by Monte Carlo simulations.

Fluidealstic instability of a cylinder in a shear flow

Experimental results show that fluidelastic instability can occur at high reduced velocity for a cylinder placed in a shear flow. To study the stability of such a system, the model for a cylinder in a cross-flow is extended to incorporate the influence of the shear flow. A quasi-steady model is used to model the vortex-induced forces while the motion-dependent forces are neglected since they are quite small at the region of high reduced velocity. For such a deterministic system, its stability depends on the eigenvalues of the system matrix $\mathbf{A}$. If the real parts of the eigenvalues are negative, the system is stable. When the reduced velocity U_r increases to a critical value, the largest real part of the eigenvalues become positive, i.e., the cylinder becomes unstable. Increasing the values of the reduced velocity U_r or the shear parameter K can destabilize the cylinder. On the contrary, increasing the mass ratio M_r, decreasing U_r, or decreasing K would make the system more stable.

To investigate the effects of turbulence on stability, the grid-generated turbulence is modeled by a real noise with Gaussian distribution and zero mean. Thus, the equations of motion for the cylinder are randomized resulting in a four-dimensional system excited by a real noise. The system has one critical mode and one stable mode. The effect of real noise on the stability of such a parametrically excited four-dimensional system is considered. The dynamic stability of the system is studied by determining the moment Lyapunov exponents and the Lyapunov exponents. For weak noise excitations, a regular perturbation method is employed to obtain second-order expansions of the moment Lyapunov exponents. and the Lyapunov exponent. The analytical method is applied to study the effects of grid-generated turbulence on the stability of a circular cylinder in a shear flow, which is subjected to fluide-

lastic instability. The correctness and the accuracy of the approximate analytical results are validated and assessed by comparing with those obtained by Monte Carlo simulations.

The analysis demonstrates that the cylinder can be stabilized by the real noise with proper parameters in the sense of both sample stability and moment stability. It is shown that grid-generated turbulence can shift the critical reduced velocity to a higher value and hence stabilize the cylinder. The stabilizing effect becomes smaller when α, which characterizes the bandwidth of the real noise, increases. This result indicates that the length scale of turbulence L_x is a key parameter for the stabilization since α is related to L_x. Furthermore, the analytical results show that the stabilizing effect of turbulence is proportional to the turbulence intensity, which agrees with the experimental observations.

It is also found that the stabilization is sensitive to the frequency ratio k between the two natural frequencies of the cylinder in the x-direction and y-direction. When the difference between the two natural frequencies becomes larger, a better stabilizing effect is observed due to stronger coupling between the critical mode and the stable mode.

Parametric resonances of a two degrees-of-freedom system induced by a bounded noise

A two degrees-of-freedom system under bounded noise excitation is considered. Depending on the central frequency of the bounded noise, various types of parametric resonance may occur in the system. The partial differential eigenvalue problem governing the moment Lyapunov exponent is established. For weak noise excitations, a singular perturbation method is employed to obtain second-order expansions of the moment Lyapunov exponents. A double Fourier series is used to solve the eigenvalue problem. The effects of the bounded noise and the detuning frequency Δ on the resonance are investigated. Stochastic stability of the system, which is in subharmonic resonance, combination additive resonance, and combined resonance when the excitation is a harmonic function, respectively, is studied. Numerical results for both the Lyapunov exponents and moment Lyapunov exponents are obtained by Monte Carlo simulation and compared with the analytical results to validate the analytical approach. The effect of noise on various types of parametric resonance, such as subharmonic resonance, combination additive resonance, and combined subharmonic

and combination additive resonance, is investigated. The effects of system parameters, such as the damping β_i and the amplitudes of bounded noise k_{ij}, on the stability are also studied.

It is shown that subharmonic resonance is associated with k_{11} or k_{22} only, while combination additive resonance is only influenced by k_{12} and k_{21}, which represents the coupling between the two degrees-of-freedom. When the subharmonic resonance and combination additive resonance occur simultaneously, the resonance results have contributions from all k_{ij}'s. Larger amplitudes of the bounded noise, which are characterized by larger values of k_{ij}'s, yield more significant resonance. Decreasing the bandwidth of the bounded noise σ has the same effect on the stability because the power spectrum of the bounded noise is more narrow-banded and the effect of parametric resonance is more prominent. The frequency detuning parameter Δ is also a key parameter on the stability of the system. When the central frequency of the bounded noise is offset from the resonance frequencies, the effect of parametric resonance is significantly reduced. The damping always has a stabilizing effect. It is also found that the combined effect of subharmonic and combination additive resonances results in not only more significant resonance in terms of larger Lyapunov exponent than either case separately, but also wider resonance region in terms of frequency detuning. This means that parametric resonance can be triggered more easily.

The accuracy of the approximate analytical results is validated and assessed by comparing with those obtained using Monte Carlo simulation. It is observed that there is an excellent agreement between the analytical results and the numerical results.

6.2 Future Work

The present research considers only one cylinder in a cross-flow. In practical industrial applications, cylinders or tubes are usually placed in an array. The motion of each cylinder will change the fluid field and thus the cylinder interacts with the adjacent cylinders. The interactions among cylinders have to be taken into account for determining the stability boundary of an array of cylinders. This results in a lot of difficulties. There are no general theoretical models which can predict the fluid forces applied on an arbitrary cylinder in an array. The fluid forces have to be measured experimentally, which is generally difficult and time-consuming. One possible solution is to consider a cell in an array such as two

side-by-side cylinders instead of the whole array. However, the study of stochastic stability of high-dimensional systems is still a challenging problem.

In the present study, the fluid-structure interaction is approximated linearly based on the quasi-steady theory for the convenience of analytical analysis. However, flow-induced vibration of cylinders in a cross-flow is essentially a nonlinear phenomenon. Chaotic vibration can occur in the flow-induced instabilities with strong nonlinearities. Modeling the nonlinearities correctly is important for determining the critical velocity and the limit cycle amplitudes of the vibrating cylinders. The turbulence effects on the stability of the nonlinear systems can be studied by stochastic bifurcation theory, which has attracted the interest of many researchers.

In addition to the urgent needs of theoretical modeling, experimental efforts are also indispensable. The fluid force coefficients depend on the Reynolds number, the reduced velocity, turbulence intensity, and the position of the cylinder in an array. Extensive experiments have to be conducted to measure the fluid force coefficients under different conditions. Experimental results can provide the information for theoretical modeling and validate the predictions from the mathematical models. With the development of computational fluid dynamics (CFD), some of the experimental work can be substituted by numerical simulations.

In summary, large gaps still remain in the flow-induced vibration of cylinders despite the fact that many efforts have been made in the experimental, theoretical, and numerical methods. Stochastic analysis is a useful tool for the study of flow-induced vibration and the mechanism of the fluid-structural interaction can be understood better with the help of the theory of stochastic systems.

APPENDIX A

A.1 The Fredholm Alternative

When the method of perturbation is applied to obtain weak noise expansions of the pth moment Lyapunov exponents, the Fredholm Alternative is used.

Consider the following elliptic partial differential equation in a smooth, bounded domain $\Omega \subset \mathcal{R}^n$,

$$\mathscr{L}u = f, \qquad \text{in } \Omega, \tag{A.1.1a}$$

where $\mathscr{L}$ is the uniformly elliptic operator

$$\mathscr{L}(u) = \sum_{i=1}^{n}\sum_{j=1}^{n} a_{ij}(\mathbf{x})\,\frac{\partial^2 u}{\partial x_i \partial x_j} + \sum_{i=1}^{n} b_i(\mathbf{x})\,\frac{\partial u}{\partial x_i} + c(\mathbf{x})\,u \tag{A.1.1b}$$

with smooth coefficients a_{ij}, b_i, and c satisfying uniform ellipticity:

$$\sum_{i=1}^{n}\sum_{j=1}^{n} a_{ij}(\mathbf{x})\xi_i\xi_j \geqslant M\left\|\boldsymbol{\xi}\right\|^2, \qquad \text{for all } \mathbf{x} \in \Omega \text{ and } \boldsymbol{\xi} \in \mathcal{R}^n \quad (M>0). \tag{A.1.1c}$$

The adjoint operator $\mathscr{L}^*$ is given by

$$\mathscr{L}^*(u) = \sum_{i=1}^{n}\sum_{j=1}^{n} \frac{\partial^2\left(a_{ij}(\mathbf{x})\,u\right)}{\partial x_i \partial x_j} - \sum_{i=1}^{n} \frac{\partial\left(b_i(\mathbf{x})\,u\right)}{\partial x_i} + c(\mathbf{x})\,u. \tag{A.1.1d}$$

The Fredholm Alternative can be stated as follows.

Theorem: Suppose the operator $\mathscr{L} : X = H^2(\Omega) \cap H_0^1(\Omega) \to L^2(\Omega)$ as in equation (A.1.1b) is uniformly elliptic with smooth coefficients. The homogeneous equations

$$\mathscr{L}y = 0, \tag{A.1.2}$$

$$\mathscr{L}^* z^* = 0, \tag{A.1.3}$$

have the same finite number of linearly independent solutions $y_1, y_2, \ldots, y_k$ and $z_1^*, z_2^*, \ldots, z_k^*$, respectively, in $\mathcal{X} = H^2(\Omega) \cap H_0^1(\Omega)$. Moreover,

1. For $f \in L^2(\Omega)$, the nonhomogeneous partial differential equation

$$\mathscr{L} u = f \tag{A.1.4}$$

can be solved if and only if f is orthogonal to the k solutions $z_1^*, z_2^*, \ldots, z_k^*$ of equation (A.1.3), i.e.

$$\left(f,\, z_i^*\right) = 0, \quad i = 1, 2, \ldots, k, \tag{A.1.5}$$

where (ϕ, ψ) denotes the inner product of functions ϕ and ψ, which are defined and integrable over the region Ω,

$$(\phi, \psi) = \int_\Omega \phi\, \psi \, \mathrm{d}\mathbf{x}. \tag{A.1.6}$$

2. For $g \in L^2(\Omega)$, the nonhomogeneous partial differential equation

$$\mathscr{L}^* v = g, \tag{A.1.7}$$

can be solved if and only if g is orthogonal to the k solutions $y_1, y_2, \ldots, y_k$ of equation (A.1.2), i.e.

$$\left(g,\, y_i\right) = 0, \quad i = 1, 2, \ldots, k. \tag{A.1.8}$$

For more details about the Fredholm Alternative, one can refer to [48] and [103]. Although the Fredholm Alternative is proved only for functions f and u in bounded domains Ω of independent variables, the theorem often applies to singular problems such as one or more of the independent variables goes to infinity (see, e.g., Davis and Thomson [28]).

In the perturbation analysis of stochastic equations, the elliptic operator in equation (A.1.1b) is usually the infinitesimal generator of a diffusion process. If the diffusion process satisfies a strong ergodicity condition, the Fredholm Alternative can be proved for both bounded and unbounded domains from the ergodic theory. Specifically, if the transition probability function satisfies the Doeblin's condition, the transition probabilities converge geometrically fast to the stationary probability. The Poisson's equation (A.1.4) can be solved if and only if

$$\left(f,\, \bar{P}\right) = 0, \tag{A.1.9}$$

where $\bar{P}$ is the stationary probability which is the solution of equation (A.1.3). Furthermore, the solution of equation (A.1.4) is unique and can be expressed in terms of the recurrent potential kernel (or Green's function) for the operator $\mathscr{L}$. For more details, refer to Papanicolaou [60].

It can be shown that the diffusion processes used in this thesis satisfy the above assumptions. Hence, the Fredholm Alternative is applicable.

Bibliography

1. P. Anagnostopoulos. Vibration induced by vortex shedding. In P. Anagnostopoulos, editor, *Flow-induced Vibrations in Engineering Practice*, pp. 1–80, Southampton, UK, 2002. WIT Press.

2. S.T. Ariaratnam. Stochastic stability of viscoelastic systems under bounded noise excitation. In A. Naess and S. Krenk, editors, *IUTAM Symposium on Advances in Nonlinear Stochastic Mechanics*, pp. 11–18. Kluwer Academic Publishers, 1996.

3. L. Arnold, H. Crauel, and V. Wihstutz. Stabilization of linear systems by noise. *SIAM Journal of Control and Optimization*, **21**, pp. 451–461, 1983.

4. L. Arnold, M.M. Doyle, and N.S. Namachchivaya. Small noise expansion of moment Lyapunov exponents for two-dimensional systems. *Dynamics and Stability of Systems*, **12**(3), pp. 187–211, 1997.

5. L. Arnold, W. Kliemann, and E. Oeljeklaus. Lyapunov exponents of linear stochastic systems. In L. Arnold and V. Wihstutz, editors, *Lyapunov Exponents*, vol. 1186 of *Lecture Notes in Mathematics*, pp. 129–159. Springer-Verlag, Berlin, 1986. Proceedings of a Workshop, Bremen, Germany, 1984.

6. L. Arnold, E. Oeljeklaus, and E. Pardoux. Almost sure and moment stability for linear Itô equations. In L. Arnold and V. Wihstutz, editors, *Lyapunov Exponents*, vol. 1186 of *Lecture Notes in Mathematics*, pp. 85–125. Springer-Verlag, Berlin, 1986. Proceedings of a Workshop, Bremen, Germany, 1984.

7. L. Arnold. A formula connecting sample and moment stability of linear stochastic systems. *SIAM Journal of Applied Mathematics*, **44**(4), pp. 793–802, 1984.

8. L. Arnold. Stabilization by noise revisited. *Z. Angew. Math. Mech.*, **70**, pp. 235–246, 1990.

9. M.K. Au-Yang. *Flow-Induced Vibration of Power and Process Plant Components: A Practical Workbook*. ASME Press, New York, 2001.

10. S. Balasubramanian and R.A. Skop. A nonlinear oscillator model for vortex shedding from cylinders and cones in uniform and shear flows. *Journal of Fluids and Structures*, **10**, pp. 197–214, 1996.

11. G.K. Batchelor. *The theory of homogeneous turbulence*. Cambridge University Press, 1953.

12. E. Berger. On a mechanism of vortex excited oscillations of a cylinder. *Journal of Wind Engineering and Industrial Aerodynamics*, **28**, pp. 301–310, 1988.

13. H.M. Blackburn and W.H. Melbourne. The effect of free-stream turbulence on sectional lift forces on a circular cylinder. *Journal of Fluid Mechanics*, **11**, pp. 267–292, 1996.

14. H.M. Blackburn and W.H. Melbourne. Sectional lift forces for an oscillating circular cylinder in smooth and turbulent flows. *Journal of Fluids and Structures*, **11**, pp. 413–431, 1997.

15. R.D. Blevins. *Flow-Induced Vibrations*. Van Nostrand Reinhold, New York, NY, second edition, 1990.

16. R.D. Blevins. Turbulence-induced vibration. In M.K. Au-Yang, editor, *in Technology for the '90s, Part III: Fluid-Structure Interaction*, pp. 681–709, ASME, New York, 1993.

17. R.V. Bobryk and A. Chrzeszczyk. Colored-noise-induced parametric resonance. *Physica A*, **316**, pp. 225–232, 2002.

18. A. Bokaian and F. Geoola. Wake-induced galloping of two interfering circular cylinders. *Journal of Fluid Mechanics*, **146**, pp. 383–415, 1984.

19. C.G. Bucher and Y.K. Lin. Stochastic stability of bridges considering coupled modes. *ACSE Journal of Engineering Mechanics*, **114**, pp. 2055–2071, 1988.

20. G.Q. Cai and C. Wu. Modeling of bounded stochastic processes. *Probabilistic Engineering Mechanics*, **19**, pp. 197–203, 2004.

21. S.S. Chen, Y. Cai, and G.S. Srikantiah. Fluid damping controlled instability of tubes in crossflow. *Journal of Sound and Vibration*, **217**(5), pp. 883–907, 1998.

22. S.S. Chen and G.S. Srikantiah. Motion-dependent fluid force coefficients for tube arrays in crossflow. *ASME Journal of Pressure Vessel Technology*, **123**, pp. 429–436, 2001.

23. S.S. Chen, S. Zhu, and Y. Cai. An unsteady flow theory for vortex-induced vibration. *Journal of Sound and Vibration*, **184**, pp. 73–92, 1995.

24. S.S. Chen. *Flow-Induced Vibration of Circular Cylindrical Structures*. Hemisphere Publishing, New York, 1987.

25. H. J. Connors, Jr. Fluidelastic vibration of tube arrays excited by cross flow. In D. D. Reiff, editor, *Flow-Induced Vibration in Heat Exchangers (Lecture Notes in Mathematics, 1186)*, pp. 42–56, New York, 1970. ASME.

26. R.M. Corless and G.V. Parkinson. A model of the combined effects of vortex-induced oscillation and galloping. *Journal of Fluids and Structures*, **2**, pp. 203–220, 1988.

27. R.M. Corless and G.V. Parkinson. Mathematical modelling of combined effects of vortex-induced vibration and galloping. part II. *Journal of Fluids and Structures*, **7**, pp. 825–848, 1993.

28. H.T. Davis and K.T. Thomson. *Linear Algebra and Linear Operators in Engineering with Applications in Mathematica*. Academic Press, 2000.

29. M.F. Dimentberg. *Statistical Dynamics of Nonlinear and Time-Varying Systems.* John Wiley & Sons, Inc., New York, 1988.

30. R.D. Gabbai and H. Benaroya. An overview of modeling and experiments of vortex-induced vibration of circular cylinders. *Journal of Sound and Vibration*, **282**, pp. 575–616, 2005.

31. C.W. Gardiner. *Handbook of Stochastic Methods for Physics, Chemistry and the Natrual Sciences*. Spriger, New York, 1985.

32. S. Granger and M.P. Païdoussis. An improvement to the quasi-steady model with application to cross-flow-induced vibration of tube arrays. *Journal of Fluid Mechanics*, **320**, pp. 163–184, 1996.

33. O.M. Griffin and G.H. Koopmann. The vortex-excited lift and reaction forces on resonantly vibrating cylinders. *Journal of Sound and Vibration*, **54**, pp. 435–448, 1977.

34. O.M. Griffin. Vortex-excited cross-flow vibrations of a single cylindrical tube. *Journal of Pressure Vessel Technology*, **102**, pp. 158–166, 1980.

35. R.T. Hartlen and I.G. Currie. Lift oscillation model for vortex-induced vibration. *ASCE Journal of Engineering Mechanics*, **96**, pp. 577–591, 1970.

36. R.A. Ibrahim. Excitation-induced stability and phase transition: a review. *Journal of Vibration and Control*, **12**(10), pp. 1093–1170, 2006.

37. S. Kang. Uniform-shear flow over a circular cylinder at low reynolds numbers. *Journal of Fluids and Structures*, **22**, pp. 541–555, 2006.

38. R.Z. Khasminskii and N. Moshchuk. Moment Lyapunov exponent and stability index for linear conservative system with small random perturbation. *SIAM Journal of Applied Mathematics*, **58**(1), pp. 245–256, 1998.

39. P.E. Kloeden and E. Platen. *Numerical Solution of Stochastic Differential Equations*. Springer-Verlag, Berlin, 1999.

40. M.T. Landahl and E. Mollo-Crristensen. *Turbulence and Random Processes in Fluid Mechanics*. Cambridge University Press, Cambridge, MA, 2nd edition, 1992.

41. R. Landl. A mathematical model for vortex-excited vibrations of bluff bodies. *Journal of Sound and Vibration*, **42**, pp. 219–234, 1975.

42. C. Lei, L. Cheng, and K. Kavanagh. A finite difference solution of the shear flow over a circular cylinder. *Ocean Engineering*, **27**, pp. 271–288, 2000.

43. J.H. Lever and D.S. Weaver. On the stability behaviour of heat exchanger tube bundles: Part 1-modified theoretical model, part 2-numerical results and comparison with experiments. *Journal of Sound and Vibration*, **107**, pp. 375–410, 1986.

44. Y.K. Lin and G.Q. Cai. *Probabilistic Structural Dynamics: Advanced Theory and Applications*. McGraw-Hill, Inc., New York, 1995.

45. Y.K. Lin and Q.C. Li. New stochastic theory for bridge statility in turbulent flow. *Journal of Engineering Mechanics*, **119**(1), pp. 113–127, 1993.

46. Q.C. Li and Y.K. Lin. New stochastic theory for bridge stability in turbulent flow II. *ASCE Journal of Engineering Mechanics*, **121**, pp. 102–116, 1995.

47. A.M. Lyapunov. Problème Générale de la Stabilité du Mouvement. *Comm. Soc. Math. Kharkov*, **2**, pp. 265–272, 1892. Reprinted in *Annals of Mathematical Studies*, vol. 17, Princeton University Press, Princeton, 1947.

48. R.C. McOwen. *Partial Differential Equations: Methods and Applications*. Prentice Hall, New Jersey, second edition, 2003.

49. S.A. Molchanov. The structure of eigenfunctions of one-dimensional unordered structures. *Math. USSR Izvestija*, **12**, pp. 69–101, 1978.

50. N. Moshchuk, R.A. Ibrahim, and R. Khasminskii. Response statistics of ocean structures to non-linear hydrodynamic loading, part i: Gaussian ocean waves. *Journal of Sound and Vibration*, **184**(4), pp. 681–701, 1995.

51. T. Myint-U and L. Debnath. *Linear Partial Differential Equations for Scientists and Engineers*. Birkhäuser, Boston, forth edition edition, 2007.

52. N.S. Namachchivaya, H.J. Van Roessel, and M.M. Doyle. Moment lyapunov exponent for two coupled oscillators driven by real noise. *SIAM Journal on Applied Mathematics*, **56**(5), pp. 1400–1423, 1996.

53. N.S. Namachchivaya and H.J. Van Roessel. Moment Lyapunov exponent and stochastic stability of two coupled oscillators driven by real noise. *ASME Journal of Applied Mechanics*, **68**(6), pp. 903–914, 2001.

54. N.S. Namachchivaya and H.J. Van Roessel. Stochastic stability of coupled oscillators in resonance: a perturbation approach. *ASME Journal of Applied Mechanics*, **71**(6), pp. 759–768, 2004.

55. N.S. Namachchivaya and L. Vedula. Stabilization of linear systems by noise: Application to flow induced oscillations. *Dynamics and Stability of Systems*, **15**(2), pp. 185–208, 2000.

56. E. Naudascher and D. Rockwell. *Flow-induced vibrations: an engineering guide*. Balkema Publishers, USA, 1994.

57. Y.I. Oseledec. A multiplicative ergodic theorem. Lyapunov characteristic number for dynamical systems. *Transactions of the Moscow Mathematical Society*, **19**, pp. 197–231, 1968. English translation.

58. M.P. Païdoussis, D. Mavriplis, and S.J. Price. A potential flow theory for the dynamics of cylinders arrays in cross flow. *Journal of Fluid Mechanics*, **146**, pp. 227–252, 1984.

59. M.D. Pandey and S.T. Ariaratnam. Stability analysis of wind-induced torsional motion of slender bridges. *Structural Safety*, **20**, pp. 379–389, 1998.

60. G.C. Papanicolaou. Asymptotic analysis of stochastic equations. In M. Rosenblatt, editor, *Studies in Probability Theory*, vol. 18, pp. 111–179. The Mthematical Association of America, 1978.

61. E. Pardoux and V. Wihstutz. Lyapunov exponent and rotation number of two-dimensional linear stochastic systems with small diffusion. *SIAM Journal of Applied Mathematics*, **48**(2), pp. 442–457, 1988.

62. D. Poirel and S.J. Price. Random binary (coalescence) flutter of a two-dimensional linear airfoil. *Journal of Fluids and Structures*, **18**, pp. 23–42, 2003.

63. S.B. Pope. *Turbulent flows*. Cambridge University Press, New York, 2000.

64. K. Popp and O. Romberg. Influence of stochastic effects on flow induced vibrations in tube bundles. In S. Narayanan and R.N. Iyengar, editors, *IUTAM Symposium on Nonlinearity and Stochastic Structural Dynamics*, pp. 197–208. Kluwer Academic Publishers, 1999.

65. S.J. Price and M.P. Païdoussis. An improved mathematical model for the stability of cylinder rows subject to cross-flow. *Journal of Sound and Vibration*, **97**, pp. 615–640, 1984.

66. S.J. Price. A review of theoretical models for fluidelastic instability of cylinder arrays in cross-flow. *Journal of Fluids and Structures*, **9**, pp. 463–518, 1995.

67. O. Romberg and K. Popp. Random excitation by fluid forces acting on a single flexible tube in bundles subjected to cross-flow. In M.P. Païdoussis, editor, *Fluid-Structure Interaction, Aeroelasticity, Flow-Induced Vibration and Noise*, vol. 53, pp. 173–181. ASME, 1997.

68. O. Romberg and K. Popp. The influence of upstream turbulence on the stabiltiy boundaries of a flexible tube in a bundle. *Journal of Fluids and Structures*, **12**, pp. 153–169, 1998.

69. M. Rottmann and K. Popp. Influence of upstream turbulence on the fluidelastic instability of a parallel triangular tube bundle. *Journal of Fluids and Structures*, **18**, pp. 595–612, 2003.

70. F. Rüdinger and S. Krenk. Stochastic analysis of self-induced vibrations. *Meccanica*, **37**, pp. 3–14, 2002.

71. G. Rzentkowski and J.H. Lever. An effect of turbulence on fluidelastic instability in tube bundles: A nonlinear analysis. *Journal of Fluids and Structures*, **12**, pp. 561–590, 1998.

72. T. Sarpkaya. Fluid forces on oscillating cylinders. *Journal of Waterway, Port, Coastal and Ocean Engineering*, **104**, pp. 275–291, 1978.

73. T. Sarpkaya. Vortex-induced oscillations — a selective review. *ASME Journal of Applied Mechanics*, **46**, pp. 241–258, 1979.

74. T. Sarpkaya. A critical review of the intrinsic nature of vortex-induced oscillations. *Journal of Fluids and Structures*, **19**, pp. 389–447, 2004.

75. R.A. Skop and O.M. Griffin. A model for the vortex-excited resonant response of bluff cylinders. *Journal of Sound and Vibration*, **27**, pp. 225–233, 1973.

76. K. Sobczyk. *Stochastic Differential Equations, With applications to Physics and Engineering*. Kluwer Acdemic Publishers, Dordrecht, 1991.

77. G. Solari and G. Piccardo. Probabilistic 3-d turbulence modeling for gust buffeting of structures. *Probabilistic Engineering Mechanics*, **16**, pp. 73–86, 2001.

78. R.M.C. So, Y. Liu, S.T. Chan, and K. Lam. Numerical studies of a freely vibrating cylinder in a cross flow. *Journal of Fluids and Structures*, **15**, pp. 845–866, 2001.

79. R.M.C. So and S.D. Savkar. Buffeting forces on rigid circular cylinders in cross flows. *Journal of Fluid Mechanics*, **105**, pp. 397–425, 1981.

80. R.M.C. So, X.Q. Wang, W.-C. Xie, and J. Zhu. Free-stream turbulence effects on vortex-induced vibration of an elastic cylinder. *Journal of Fluids and Structures*, accepted.

81. R.L. Stratonovich. *Topics in the Theory of Random Noise*, vol. 2. Gordon and Breach Science Publishers, Inc., New York, 1967.

82. H. Tanaka, S. Takahara, and K. Ohta. Flow-induced vibration of tube arrays with various pitch-to-diameter ratio. *Journal of Pressure Vessel Technology*, **104**, pp. 168–176, 1982.

83. H. Tanaka and S. Takahara. Fluid elastic vibration of tube array in cross flow. *Journal of Sound and Vibration*, **77**, pp. 19–37, 1981.

84. B.J. Vickery and R.I. Basu. Across-wind vibrations of structures of circular cross-section. part I: Development of a mathematical model for two-dimensional conditions. *Journal of Wind Engineering and Industrial Aerodynamics*, **12**, pp. 49–73, 1983.

85. X.Q. Wang, R.M.C. So, and K.T. Chan. A nonlinear fluid force model for vortex-induced vibration of an elastic cylinder. *Journal of Sound and Vibration*, **260**, pp. 287–305, 2003.

86. X.Q. Wang, W.-C. Xie, and R.M.C. So. Force evolution model for vortex-induced vibration of one elastic cylinder in cross flow. In *Proceedings of the 2006 ASME Pressure Vessels and Pipeline Division Conference*, number PVP2006-ICPVT11-93875, Vancouver, Canada, July 2006.

87. D.S. Weaver and J.A. Fitzpatrick. A review of flow induced vibrations in heat exchangers. *Journal of Pressure Vessel Technology*, **2**, pp. 73–93, 1988.

88. D.S. Weaver, S. Ziada, M.K. Au-Yang, and et al. Flow-induced vibration in power and process plant component–progress and prospects. *Journal of Pressure Vessel Technology*, **22**, pp. 339–348, 2000.

89. D.S. Weaver. Vortex shedding and acoustic resonance in heat exchanger tube arrays. In M.K. Au-Yang, editor, *Technology for the '90s, Part III: Fluid-Structure Interaction*, pp. 775–810, ASME, New York, 1993.

90. D.P. Weber, R. Brewster, S.S. Chen, and T.Y.C. Wei. A numerical method for fluidelastic instability evaluation in nuclear reactor system and plant components. In V. Matzen, editor, *The 16th International Conference on SMiRT*, Washington DC, 2001.

91. W. Wedig. Lyapunov exponent of stochastic systems and related bifurcation problems. In S. T. Ariaratnam, G. I. Schuëller, and I. Elishakoff, editors, *Stochastic Structural Dynamics–Progress in Theory and Applications*, pp. 315–327. Elsevier Applied Science, London, 1988.

92. W. Wedig. Analysis and simulation of nonlinear stochastic systems. In W. Schiehlen, editor, *Nonlinear Dynamics in Engineering Systems*, pp. 337–344. Springer-Verlag, Berlin, 1989.

93. C.H.K. Williamson and R. Govardhan. Vortex-induced vibrations. *Annual Review of Fluid Mechanics*, **36**, pp. 413–455, 2004.

94. A. Wolf, J. Swift, H. Swinney, and A. Vastano. Determining Lyapunov exponents from a time series. *Physica D*, **16**, pp. 285–317, 1985.

95. W.-C. Xie and Q. Huang. Simulation of moment lyapunov exponents for linear homogenous stochastic systems. *ASME Journal of Applied Mechanics*, submitted.

96. W.-C. Xie. Moment Lyapunov exponents of a two-dimensional system under real noise excitation. *Journal of Sound and Vibration*, **239**(1), pp. 139–155, 2001.

97. W.-C. Xie. Moment Lyapunov exponents of a two-dimensional viscoelastic system under bounded noise excitation. *ASME Journal of Applied Mechanics*, **69**(3), pp. 346–357, 2002.

98. W.-C. Xie. Moment Lyapunov exponents of a two-dimensional system under bounded noise parametric excitation. *Journal of Sound and Vibration*, **263**(3), pp. 593–616, 2003.

99. W.-C. Xie. *Dynamic Stability of Structures*. Cambridge University Press, 2006.

100. M. Yu, C. Yu, and K. Chen. Fluid elastic instability of a small circular cylinder in the shear layer of a two-dimensional jet. *Physics of Fluids*, **16**(7), pp. 2357–2370, 2004.

101. E. Zauderer. *Partial Differential Equations of Applied Mathematics*. John Wiley & Sons, New York, second edition, 1989.

102. M.M. Zdravkovich. *Flow around circular cylinders*, vol. 1. Oxford University Press, New York, 1997.

103. E. Zeidler. *Applied Functional Analysis: Main Principles and Their Applications*. Springer-Verlag, New York, 1995.

104. J. Zhu, X.Q. Wang, W.-C. Xie, and R.M.C. So. Flow-induced instability under bounded noise excitation in cross-flow. *Journal of Sound and Vibration*, in press.

105. S. Zhu, S.S. Chen, and Y. Cai. Vibration and stability of two tubes in crossflow. In M.J. Petttigrew, editor, *Flow-Induced Vibration*, vol. 298, pp. 1–12. ASME, 1995.